#073

#3073

PRESSURE GRADIENTS AND THE LOCATION OF THE NEUTRAL PRESSURE AXIS FOR LOW-RISE STRUCTURES UNDER PURE STACK CONDITIONS

John P. Chastain, M.S. Thesis, 1987
University of Kentucky

Air Infiltration and Ventilation Centre
University of Warwick Science Park
Barclays Venture Centre
Sir William Lyons Road
Coventry CV4 7EZ
Great Britain
Telephone: (0203) 692050
Telex: 312401
Fax: (0203) 410156

LOAN

1st copy

8. 1. 90		
16. 3. 90		
20. 3. 90		
25. 4. 90		

ABSTRACT OF THESIS

PRESSURE GRADIENTS AND THE LOCATION OF THE NEUTRAL PRESSURE AXIS FOR LOW-RISE STRUCTURES UNDER PURE STACK CONDITIONS

A discharge coefficient equation was incorporated into a mass balancing procedure to compute the elevation of the neutral pressure axis (NPA) for a general distribution of openings. An equation was developed to compute the discharge coefficient of an arbitrary opening as a function of the three dimensional geometry, the pressure, difference, the total minor loss coefficient, and the air properties.

A two cell environmental chamber was constructed to simulate the temperature gradients across a wall and ceiling section of a two story residence. Idealized openings could be mounted in the wall at nine different elevations and one mounting location was provided in the ceiling section.

An experiment was designed to investigate the factors which influence the location of the NPA and to test the validity of the mass balancing procedure. A total of eight opening distributions were defined. Four of these distributions included an opening placed in the ceiling section. The parameters varied were: the total leakage area mounted in the test sections; the size of the individual openings, the geometry of the openings; the vertical placement and the mean temperature difference.

The results indicated that the location of the NPA depends on the relative size of the openings in a distribution, a variable discharge coefficient, and the vertical placement of the openings. The location of the NPA was not a function of the mean temperature difference and the observed degree of temperature stratification had no effect on the NPA. The location of the NPA was predicted within $\pm$ 2.22 percent of the eave height for each case using the mass balancing procedure.

Application of the mass balancing procedure to an actual structure would require a method to model the air flow through components of envelope leakage as an equivalent opening. A modeling equation was developed which could be used to determine the

cross-sectional area and the three dimensional geometry of an equivalent straight rectangular opening which would provide the same air flow as the modeled component.

An experiment was performed to develop the concept of modeling components of envelope leakage as an equivalent straight rectangular opening. Differential pressure measurements were obtained for a group of straight openings which ranged in cross-sectional geometry from a near infinite rectangular slot to a cylinder. The dimensionless flow length, z/D_h, of the openings was varied from 2.0 to 15.9.

It was apparent from the results that the equivalent opening areas were in close agreement with the actual areas of the defined openings. Also, the observed flow rates were predicted within the uncertainties of the measurements using a single mean total minor loss coefficient with the discharge coefficient equation and the equivalent opening parameters obtained by application of the modeling equation.

(Author's Name)

(Date)

PRESSURE GRADIENTS AND THE LOCATION OF THE NEUTRAL PRESSURE AXIS FOR LOW-RISE STRUCTURES UNDER PURE STACK CONDITIONS

THESIS

A thesis submitted in partial fulfillment of the requirements for the degree of Master of Science in Agricultural Engineering at the University of Kentucky

By

John P. Chastain

Lexington, Kentucky

Director: Dr. Donald G. Colliver, Associate Professor
of Agricultural Engineering
Lexington, Kentucky

1987

PRESSURE GRADIENTS AND THE LOCATION OF THE NEUTRAL
PRESSURE AXIS FOR LOW-RISE STRUCTURES
UNDER PURE STACK CONDITIONS

By

John P. Chastain

____
(Director of Thesis)

____
(Director of Graduate Studies)

____
(Date)

RULES FOR THE USE OF THE THESES

Unpublished theses submitted for the Master's and Doctor's degrees and deposited in the University of Kentucky Library are as a rule open for inspection, but are to be used only with due regard to the rights of the authors. Bibliographical references may be noted, but quotations or summaries of parts may be published only with the permission of the author, and with the usual scholarly acknowledgements.

Extensive copying or publication of the thesis in whole or in part requires also the consent of the Dean of the Graduate School of the University of Kentucky.

A library which borrows this thesis for use by its patrons is expected to secure the signature of each user.

Name and Address	Date

MASTER'S THESIS RELEASE

______ I authorize the University of Kentucky Libraries
to reproduce this thesis in whole or in part for
______ purposes of research.

______ I do not authorize the University of Kentucky Libraries
to reproduce this thesis in whole or in part for
______ purposes of research.

Signed: ______________________________

Date: ______________________

THESIS

John P. Chastain

The Graduate School

University of Kentucky

1987

ACKNOWLEDGEMENTS

The author wishes to express sincere appreciation to the following individuals for their valuable contributions to this work.

To Dr. Donald Colliver for serving as the director of the thesis, for his advice and encouragement, and for his efforts on the design and installation of the refrigeration system.

To Dr. I. J. Ross for arranging the financial support for this research, for offering timely encouragement, and for soldering the pipe for the refrigeration system.

To Dr. Gerald White for his patience with all of the ''one-minute'' questions which lasted hours and for serving on the examining committee.

To Dr. John Walker and Dr. James Funk for their valuable criticisms and advice while serving on the examining committee.

To Dr. Paul Cornelius for his advice concerning the statistical analysis.

To Joe Yeoman for his willingness and patience in wiring the controls for the refrigeration system and for setting up the data logger.

To James Penman for wiring the two cell environmental chamber and for sharing his carpentry experience.

To Dean Roberts for loaning to me a countless number of tools and for sharing his expertise in carpentry and refrigeration systems.

To Steve Shipman for allowing me to use many tools and instruments, and for aiding in setting up the pressure transducer.

To Thomas Gettings, Robert Curtis, and Anthony Osborne for their excellent performance as student workers.

To Lee Rechtin for teaching me how to use the milling machine and answering my many questions.

To Carl King for his willigness to help and for sharing some of his expertise.

To Ruth Durham for her excellent work on typing and for her words of encouragement during times of critical hyperactivity.

To Buren Plaster for his patience and excellent work on the drawings.

To Wid Winner for the many valuable hours spent on discussion and for permitting the use of his test box.

To Nat Peters, Mike Bader, Mark Casada and others for giving valuable insights and criticisms concerning ''how to do a thesis''.

To my wife, Kimberly, for her love, support and encouragement which were responsible for maintaining my sanity throughout the course of this thesis.

To my parents who always encouraged me to strive for excellence in any endeavor.

TABLE OF CONTENTS

Page

Page

LIST OF TABLES

LIST OF FIGURES

Figure		Page

work remains to be done to develop a complete understanding of the infiltration process.

Infiltration is a major source of heat loss during the heating season. It has been estimated that 33 to 50 percent of the total heat loss of a residence is due to infiltration (Sherman, 1980). A preliminary study at the University of Kentucky concluded that infiltration accounted for about one third of the heat loss for several all electric homes which were classified as well insulated (R-11 walls and R-30 or greater ceilings) and weatherstripped (Colliver et al. 1982). It was also determined that the added heat loss due to a 16 km/hr (10 mph) wind at an external temperature of 0° C (32° F) was equivalent to an additional temperature difference of 9.3° C (17° F).

The mass transport process associated with infiltration is not only an important energy loss factor, but it is also a major factor in the maintenance of indoor air quality in residential structures. When the doors and windows are closed infiltrating air is the only source of fresh air for a dwelling. Fresh air is needed to replenish the oxygen supply and infiltrating air removes indoor air contaminants. Most of the indoor air contaminants in residences may be classified as products of combustion, chemical vapors from cleaning products and building materials, organic particulates, excess moisture, and radon (Diamond and Grimsrud, 1984; McNall, 1986). In very tight houses, without mechanical ventilation, the concentrations of several of these contaminants have been observed to reach levels which exceed the Environmental Protection Agency standards for outside air (Diamond and Grimsrud, 1984; McNall, 1986). It has been

the infiltration process. One of the major goals of infiltration research is to adequately describe the infiltration process so that responsible energy conservation techniques may be developed which do not endanger the quality of the indoor environment.

The pressure differences which drive infiltration arise from two components: the effects of thermal buoyancy and the momentum from wind velocities. A temperature difference between the interior and exterior of the structure results in a difference in air density. In turn, the density difference induces a pressure difference. On a typical day during the heating season, the internal air of a structure will be less dense than the external air. Therefore, the warm air will rise and exit the structure through the leaks in the upper portion of the envelope. The more dense outside air will flow into the building through the leakage of the lower portion of the envelope. The two opposite directions of flow suggests that there must be a reverse in sign of the pressure difference across the envelope. In addition, there exists a level in the vertical plane where the pressure difference is equivalent to zero (Emswiler, 1926; and ASHRAE, 1985, Ch. 22). This reference plane is termed the neutral pressure axis (NPA) (refer to Figure 1.1). The flow of air induced by the pressure gradients due to thermal buoyancy are similar to the draft associated with a chimney. Hence, the infiltration resulting from thermal gradients is called the stack effect (ASHRAE, 1985). During the cooling season the internal air is cooler than the external air and the flow directions are reversed. The pressure gradients due to the stack effect are also typically smaller in magnitude.

When wind strikes the exterior of a structure the momentum of the air molecules is dissipated and the kinetic energy is converted into a pressure. The induced pressure may be estimated by the velocity head term of Bernoulli's equation. Wind velocities are not uniform across the surface of the structure and the magnitudes of the velocities that strike a residence depend on several site dependent parameters which are difficult to describe. Local shielding from nearby buildings and trees will tend to reduce the wind velocity or obstruct it entirely. The orientation of the building with respect to the prevailing winds will also influence the magnitudes of the wind pressures. Because of the extreme variability of actual wind velocities an average design wind velocity is often used.

The pressure differences due to the wind and stack effect are independent. Therefore, the total differential pressure profile may be obtained by addition of the two components (ASHRAE, 1985; Sherman, 1980). The volumetric flow rates of each component do not add because the flow rate is a nonlinear function of the pressure differences. Also, the elevation of the neutral pressure axis will be shifted by the effects of the wind pressures. Figure 1.2 represents an idealized differential pressure distribution across the walls of a residence due to the combined influence of the stack effect and wind. The pressure distribution resulting from the wind has been assumed to be uniform on each wall with the pressure on the windward side being positive and the leeward side being negative.

The total infiltration rate is defined as the total mass of outside air which enters a structure driven by the pressure differences resulting from the stack effect and the wind velocities.

position of the neutral pressure axis for a residential structure under pure stack conditions has not been developed.

The primary objectives of this investigation are as follows:

1. To describe the differential pressure distribution across the envelope of a residence due to the stack effect;
2. To identify and describe the factors which influence the elevation of the neutral pressure axis;
3. To develop a procedure to compute the location of the neutral pressure axis (NPA) under pure stack conditions for distributions of openings considered characteristic of the envelope leakage common to residences; and
4. To develop a method to model the leakage of a building component (such as a door or window) as a single near infinite straight rectangular slot.

Equation 2.2 was integrated under the following assumptions.

1. The temperature of the air column is uniform throughout. Therefore, the air density is constant.
2. The variation of the acceleration due to gravity is negligible.
3. The distance from the reference plane, H, is considered positive when measured downward from the reference plane, y_{ref}.

Equation 2.2, which many refer to as the static fluid equation, only describes the variation of pressure in a single column of air of constant density. The equation which represents the variation of the pressure difference induced by the effect of thermal buoyancy (i.e. stack effect) may be developed by the direct application of the static fluid equation to the two volumes of air inside and outside of a structure.

The temperature within the structure, T_i, is assumed to be greater than the outside temperature, T_o and both temperatures are assumed to be constant with respect to elevation. Application of the static fluid equation to the volumes of air inside and outside of the building yields the following pair of equations.

$$P_i = P_{ref} + \rho_i \; g \; H \qquad (2.3)$$

$$P_o = P_{ref} + \rho_o \; g \; H \qquad (2.4)$$

where; i = inside,

o = outside,

P_{ref} = the barometric pressure at the reference plane.

Reference to Figure 2.1 indicates that the pressure in each

volume of air will vary with the distance from the reference plane independently. The pressure difference due to the stack effect at a particular distance from the reference plane is the difference between the two pressures P_o and P_i. At the reference plane the pressure difference is equal to zero. The neutral pressure axis (NPA) is defined as the elevation where the pressure difference across the envelope of a structure is zero. Therefore, the reference plane (shown in Figure 2.1) is the neutral pressure axis.

Since the external pressure (P_o) is greater in magnitude than the internal pressure (P_i) the expression for the variation of pressure difference with respect to elevation is obtained by simply subtracting equation 2.4 from equation 2.3.

$$\Delta P = g \ \Delta\rho \ H \tag{2.5}$$

where; ΔP = the pressure difference due to the stack effect, and
$\Delta\rho = (\rho_o - \rho_i)$.

In the above equation it can be seen that at the reference plane the pressure difference induced by the stack effect is the net pressure difference owing to the density difference. The slope of the linear differential pressure distribution is a function of the average densities of the two volumes of air and it is independent of the location of the neutral pressure axis (Emswiler, 1926; Lee et al., 1985; Tamura and Wilson, 1966). Furthermore, pressure differences above the NPA are negative as a result of the sign convention.

If the floor of the structure is considered to be at an elevation of zero (refer to Figure 2.2) then the vertical distance from the NPA to any point on the envelope may be redefined as:

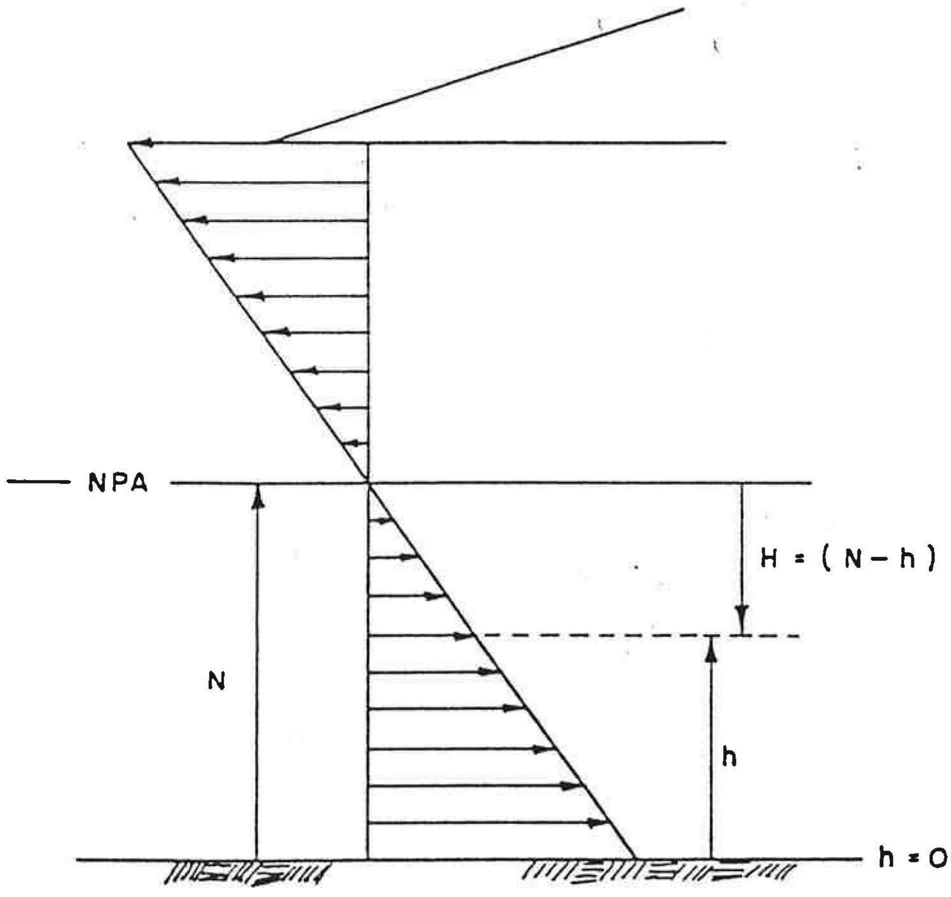

Figure 2.2 The distance from the NPA defined in terms of the elevation of the NPA and the elevation of the point in question.

T_i = internal temperature (K).

As a result, the variation of the pressure difference due to the stack effect may be written as:

$$\Delta P = g\ \rho_o \left(\frac{\Delta T}{T_i}\right) (N - h) \tag{2.11}$$

Factors Which Influence the Position of the Neutral Pressure Axis

The neutral pressure axis is a structure dependent parameter which has been observed to vary greatly between buildings (ASHRAE, 1985; Emswiler, 1926; Shaw, 1980; Shaw and Brown, 1982). The phenomenon of a variable plane of zero pressure difference is not confined to infiltration, but it is also a controlling factor in any natural ventilation system. Much of the present knowledge concerning the factors which affect the location of the NPA are the result of Emswilers' (1926) original study of natural ventilation in foundries. The following conclusions pertaining to the structural dependency of the location of the neutral pressure axis under pure stack conditions have been presented from Emswilers' analysis :

1. If the openings are uniformly distributed throughout a building and there is no significant stratification of internal temperature then the vertical location of the NPA will be at the mid-height of the structure.
2. If a significant degree of internal temperature stratification exists then the NPA would be expected to be slightly displaced toward the region of the greatest internal temperature.
3. If the majority of the openings are concentrated in a

particular region of a structure then the NPA will be located close to the elevation of that region.

4. The neutral pressure axis will always be located at a position such that the flow of air into a building will equal the flow of air out.

A more recent study of the neutral pressure axis in model tall buildings further verified most of Emswiler's observations except for the effects of temperature stratification (Lee et al. 1985). Lee's experimental apparatus was constructed and controlled so as to eliminate temperature stratification. Lee et al. (1985) verified experimentally that the horizontal distribution of the openings within a structure and the mean temperature difference were not significant factors in the location of the neutral pressure axis.

The presence of chimneys in residential structures also influences the position of the neutral pressure axis (ASHRAE, 1985). Shaw and Brown (1982) observed that during the heating season the presence of a gas furnace chimney tended to raise the level of the NPA significantly (also see ASHRAE, 1985, Ch 22. Figure 6). The pressures which drive the air flow through the chimney of any type of combustion appliance are not a result of the stack effect only. The pressure difference across a chimney will fluctuate with the operation cycle of the appliance. The description of the pressure differentials across a chimney is a complicated interaction of several variables which merits a separate investigation. It is believed that the additional pressures due to the draft of a chimney will cause the NPA to fluctuate in the vertical direction as the temperature of the chimney oscillates with the combustion of the appliance. The present study shall focus upon the determination of the position of the neutral pressure axis as influenced by openings in the envelope of a residence. The only source of flow potential will be the stack effect. Once a practical procedure for locating the NPA for the envelope leakage of a residence has been developed, the effect of wind pressures and the pressures from the draft of a chimney would be incorporated.

In general, a review of the literature suggests that the position of the neutral pressure axis for envelope leakage under pure stack conditions depends upon the relative size of the individual openings, their resistance to flow, their vertical distribution and to a lesser extent the degree of interior temperature stratification (Emswiler, 1926; and Lee et al. 1985).

<u>Review of Previous Methods to Determine The Location of the Neutral Pressure Axis</u>

The first procedure to determine the position of the neutral pressure axis for a particular building was developed by Emswiler (1926). The procedure was based upon the assumption that the pressure difference at each opening will have a value such that the total volumetric air flow into the building will be identical to the total air flow out of the building. As a result, Emswiler's method to determine the position of the NPA consisted of a direct application of the continuity equation over the entire envelope of the building. The air flow into the building was assumed to be positive, and the continuity equation was written as;

$$\sum_{j=1}^{n} Q_j = 0 \qquad (2.12)$$

where; Q_j = the volumetric flow rate through the j^{th} opening,

n = the total number of openings in the natural ventilation system.

Since Emswiler was concerned with the natural ventilation of foundries, all of the openings in the shell of the building were similar to a large window and they were treated as large orifices. The volumetric flow rate was computed using the orifice equation with a discharge coefficient of 0.65. The elevation of the neutral pressure axis was determined by iteration. For each elevation of the NPA chosen, the pressure difference due to the stack effect and the corresponding flow rates were computed. The correct position of the neutral pressure axis resulted when the continuity equation (equation 2.12) had been satisfied. This iterative procedure was referred to as the flow balancing procedure.

The flow balancing procedure was tested on an actual foundry. All of the openings used were on the leeward side of the building. The average internal temperature of the foundry was 59°F and the outside temperature was 20°F. The location of the NPA was determined for a distribution of four openings using the flow balancing procedure and the air flow through the lowest opening was measured using an anemometer. The flow measured was 12,500 cfm whereas the flow computed by the orifice equation was 10,260 cfm. The agreement was within 18 percent. It was stated that for a second trial the calculated and the measured flow rates differed by only 7 percent.

Emswiler's procedure to determine the position of the neutral pressure axis for a building under pure stack conditions has been widely accepted for use in natural ventilation systems but it has a fundamental error. In a closed system the mass of the air will be conserved and not the volume. Therefore, to be theoretically correct the continuity equation should be written in terms of the mass flow rate. This is particularly true when the air flowing into a building is much colder than the air flowing out.

The ASHRAE Handbook of Fundamentals (ASHRAE, 1985, Ch. 22) gives the following equation to compute the location of the neutral pressure axis for the case of natural ventilation due to two openings.

$$h = \frac{H}{1 + \left[\left(\frac{A_1}{A_2}\right)^2 * \left(\frac{T_i}{T_o}\right)\right]} \qquad (2.13)$$

where; H = the vertical distance between the two openings,

A_1 and A_2 = the opening areas,

h = elevation of the NPA measured from the lowest opening,

T_i = internal temperature, and

T_o = outside temperature.

Equation 2.13 cannot be applied to most cases of either natural ventilation or infiltration because of its limitation to only two openings and the assumption that the discharge coefficients of the two openings are equal. Lee et al. (1985) showed experimentally that even for the case of two openings equation 2.13 could only predict the elevation of the NPA within 25 percent.

Lee et al. (1985) developed a procedure to compute the position of the neutral pressure axis for a model tall building using the following assumptions:

1. There are no internal partitions between floors;

2. The inside and outside temperatures do not vary with elevation;
3. The inside temperature is greater than the outside temperature;
4. The only pressure gradients are due to the stack effect (i.e. no wind);
5. The openings are of circular cross-section; and
6. The flow through the openings is steady, smooth, laminar and in hydrodynamic transition.

From the law of conservation of energy the pressure drop across an opening was formulated as shown:

$$\Delta P_k = \frac{1}{2}\left[\rho\,\bar{V}^2\,(1 + K_{f1}) + B\,\bar{V}\left(\frac{\mu L}{D^2}\right)\right]_k \tag{2.14}$$

where; ΔP_k = the total pressure drop across the k^{th} opening,

$\bar{V}$ = the average velocity,

B = 64, the laminar friction coefficient for a circular cross-section,

L = the flow length,

D = the diameter,

K_{f1} = the sum of the minor losses due to the entrance effects and any contractions or expansions,

μ = the dynamic viscosity, and

ρ = the density.

The pressure difference due to the stack effect was expressed in the following form.

$$\Delta P_{stack} = K_1\left(\frac{1}{T_{out}} - \frac{1}{T_{in}}\right)(NPA - Z) \tag{2.15}$$

where; K_1 = a constant = $\dfrac{g\ P_o}{R}$

P_o = the standard atmospheric pressure,

NPA = the elevation of the neutral pressure axis, and

Z = the elevation of the opening from the ground.

For each opening the pressure difference due to the stack effect was equated to the total pressure drop across the opening (equation 2.14). The general equation to compute the elevation of the NPA for a building with n openings in the envelope was presented by Lee as follows:

$$NPA = \frac{H_j + (X_j/X_i)\ H_i}{1 + (X_j/X_i)} \tag{2.16}$$

where; $X_{i\ or\ j} = \left[\left(\dfrac{P_o}{RT}\right) \bar{V}^2 (1 + \sum K_{f1}) + \left(\dfrac{B\ \mu\ L}{D^2}\right) \bar{V} \right]_{i\ or\ j}$

i - denotes openings below the NPA,

j - denotes openings above the NPA.

$H_{i\ or\ j}$ = the distance of a particular opening from the bottom opening.

The solution to equation 2.16 for n openings involves a set of n non-linear equations to be solved iteratively in terms of velocity. The only explanation which the author gave for the solution of the equation is that ''a standard computational method available for computers'' was employed (Lee et al. 1985, p. 4).

Lee's et al. (1985) experimental investigation was carried out using a model building that stood 18.2 m (59.71 ft) high. There were no internal partitions of any kind within the model and six identical cylindrical openings were installed at four different elevations.

Two openings were placed at the top and the bottom of the model building. The remaining two openings were equally spaced above and below the mid-height of the building. All of the openings were in the side walls and each opening could be opened or closed independently.

Twenty individually controlled electrical heating elements were used throughout the height of the model building. A uniform temperature inside the model building was achieved by adjusting the power supply to each of the electrical heaters. The supply voltage, the current to each heater and the temperature profile were monitored continuously. The maximum allowable temperature deviation between points was 3°C (5.4°F). By heating the interior of the model building, temperature gradients from 25°C (45°F) to 60°C (108°F) were obtained.

Differential pressure measurements were obtained from seven pairs of pressure taps placed at intervals of 3.0 m (9.84 ft). Each pair of pressure taps was connected to a single pressure transducer with an error of $\pm$ 0.2 Pa.

The position of the NPA was observed for twelve different opening distributions and five different temperature differentials (25°, 30°, 40°, 50° and 60°C). No variation in the position of the NPA was observed over the entire range of mean temperature differentials. It was stated that the position of the NPA was predicted by equation 2.16 within 6 percent in all cases.

Overlooking the extreme complexities of applying Lee's method to a practical situation, three of the initial assumptions are unreasonable. First if the intended application is for high-rise buildings, then several of the references indicate that the pressure of internal separations can greatly influence the location of the NPA in tall buildings (Shaw and Tamura, 1977; Tamura and Shaw, 1976; Tamura and Wilson, 1966; and Tamura and Wilson, 1967). The assumption that internal separations are absent is not a reasonable assumption for a tall building. Secondly, the effects of temperature stratification needs to be addressed experimentally. Even in a residence an appreciable degree of stratification of internal temperature can occur. Finally, a visual inspection of the envelope leakage of a building suggests that most of the openings typical of infiltration are of a rectangular cross-section and not circular.

Up to this point only methods to actually compute the elevation of the NPA have been presented. Several empirically based mathematical models of infiltration are available that include the elevation of the NPA as one of the parameters. Usually the NPA is assumed to be located at the midheight of the structure or an elevation is assumed based upon a visual inspection of the distribution of known sources of leakage such as doors, windows, and penetrations for ductwork or plumbing (Liddament and Allen, 1983). A better estimate of the elevation of the NPA should be able to improve the estimates obtained from the empirical models.

Chapter 3

THEORETICAL DEVELOPMENT

Introduction

The review of the literature revealed that the computation of the pressure differences which are induced by the stack effect depend upon the knowledge of the position of the neutral pressure axis (NPA). Furthermore, the position of the NPA is a structure dependent parameter which varies with respect to the relative size of the openings in the envelope, their resistance to flow, and their vertical distribution (Emswiler, 1926; Lee et al. 1985). Assuming that the outside temperature is invariant, stratification of temperature within a structure is believed to cause a slight displacement of the NPA towards the region of the greatest internal temperature (Emswiler, 1926). Temperature stratification is thought to be a minor factor that can be neglected, but its importance has not been ascertained experimentally.

The factor that influences the location of the NPA which is subject to the greatest ambiguity is the description of the flow resistance of small openings characteristic of the envelope leakage of residences. Due to the small size and the great number of openings in a structure, the leakage of a single component, or even the entire building envelope is often modeled as a single equivalent orifice (ASHRAE, 1985; Keil et al. 1985). The flow resistance of an orifice may be defined as the product of the cross-sectional area and a discharge coefficient. The area and the discharge coefficient of the equivalent orifice are lumped into a single parameter known as the effective leakage area, $A_e(m^2)$. The flow through the effective leakage area is defined by the following simplification of the orifice equation:

$$Q = A_e \sqrt{\frac{2\Delta P}{\rho}} \qquad (3.1)$$

where; Q = the volumetric flow rate (m^3/s),

ΔP = the pressure difference (Pa), and

ρ = the air density (kg/m^3).

To determine the effective leakage area of a building component (or an entire structure) the current practice involves the measurement of the volumetric flow rate through the component at several pressure differences in the range of 12.5 to 75 Pascals (ASTM, 1985). The data is then fitted to a power law of the following form:

$$Q = C\ (\Delta P)^n \qquad (3.2)$$

where; C = the flow coefficient ($m^3/s * Pa^n$), and

n = the flow exponent.

The value of the flow exponent, n, is typically between 0.5 and 1.0. An exponent of 0.5 is believed to correspond to orifice flow and an exponent of 1.0 is thought to represent fully developed laminar flow (Keil et al. 1985).

The effective leakage area is calculated from the data by equating equation 3.1 to equation 3.2 and solving for the effective leakage area at a given reference pressure drop (Keil et al. 1985).

$$A_{e,ref} = C \left(\frac{\rho}{2}\right)^{0.5} \Delta P_{ref}^{(n-0.5)} \quad . \qquad (3.3)$$

The description of the leakage area and the flow resistance of a building component as an equivalent leakage area is inadequate for the following reasons:

1. The effective leakage area, A_e, will vary with the reference pressure drop used. Therefore, it lacks physical significance.
2. The flow exponent, n, and the flow coefficient, C, are merely products of regression and do not adequately describe the physics of the flow.
3. The dimensions are not homogeneous.
4. The pressure differences which are typical of the stack effect in residences are less than ten Pascals. Computation of an effective leakage area at pressure differences below the range of data is a statistically invalid procedure.
5. The use of an effective leakage area to model a building component is analogous to modeling the component as an equivalent orifice with a constant discharge coefficient over the entire range of data. As a result, the variation of the element of resistance due to the presence of a flow length is neglected.

A general survey of the leakage about doors and windows suggests that most of the openings common to infiltration approximate rectangular slots. It is believed that the flow length of the openings common to envelope leakage contributes significantly to the flow resistance (Beavers et al. 1970; Etheridge, 1977; Han, 1960; and

Hopkins and Hansford, 1974). As a result, the openings which are characteristic of infiltration should be modeled as rectangular slots and not orifices. Furthermore, previous work concerning flow through small rectangular slots with cross-sectional dimensions similar to envelope leakage concluded that the openings common to infiltration had hydraulic diameters (D_h) small enough to treat the flow as laminar (Etheridge, 1977; Hopkins and Hansford, 1974).

Beginning with the solution to the Navier-Stokes equation for the idealized case of flow between infinite parallel plates, a semi-empirical equation to directly compute the discharge coefficient for laminar flow through an arbitrary rectangular channel will be developed. The discharge coefficient may be viewed as a dimensionless flow resistance parameter which varies with the geometry of the channel as well as the pressure drop. The geometric component of the discharge coefficient may be described by the cross-sectional area and a geometric parameter, gamma, which takes into account the flow length and the dimensionless properties of the cross-section. By means of the general energy equation, the analysis will be extended to include openings of a circular cross-section.

Once the discharge coefficient relationship has been developed it shall be incorporated into a procedure to compute the position of the neutral pressure axis for any distribution of openings.

Derivation of the Discharge Coefficient Equation

The solution to the Navier-Stokes equation for the idealized case of flow between infinite parallel flat plates is provided in Appendix B. The solution is stated in terms of the volumetric flow per unit width as:

$$\frac{Q}{w} = \frac{d^3\ \Delta P}{12\ \mu\ z} \tag{3.4}$$

where; Q = the volumetric flow rate (m^3/s),

d = the channel thickness (m),

z = the flow length (m),

w = the width (m),

μ = the dynamic viscosity ($N*s/m^2$), and

ΔP = the pressure difference (Pa).

The following assumptions were applied to obtain equation 3.4:

1. The fluid is viscid and incompressible;
2. The flow is steady, fully developed and laminar;
3. The velocity varies one dimensionally across the thickness (d);
4. The pressure varies linearly in the direction of flow;
5. The gravity effects are negligible;
6. There are no entrance or exit losses;
7. The no-slip boundary condition exists; and
8. A positive pressure difference yields a positive flow.

By dimensional analysis, equation 3.4 may be expressed in terms of the total dimensionless pressure drop.

$$\frac{2\Delta P}{\rho \bar{V}^2} = \frac{96}{Re}\left(\frac{z}{D_h}\right) \tag{3.5}$$

For laminar flow the friction factor is defined by:

$$f = \frac{B}{Re} \tag{3.6}$$

Therefore, equation 3.5 indicates the value of the friction coefficient, B, is 96 for infinite parallel flat plates. The

Reynolds number is given by:

$$Re = \frac{\bar{V}\, D_h}{\nu} \tag{3.7}$$

Where, ν, is the kinematic viscosity and the hydraulic diameter (D_h) is defined as:

$$D_h = \frac{4A}{\text{wetted perimeter}} \tag{3.8}$$

For rectangular cross-sections the hydraulic diameter may be written in terms of the thickness, d, and the aspect ratio, α, (Fox and McDonald, 1978).

$$D_h = \frac{2d}{(1 + \alpha)} \tag{3.9}$$

Where the aspect ratio is given by:

$$\alpha = \frac{d}{w} \tag{3.10}$$

For the case of infinite parallel flat plates, the aspect ratio is equal to zero and the hydraulic diameter becomes:

$$D_h = 2d \tag{3.11}$$

The mean velocity, $\bar{V}$, is defined by:

$$\bar{V} = \frac{Q}{A} \tag{3.12}$$

Substitution of the definition of the mean velocity into the definition of the Reynolds number in equation 3.5, and solving for the flow rate gives:

$$Q = C_d\, A \sqrt{\frac{2\Delta P}{\rho}} \tag{3.13}$$

Where the discharge coefficient for idealized flow is defined by the expression:

$$C_d = \sqrt{\frac{D_h \ Re}{z \ B}} \tag{3.14}$$

The general form of equation 3.13 has been used extensively to compute the flow through rectangular as well as circular channels, but equation 3.14 is not adequate to compute the discharge coefficient for an actual situation. The inadequacy arises from the neglect of the losses at the entrance and exit of the flow channel. In order to apply the flow equation to an actual flow situation, the entrance and exit effects must be included in the discharge coefficient.

Another discharge coefficient which includes the entrance and exit losses is described by the following functional statement:

$$C_z = f\left(\frac{z}{D_h}, \frac{B}{Re}, K\right) \tag{3.15}$$

The term, z/D_h, defines a dimensionless flow length and K is the total minor loss coefficient which represents the sum of the dimensionless pressure losses due to the entrance and exit effects. In addition to eliminating assumption 6, which was required to solve the Navier-Stokes equation, it will be shown later that the effects of undeveloped flow are also included in K (assumption 2).

Based upon the law of conservation of energy, the general energy equation for laminar flow through an arbitrary channel is given by:

$$\Delta P = \frac{1}{2} \rho \bar{V}^2 B \left(\frac{z}{D_h Re}\right) + \frac{1}{2} \rho \bar{V}^2 K \tag{3.16}$$

Assuming that the mean velocity is not zero and dividing equation 3.16 by the velocity head gives the equation for the total dimensionless pressure drop across an arbitrary channel.

$$\frac{2\,\Delta\,P}{\rho\,\bar{V}^2} = B\left(\frac{z}{D_h Re}\right) + K \qquad (3.17)$$

Thus, the total dimensionless pressure drop is the sum of the friction loss, $B(z/D_h Re)$, and the total minor loss coefficient, K.

Etheridge (1977), defined a discharge coefficient for straight rectangular openings with a finite flow length as:

$$C_z = \frac{Q}{A}\sqrt{\frac{\rho}{2\,\Delta\,P}} \qquad (3.18)$$

Substitution of the average velocity into the above equation and solving for the total dimensionless pressure drop yields:

$$\frac{2\,\Delta\,P}{\rho\,\bar{V}^2} = \frac{1}{C_z^{\,2}} \qquad (3.19)$$

Combining equations 3.17 and 3.19 gives the following linear relationship between the squared inverse of the discharge coefficient and the term, $(z/D_h Re)$ (Etheridge, 1977).

$$\frac{1}{C_z^{\,2}} = B\left(\frac{z}{D_h Re}\right) + K \qquad (3.20)$$

The discharge coefficient, C_z, as defined by equation 3.18, was determined experimentally by Hopkins and Hansford (1974), for several straight slots. The slot thickness ranged from about 1 mm (0.039 in) to 10 mm (0.394 in) and the flow length, z, ranged from approximately 6mm (0.25 in) to 50 mm (2 in). The aspect ratio was assumed to be zero for all cases. Etheridge (1977) pooled all of the data into one linear regression. The results gave a mean friction coefficient (B) of 95.7 and a mean total minor loss coefficient (K) of 1.5. The technique presented by Etheridge (1977) to calculate the flow rate for a rectangular slot involved an iteration on the Reynolds number using equation 3.20 in conjunction with the following flow equation:

$$Q = C_z A \sqrt{\frac{2 \Delta P}{\rho}} \tag{3.21}$$

Etheridge's analysis was confined to rectangular openings with near infinite cross-sections, sharp-edged inlets, and finite flow lengths. The following development is devoted to the derivation of an equation to compute the discharge coefficient directly and to expand the analysis to include rectangular cross-sections of any aspect ratio as well as openings with circular cross-sections. The analysis may be extended to include rectangular slots of any aspect ratio by using the expression for the hydraulic diameter presented in equation 3.9. A diagram of a typical rectangular channel is shown in Figure 3.1.

Substitution of the definition of the mean velocity into equation 3.17 and equating the expression to zero gives:

$$\frac{2 \Delta P A^2}{\rho Q^2} - \frac{\nu B z A}{Q D_h^2} - K = 0 \tag{3.22}$$

Multiplication of equation 3.22 by the square of the flow rate, employing the expression for D_h given in equation 3.9, and simplifying gives the following quadratic flow equation:

$$\frac{8 \Delta P A^2}{\rho} - \frac{Q\nu}{\gamma} - Q^2 4K = 0 \tag{3.23}$$

Where the geometric parameter, gamma, for a rectangular cross-section is defined as:

$$\gamma = \frac{\alpha}{Bz(1 + \alpha)^2} \tag{3.24}$$

The quadratic flow equation was solved by means of the quadratic

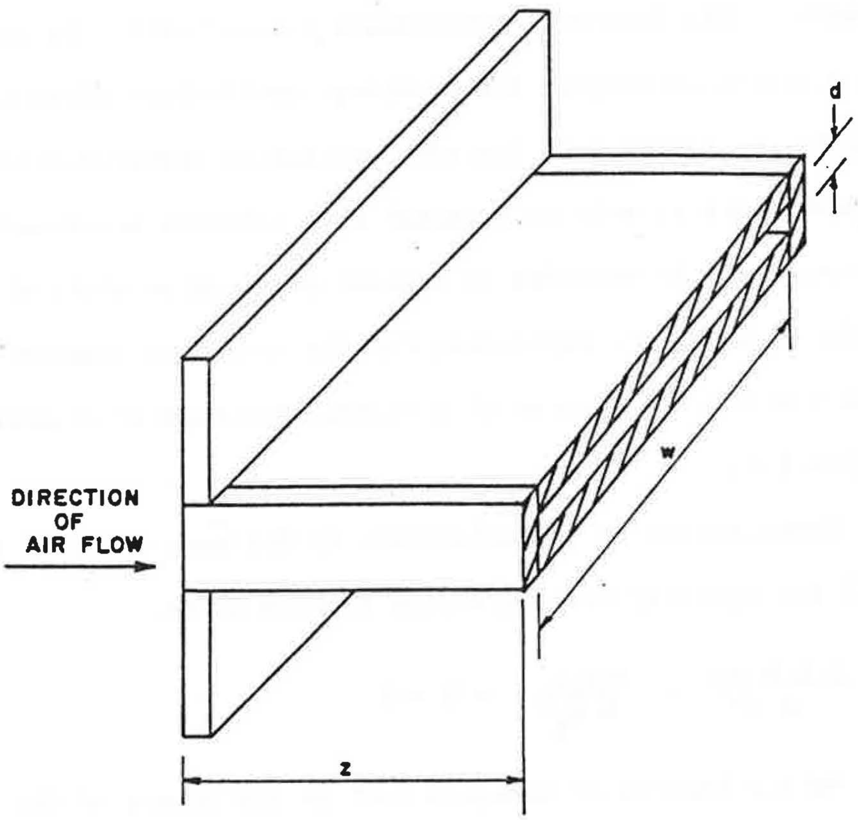

Figure 3.1   A typical straight rectangular opening.

formula. The positive root was determined to be the only root with physical significance.

$$Q = \left(\frac{-\nu}{8K\gamma}\right) + \left[\left(\frac{\nu}{8K\gamma}\right)^2 + \frac{2\ A^2\ \Delta\ P}{K\ \rho}\right]^{0.5} \qquad (3.25)$$

Substitution of equation 3.25 into the definition for the Reynolds number of equation 3.20 and simplifying gives the following equation for the squared inverse of the discharge coefficient:

$$\frac{1}{C_z^{\,2}} = \frac{2K}{\left[1 + (A\ \gamma)^2\ \dfrac{128\ K\ \Delta\ P}{\rho\ \nu^2}\right]^{0.5} - 1} + K \qquad (3.26)$$

The above equation was derived under the assumption that the aspect ratio is greater than zero. Inspection of the definition of gamma (equation 3.24) reveals that for an aspect ratio of zero, gamma is equal to zero. This would cause the discharge coefficient equation (equation 3.26) to become undefined.

This singularity was removed by rederiving the discharge coefficient equation using a hydraulic diameter of 2d (i.e. $\alpha = 0$) and a friction coefficient (B) of 96. The quadratic flow equation (Equation 3.23) was written in terms of the flow per unit width and solved to yield the following equation for the flow per unit width:

$$\frac{Q}{w} = -12\ \left(\frac{z\nu}{Kd}\right) + \left[144\ \left(\frac{z\nu}{Kd}\right)^2 + \frac{2d^2\ \Delta P}{\rho K}\right]^{0.5} \qquad (3.27)$$

The discharge coefficient equation was found to be of exactly the same form as given in Equation 3.26. The only difference was in the expression for the area-gamma product, $(A\gamma)$. If it is desired to compute the discharge coefficient using an aspect ratio of zero the following expression for $(A\gamma)$ is to be used with Equation 3.26:

$$(A\gamma) = \frac{d^2}{96z} \tag{3.28}$$

For very small aspect ratios the value of $(A\gamma)$ determined from the cross-sectional area and the definition of gamma given by Equation 3.24 will approach the value determined by using Equation 3.28. The point at which the aspect ratio is small enough to be considered to be zero is dependent upon the application. In actuality, no rectangular channel is truly infinite. In the application of these concepts to the modeling of building components it is more descriptive to include the aspect ratio.

It should be noted that since the discharge coefficient equation was developed from the dimensionless energy equation (equation 3.17) the assumption that the mean velocity is not zero also applies. Therefore the pressure difference cannot be zero. Furthermore, the square root requires the use of the absolute value of the pressure difference.

For a straight cylinder the total dimensionless pressure drop is of the same form as shown in equation 3.19 and the characteristic dimension is the diameter of the opening. Using the same analysis as for a rectangular channel, the quadratic flow equation for a cylinder is the same as shown in equation 3.23. The geometric parameter, gamma, for a cylinder is defined as:

$$\gamma = \frac{1}{B \pi z} \tag{3.29}$$

The discharge coefficient for a cylinder may be calculated by using equation 3.26 with the definition of gamma for a cylinder (equation 3.29). The value of the friction coefficient for a circular cross-section is 64 and it may be obtained in a manner analogous to that presented for infinite parallel flat plates (Currie, 1974; Fox and McDonald, 1978).

Physical Significance of the Area-Gamma Product

It has been shown that the flow through an arbitrary rectangular or circular channel is a function of the pressure difference, the cross-sectional area, gamma, the minor losses, and the air properties. The flow rate may be calculated directly either by equation 3.25 or by first determining the discharge coefficient by equation 3.26 and then computing the flow rate by equation 3.21. Either method yields the same result.

The discharge coefficient method is advantageous because it is able to provide additional insight concerning the factors which influence the flow rate. A closer look at equation 3.26 indicates that the discharge coefficient describes the total resistance of a flow channel. For a particular set of air properties and a known total minor loss coefficient, the discharge coefficient is a function of the area-gamma product and the total pressure drop. Therefore, the term $(A\gamma)$ describes the total geometric contribution to the resistance of the channel. The geometric parameter, gamma, includes the contribution of the flow length, the friction coefficient, and a dimensionless constant that represents the cross-sectional geometry. For a cylinder the constant is $1/\pi$ and for a rectangular cross-section the constant is given by $\alpha/(1 + \alpha)^2$. As a result, gamma may be viewed as a three dimensional scale factor of a channel.

An inspection of the work of Hopkins and Hansford (1974), and Etheridge (1977) suggest the effects of channel geometry on the friction coefficient and the total minor loss coefficient need closer examination.

Variation of the Friction Coefficient with the Cross-Sectional Geometry

A number of researchers (Beavers, et al. 1970; Fox and McDonald, 1978; Han, 1960; Kays and Crawford, 1980; Langhaar, 1942), agree that the friction coefficient is a parameter that is determined by the cross-sectional geometry of the channel. A friction coefficient of 64 is always used with a circular cross-section. For rectangular cross-sections, the friction coefficient is a function of the aspect ratio (Beavers et al. 1970; Han, 1960; Kays and Crawford, 1980). The curve presented in Figure 3.2 indicates that as the aspect ratio increases from zero the theoretical value of the friction coefficient decreases from 96 to a minimum of about 57 which corresponds to a square (α = 1.0), (Kays and Crawford, 1980; Han, 1960). The following regression equation to compute the friction coefficient was obtained from a least squares best fit of this curve for aspect ratios from zero to 0.075:

$$B = 96.0 - 106.67\alpha \tag{3.30}$$

Variation of the Total Minor Loss Coefficient

The total minor loss coefficient (K) for any type of straight channel is an empirically determined value which is the sum of the entrance and exit effects. The magnitude of the entrance effect can vary considerably depending upon the inlet geometry and the degree of hydrodynamic development. Also, two similar channels can have different values of K due to inaccuracies in fabrication. The variation of the components of the total minor loss coefficient will be

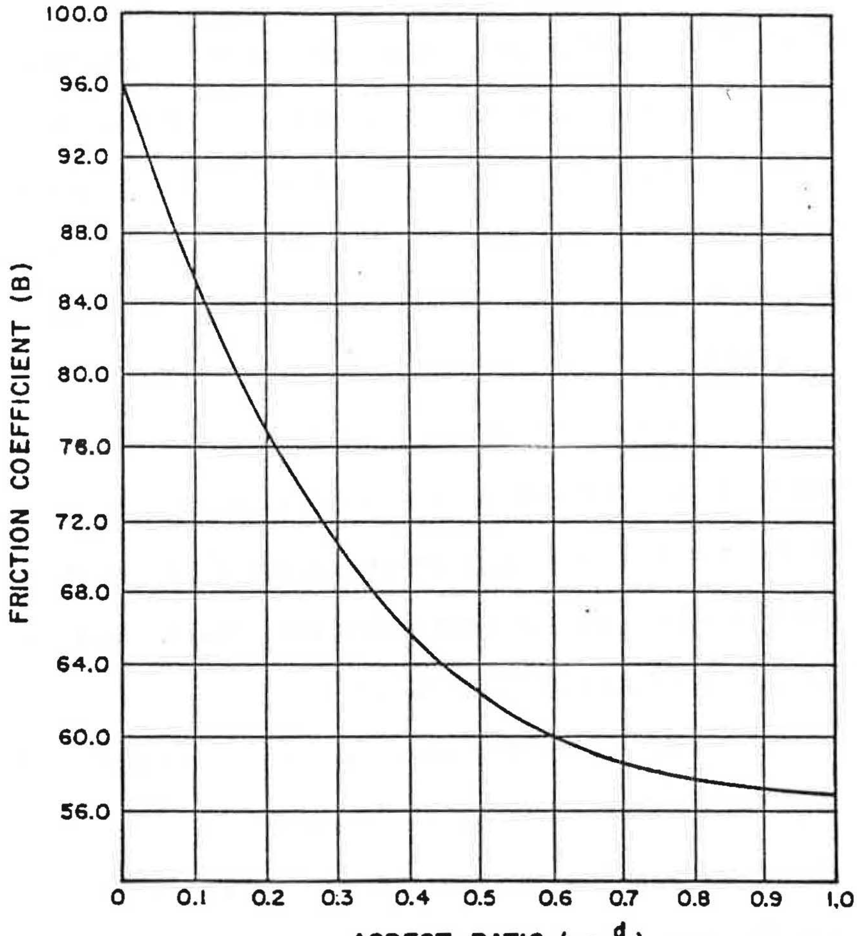

Figure 3.2 Friction coefficients for laminar flow through channels of rectangular cross-section (Kays and Crawford, 1980; Han, 1960).

presented in the following discussion.

According to many fluid mechanics texts the kinetic energy is considered to be completely dissipated when the fluid exits a pipe into an infinite expansion. As a result, the dimensionless pressure loss due to the exit (K_{ex}) is 1.0 for all cases (Fox and McDonald, 1978). The entrance effect is the sum of the losses induced by the inlet geometry (K_{inlet}) and the degree of hydrodynamic development (K_{hd}). The loss coefficient of the inlet can be expected to vary from about 0.04 for a well rounded inlet to 0.5 for a sharp edged inlet (Fox and McDonald, 1978). For practical purposes the dimensionless pressure loss of a well designed rounded inlet may be considered negligible (Beavers, et al. 1970; Fox and McDonald, 1978).

The loss coefficients for developing laminar flow (K_{hd}) through long straight ducts of rectangular cross-section were determined by Beavers et al. (1970) for aspect ratios from 0.0196 to 1.0. For this work the inlets of the ducts were well rounded and the inlet loss (K_{inlet}) was considered to be zero.

Beavers et al. (1970) observed that the value of K_{hd} was zero at the inlet and increased to a maximum value at a point down-stream and then remained constant. The distance from the inlet to the point where K_{hd} attained a maximum was defined as the entrance length of the duct (L_e). It was also determined that the flow may be treated as fully developed when K_{hd} attains 95 percent of the fully developed value (Beavers et al., 1970).

The fully developed values of K_{hd} varied linearly for aspect ratios (α) from 0.0196 to 0.50. The fully developed value of K_{hd} was 0.6 for an α of 0.0196 and 1.1 for an α of 0.50. For a square (α

= 1.0) the fully developed value of K_{hd} was 1.2.

The total minor loss coefficient (K) for fully developed laminar flow in a long circular pipe with a well rounded inlet was determined to be 2.2 by Langhaar (1942). In this case the total minor loss coefficient was equal to the sum of the losses due to hydrodynamic development and the exit (K_{ex} = 1). By subtracting the exit loss from the total minor loss coefficient it was observed that the fully developed value of K_{hd} for a long circular pipe was 1.2. The entrance length for a long circular pipe was defined in the same manner as discussed previously for a rectangular duct.

The variation of the total minor loss coefficient, $K = (K_{hd} + K_{ex})$, for developing laminar flow through long rectangular ducts and circular pipes has been compared in Figure 3.3. The exit loss was added to the data presented by Beavers et al. (1970) to facilitate comparison with the values for a long circular pipe (Langhaar, 1942). It should be noted that the best estimate of the total minor loss coefficient for developing laminar flow in long pipes with sharp edged inlets would be obtained by adding the inlet loss (K_{inlet} = 0.5) to the values presented in Figure 3.3.

Any type of straight channel may be classified as either (1) a long pipe, (2) a short pipe or (3) an orifice based upon a comparison of the magnitudes of the dimensionless friction loss and the total minor loss coefficient (refer to Figure 3.3 and Equation 3.17). A long pipe has a flow length (z) which is much longer than the required entrance length to insure fully developed laminar flow (L_e). In this case $B(z/D_hRe)$ is much larger than K. That is, the dimensionless friction loss is the greatest component of the

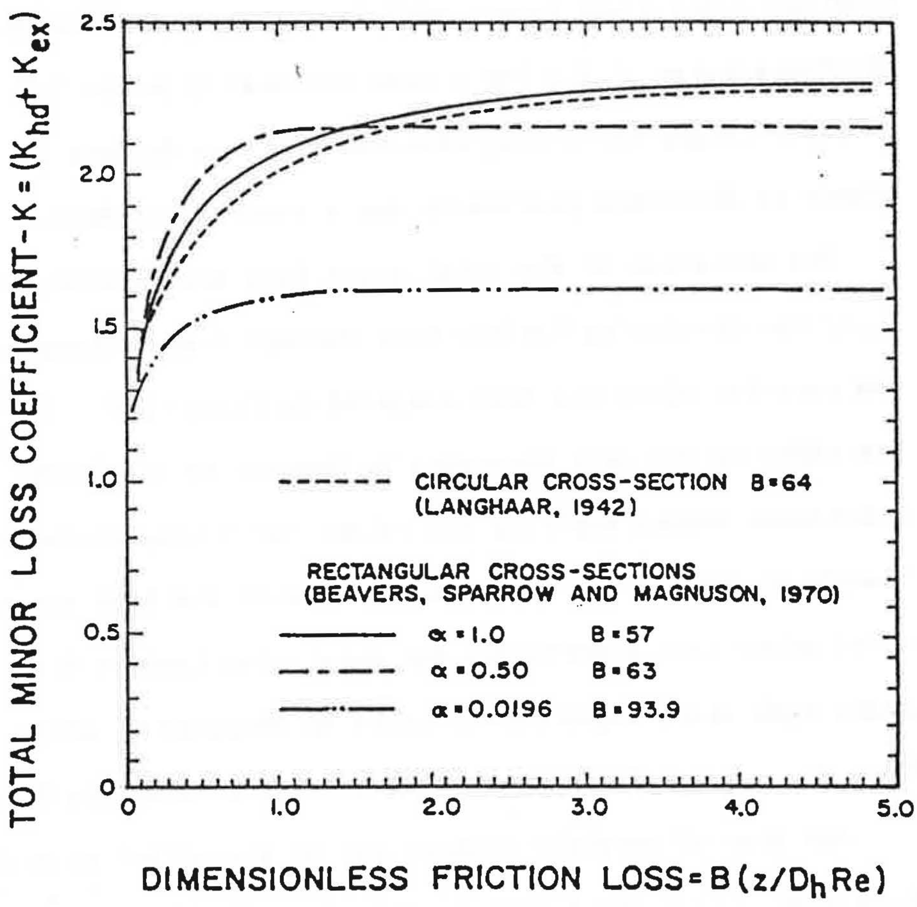

Figure 3.3 Comparison of the total minor loss coefficients for hydrodynamically developing laminar flow in long rectangular ducts and circular pipes with well rounded inlets.

total dimensionless pressure drop across a long pipe. A short pipe has a flow length that is less than or equal to the required entrance length. The flow is not fully developed or the profile may develop just before the fluid exits the pipe. If the flow length is less than the required entrance length, then the total minor loss coefficient is the greatest component of the total dimensionless pressure drop. If z is equal to L_e then the dimensionless friction loss will be approximately equal to K. The magnitude of the total minor loss coefficient will depend upon the degree of hydrodynamic development and will vary with the Reynolds number. An orifice does not have a flow length and the dimensionless friction loss is zero. The total minor loss coefficient for an orifice is simply the sum of K_{inlet} and K_{ex}. Also, K is equal to the total dimensionless pressure drop which varies with the mean velocity.

The Procedure to Determine the Position of the Neutral Pressure Axis

The simplest and most fundamental approach to compute the location of the neutral pressure axis is a direct application of the conservation of mass for a closed system. The system is defined as a residential structure and the surrounding atmosphere subject to the following constraints (refer to Figure 3.4):

1. There is no wind impending upon the structure (i.e. pure stack conditions exist);
2. The openings are characterized as straight openings with cross-sectional dimensions similar to those found in a dwelling;
3. The flow through the openings is characterized as steady, smooth and laminar;

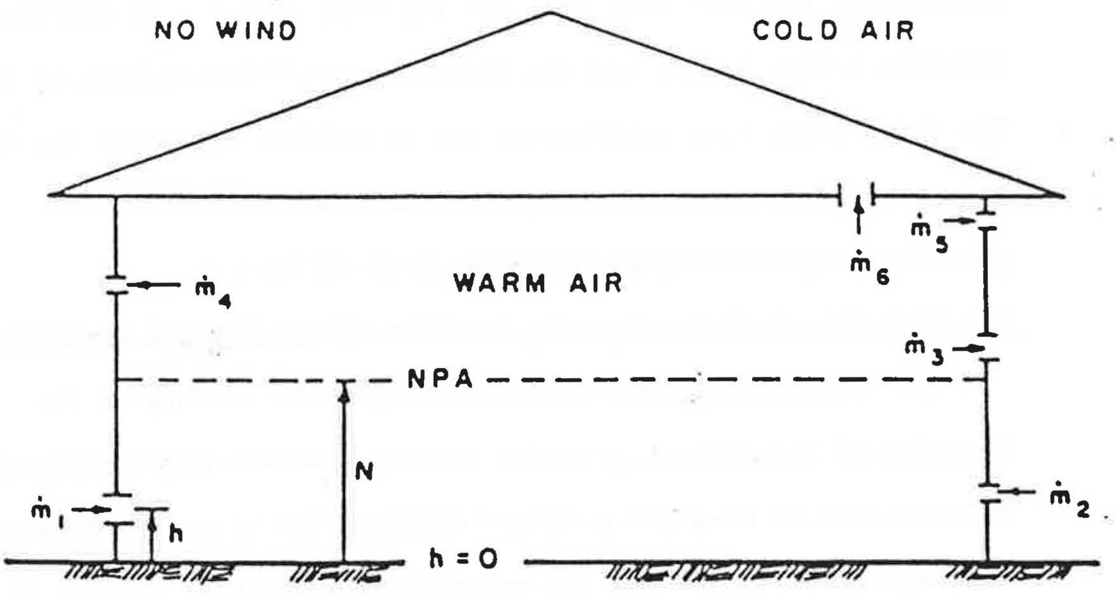

Figure 3.4 The stack effect for a residence.

4. The inside and outside temperatures (T_i and T_o) are constant with respect to elevation;

5. The discharge coefficient does not depend on the direction of flow through the openings;

6. The only openings which exist are in the walls, floor and ceiling of the structure (i.e. no chimneys); and

7. There are no internal partitions which significantly obstruct the flow of air.

The pressure difference induced by the stack effect may be determined by the following equation.

$$\Delta P_j = g \, \Delta\rho \, (N - h_j) \tag{3.31}$$

ΔP_j = the pressure difference (Pa),

N = elevation of the NPA above the floor of the structure (m),

h_j = the elevation of the j^{th} opening above the floor (m), and,

$\Delta\rho$ = the mean density difference (kg/m^3).

Under the assumption that mass flow into the structure is positive the continuity equation is stated as:

$$\sum_{j=1}^{n} = \dot{m}_j = 0 \tag{3.32}$$

where; $\dot{m}_j$ = the mass flow rate through the j^{th} opening (kg/s), and

n = the total number of openings.

Multiplication of the volumetric flow rate equation (equation 3.21) by the density of the air flowing through the opening gives the following equation for the mass flow rate through an opening:

$$\dot{m}_j = (C_z\ A)_j \sqrt{2\ \Delta P_j\ \rho_j} \tag{3.33}$$

where; C_z = the discharge coefficient of the j^{th} opening (computed by equation 3.26 using ρ_j and ν_j),

A = the cross-sectional area of the j^{th} opening (m^2),

ΔP_j = the absolute value of the pressure difference at the elevation of the j^{th} opening, (Pa), and

ρ_j = the density of the air flowing through the j^{th} opening (ρ_o or ρ_i), (kg/m^3).

The position of the neutral pressure axis for an arbitrary distribution of openings in the envelope of a residence may be determined by the following mass balancing procedure.

1. Select an initial elevation of the NPA, N.
2. Compute the pressure difference across each opening using equation 3.31.
3. Determine the discharge coefficient from equation 3.26 and the mass flow rate from equation 3.33 for each opening using the absolute value of the pressure difference.
4. Using the sign of the pressure drop across each opening compute the sum of the mass flow rates.
5. If the sum of the mass flows is not zero then select another elevation for the NPA and repeat the process until equation 3.32 is satisfied.

Chapter 4

DESCRIPTION OF THE EXPERIMENTAL APPARATUS

Introduction

A two cell environmental chamber was constructed to simulate the temperature gradients across the envelope of a structure. The facility was built as air tight as possible and it is capable of producing temperature differences as great as 60°C (108°F) across a thermal barrier. The thermal barrier consists of two removable test sections which can simulate a two story wall with a ceiling. The wall section has nine different locations where an idealized opening may be mounted into the wall to simulate structural leakage. The ceiling section has one mounting plate for an idealized opening and a circular mounting plate which will enable the study of a chimney at a later date. Eight straight rectangular openings and six cylindrical openings were fabricated of acrylic sheet (often referred to as ''plexiglass'').

Construction of the Two Cell Environmental Chamber

The base of the chamber has outside dimensions of 4.343 m (14.25 ft) by 5.918 m (19.42 ft) and the external height is 5.944 m (19.5 ft) (refer to Figure 4.1). The walls are of double stud construction with a thickness of 31.75 cm (12.5 in). The insulation value of the wall is approximately R-42. A construction detail of a typical wall section is provided in Figure 4.2. A continuous polyethylene vapor barrier was installed beneath the exterior plywood of each of the four walls. The vapor barrier of each of the walls was overlapped a

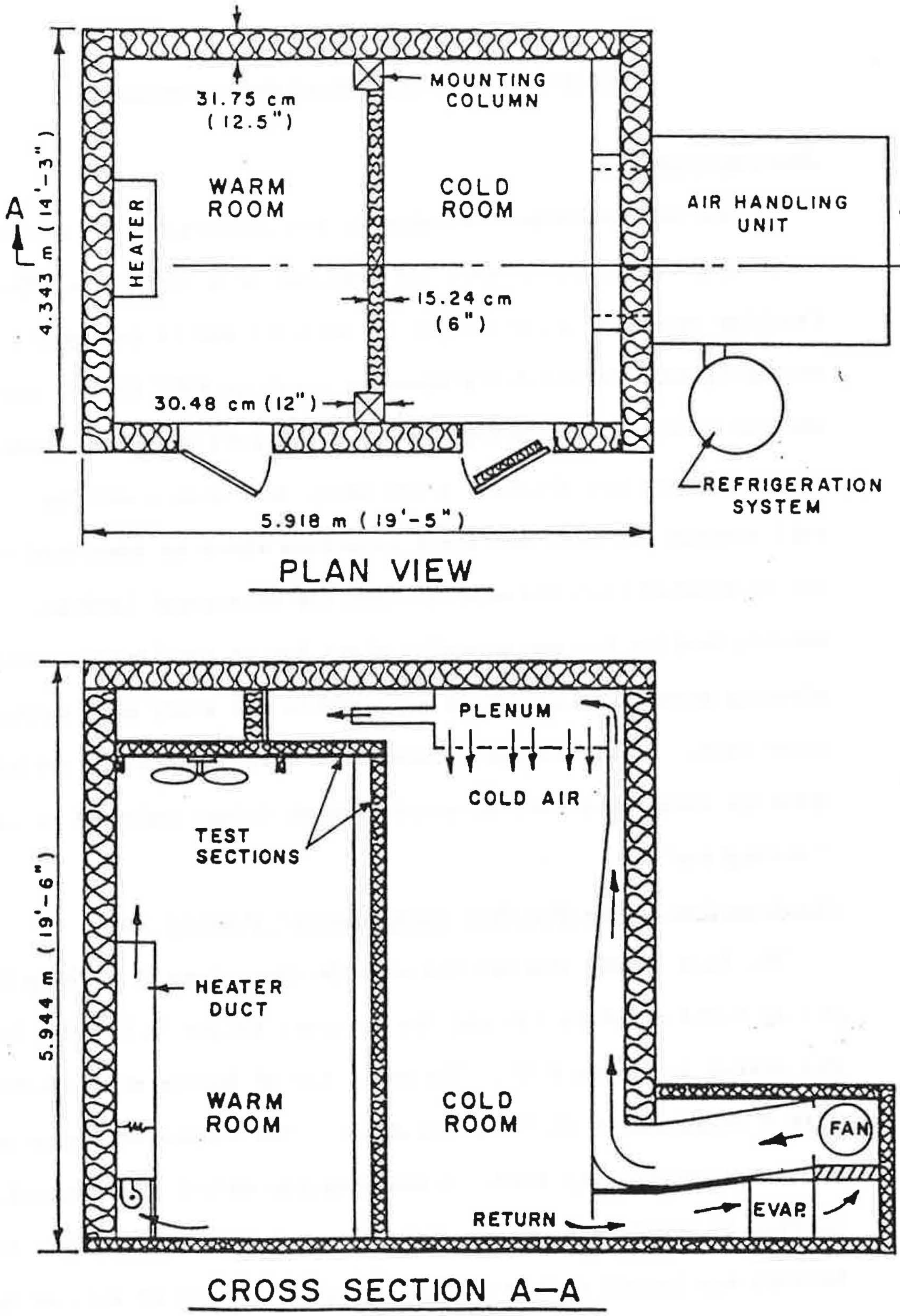

Figure 4.1 The two cell environmental chamber.

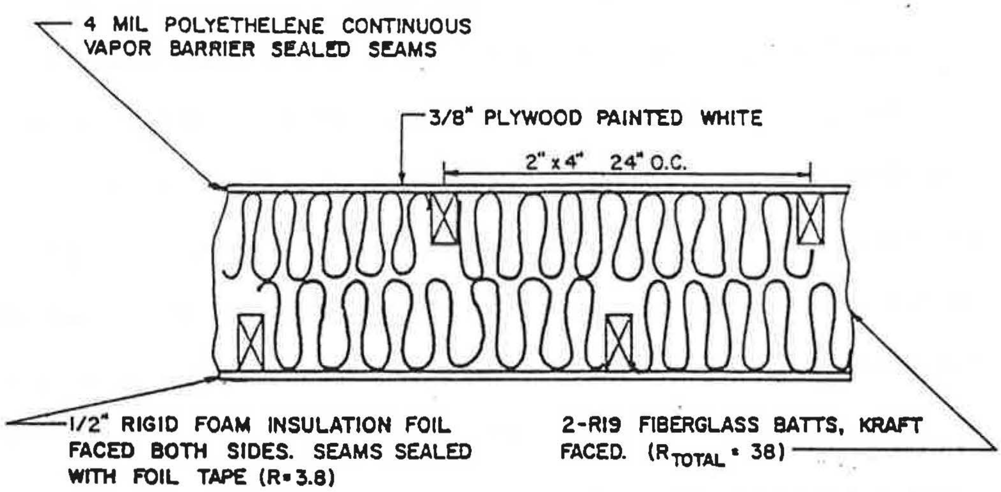

Figure 4.2 Detail of the wall construction.

minimum of 1.22 m (4 ft) at the corners and sealed with an adhesive sealant. A second continuous vapor barrier was formed on the interior of the chamber by sealing all of the seams and nail holes in the foil faced foam board insulation with foil tape. The interior vertical joint at the corners was also sealed using foil tape. The use of the foil faced rigid insulation provided a highly reflective finish on the interior of all of the permanent walls. To minimize the number of penetrations in the walls, all electrical outlets, switches, and conduit were surface mounted on plywood bases. Any penetrations that were made were sealed with silicone caulk.

The ceiling was also insulated to a value of R-42. A detail of the placement of the ceiling insulation and the ceiling-wall joint is presented in Figure 4.3. A single sheet of polyethylene plastic was spread over the outside layer of ceiling insulation and the edges were lapped 1.22 m (4 ft) over all four sides of the chamber and sealed to the vapor barriers of each of the walls. The interior vapor barrier was made complete by taping the joint between the ceiling and the walls. The seams and nail holes in the rigid insulation used on the interior of the ceiling were also taped.

The floor of the environmental chamber was constructed of 2 x 6 lumber (16 in. O.C.) on a concrete floor (refer to Figure 4.4). The cavities between the floor joists were insulated with R-19 fiberglass insulation. The floor section beneath the test wall and the mounting columns (refer again to Figure 4.1) was designed and built to support the dead load of a concrete block wall. The cavities in this floor section were insulated using extruded polystyrene foam board to provide a thermal break with an R value of about 50. The thermal

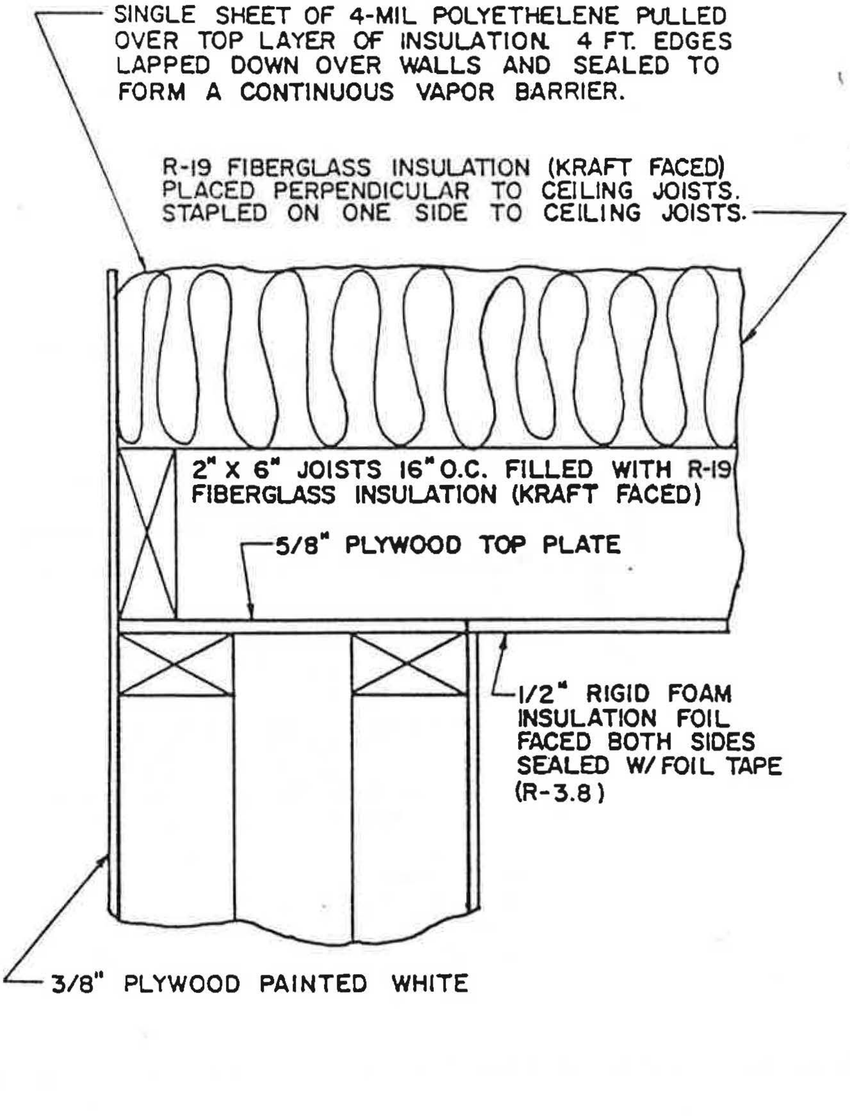

Figure 4.3 Cross-sectional view of the ceiling and wall joint.

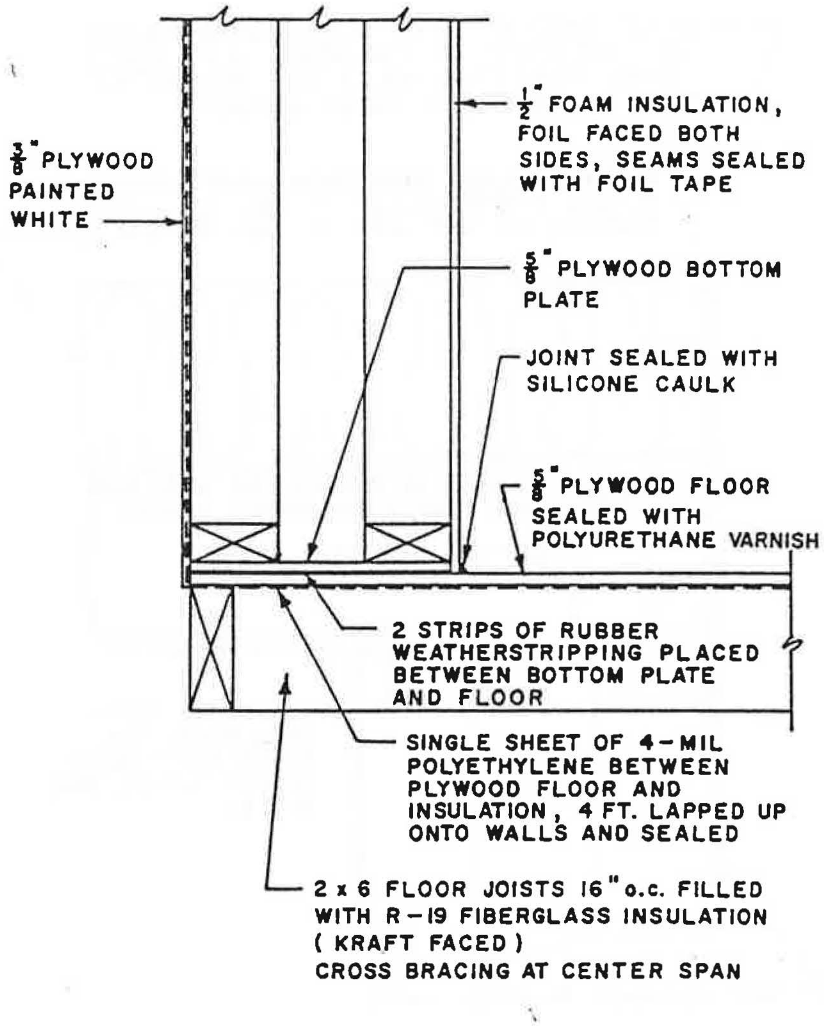

Figure 4.4 Cross-sectional view of the wall and floor joint.

break was installed to prevent excessive heat flow underneath the test wall. A continuous vapor barrier was placed between the floor joists and the plywood floor. The edges of the vapor barrier were sealed to the exterior vapor barrier of the walls in the same fashion as described for the ceiling. In order to prevent the leakage of air underneath the bottom plate of the walls, two strips of rubber weatherstripping were placed between the bottom plate of the walls and the floor. Also, the joint between the rigid foam insulation on the walls and the floor was sealed with silicone caulk. The joints in the plywood floor were caulked and then the floor was painted with three coats of polyurethane varnish to prevent moisture uptake by the wood and to complete the internal vapor barrier.

An insulated steel access door was furnished for each side of the environmental chamber. The doors had a foam insulation core which was rated R-14 by the manufacturer and each door was equipped with magnetic seals. An additional 4 inches of foam insulation was added to the access door of the cold room by gluing polystyrene foam board to the inside surface.

The Cooling System

The temperature of the cold room was capable of being controlled between -32° (-25°F) and 18°C (65°F). The cooling was provided by a five ton R-502 refrigeration system with a water cooled shell-in-tube condensing unit. The refrigeration system was designed to provide 7.03 KW (24,000 BTU/hr) of heat removal at a room temperature of -32°C (-25°F).

The air handling unit was equipped with a fan that delivered the design air flow rate of 2.12 m^3/s (4,500 cfm). This was equivalent to 2.6 complete air changes per minute. The fan, the duct work and the evaporator were insulated with rigid foam insulation (R = 3.8). The entire air handling system was housed in a wooden frame constructed of 2 x 6 lumber and insulated with fiberglass batts (R = 19). The motor which drives the fan was mounted outside of the housing.

The refrigerated air entered the cold room by way of a penetration in the wall and the air was discharged into a duct with a cross-section of 0.30 m (1 ft) by 1.83 m (6 ft). The air flow was directed upwards by means of a turning vane. At the point of discharge into the plenum, the air supply duct was as wide as the interior of the building and the cross-sectional dimensions were 0.15 m (0.5 ft) by 3.66 m (12 ft). The plenum was permanently built into the ceiling and it measured 1.83 m (6 ft) by 3.66 m (12 ft) by 0.61 m (2 ft) deep. A front view of the air supply duct is shown in Figure 4.5. The air supply duct and the plenum were constructed of 2 x 2 framework with 3/8 in plywood forming the interior surface. All of the wood was covered with three coats of polyurethane varnish to prevent the absorption of moisture. The bottom of the plenum consisted of an air diffusing grid fabricated of sheets of 1.27 cm (0.5 in) polyester fiber filter material stapled to a wooden frame. Two circular fiberglass ducts extended horizontally from the front of the plenum to directly supply cooling air to the space above the ceiling of the test section (refer to Figure 4.1).

The air flow into the plenum was made uniform across the width of the building by means of two large manually adjustable baffles which were positioned in the air supply duct below the point of discharge

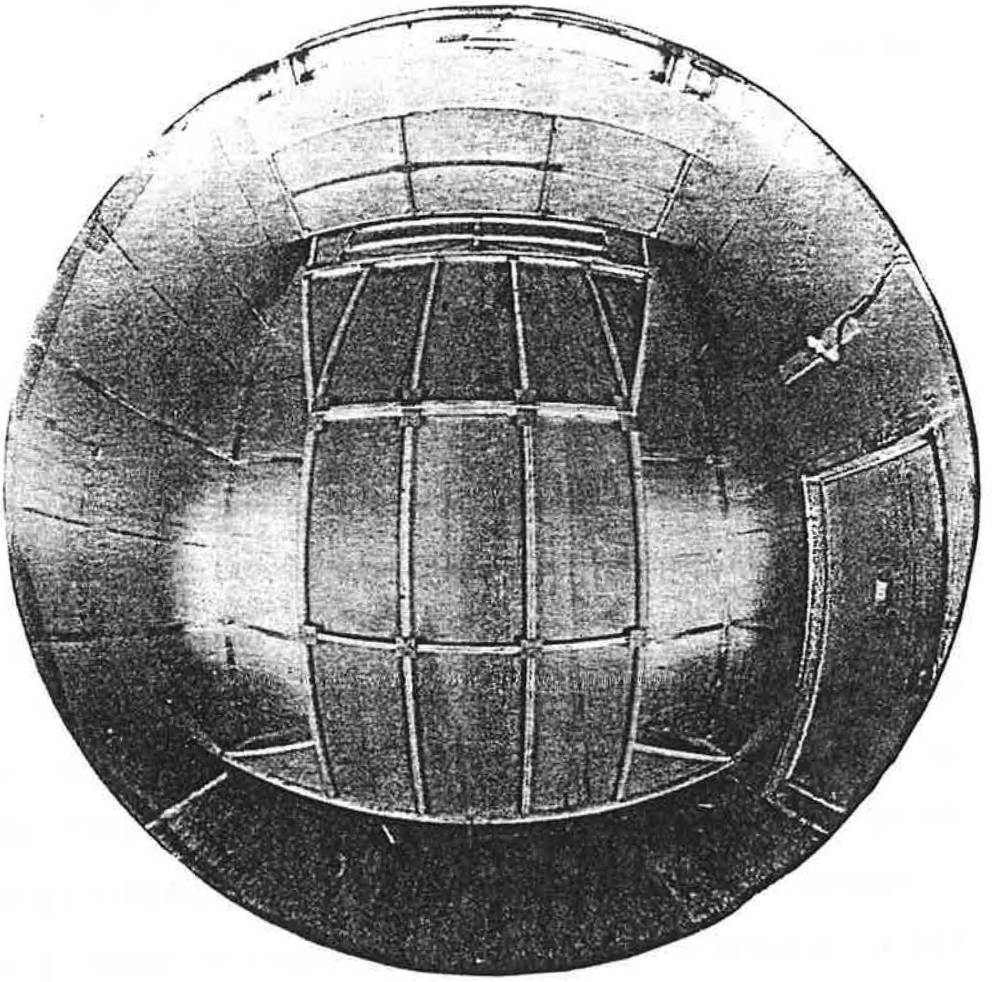

Figure 4.5 The refrigeration duct as seen from inside the cold room.

into the plenum. The effect of the plenum was to receive the refrigerated air at an average velocity of 3.8 m/s (750 fpm) in the horizontal direction and to discharge the air flow in the downward direction at a face velocity of about 0.5 m/s (100 fpm) or less.

The return duct extended the width of the interior of the cold room and it had a cross-sectional area of 0.557 m^2 (6 ft^2). The face of the return was covered with a wire screen.

<u>The Heating System</u>

The warm room was equipped with an electric heater which could maintain a room temperature from 10°C (50°F) to 29° (84°F). A small blower was mounted at the base of the heater duct. The blower was operated continuously at an air flow rate of about 0.061 m^3/s (130 cfm). Four resistance heating elements were mounted downstream from the blower and the heating elements could be either controlled by the thermostat or manually. Under manual operation room temperatures of 43°C (110°F) could be obtained. The output power of the heater could be varied infinitely from 0 to 880 W by means of four small variable voltage transformers (one for each element). A reflective metal shield was mounted around the heating elements and perpendicular to the direction of air flow to protect combustible materials from the radiant heat. The air flow was directed towards the ceiling where the heated air could be uniformly distributed by means of a variable speed paddle fan. The heating system is shown in Figure 4.6.

<u>The Test Sections</u>

A removable wall section and ceiling section were constructed between the two permanent mounting columns within the environmental chamber. Except for the dimensions, the test sections were

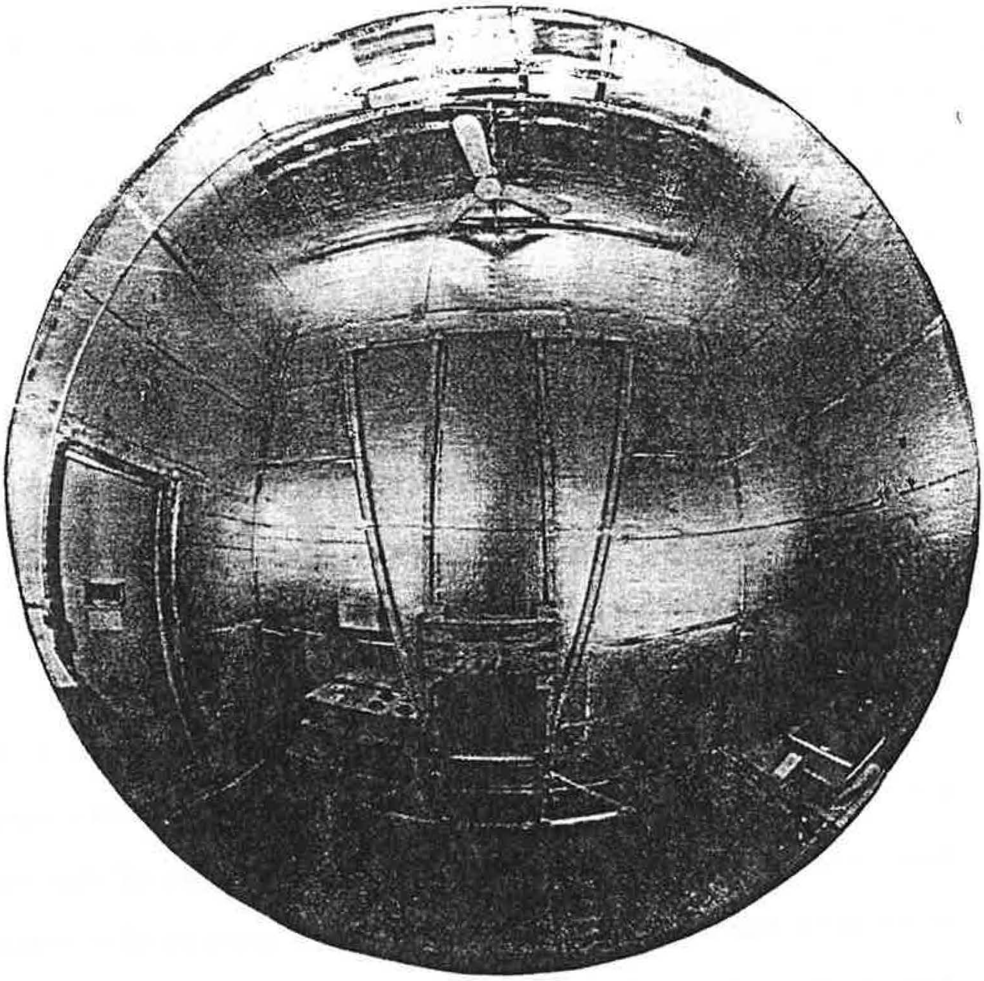

Figure 4.6 The heating system as viewed from inside the warm room.

constructed in the same fashion. The wall section was 3.05 m (10.0 ft) wide by 4.969 m (16.27 ft) tall. The ceiling section measured 3.71 m (12.17 ft) wide by 2.79 m (9.17 ft) in length. Referring back to Figure 4.1, it can be seen that the ceiling section is supported by the two mounting columns as well as two 2 x 6 beams which are as wide as the interior of the chamber. The beam supporting the end of the ceiling section opposite the test wall is fastened to the framing of the chamber wall along its entire length. The other beam is positioned about 0.76 m (2.5 ft) from the test wall. The ends of this beam penetrate the wall finish and they are bolted to the frame of the chamber wall. The joints between the test ceiling and the permanent chamber walls were sealed on all sides using silicone caulk and foil tape. On the cold side of the test ceiling an R-23 insulation barrier was placed at about 0.91 m (3 ft) back from the test wall. The test ceiling was insulated in a manner similar to that shown below for the test wall.

The construction of the test wall has been presented in Figure 4.7. All of the cavities, except for the center cavity, were insulated to a value of R-23 as shown. Both sides of the center section of the wall (and the ceiling) were covered with removable foam insulation panels. The panels on the warm side were cut into two pieces. The smaller pieces were hinged to the test wall by means of foil tape and they were used to access the center cavity once the other panels were in place. The center section of the wall and ceiling were fabricated in this manner to facilitate the mounting of pressure taps.

An enlarged cross-section of the center wall section and the

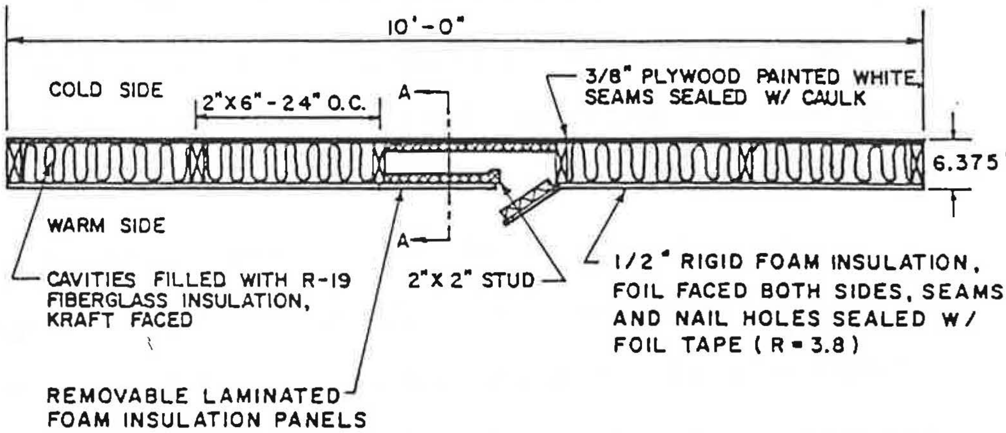

Figure 4.7 Construction detail of the test wall.

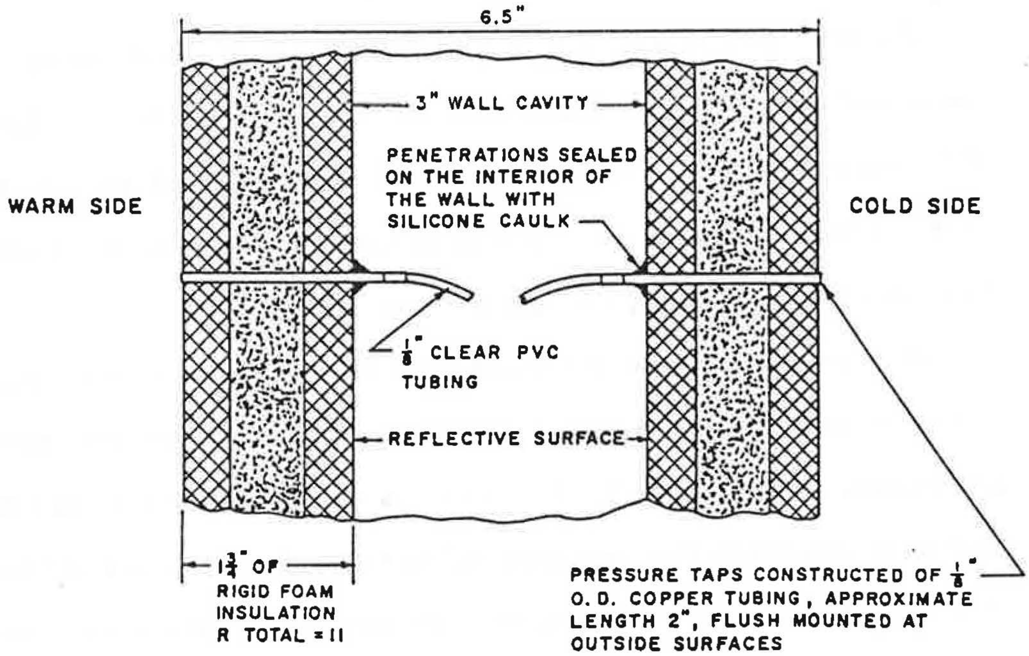

CROSS SECTION A-A OF THE TEST WALL

Figure 4.8 Technique used for mounting pressure taps.

technique employed to mount the pressure taps is presented in Figure 4.8. The insulated panels were formed by gluing two layers of 0.5 inch foam board around a single layer of 0.75 inch extruded polystyrene foam insulation. The three layers of insulation board were also taped together on all edges.

Once the construction of the wall was complete the joint between the test wall and the floor was sealed on both sides with a generous application of silicone caulk. Any large gaps between the mounting columns and the test wall were filled with sprayable foam insulation. Then the joints between the columns and the test wall were sealed on both sides using silicone caulk. The vapor barrier on the warm side of the test sections was made continuous by sealing all penetrations with silicone and sealing all seams in the foil faced insulation with foil tape.

The test sections were built in such a way as to allow an idealized opening to be mounted in ten vertical locations. Nine of the ten mounting locations were in the test wall and one was in the test ceiling. A circular mounting plate for a chimney was also provided in the ceiling for a future study.

In order to measure the pressure difference across the test sections as a function of elevation, pairs of pressure taps were positioned at twenty different locations. A schematic of the test sections depicting the positions of the mounting plates and the differential pressure measurements is given in Figure 4.9. The pairs of pressure taps mounted in the ceiling were considered to be at an elevation of 4.959 m (16.27 ft). A view of the test wall from the cold room is shown in Figure 4.10.

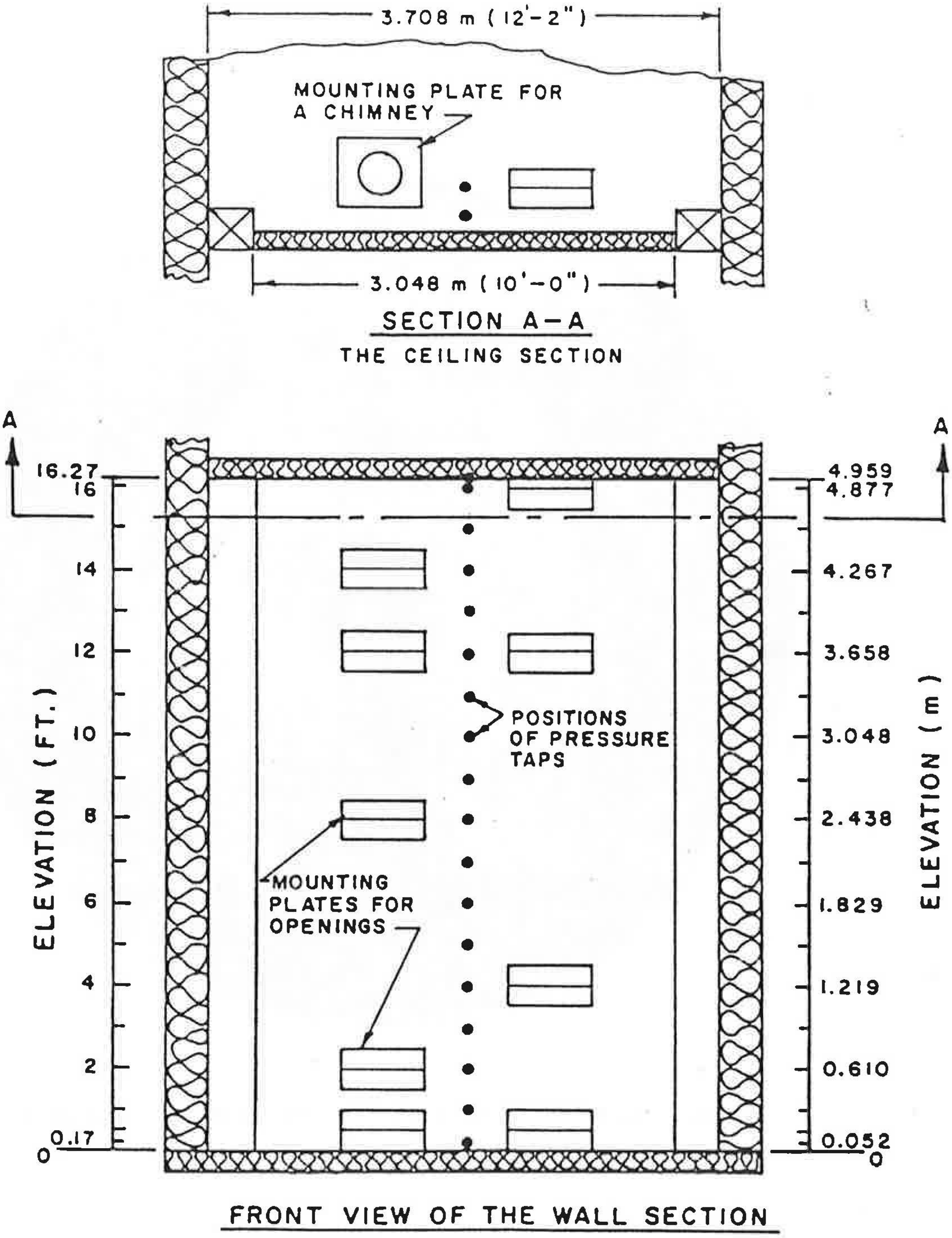

Figure 4.9 Schematic of the test sections as viewed from the warm room.

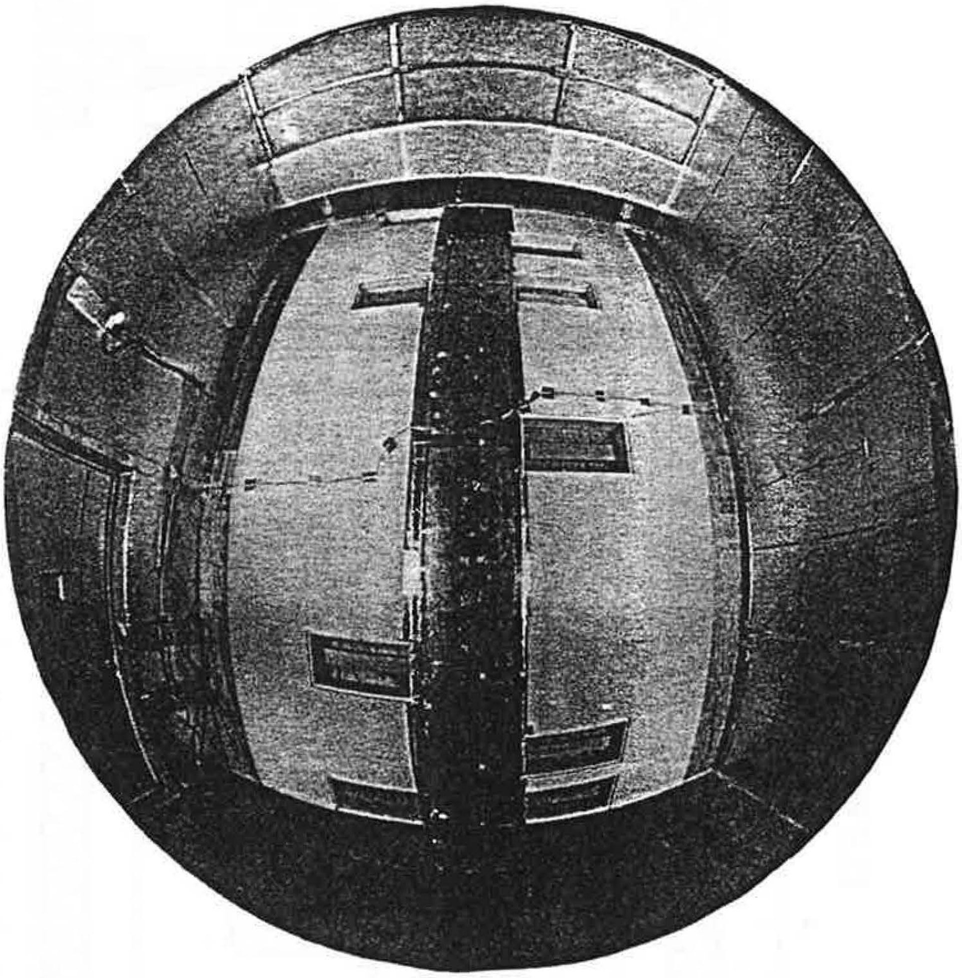

Figure 4.10 The test wall as seen from the cold room.

Figure 4.11 provides a detailed illustration of the method used to install the mounting plates for the idealized openings. The technique used to clamp an opening to the mounting plate has been depicted in Figure 4.12. Inspection of both of these figures reveals that the openings were clamped to the mounting plate using six carriage bolts. The tightening of the plywood clamps not only held the centerline of the opening at the correct elevation but also created a seal between the plywood plate and the idealized opening by compressing the foam rubber weatherstripping. The foam rubber was glued around the perimeter of the opening in the mounting plate. Extra pieces of weatherstripping were overlapped at the seams to attempt to create a continuous seal. The elevation to mount the centerline of an opening was marked on each end of the mounting plates. Using these marks as a guide, the centerline of the idealized openings could be consistently placed at the correct elevation to within approximately $\pm$ 0.318 cm (0.125 in). The joints between the mounting plates and the test sections were sealed as noted in the illustrations.

<u>Fabrication and Description of the Idealized Openings</u>

Eight straight rectangular openings and six cylindrical openings were fabricated for use in the experimental investigation of the neutral pressure axis. All of the openings were fabricated of 6.25 mm (0.246 in, 1/4 in nominal) acrylic sheet. The uncertainty of the dimensions was approximately $\pm$ 0.25 mm (0.01 in).

A detailed description of the rectangular openings is shown in Table 4.1. The slot thickness, d, ranged from 0.8 mm (0.03 in) to 16.0 mm (0.63 in) and the flow lengths, z, were in the range of 12.7

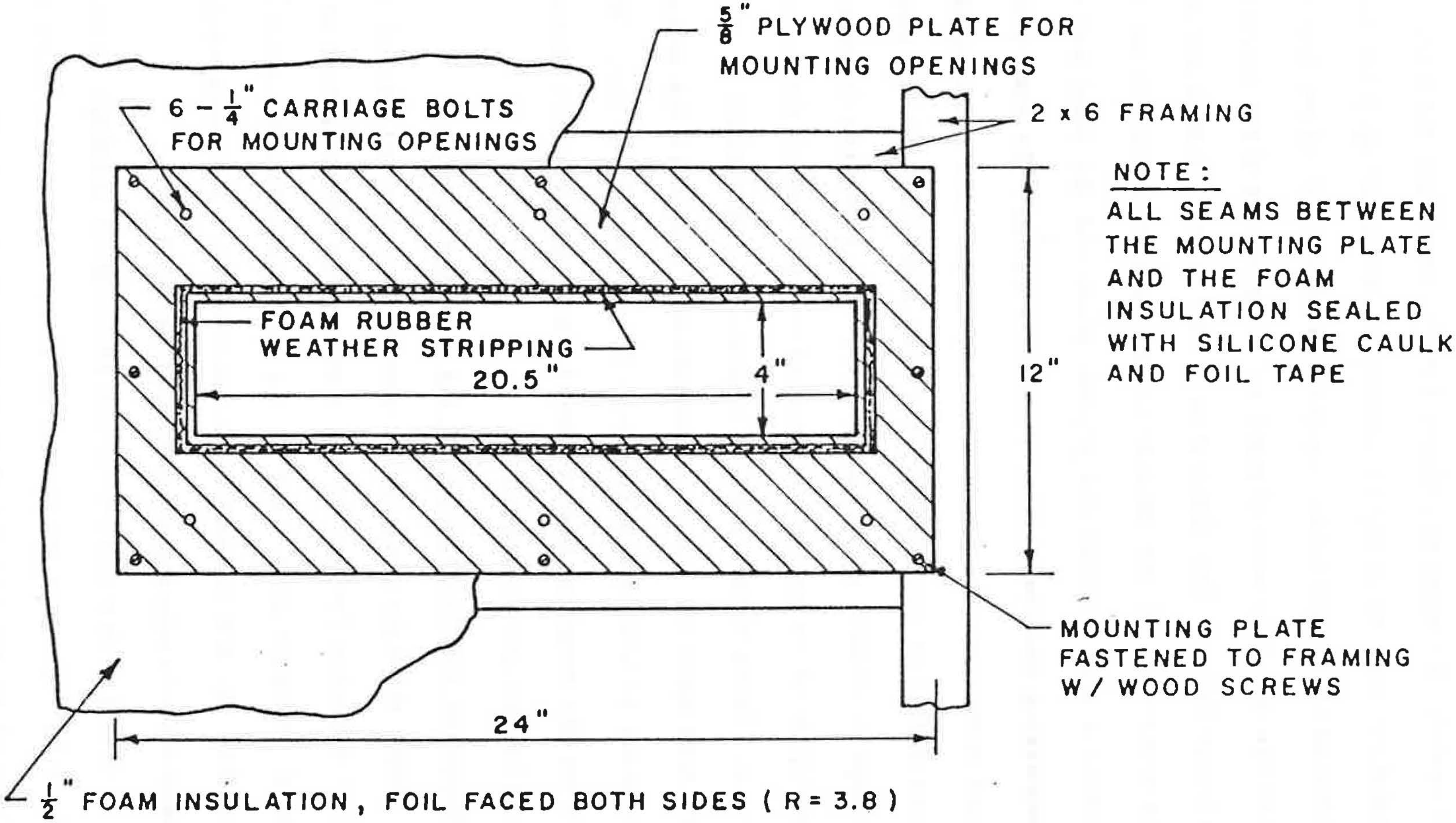

Figure 4.11 Typical installation of a mounting plate.

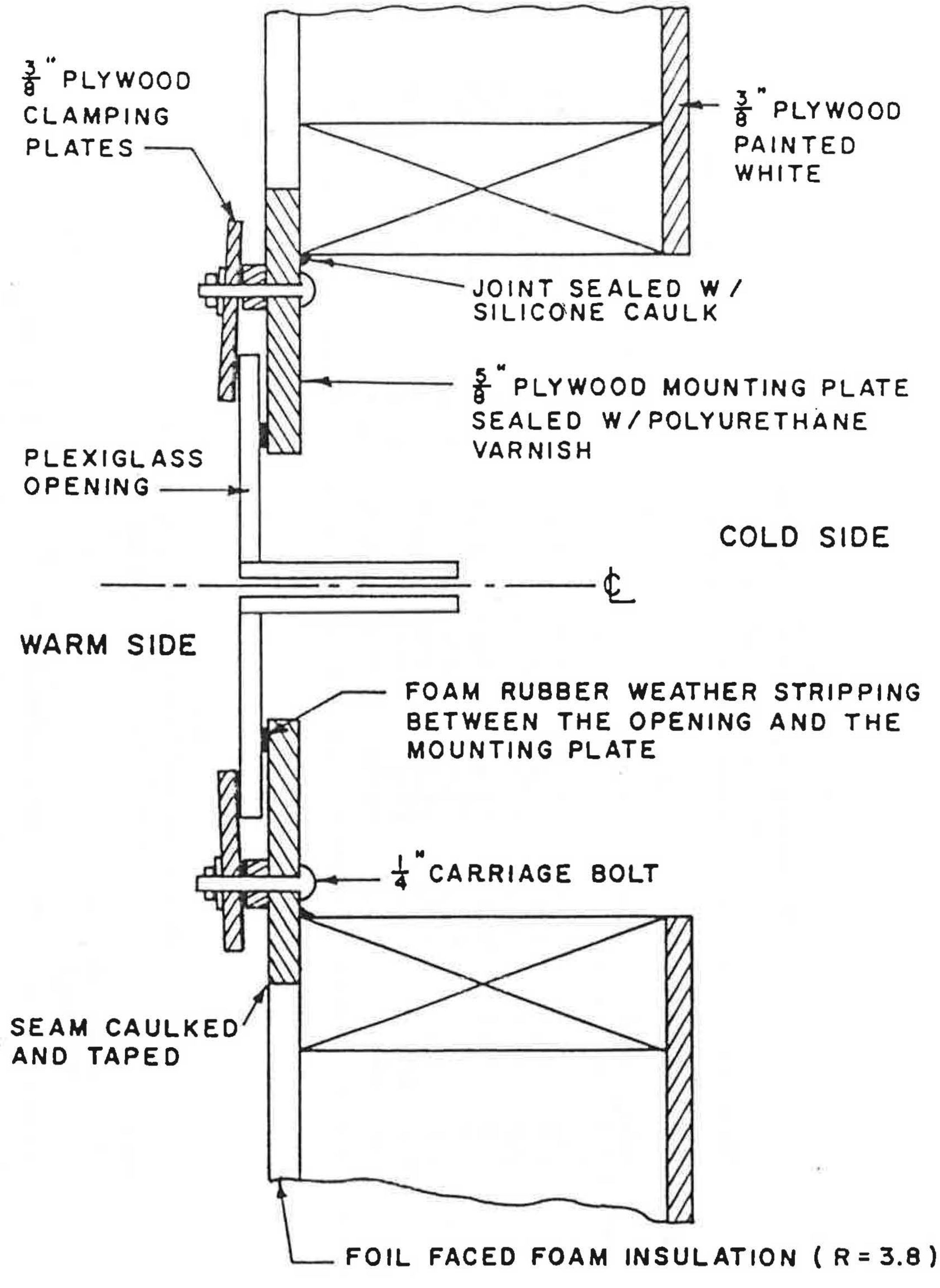

Figure 4.12 Technique used to mount an opening in the test sections.

Table 4.1
Dimensions and Geometric Parameters of
the Rectangular Openings

ID.	d (mm)	z (mm)	w (mm)	A (cm^2)	α	B	γ $x10^{-4}(m^{-1})$	$(A\gamma)$ $x10^{-5}(m)$	z/D_h
A	0.8	25.4	500.1	4.00	0.0016	95.8	6.55	0.026	15.9
B	1.7	50.8	500.1	8.50	0.0034	95.6	6.95	0.059	14.9
C	2.0	12.7	500.1	10.00	0.0040	95.6	32.68	0.327	3.2
D	3.3	44.5	500.1	16.50	0.0066	95.3	15.36	0.253	6.7
E	6.3	88.9	499.3	31.45	0.0126	94.7	14.60	0.459	7.2
F	12.9	50.8	498.5	64.31	0.0259	93.2	51.98	3.343	2.0
G	13.4	152.4	500.1	67.01	0.0268	93.1	17.91	1.200	5.8
H	16.0	123.8	500.1	80.02	0.0320	92.6	26.21	2.097	4.0

Table 4.2
Dimensions and Geometric Parameters of
the Cylindrical Openings

ID.	Number of Openings	D (mm)	z (mm)	A (cm^2)	γ $x10^{-4}(m^{-1})$	$(A\ \gamma)$ $x10^{-5}(m)$	z/D_h
X	2	6.4	50.8	0.32	979.05	0.313	7.9
Y	2	12.7	50.8	1.27	979.05	1.243	4.0
Z	2	50.8	50.8	20.27	979.05	19.845	1.0

mm (0.5 in) to 152.4 mm (6.0 in). All of the openings had a width, w, of about 500 mm (19.685 in).

These dimensions gave a range of aspect ratio, α, from 0.0016 to 0.032 and a range of dimensionless flow length, z/D_h, from 2.0 to 15.9. As was stated previously, the aspect ratio describes the cross-sectional geometry of a rectangular opening. The magnitude of the dimensionless flow length is an indicator of the relative importance of the contribution of the flow length to the total dimensionless pressure drop (refer to equation 3.17). An opening with a very small dimensionless flow length would be expected to contribute a negligible friction loss and behave as an orifice. Openings with relatively large values of z/D_h would contribute a more significant friction loss characteristic of laminar flow through a pipe. Furthermore, the openings with small aspect ratios (slots A through D) are considered the most characteristic of structural leakage in a residence. The rectangular slots with larger aspect ratios (and smaller z/D_h) are more representative of natural ventilation. In particular slot F (α = .0259; z/D_h = 2.0) may be expected to behave in a manner similar to a window which has been slightly raised.

A typical profile of the construction of a rectangular opening was presented previously in Figure 3.1. The sawn edges of the acrylic sheet were milled to produce a smooth edge as well as to even up the dimensions. It should be noted that the ends of the slots are closed.

Even though the majority of the openings in the envelope of a structure are of rectangular cross-section, a few cylindrical openings were included in the study. The dimensions and the geometric parameters of the cylindrical openings are presented in Table 4.2. Three different diameters (D) were used and all of the openings had a flow length equal to 50.8 mm (2.0 in). As a result, the dimensionless flow length, z/D_h, was in the range of 1 to 7.9.

The cylinders identified as X and Y were fabricated by drilling successively larger holes in a block of laminated acrylic sheet until the desired diameter was obtained. To obtain a diameter of 50.8 mm (2.0 in), a pilot hole was drilled in a laminated block of plexiglass and the diameter was enlarged on a milling machine using a boring tool. Two openings were fabricated for each diameter to give a total of six cylindrical openings. The openings X2 and Y2 were drilled side by side in the same block of material.

Instrumentation

In order to test the validity of the mass balancing procedure to compute the location of the neutral pressure axis, the differential pressure profile due to the stack effect and the psychrometric data to compute the air properties were measured. The air properties required to compute the mass flow rate through an idealized opening are the density, the dynamic viscosity and the kinematic viscosity. The dynamic viscosity, μ, is a function of the air temperature alone. The density, ρ, is a function of the local barometric pressure, the temperature and the moisture content of the air. The kinematic viscosity, ν, may be determined from the dynamic viscosity and the density. To calculate the air properties, the measurements required were the local barometric pressure, the dry-bulb temperature, and the wet-bulb temperature (for the warm air) or the dewpoint (for the cold air). The relationships used to compute the air properties from the data are provided in Appendix C. The experimental setup is shown in Figure 4.13. All of the measurements were taken from the warm side.

Twenty pairs of static pressure taps were installed in the test sections at the elevations indicated. The pressure taps were about 50.8 mm (2.0 in) in length and they were fabricated of 3.18 mm (0.125 in nominal, O.D.) copper tubing. All rough edges caused by cutting the tubing were filed smooth. A long piece of flexible, clear, PVC tubing with an outside diameter of about 3.18 mm (0.125 in) was pushed onto the end of the pressure taps (refer to Figure 4.8). The PVC tubing fit the copper tubing very tightly and the tubes for each pair of pressure taps were of the same length. Each pair of tubes was lightly twisted together and taped at several intervals. This enabled a pair of tubes to be routed together and any variations of temperature in the environment surrounding the tubes would not affect the differential pressure reading. Each pair of tubes came out of the test wall cavity (refer to Figure 4.7) at the elevation of placement (refer to Figure 4.9) by way of a small hole in the insulated panel on the warm side of the test wall. The tubes were routed down the surface of the test wall to the pressure transducer. The penetrations in the insulation panel were sealed around the tubes with silicone caulk and the tubes were taped to the test wall with foil tape.

Initially, the tubes were routed to the pressure transducer individually within the cavity of the test wall. The temperature variations within the wall cavity interfered with the pressure

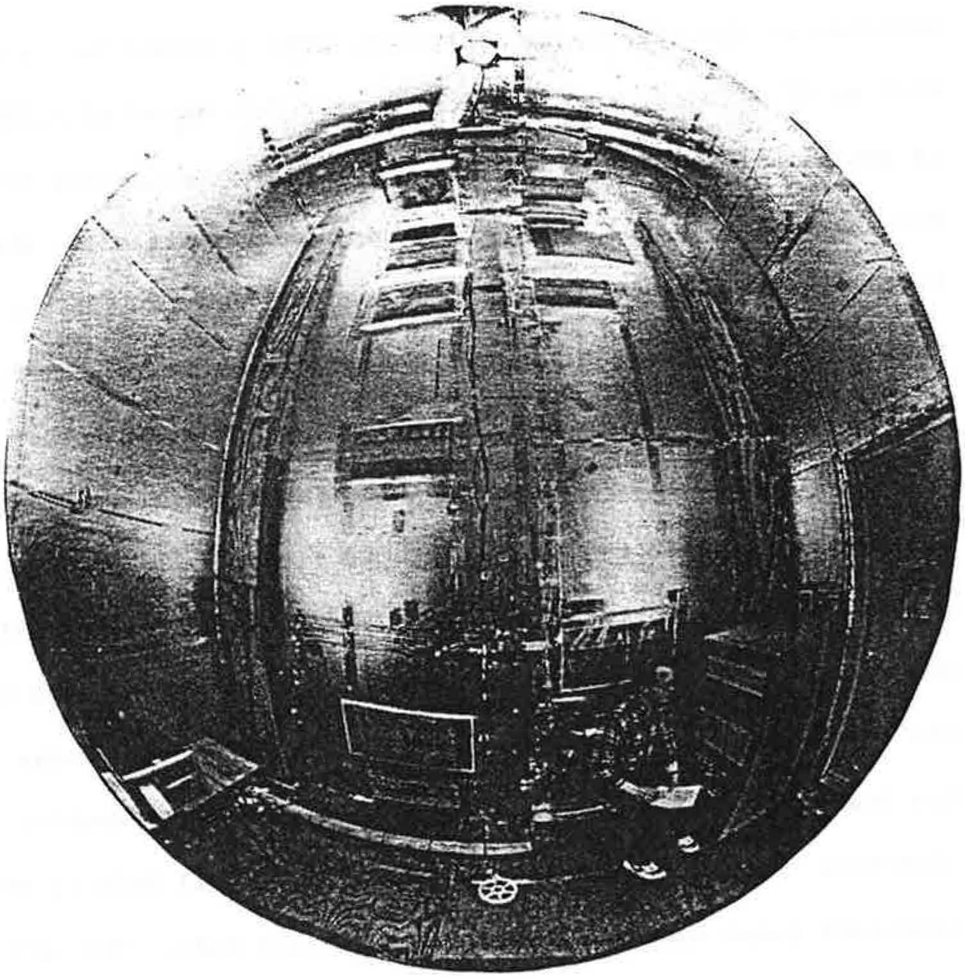

Figure 4.13 The experimental setup as seen from the warm room.

measurements so they were moved to the warm side of the test wall.

A single differential pressure transducer was used to measure the pressure difference at each elevation. Eighteen of the twenty pairs of tubes were attached to the transducer by means of a manual switching valve (Scanivalve Type W1260 Fluid Wafer Switch) . The remaining two pairs of tubes were attached directly to the transducer when a measurement was desired. The differential pressure measurements were taken using an MKS Baratron (type 77H-10) pressure meter which has a resolution of 0.013 Pa (0.0001 mm Hg), 0.027 Pa (0.0002 mm Hg) and 0.133 Pa (0.001 mm Hg) on the three scales used.

The standard barometric pressure was obtained on an hourly basis from the Kentucky Weather Wire Service, Bluegrass Airport, Lexington, Kentucky located approximately 11 miles from the test chamber. The elevation of the laboratory in the Agricultural Engineering building is 304.8 m (1000 ft) above sea level. The local barometric pressure was determined by subtracting 3556 Pa (1.05 in Hg) from the standard barometric pressure reading.

According to the literature cited (ASHRAE, 1985; Emswiler, 1926; Lee et al. 1985), the mean internal and external temperatures are sufficient to estimate pressure differences due to the stack effect if the elevation of the neutral pressure axis is known (refer to equation 2.11). Emswiler (1926) theorized that if the temperature within a building increased with elevation then the NPA would be displaced slightly towards the ceiling. Therefore, it was desired to not only take measurements to estimate the mean temperature of each room but also to measure the variation of temperature with respect to elevation. A temperature measuring cable was suspended about 0.76 m

(2.5 ft) from the center section of each side of the test wall. A total of nineteen individual temperature measurements were taken which allowed the computation of ten temperature differences. Thermocouple number 9 was used with number 18 to determine the temperature difference at the height of 4.877 m (16.0 ft) and with number 19 to determine the temperature difference across the test ceiling. Thermocouple number 19 was suspended from the ceiling of the chamber and was used to measure the cold air temperature above the test ceiling. Thermocouples 1 and 10 measured the temperatures near the floor at an elevation of approximately 5.08 cm (2.0 in). The remaining eight pairs were equally spaced at intervals of about 0.610 m (2.0 ft). The thermocouple wires from the cable in the cold room were passed through a single penetration in the insulated panels to the warm room where all nineteen temperatures were recorded using an Esterline Angus model PD2064 programmable data logger. The uncertainty of the temperature measurements was estimated to be $\pm$0.6°C (1°F). The thermocouple penetration through the test wall was sealed on both sides with silicone caulk.

In addition to the room temperature measurements previously described, two additional thermocouples were installed in each room. In the warm room, a thermocouple was taped near the center of the wall across from the door (refer to Figure 4.1) at about 2.43 m (8 ft) above the floor. A second thermocouple was placed directly above the access door and about 0.61 m (2 ft) below the ceiling. The other two thermocouples were installed in the cold room in approximately the same corresponding locations. The wires were routed in the same fashion as described for the other temperature measurements in the cold room. All four pairs of thermocouple leads were passed through a small hole in the wall of the warm chamber next to the access door and sealed. The four temperature measurements were read outside of the two cell environmental chamber using an Omega 2176 multipoint digital thermometer.

Originally, the thermocouples to measure the two room temperatures as a function of elevation were mounted in the test sections in a manner similar to that described for the pressure taps. The main difference was that the thermocouple bulbs protruded about 5.08 cm (2.0 in) out from the wall on each side. During the testing of the instrumentation it was determined that these thermocouples were significantly influenced by the heat transfer through the wall. Comparison of the temperatures indicated by the digital thermometer with the measurements very near the test sections showed that the measurements on the warm side of the test walls were consistently less than the average room temperature. The measurements on the cold side of the test wall were consistently greater than the mean room temperature. As a result, the thermocouples mounted on the cables were substituted.

During operation of the refrigeration system, the air exiting the evaporator coils is very close to saturation. Therefore, a thermocouple placed downstream from the evaporator would indicate a close approximation of the dewpoint temperature (Figure 4.14). Recalling that the air handling system provides 2.6 complete air changes per minute, the dew point measured downstream from the evaporator is also a close estimate of the dewpoint within the cold room. If the barometric pressure, the dry bulb temperature and the

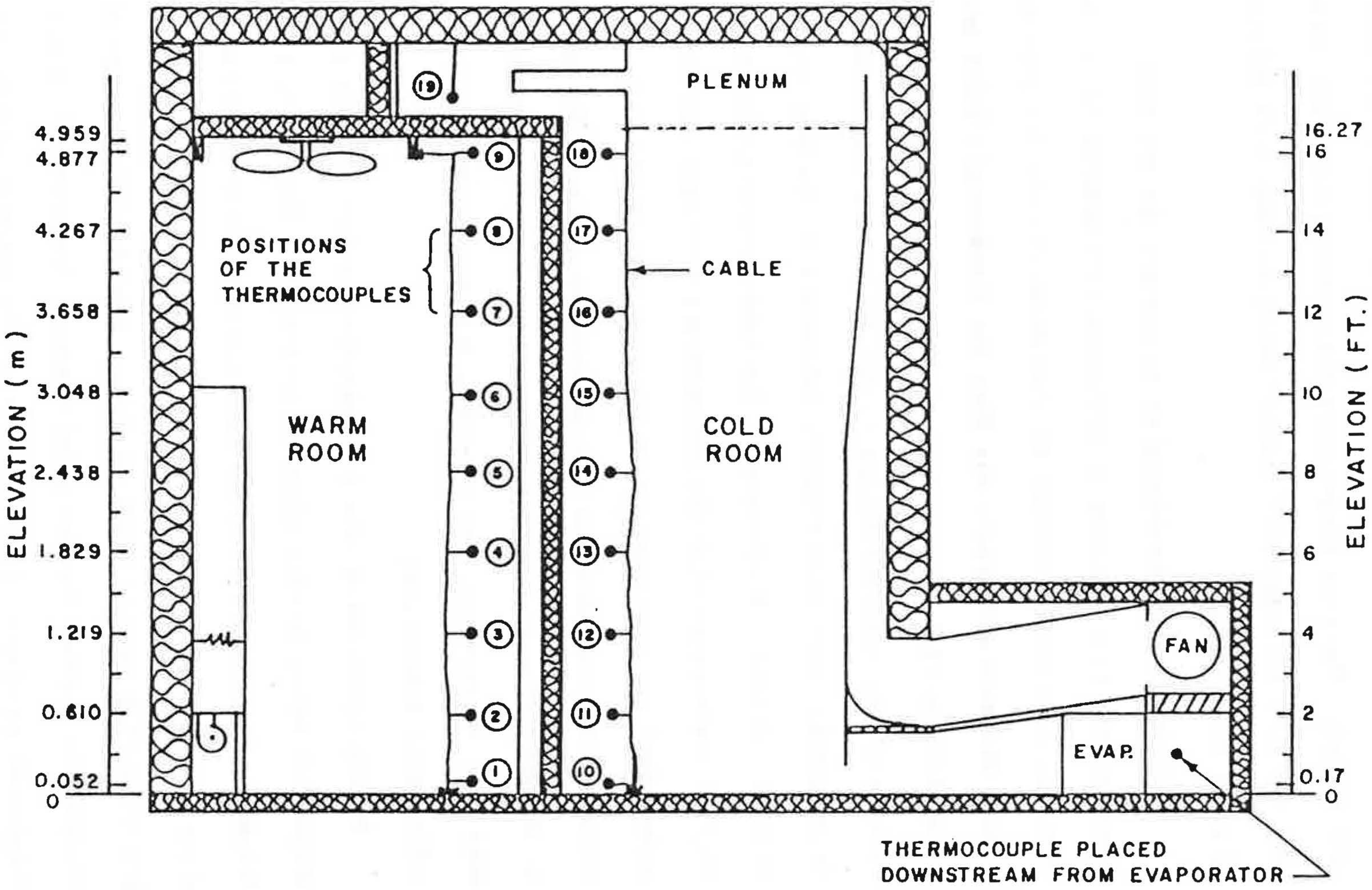

Figure 4.14 Positions of the temperature measurements.

dewpoint temperature are known then the air properties may be calculated (ASHRAE, 1985). The dewpoint temperature was read with the Omega digital thermometer.

The wet-bulb temperature was required to calculate the air properties of the warm air. The wet-bulb temperature was determined for the warm room using a mechanical wet-bulb psychrometer. The uncertainty of the measurement was ± 0.6°C (± 1°F).

Chapter 5

SENSITIVITY ANALYSIS OF THE DISCHARGE COEFFICIENT EQUATION

A detailed sensitivity analysis was performed on the discharge coefficient equation which was derived from the dimensionless energy equation for laminar flow through any type of rectangular or cylindrical opening (equation 2.17). The discharge coefficient equation was given in equation 3.26 and it has been restated below along with several defining expressions for convenience.

$$\frac{1}{C_z^2} = \frac{2K}{\left[1 + (A\ \gamma)^2 \frac{128\ K\ \Delta\ P}{\rho\ \nu^2}\right]^{0.5} - 1} + K$$

where; C_z = the discharge coefficient for real laminar flow,

$(A\gamma)$ = the area-gamma product (m),

A = the cross-sectional area (m^2),

γ = a geometric parameter which describes the three dimensional scale of an opening (m^{-1}),

ΔP = the total pressure drop across an opening (Pa),

K = the total minor loss coefficient,

ρ = the fluid density (kg/m^3),

$\nu = \mu/\rho$ = the kinematic viscosity (m^2/s), and

μ = the dynamic viscosity ($N * s/m^2$).

The definition of gamma for a rectangular cross-section of any aspect ratio was given in equation 3.24 as:

$$\gamma = \frac{\alpha}{Bz(1 + \alpha)^2}$$

where; $\alpha = \frac{d}{w}$ = the aspect ratio, B = the friction coefficient = 96.0 - 106.67α (eq. 3.30),

d = the thickness (m),

w = the width (m), and

z = the flow length (m).

Equation 3.29 gave the definition of gamma for a circular cross-section as follows:

$$\gamma = \frac{1}{B \pi z} \quad \text{and}$$

B = 64.

The discharge coefficient (C_z) may be viewed as a total dimensionless flow resistance and is described by the following functional statement:

$$C_z = f\ [(A\gamma),\ \Delta P,\ K,\ \mu,\ \rho]$$

The total geometric contribution to the flow resistance of an opening may be described by the area-gamma product ($A\gamma$). It can also be shown that the dimensionless friction loss, $B(z/D_h Re)$, may be written as follows:

$$\text{Dimensionless friction loss} = B\left(\frac{z}{D_h Re}\right) = \frac{\nu}{4Q\gamma}$$

As a result, the geometric component of the dimensionless friction loss of an opening may be described by the geometric parameter gamma. Furthermore, for a given total minor loss coefficient and set of air properties, any two openings which have the same value of ($A\gamma$) would also have the same discharge coefficient for a particular pressure drop.

Discharge coefficients were computed for a large range of $(A\gamma)$ at pressure differences which are typical of infiltration in residences. A total minor loss coefficient of 1.5 was used based upon the experimental results presented by Etheridge (1977). The variation of the discharge coefficient with respect to $(A\gamma)$ and the pressure difference has been shown in Figure 5.1. The following observations may be confirmed from the figure and the defining equations of gamma.

1. As the value of $(A\gamma)$ decreases the discharge coefficient also decreases. This indicates a greater resistance to flow.

2. The dimensionless energy equation was given in terms of the squared inverse of the discharge coefficient (equation 3.20) as:

$$\frac{1}{C_z^2} = B\left(\frac{z}{D_h Re}\right) + K.$$

For the case of an orifice (z=0) the value of $1/C_z^2$ is equal to the total minor loss coefficient. Inspection of the discharge coefficient equation indicates that as the value of $(A\gamma)$ increases the first term on the right side of the equation approaches zero which yields the same result. Consequently, a total minor loss coefficient of 1.5 sets the maximum value of the discharge coefficient at 0.816. Therefore, openings with large values of $(A\gamma)$, such as 10.0 x 10^{-5} m, behave like an orifice.

3. If the cross-sectional geometry of an opening is held constant then the magnitude of $(A\gamma)$ will decrease as the flow length increases. As a result, small values of $(A\gamma)$, such as

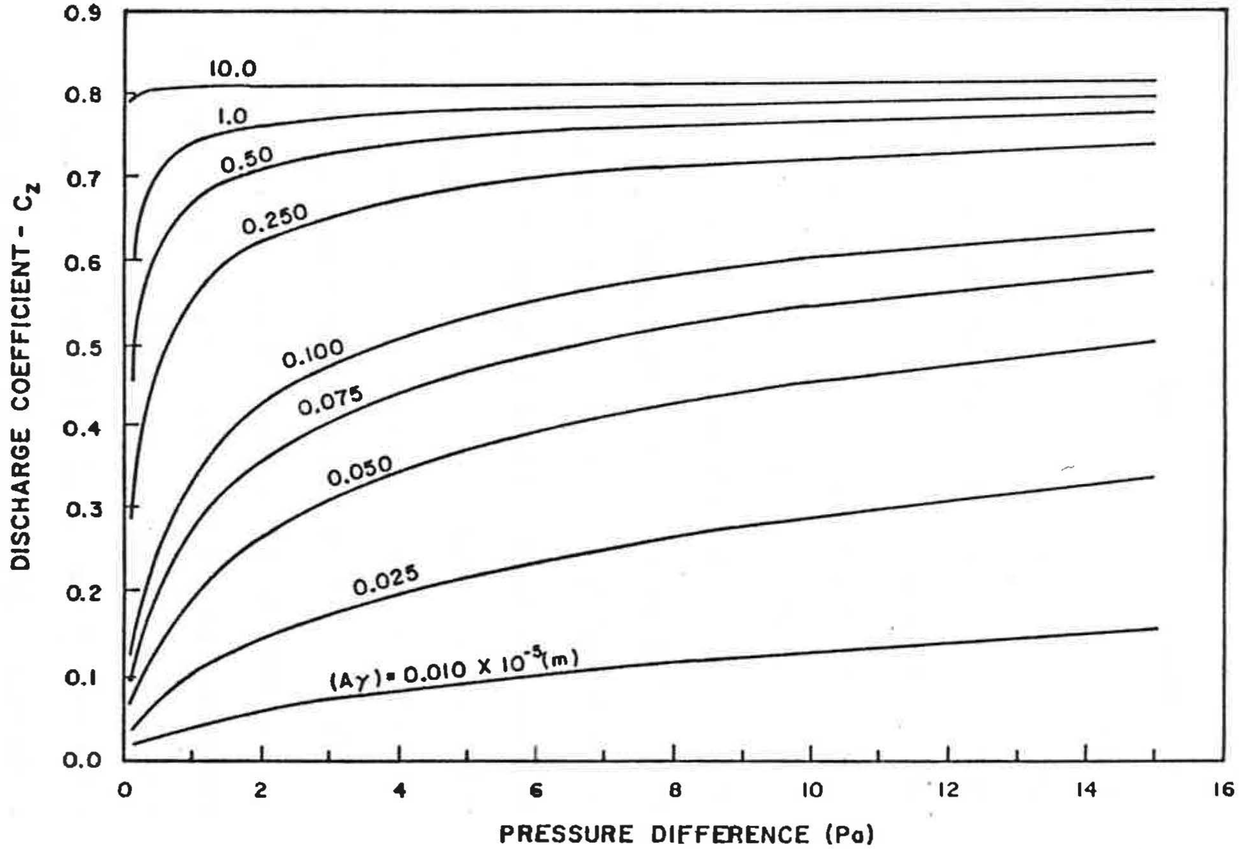

Figure 5.1 Variation of the discharge coefficient due to variations in the pressure difference and the area-gamma product ($T = -25°C$ ($-13°F$); $\rho = 1.380$ kg/m^3; $\nu = 1.150 \times 10^{-5}$ m^2/s; $K = 1.5$).

0.010×10^5 m, indicate laminar pipe flow.

4. Values of $(A\gamma)$ between 10.0×10^{-5} and 0.010×10^{-5} m represent short pipes which are at various points of transition between a long pipe and an orifice.

5. If the area and the flow length of a rectangular opening are held constant then the magnitude of $(A\gamma)$ will decrease as the aspect ratio decreases. Hence, long thin rectangular slots have a greater resistance to flow due to their cross-sectional geometry than square or cylindrical openings.

6. For pressure differences between one and fifteen Pascals the discharge coefficient can vary by as much as a factor of three for a particular value of $(A\gamma)$.

7. If the opening beneath an exterior entrance is modeled as a rectangular slot with a thickness (d) of 2.1 mm (0.0827 in), a width (w) of 91.44 cm (3 ft), and a flow length (z) of 4.445 cm (1.75 in) then the area-gamma product is 0.10×10^{-5} m. The discharge coefficient for the opening would range from 0.34 at a pressure drop of 1.0 Pa to 0.64 at a pressure drop of 15.0 Pa. The effective leakage area as given in equation 3.1 is equal to the product of the discharge coefficient and the area. As a result, the effective leakage area of this opening would vary from 6.60 cm^2 to 12.21 cm^2 (a factor of 1.85) over the range of differential pressures common to residences. Therefore, the concept of an effective leakage area is not adequate to describe the flow resistance of a building component. The inadequacy arises from the neglect of the flow length.

The variation of the discharge coefficient induced by a large variation in the air properties is presented in Figure 5.2. The difference in the air properties indicated in the figure corresponds to a variation in air temperature from approximately -25°C (-13F) to 23°C (73°F). This 48°C (86°F) increase in temperature was equivalent to a 19.8 percent decrease in density and a 27.4 percent increase in kinematic viscosity.

The greatest change in C_z was for the opening described by an $(A\gamma)$ of 0.026×10^{-5} m. At a pressure difference of 15.0 Pa, the large decrease in air properties resulted in a decrease in C_z from 0.346 to 0.292 (15.6%). For an $(A\gamma)$ of 0.459×10^{-5} m the variation in the air properties resulted in a decrease in C_z which ranged from 1.7 percent at 2.0 Pa to 1.3 percent at 15.0 Pa. Since openings with small values of $(A\gamma)$ have a significant friction loss, it was concluded that the degree of variation in C_z with respect to a change in the air properties is directly proportional to the relative importance of the friction loss. A variation in the air properties would have no effect on the discharge coefficient of an orifice $(B(z/D_hRe) = 0)$. Furthermore, it was concluded that small changes in the air properties would have an insignificant effect on the magnitude of C_z.

The influence of the variation of the total minor loss coefficient (K) on the discharge coefficient has been described in Figure 5.3. The discharge coefficients were computed over a range of $(A\gamma)$ from 0.025×10^{-5} to 25.0×10^{-5} m. For a square edged orifice the minimum value of K would be expected to be 1.5. The total minor loss coefficient was varied from 1.5 to 1.8 to yield a 20 percent variation in K. The variation of the total minor loss coefficient was normalized

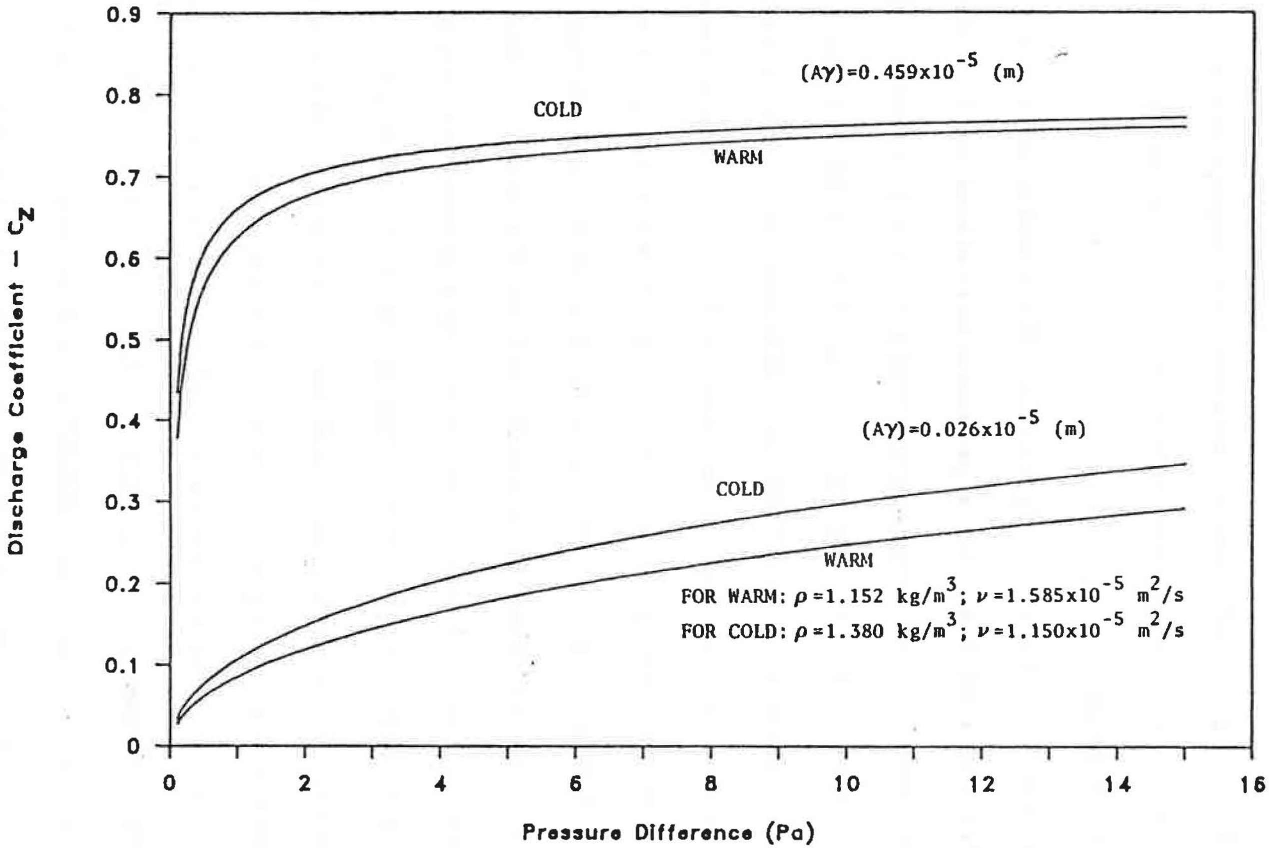

Figure 5.2 The influence of a large variation in the air properties on the discharge coefficient.

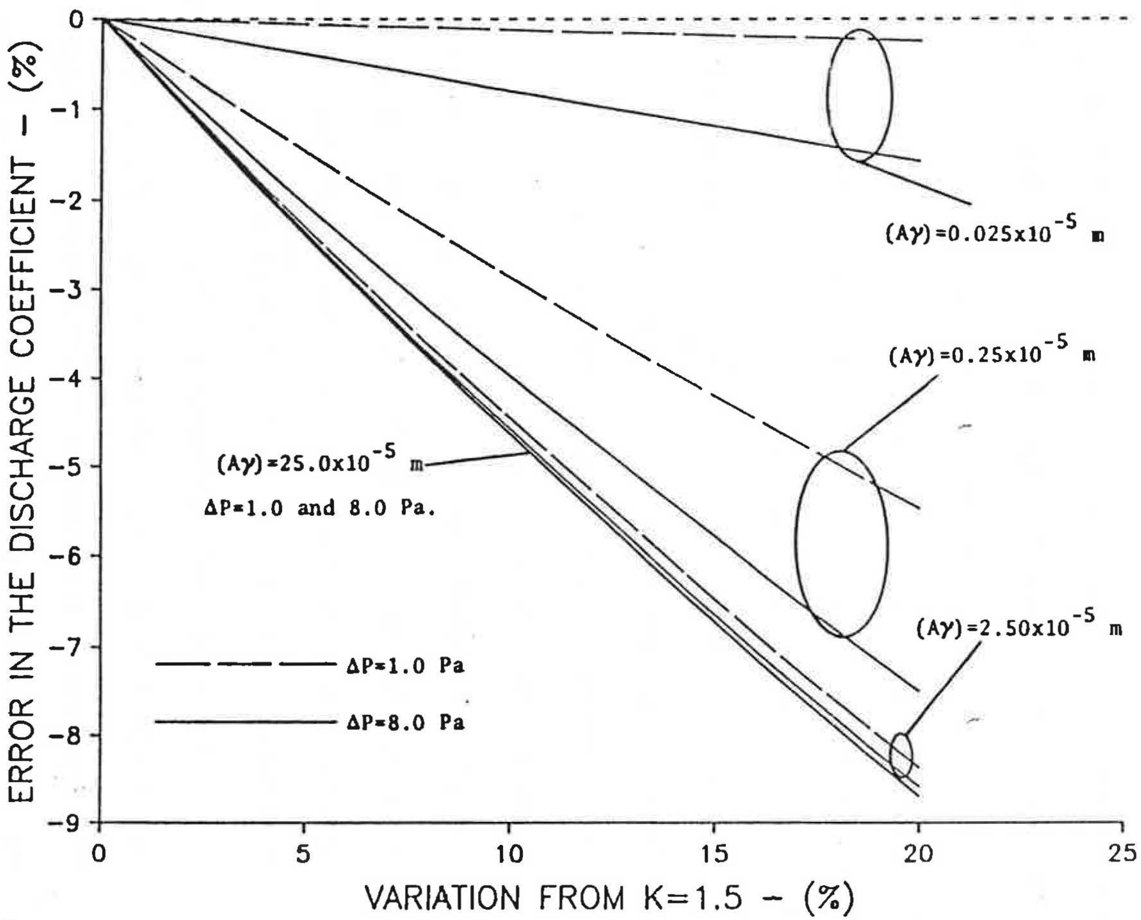

Figure 5.3 Influence of the variation of the total minor loss coefficient on the discharge coefficient ($T = -6°C$ ($21°F$); $\rho = 1.277\ kg/m^3$; $\nu = 1.319 \times 10^{-5}\ m^2/s$).

as the percent difference from K equal 1.5. The resulting variation in the discharge coefficient was normalized as the percent difference from C_z computed using K equal 1.5. Pressure differences of 1.0 and 8.0 Pascals were chosen because it was clear from Figure 5.1 that the greatest variation of the discharge coefficient occurred for pressure differences in this range. Also, it was estimated (using equation 3.31) that the pressure differences induced by the stack effect would be within this range for a two story residence.

It was determined that a 20 percent variation in the total minor loss coefficient could induce a variation in the discharge coefficient from 0.3 to 8.7 percent depending upon the magnitude of $(A\gamma)$ and the pressure difference. The following additional observations are apparent from the results presented in Figure 5.3.

1. As the total minor loss coefficient was increased the discharge coefficient decreased.
2. The greatest variation of C_z occurred for the opening described by an $(A\gamma)$ of 25.0×10^{-5} m. This opening represented an orifice and the discharge coefficient was primarily a function of K (i.e. $C_z = \sqrt{1/K}$).
3. As the value of $(A\gamma)$ was decreased from 25.0×10^{-5} m to 0.025×10^{-5} m the degree which the discharge coefficient was affected by a variation in K decreased. The magnitude of the pressure difference also began to influence the variation of C_z as $(A\gamma)$ was decreased. Therefore, openings with relatively large friction losses are less influenced by variations in the total minor loss coefficient and more influenced by variations in the pressure difference.

4. The magnitude of the pressure difference exerted the greatest influence on the variation of C_z for an $(A\gamma))$ of 0.25×10^{-5} m. Reference to Figure 5.1 indicated that this opening had the sharpest increase in the discharge coefficient with respect to ΔP.

The only parameter in the discharge coefficient equation which could not be obtained from measurements was the total minor loss coefficient (K). Therefore, an appropriate value was selected based upon the values presented in the literature and judgement.

The dimensions and geometric parameters of the rectangular openings used in the experiments were given in Table 4.1. The dimensionless flow length (z/D_h) of the rectangular openings ranged from 2.0 to 15.9 and the values of $(A\gamma)$ ranged from 0.026×10^{-5} to 3.343×10^{-5} m. It was stated previously that Etheridge (1977), experimentally determined that the average value of K was 1.5 for a set of near infinite straight rectangular openings. The data used by Etheridge was presented earlier by Hopkins and Hansford (1974) and the only slot dimensions given were the thickness (d) and the flow length (z). The aspect ratio $(\alpha = d/w)$ was assumed to be zero and the width, w, was not reported. Using the dimensions given and an aspect ratio of zero, it was determined that the minor loss coefficient of 1.5 was determined from a set of rectangular slots with dimensionless flow lengths from 0.3 to 25 $(D_h = 2d)$. The relationship to compute the area gamma product for the case of zero aspect ratio was given in equation 3.27 as:

$$(A\gamma) = \frac{d^2}{96z}$$

As a result, the slots used by Etheridge had values of ($A\gamma$) in the approximate range of 0.021×10^{-5} to 17.36×10^{-5} m. Therefore, a total minor loss coefficient of 1.5 was used for all of the rectangular openings in this study.

From Table 4.2, it can be seen that the largest cylindrical opening (Z) had a dimensionless flow length of 1.0 and an ($A\gamma$) of 19.845×10^{-5} m. It is clear from the sensitivity analysis that this cylindrical opening closely approximates an orifice. The total minor loss coefficient of an orifice is best estimated as the sum of the inlet and exit losses. Since this opening had a square edged inlet the total minor loss coefficient was assumed to be 1.5 (Fox and McDonald, 1978; ASHRAE, 1985).

The dimensionless flow lengths for openings X and Y were 7.9 and 4 respectively and the values of ($A\gamma$) were 0.313×10^{-5} for X and 1.243×10^{-5} for Y. No experimentally determined values for the total minor loss coefficients were found in the literature that were directly applicable to these two openings. Theoretically the total minor loss coefficients of these two openings would be the sum of the minor losses due to the inlet and exit losses plus the losses due to hydrodynamic development. Since all of the openings have square edged inlets the total minor loss coefficients of these two openings would be 1.5 plus any loss due to hydrodynamic development.

The magnitudes of ($A\gamma$) for the openings X and Y indicates that they may be classified as very short pipes. It is doubtful that a significant degree of hydrodynamic development would occur for either opening. Furthermore, the greatest amount of development would occur at the lowest pressure differences. At the low pressures associated with infiltration due to the stack effect, a 20 percent error in the estimate of the total minor loss coefficient would not be expected to induce a significant error in the calculation of the mass flow rate for very small openings .

The results of the sensitivity analysis given in Figure 5.3 indicated that for values of (Aγ) between 0.250 x 10^{-5} to 2.50 x 10^{-5} m a 20 percent error on the total minor loss coefficient would yield a decrease in the discharge coefficient in the range of 7 to 8 percent. Therefore the computed mass flow rate would be overpredicted by 7 to 8 percent.

The mass flow rate was computed using a K of 1.5 for openings X, Y, and Z at a pressure difference of 4.0 Pa (ρ = 1.2767 kg/m^3; ν = 1.3193 x 10^{-5} m^2/s). The resulting mass flow rates are given as follows:

for X $\quad \dot{m}$ = 7.04 x 10^{-5} kg/s (0.12 cfm);

for Y $\quad \dot{m}$ = 3.174 x 10^{-4} kg/s (0.53 cfm); and

for Z $\quad \dot{m}$ = 5.275 x 10^{-3} kg/s (8.75 cfm).

Considering the magnitudes of the mass flow rates for X and Y, a 7 or 8 percent overprediction of the mass flow rate would not constitute an appreciable error. Comparison of the size of the mass flow rates through openings X and Y relative to the mass flow through opening Z suggested than an 8 percent overprediction of the mass flows through X and Y would not induce a significant error in the prediction of the elevation of the NPA using the mass balancing procedure.

From the sensitivity analysis it was determined that the two parameters which cause the greatest variation in the discharge coefficient are the pressure difference and the area-gamma product. The variation of the air properties induced the least variation in the magnitude of the discharge coefficient. Based upon the results presented in Figure 5.3 and the information available in the literature cited, a total minor loss coefficient of 1.5 was chosen to be used with all of the cylindrical and rectangular openings in the mass balancing procedure. Furthermore, the properties of the air flowing through each opening will be computed from the temperature data at the elevation of each opening.

Chapter 6

EXPERIMENTAL DESIGN AND PROCEDURE

Experimental Design

A series of experiments were performed in the two cell environmental chamber to further investigate the factors which influence the location of the neutral pressure axis (NPA) and to test the mass balancing procedure of computing the position of the NPA. As was discussed in the review of the literature, the main factors which affect the location of the NPA for a particular opening distribution are the relative size of the individual openings, their vertical distribution and their resistance to flow (Emswiler, 1926; Lee et al. 1985). The effect of internal temperature stratification was only addressed by Emswiler (1926) on an analytical basis and in previous experimental studies it was neglected entirely. Furthermore, the variation of the mean temperature and the horizontal distribution of the openings are not believed to influence the elevation of the NPA for a particular opening distribution (Lee et al. 1985). A potential factor which has not been included in a previous investigation is the orientation of an opening in the ceiling which discharges air into a semi-enclosed space such as an attic. The opening in the test ceiling has been included to simulate this type of situation. If the air flow from the warm room significantly warms the space above the test ceiling then the elevation of the neutral pressure axis may be affected.

In an effort to make the present investigation as comprehensive as possible, the parameters varied were: the total leakage area mounted in the test sections, the vertical distribution of the openings, the size of the individual openings, the geometry of the openings, and the mean temperature difference. The geometry of the openings used varied according to the cross-sectional geometry and the flow length as shown in Tables 4.1 and 4.2. It has been shown that a variation in the geometry as well as the total pressure drop across an opening induces a variation in the flow resistance, or discharge coefficient, of an opening (Chapter 5). The stratification of temperature on both sides of the test sections was observed via the temperatures measured with the thermocouples indicated in Figure 4.14.

Several groups of openings at various vertical placements and differential temperature conditions were included in the study. A total of sixteen treatments were defined. The design of twelve of the treatments is described in Table 6.1. There were two primary purposes of the experimental design. The first objective was to determine if the variation of the mean temperature difference across the test sections has an influence on the position of the neutral pressure axis. Three mean temperature conditions classified as high, medium and low were used. Ranges of mean differential temperatures were used instead of exact temperature differences due to the limitations of the heating and cooling controls. The second objective was to ascertain if the placement of an opening in the ceiling has any intrinsic effect on the position of the NPA. In addition, it can be seen in Table 6.1 that the total opening area of the opening distribution identified as Group 2 (G2) is roughly three

Table 6.1
Opening Groups and Placements Used to Investigate the Effects of Variation of $\overline{\Delta T}$ and the Placement of an Opening in the Ceiling.

GROUP 1 - G1			GROUP 2 - G2			PLACEMENT H1	PLACEMENT H2
ID.	A (cm^2)	($A\gamma$) $\times 10^{-4}$ (m^{-1})	ID.	A (cm^2)	($A\gamma$) $\times 10^{-5}$ (m)	h (m)	h (m)
B	8.50	0.059	E	31.45	0.459	4.877	3.658
E	31.45	0.459	H	80.02	2.097	2.438	4.959*
D	16.50	0.253	F	64.31	3.343	0.152	0.152
$\Sigma A = 56.46\ cm^2$			$\Sigma A = 175.78\ cm^2$				

*An opening placed in the ceiling.

NOTE: Each of the defined opening groups were combined with the two vertical placements. Also, each opening group and placement combination was used with three ranges of ΔT. This gave twelve treatments.

times greater than the total opening area of Group 1 (G1).

The other four treatments are defined by the opening groups and placements presented in Table 6.2. All of these experiments were performed at a mean differential temperature of about 35-40°C (63-75°F). The objective was to test the application of the mass balancing procedure for a wide range of opening distributions, geometries, and total opening areas.

The two opening groups presented in Table 6.2a (REC1 and REC2) only differ by one opening. The cross-sectional area of opening F is greater than opening A by a factor of about 16. Comparison of the results of these two treatments should indicate the importance of the relative size of the openings in a distribution.

The opening distributions displayed in Table 6.2b provide a direct comparison of geometric extremes. The distribution labeled CYL contained cylindrical openings exclusively. The treatment labeled CYLREC consisted of openings with circular cross-sections and rectangular openings of small aspect ratio (0.004 and 0.0066). Another unique element of these treatments is the positioning of two openings at the same elevation. The cylindrical openings X2 and Y2 were drilled side by side in the same laminated block of acrylic. Also, the total opening areas of each of these distributions were very small.

During the initial testing of the instrumentation, several trials of differential pressure profiles were taken of the test sections alone. Each mounting location on the test section was covered with an insulated plywood plug plate. The plugs were mounted using a method analogous to that shown in Figure 4.12. For each trial a

Table 6.2
Opening Distributions and Placement of Four Treatments Defining Additional Variations of Opening Geometry and Placement.

Table 6.2a

$\overline{\Delta T}$ = 35–40°C

REC 1			REC 2			PLACEMENT
ID.	A (cm^2)	($A\gamma$) $x10^{-5}$ (m)	ID.	A (cm^2)	($A\gamma$) $x10^{-5}$ (m)	h (m)
C	10.00	0.327	C	10.00	0.327	4.959*
F	64.31	3.343	A	4.00	0.026	3.657
D	16.50	0.253	D	16.50	0.253	2.438
E	31.45	0.459	E	31.45	0.459	0.152
ΣA = 122.26 cm^2			ΣA = 61.95 cm^2			

*An opening placed in the ceiling.

Table 6.2b

$\overline{\Delta T}$ = 35–40°C

CYL				CYLREC			
ID.	A (cm^2)	($A\gamma$) $x10^{-4}$ (m)	h (m)	ID.	A (cm^2)	($A\gamma$) $x10^{-4}$ (m)	h (m)
X2	0.32	0.313	4.877	C	10.00	0.327	4.877
Y2	1.27	1.243	4.877	Y1	1.27	1.243	3.658
Y1	1.27	1.243	3.658	D	16.50	0.253	2.438
X1	0.32	0.313	2.438	Y2	1.27	1.243	0.152
Z1	20.27	19.845	0.152	X2	0.32	0.313	0.152
ΣA = 23.45 cm^2				ΣA = 29.36 cm^2			

Note: X2 and Y2 were drilled in the same block of plexiglass.

neutral pressure axis was observed at an elevation above the floor. This gave evidence of leakage in the facility. Many attempts were made to locate the source of leakage and eliminate it. Extra foil tape was applied at seams in the interior finish which appeared to have pulled away from the surface. The access door of the cold room was covered with a sheet of polyethylene plastic and sealed to the exterior with duct tape. Likewise, each opening mounting location was covered with a piece of heavy plastic and sealed to the test wall (or ceiling) with foil tape whenever it was not in use. This can be seen in Figure 4.13. All attempts to totally eliminate the leakage in the environmental chamber were unsuccessful. The only effect was to vary the position of the NPA observed. The position of the NPA changed as the leakage characteristic of the environmental chamber was changed by the attempts to completely seal the facility. The leakage inherent to the two cell environmental chamber was termed the background leakage. A typical differential pressure profile when a ΔT of 30°C existed across the test sections is shown in Figure 6.1.

In order to take the background leakage into account in the prediction of the NPA by the mass balancing procedure, four treatments were added to the experiment. The differential pressure profile of the background leakage was observed at the four ranges of differential temperature conditions used by the other 16 treatments. These treatments were termed the no cracks situation (NC). The twenty treatments have been summarized in Table 6.3. Each of the twenty treatments was replicated three times.

Experimental Procedure

The presence of the background leakage was not the only

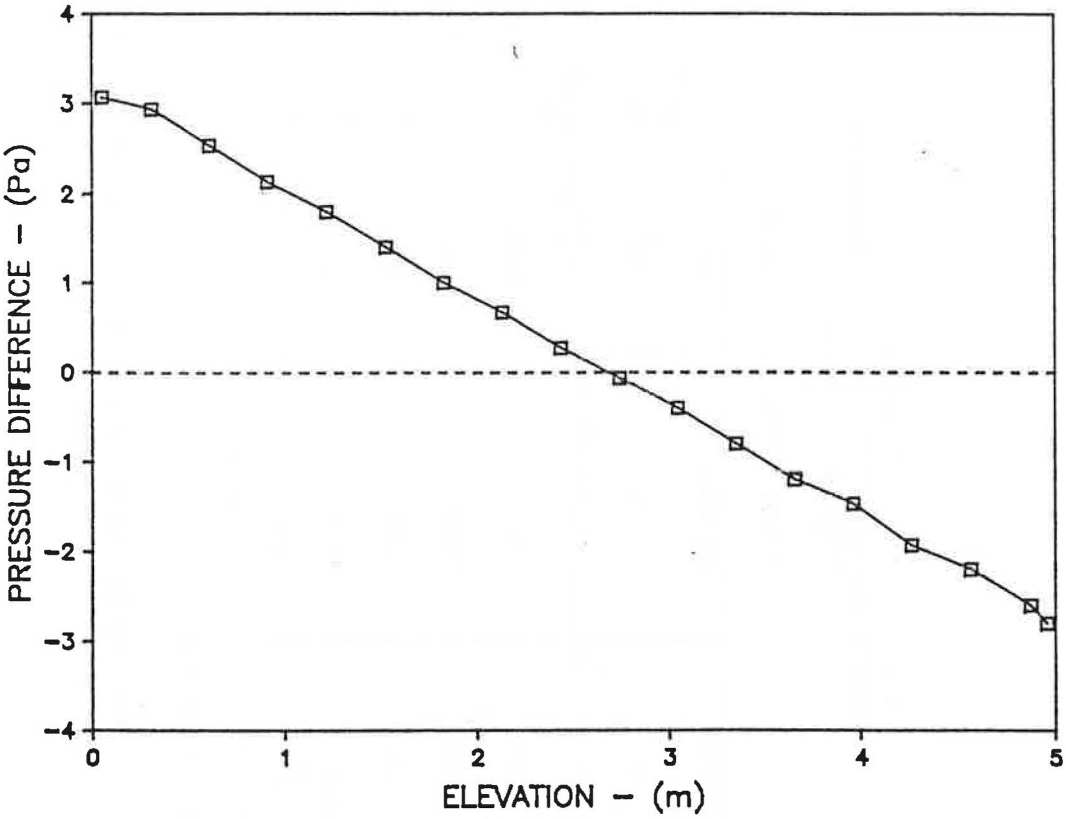

Figure 6.1 A typical differential pressure profile observed for the background leakage.

Table 6.3
Combinations of Opening Group, Placement, and Temperature Conditions

TEMPERATURE CONDITIONS

	HIGH	MEDIUM	LOW	
	T1	T2	T3	T35
	$\overline{\Delta T}$ = (40-45°C)	$\overline{\Delta T}$ = (25-30°C)	$\overline{\Delta T}$ = (15-20°C)	$\overline{\Delta T}$ =(35-40°C)
OPENING	G1H1	G1H1	G1H1	REC1
GROUP	G1H2	G1H2	G1H2	REC2
AND	G2H1	G2H1	G2H1	CYL
PLACEMENT	G2H2	G2H2	G2H2	CYLREC
COMBINATIONS	NC*	NC	NC	NC

* NC - No Cracks

Note: Three replications were made for each treatment to give a total of 60 observations.

complication that was discovered during the initial trials. Entering the warm room disturbed the differential pressure profile in two ways. Opening the access door caused a suction on the warm side and the warm side was pressurized when the door was closed (both access doors opened to the outside). The excess pressure then bled out of the chamber through the cracks around the access door. As a result, a period of time was required for the differential pressure profile to redevelop. The profile became stable again once the air flow through the openings mounted in the test sections reached equilibrium.

The measurement of consecutive differential pressure profiles immediately after entering the chamber revealed that while the air flow between the two rooms was equilibrating the position of the NPA would tend to either rise or fall and the distribution of the pressure differences tended to become more linear. It was assumed that the system attained equilibrium when the elevation of the neutral pressure axis remained constant. It was found that the time required for the system to equilibrate was a function of the total opening area placed in the test sections and the mean temperature difference between the two rooms. The opening distributions with the larger total opening areas would reach steady conditions more rapidly than the distributions with smaller opening areas. The treatments performed at the relatively high differential temperatures (i.e. $\overline{\Delta T}$ = 40-45°C) also tended to equilibrate faster. The data presented in Figures 6.2a and 6.2b allow a comparison between trials for the opening groups G1 mounted at the elevations defined by placement H2 at the two extreme differential conditions (T1 and T3).

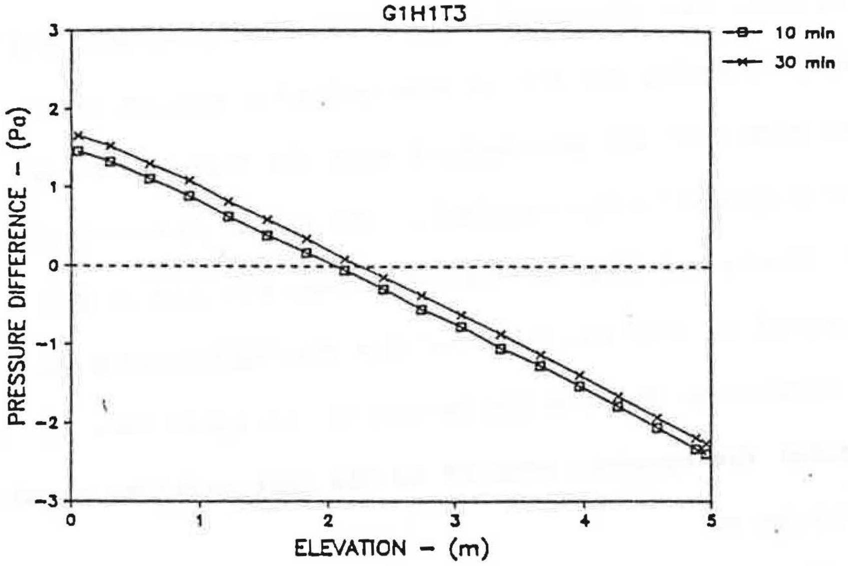

Figure 6.2a.

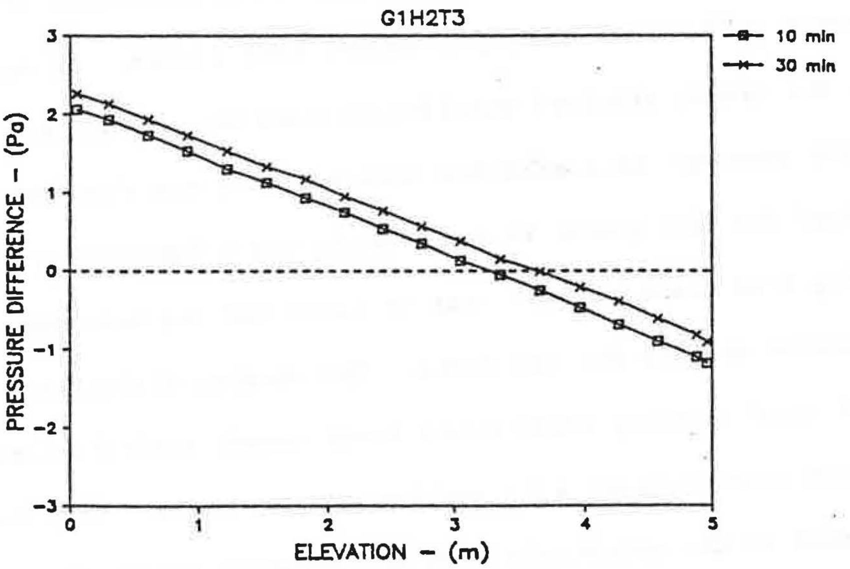

Figure 6.2b.

Figure 6.2 Variation of the differential pressure profile with respect to time after entering the warm room.

Table 6.4 indicates the length of time allowed for each treatment to attain equilibrium and the time intervals used for the measurement of the differential pressure profiles and the temperatures. These intervals were determined from trial runs and were used to ensure that equilibrium was obtained.

Reference to Figure 4.9 shows that a total of twenty pairs of static pressure taps were installed in the test sections. Eighteen pairs were mounted in the wall and two sets of pressure taps were mounted in the ceiling. After several days of maintaining the cold room at about -25°C (-13 °F) the two pressure taps on the cold side of the test ceiling became clogged with ice. The only way to remove the ice was to warm the cold side until the ice melted and then remove the moisture from the tubes by means of a small hand operated vacuum pump. This procedure proved to be futile because the taps would freeze again after just a few days of operation. As a result, only the eighteen pairs of pressure taps mounted in the test wall were used. In order to prevent the freezing of pressure taps on the cold side of the test wall, all of the remaining pressure taps were evacuated of moisture twice a day using a hand operated vacuum pump.

Considering the complications discussed, the experimental procedure for each replication of each treatment is summarized as follows.

1. The openings were mounted in the test sections at the appropriate elevations.
2. The mounting plates that were not used were covered with a piece of heavy plastic and sealed to the surface of the test sections using foil tape.

Table 6.4
Total Time Allowed for Each Treatment to Reach Equilibrium and the Intervals Over Which the ΔP Profiles were Checked

TEST ID.	TOTAL TIME ALLOWED (min.)	MEASUREMENT INTERVAL (min.)
G1H1T1	25	5
G1H1T2	50	10
G1H1T3	50	10
G1H2T1	25	5
G1H2T2	50	10
G1H2T3	50	10
G2H1T1	20	5
G2H1T2	40	10
G2H1T3	40	10
G2H2T1	20	5
G2H2T2	40	10
G2H2T3	40	10
REC1	25	5
REC2	30	5
CYL	40	10
CYLREC	30	10
NCT1	30	5
NCT2	80	20
NCT3	80	20
NC35*	40	10

*Indicates ΔT range used with REC1, REC2, CYL and CYLREC.

3. The sheet of polyethylene plastic covering the door to the cold room was periodically checked. If the tape had pulled away from the exterior of the environmental chamber then more tape was applied.
4. The mean temperatures of the warm room and the cold room were monitored from the exterior using the digital thermometer.
5. Once the desired mean differential temperature was attained, the dew point of the cold room was measured using the thermocouple placed downstream from the evaporator (see Figure 4.14).
6. The refrigeration system was turned off.
7. Upon entering the warm room, the door was closed, the timer was started and the heating system and the paddle fan were turned off.
8. The mechanical psychrometer was started (3 minutes of operation was required for a reading).
9. The interior of the door to the warm room was covered with polyethylene plastic and sealed with foil tape to a strip of cloth duct tape around the perimeter of the door. It should be noted that the time required to begin the wet bulb measurement and to tape the plastic over the access door was more than adequate for the excess pressure in the warm room to bleed out through the cracks around the door.
10. The wet bulb temperature was recorded.
11. Differential pressure measurements were taken at the time intervals shown in Table 6.4 according to the following

procedure.

a. The data logger was manually activated to scan all thermocouples.

b. The differential pressure profile was measured (approximately 4 min required).

c. The data logger was again manually activated to scan all thermocouples.

d. The starting and ending temperature measurements were averaged to give a single temperature profile for each room.

12. Once the final set of differential pressure and temperature data was obtained the heating and cooling systems were reactivated.

13. Several hourly barometric pressure readings were obtained during the period over which data was taken. All of the barometric pressure readings for a particular day were averaged and the mean was used to compute the air properties for all of the replications performed on that day.

Determination of the Elevation of the NPA and the Mean Density Difference from the Observed Differential Pressure Profiles

The differential pressure data for each replication was fitted to a linear equation of the following form:

$$y = a + b\,x \tag{6.1}$$

Where, the independent variable was the elevation and the dependent variable was the pressure difference. It can be seen that the slope (b) and the y-intercept (a) have physical significance by expanding equation 3.31 to give:

$$\Delta P = \Delta\rho g\ N - \Delta\rho\ g\ h \tag{6.2}$$

where; ΔP = the differential pressure (Pa),

h = the elevation (m),

$\Delta\rho$ = the mean density difference (kg/m^3),

N = the elevation of the NPA (m), and

g = the acceleration due to gravity (m/s^2).

Comparing equation 6.2 to 6.1 indicates that the slope of the regression equation is always negative and it is equal to the product of the acceleration due to gravity and the mean density difference. Therefore, the mean density difference may be estimated by:

$$\Delta\rho = |b/g| \tag{6.3}$$

In the same manner, the elevation of the NPA may be computed from the constants of the regression equation by:

$$N = |a/b| \tag{6.4}$$

The relationships used to compute the slope, the y-intercept, the coefficient of determination, and the respective 95 percent confidence intervals are presented in detail in Appendix D.

Chapter 7

ANALYSIS AND RESULTS

Results of Regression On the Observed Differential Pressure Profiles

The differential pressure and temperature measurements, the computed mean air properties and the results of the regression procedure for each replication of all of the treatments are presented in Appendix E. Sixty differential pressure profiles were obtained (20 treatments x 3 replications). As was expected, there was a high degree of linear correlation between the pressure difference measurements and the elevation of measurement. The coefficients of determination (r^2) of 59 of the 60 profiles observed were between 0.99916 and 0.99992. These high levels of correlation yielded 95 percent confidence intervals for the positions of the NPA from $\pm$0.7 cm ($\pm$0.276 in.) to $\pm$2.5 cm ($\pm$0.984 in.). The corresponding range of 95 percent confidence intervals of the slope of the regression equation (Pa/m) was $\pm$0.47 to $\pm$1.53 percent. The lowest coefficient of determination was for the third replication of NCT3 in which the value of r^2 was 0.99861 and the 95 percent confidence intervals were $\pm$3.1 cm ($\pm$1.220 in.) for the NPA and $\pm$1.98 percent for the slope. In summary, the location of the NPA was known to within $\pm$ 3.1 cm ($\pm$1.22 in) for all cases.

The range of 95 percent confidence intervals for the slope of the regression equation have been expressed as percentages because the confidence interval of the mean density difference (as computed by equation 6.3) is equivalent to the confidence interval of the slope in percent. The regression procedure was the only practical way to ''observe'' the elevation of the NPA and the slope of the regression equation yielded the best estimate of the mean density difference between the cold and warm rooms. Therefore, the confidence intervals for the NPA and the mean density difference were considered analogous to uncertainties of measurement. Each of the 95 percent confidence intervals are based upon an estimate of the variance about each individual regression line with sixteen degrees of freedom (refer to Appendix D).

The elevations of the NPA for each treatment along with the treatment means and standard deviations are presented in Table 7.1. A survey of the data in the table affords several important observations.

a. The relative size of the openings in a group and the vertical distribution of the openings induced a large variation in the elevation of the NPA.

b. A comparison of all the treatments involving opening groups G1 and G2 indicated that the variation in the elevation of the NPA was greater when the openings were distributed according to placement H2 than placement H1. The primary difference between the two placements was an opening was placed in the test ceiling for H2. In addition, the greatest variability occurred for the three treatments involving G1H2.

c. Comparison of the No Cracks (NC) treatments with the original sixteen treatments indicates that in general the variability of the No Cracks data was greater than all other treatments.

Table 7.1
Observed Elevations of the NPA (cm)

Opening Group and Placement		T1	T2	T3	Opening Group and Placement	T35
	Rep 1	220.5	224.9	222.9		305.9
G1H1	Rep 2	221.1	221.6	221.3	REC1*	305.6
	Rep 3	220.8	218.6	224.9		304.2
	Mean	220.8	221.7	223.0		305.2
	std. dev.	0.30	3.15	1.80		0.91
	Rep 1	349.2	353.9	361.5		155.2
G1H2*	Rep 2	350.2	360.2	361.6	REC2*	152.2
	Rep 3	347.2	349.6	365.5		151.1
	Mean	348.9	354.6	362.9		152.8
	std. dev.	1.53	5.33	2.28		2.12
	Rep 1	206.2	211.0	206.3		76.0
G2H1	Rep 2	207.9	207.5	205.0	CYL	78.5
	Rep 3	209.0	207.8	209.2		75.3
	Mean	207.7	208.8	206.8		76.6
	std. dev.	1.41	1.94	2.15		1.68
	Rep 1	313.5	318.1	320.6		292.2
G2H2*	Rep 2	315.6	322.5	317.1	CYLREC	293.3
	Rep 3	315.8	318.5	318.4		291.6
	Mean	315.0	319.7	318.7		292.4
	std. dev.	1.27	2.43	1.77		0.86
	Rep 1	261.9	310.2	284.4		312.0
NC	Rep 2	256.2	258.1	307.9		280.8
	Rep 3	259.5	268.9	272.9		280.6
	Mean	259.2	279.1	288.4		291.1
	std. dev.	2.86	27.50	17.84		18.07

*Placements with an opening mounted in the test ceiling.

NOTE: For T1 ΔT = 40-45°C
For T2 ΔT = 25-30°C
For T3 ΔT = 15-20°C
For T35 $\Delta T \cong$ 35°C

Sample differential pressure profiles for G1H1, G1H2, G2H1, G2H2 and NC have been presented in Figures 7.1 through 7.5. For clarity only the data for two of the three replications for each range of mean temperature difference are shown. The replications with the highest and lowest mean temperature differences were chosen since the third replication was between these two extremes.

The data in the 5 figures indicated that the variation of the mean temperature difference had little if any effect on the position of the NPA. It can also be seen that the slope of the differential pressure profiles, and in turn the magnitudes of the pressure differences, were a function of the mean temperature differences. The additional variation of the elevation of the NPA for the placement H2 may be clearly seen by comparison of the profiles given in Figures 7.1 through 7.4. In addition, a comparison between all five figures provides further evidence that the variance of the location of the NPA for the No Cracks treatments and the other sixteen treatments were different. As a result, the original sixteen treatments and the No Cracks treatments were considered to be two independent blocks of data.

In order to determine if the observed differences in the treatment means were significant, a one-way analysis of variance was performed on each block of data independently. The results of the analysis of variance for the No Cracks data has been displayed in Table 7.2 and the analysis of variance for the original sixteen treatments has been shown in Table 7.3.

The overall variance of the No Cracks treatments was shown to be significantly greater than the overall variance of the original

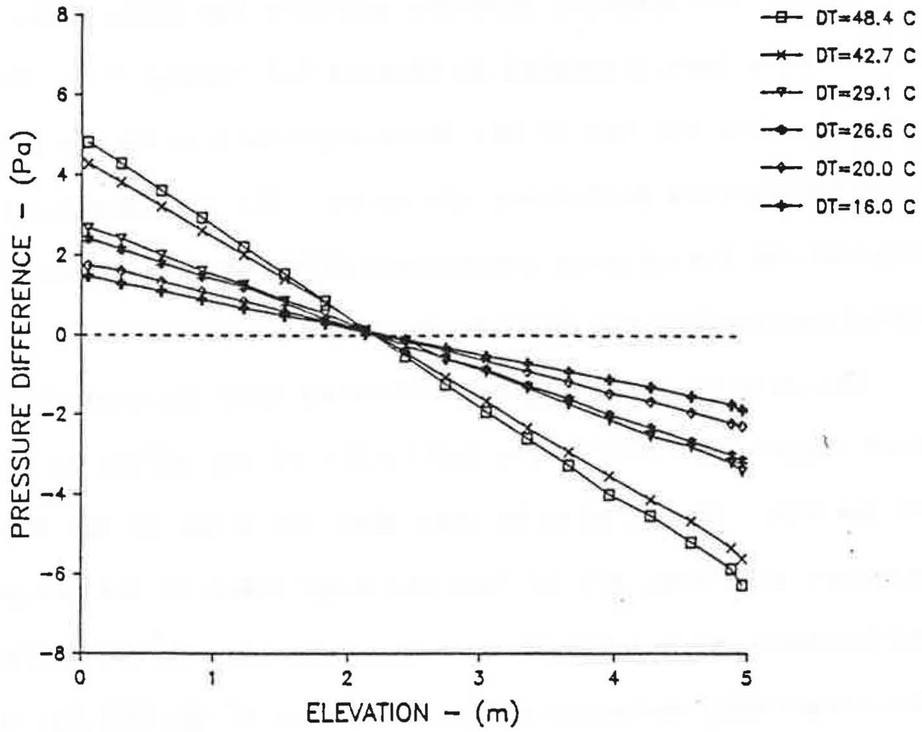

Figure 7.1 Differential pressure profiles for G1H1.

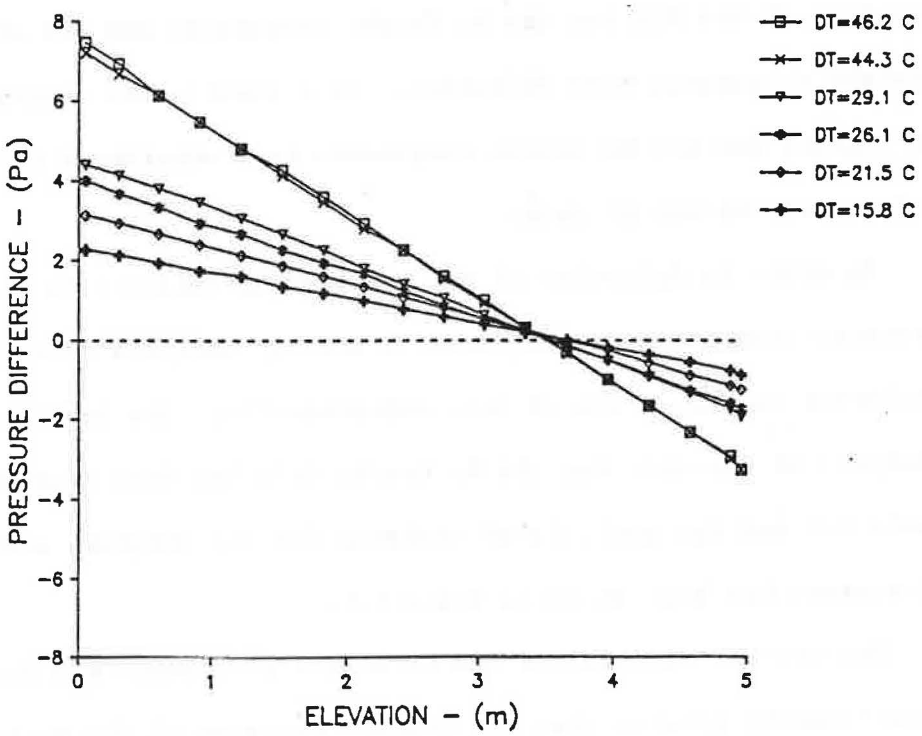

Figure 7.2 Differential pressure profiles for G1H2.

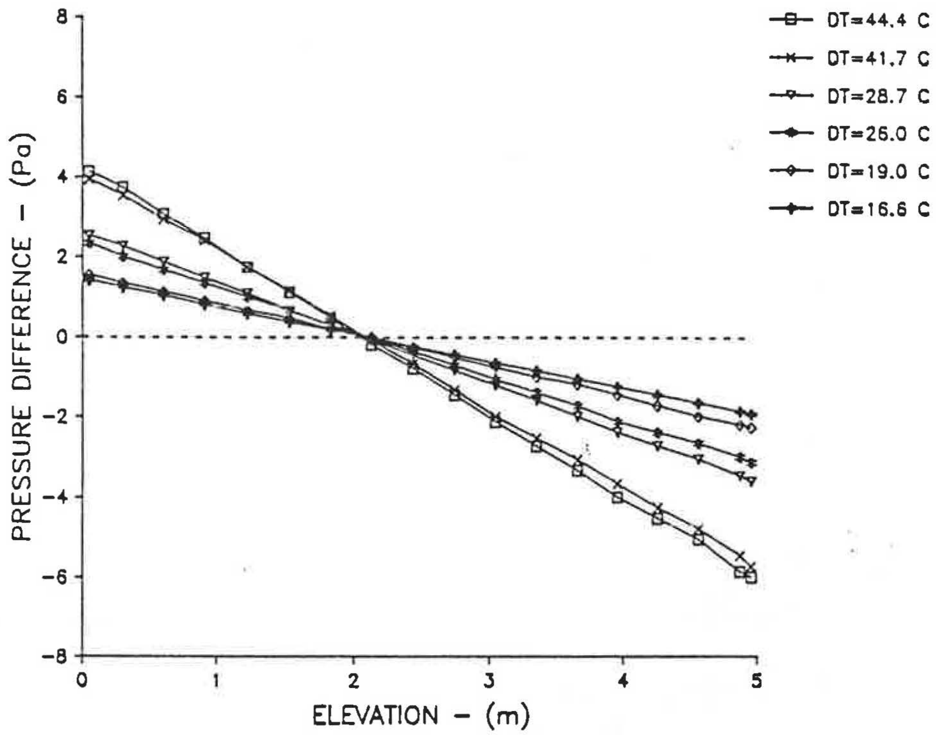

Figure 7.3 Differential pressure profiles for G2H1.

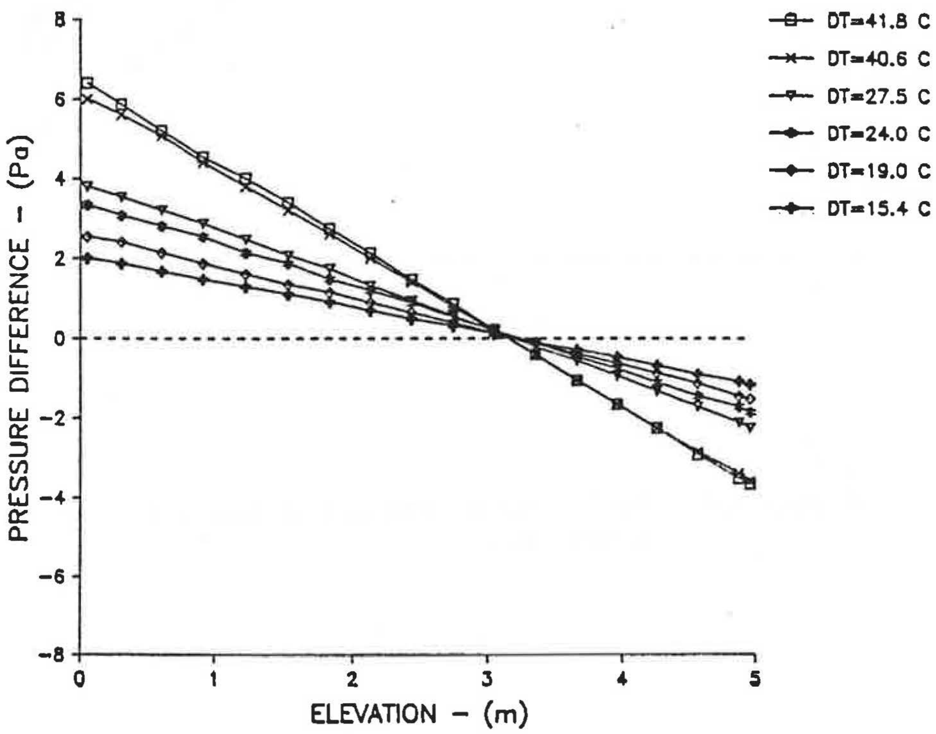

Figure 7.4 Differential pressure profiles for G2H2.

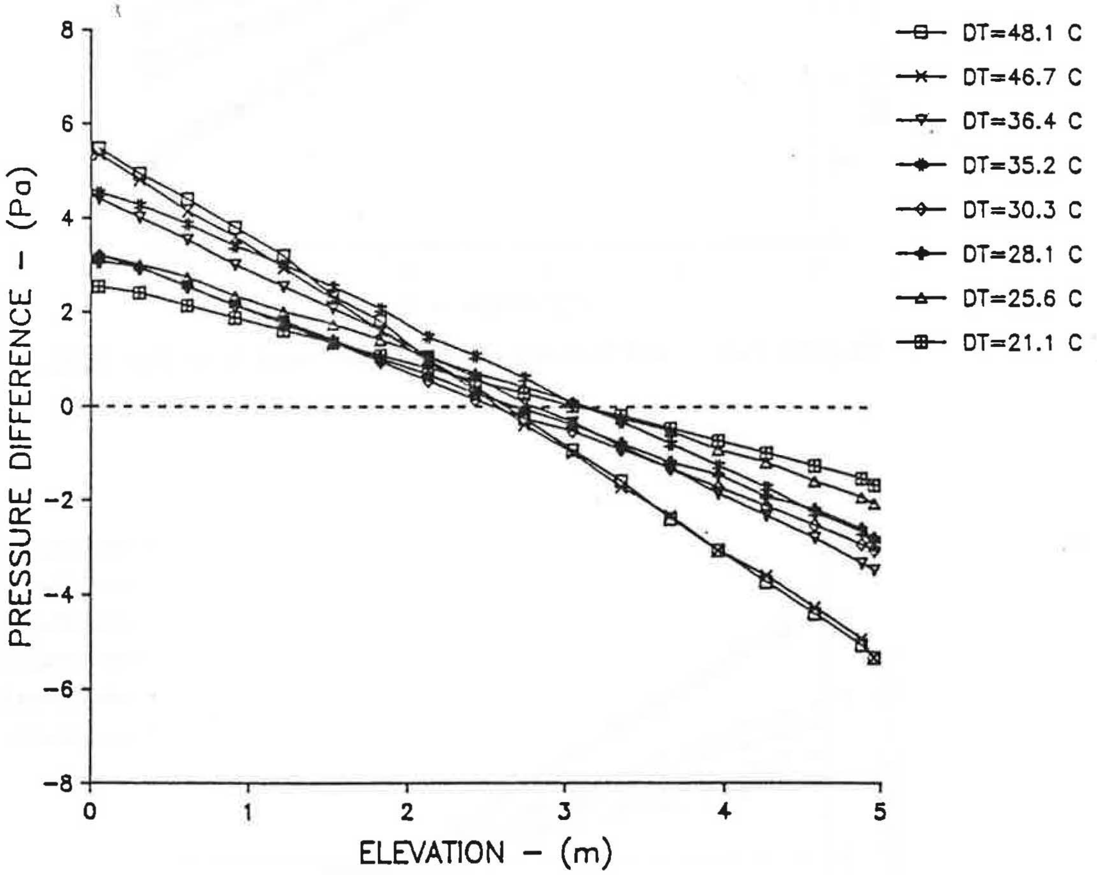

Figure 7.5 Differential pressure profiles for the No Cracks treatments.

Table 7.2
Analysis of Variance for the No Cracks Data

Source of Variation	df	SS	MS	F
Treatment	3	1880.4367	626.8122	1.799^{ns}
Error	8	2818.2733	352.2842 = s_y^2	
Total	11	4698.7100		

ns - Not significant.

s_y = 18.7692 cm

Standard Error = $\sqrt{s_y^2/r}$ = 10.8364 cm

Grand Mean NPA = 279.5 cm

95% Confidence Interval = $\pm$25 cm

Table 7.3
Analysis of Variance for All Treatments
Excluding the No Cracks Data

Source of Variation	df	SS	MS	F
Treatment	15	294558.6123	19637.2408	3968.0011**
Error	32	158.3667	4.9489 = s_y^2	
Total	47	294716.9790		

** - Significant to the .01 level.

s_y = 2.2246 cm

Standard Error = $\sqrt{s_y^2/r}$ = 1.2844 cm

95% Confidence Interval = $\pm$2.6 cm

sixteen other treatments by performing a two-tailed F-test on the variances of the two blocks of data. The estimate of the variance (s_y^2) of each of the populations is equivalent to the mean square (MS) of the error in the respective analysis of variance tables. The F-statistic was computed as follows (Steel and Torrie, 1980):

$$F = \frac{\text{the larger } s_y^2}{\text{the smaller } s_y^2} = 71.18$$

The degrees of freedom for the numerator and the denominator were equivalent to the error degrees of freedom associated with each variance. The tabulated F-statistic was found to be:

$F_{0.005\ (8,32)} = 3.53$

Since the computed F was greater than the tabulated value the two variances were significantly different at the 1 percent level. Therefore, it would be incorrect to pool the No Cracks treatment with the other sixteen treatments.

The conclusions from the two analysis of variance tables as well as the factors which caused the variation in the position of the NPA will be discussed independently in the following sections.

Variation of the No Cracks Treatments

The analysis of variance of the observed positions of the NPA for the No Cracks data indicated that the difference between the treatment means was not significant. The mean of all twelve elevations of the NPA was 279.5 cm and the 95 percent confidence interval about the grand mean was $\pm$25 cm.

Examination of the differential pressure profiles gave no indication of any type of systematic error. Likewise, the temperature data for each room was examined and nothing unusual was found.

It was concluded that the variation of the position of the NPA for the No Cracks data was due to a variation of the background leakage of the two cell environmental chamber. A plot of the position of NPA for all of the No Cracks treatments with respect to time has been presented in Figure 7.6. The unit of time used was the day on which data were taken (a table relating day number to the date is given in Appendix E).

The variation of the elevation of the NPA shown in the figure was the result of the variation of the leakage of the two cell environmental chamber (or background leakage). Probably the greatest source of variation was the result of not being able to exactly replicate the sealing of the mounting plates that were not in use. The plywood mounting plates were generally much colder than the temperature of the warm room. As a result, condensation periodically formed on the mounting plates, ran down the test wall, and caused the duct tape which created the seal between the plastic covering the mounting plate and the test wall to loosen. The next most likely source of variation in the background leakage was the loosening of the duct tape which held the plastic cover over the exterior of the cold room door. The balloon action caused by the cold air attempting to flow out of the cold room caused the tape to pull away. Whenever this occurred the tape was replaced.

Variation of the NPA for the Original Sixteen Treatments

The analysis of variance shown in Table 7.3 indicated that the difference between the treatment means was highly significant. A 95

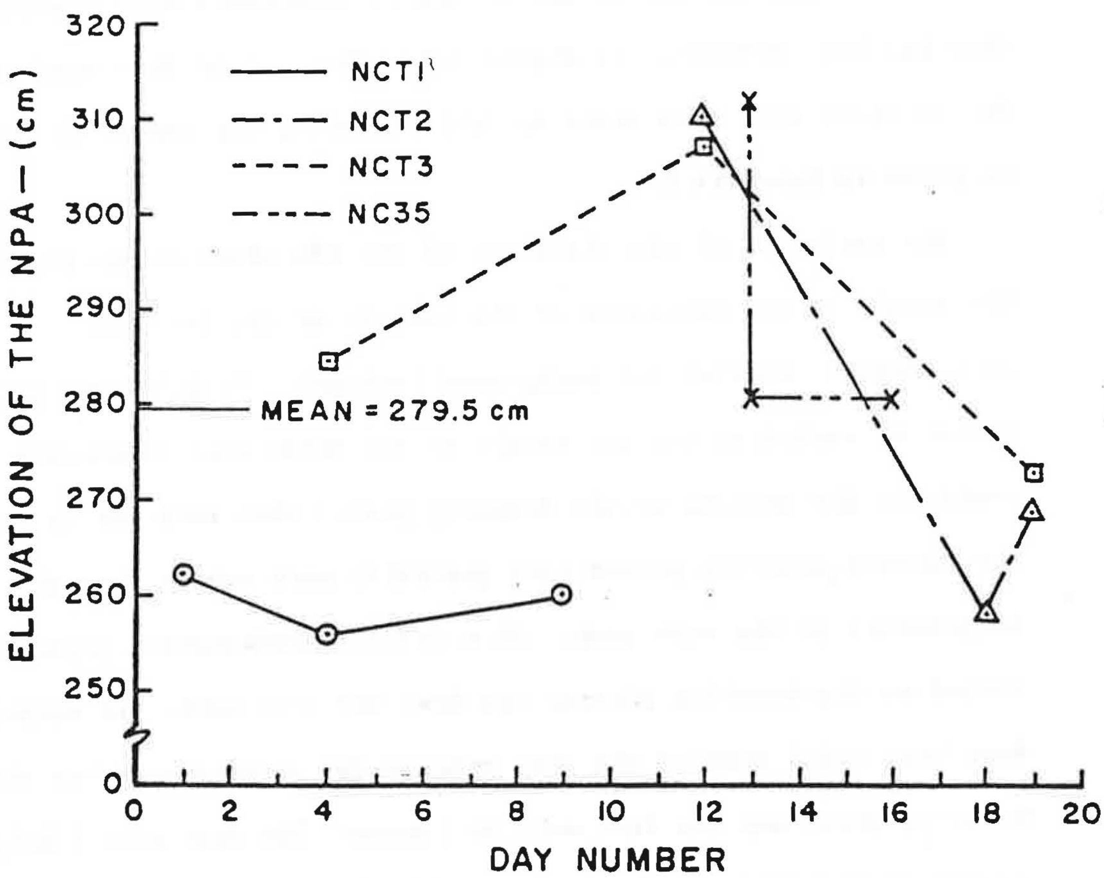

Figure 7.6 **Variation of the position of the NPA for the No Cracks treatments with respect to the day on which data were taken.**

percent confidence interval about any treatment mean was determined from the standard error to be ±2.6 cm.

The least significant difference method (Steel and Torrie, 1980) was used to determine if there was a significant variation of the NPA with respect to the mean temperature difference. The comparisons between the treatment means of G1H1, G1H2, G2H1 and G2H2 have been given in Table 7.4.

From the comparisons between the selected treatment means it was observed that:

a. When both opening groups (G1 and G2) were mounted in the test wall at the elevations defined by placement H1 no significant variation of the NPA with respect to the mean temperature difference was observed;

b. When one of the Group 1 openings was mounted in the test ceiling as defined by placement H2 the differences between the three treatment means were significant to the 1 percent level; and

c. When the Group 2 openings were mounted in the test sections according to placement H2 the only significant difference was between the means of the treatments G2H2T1 and G2H2T2 (high and medium ΔT).

The position of the NPA varied significantly with variation of the mean temperature difference only for the cases when an opening was mounted in the test ceiling (placement H2). Therefore, it was concluded that the placement of an opening in the test ceiling had some influence on the position of the NPA.

Table 7.4
Comparison of Select Treatment Means Using the
Least Significant Difference Method (LSD)

$$LSD = t_{\alpha/2(\text{error df})} \sqrt{2 s_y^2 / r}$$

LSD(.05) =3.7 cm LSD(.01)=5.0 cm
* - Significant to the 5% Level
** - Significant to the 1% Level

G1H1T1 N=220.8	G1H1T2 N=221.7	G1H1T3 N=223.0
|<----0.9---->|	|<----1.3---->|	
|<------------2.2------------>|		
G1H2T1 N=348.9	G1H2T2 N=354.6	G1H2T3 N=362.9
|<----5.7**---->|	|<----8.3**---->|	
|<------------14.0**------------>|		
G2H1T1 N=207.7	G2H1T2 N=208.8	G2H1T3 N=206.8
|<----1.1---->|	|<----2.0---->|	
|<------------0.9------------>|		
G2H2T1 N=315.0	G2H2T2 N=319.7	G2H2T3 N=318.7
|<----4.7*---->|	|<----1.0---->|	
|<------------3.7------------>|		

Note: For T1 ΔT = 40-45°C
For T2 ΔT = 25-30°C
For T3 ΔT = 15-20°C

Examination of the treatment means in Table 7.4 indicated that when an opening was located in the test ceiling the NPA tended to assume a higher elevation at the lower mean temperature differences. The only exception was for the treatment G2H2T3 where the mean of the three replications was slightly lower than for G2H2T2.

Noting that the direction of air flow is upward for an opening in the ceiling, it was hypothesized that the weight of the air above an opening in the ceiling would induce a body force in the direction opposite to the flow of air. Such a force would cause an additional flow restriction for an opening placed in the test ceiling. Also, the magnitude of the body force would be directly proportional to the density of the air above the test ceiling. According to theory, the NPA assumes a position such that the mass flow into the warm room is equal to the mass flow out. In order to maintain continuity of mass flow, the position of the NPA would be expected to move slightly downward as the density above the ceiling increased. The downward shift of the NPA would compensate for the added flow restriction in two ways. A lower NPA would result in a higher pressure difference across the ceiling to overcome the effects of the body force and lower pressure differences below the NPA would reduce the total mass flow into the warm room. The position of the NPA would be expected to be lower for the higher temperature differences.

The variation of the elevation of the NPA with respect to the air density above the test ceiling for the opening group and placement conditions of G1H2 and G2H2 have been presented in Figures 7.7 and 7.8, respectively. The density of the air above the ceiling was computed from the barometric pressure and temperature data for each

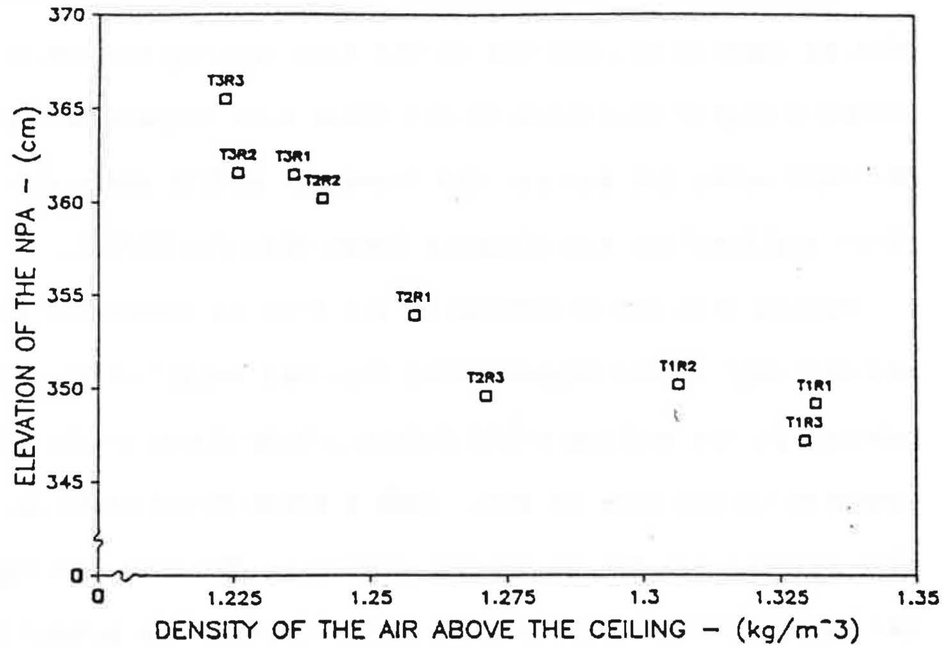

Figure 7.7 Variation of the NPA for the case of an opening in Group 1 placed in the ceiling.

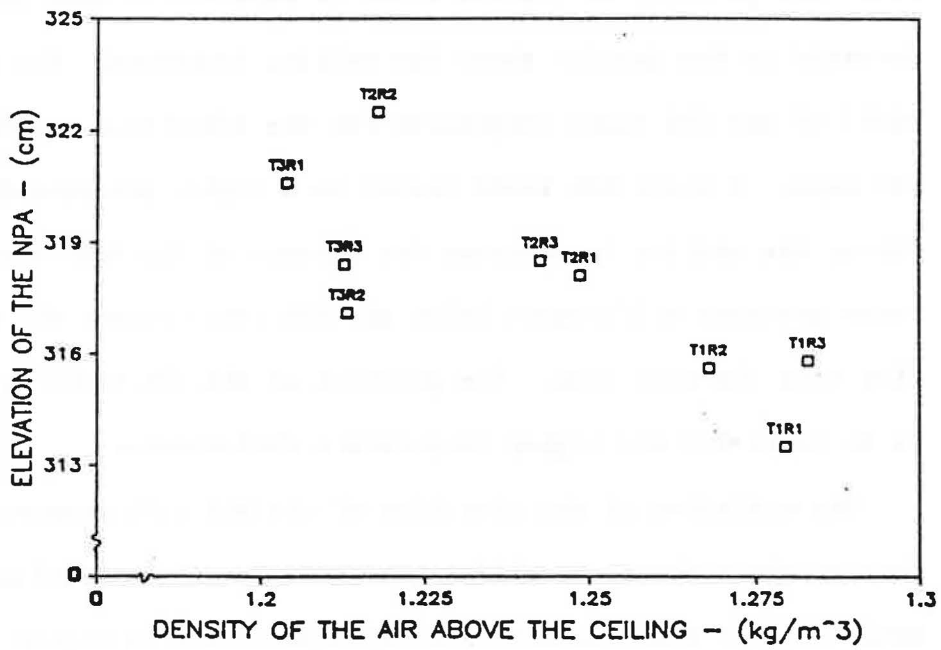

Figure 7.8 Variation of the NPA for the case of an opening in Group 2 placed in the ceiling.

replication using the relationships provided in Appendix C. Each of the observed elevations was labeled to designate the temperature difference range and the replication number. The two figures suggest that the variation of the density of the air above the test ceiling was the source of the significant differences between the treatment means indicated in of Table 7.4.

Observed Temperature Stratification

To observe the stratification of temperature of both rooms the differences between the mean room temperature and the individual temperature measurements on the cable were plotted against the elevation of measurement. The greatest amount of temperature stratification was observed for the opening group G2 at the greatest temperature differences (T1). A sample plot for each of the placement conditions (H1 and H2) have been presented in Figures 7.9 and 7.10, respectively. An opening was placed at 0.152 m (0.5 ft) for each of the sixteen original treatments. The cold air which entered the warm room would settle near the floor. Consequently the temperature near the floor of the warm room was generally considerably cooler than the temperature observed at any other elevation. As would be anticipated, the warmest temperatures observed in the cold room were near the top of the test wall and in the space above the test ceiling (thermocouple number 18 and 19 in Figure 4.14). The space above the test ceiling was significantly warmer whenever an opening was mounted in the test ceiling as indicated by the data in Figure 7.10.

Figure 7.9 represents the typical temperature variation observed for all of the treatments that did not include an opening placed in

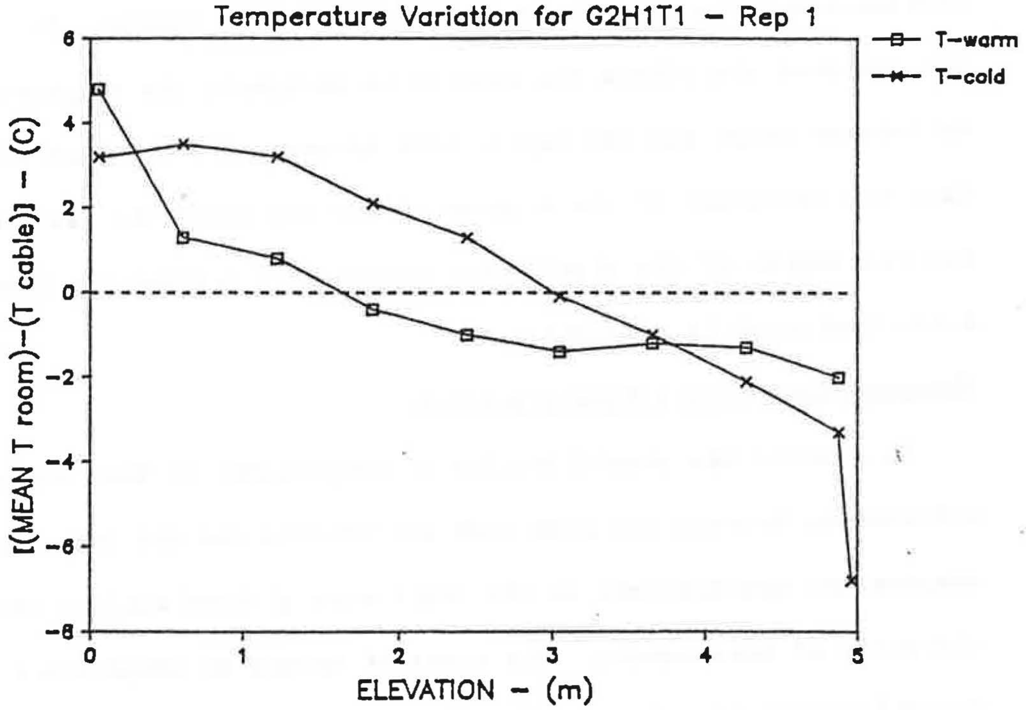

Figure 7.9 Temperature stratification for distributions without an opening in the ceiling.

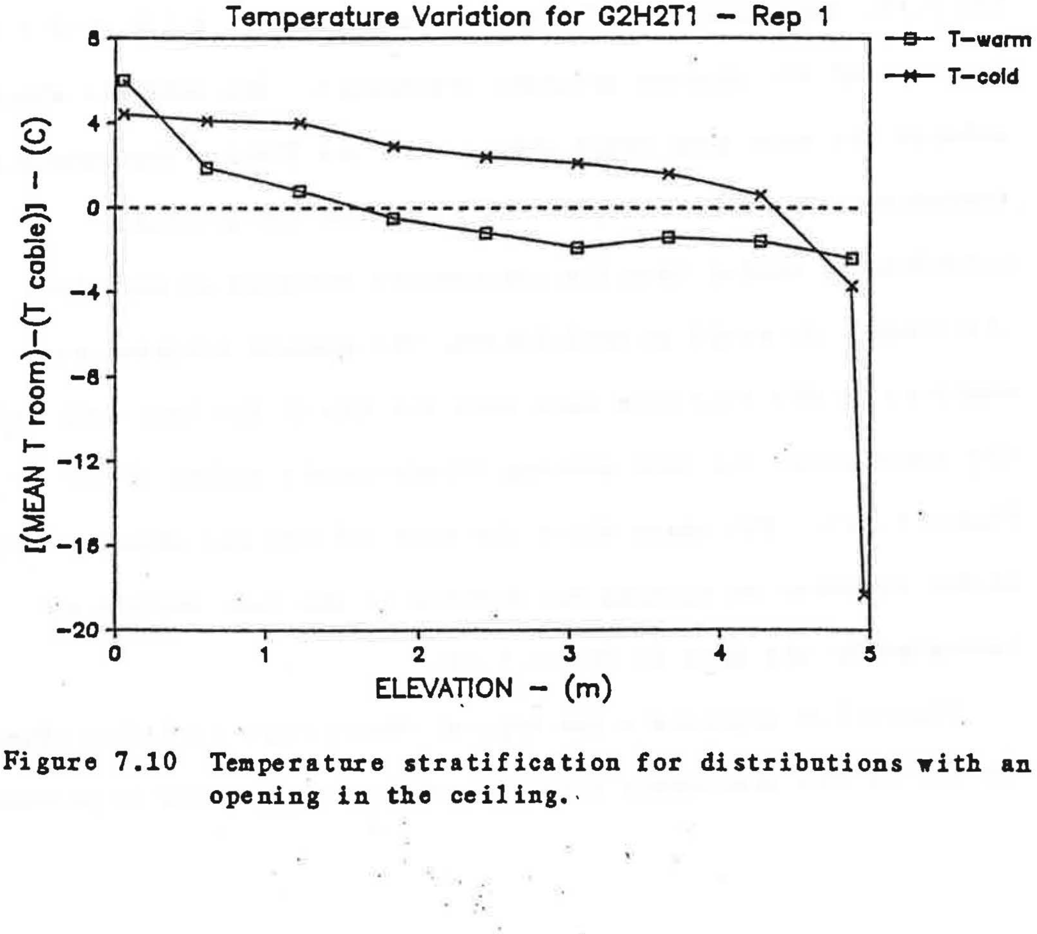

Figure 7.10 Temperature stratification for distributions with an opening in the ceiling.

the ceiling. Figure 7.10 describes the typical variation of temperature for all of the treatments for which an opening was mounted in the ceiling. Since the cases presented here are for high differential temperature conditions most of the differences between the mean room temperature and individual temperature measurements were less than those shown.

In order to determine if the observed degree of temperature stratification had a significant influence on the prediction of the differential pressures the following computations were performed on each of the sixty sets of differential pressure and temperature data:

1. The differential pressures were predicted using the regression equations and compared with the measured values;
2. A 95 percent prediction interval (refer to Appendix D) was computed about each predicted value of ΔP;
3. The residuals were compared with the prediction intervals; and
4. The density difference was computed at each elevation of temperature measurement.

It was found that only 8 (0.7%) of the 1080 (60 x 18) data points were outside of the 95 percent prediction intervals. A typical plot of the residuals and the 95 percent prediction intervals has been provided in Figure 7.11.

Based upon a detailed inspection of the variation of $\Delta\rho$ with respect to elevation, and the high levels of linear correlation of the differential pressure measurements with respect to elevation it was determined that the observed degree of temperature stratification did not have a significant influence on the differential pressure

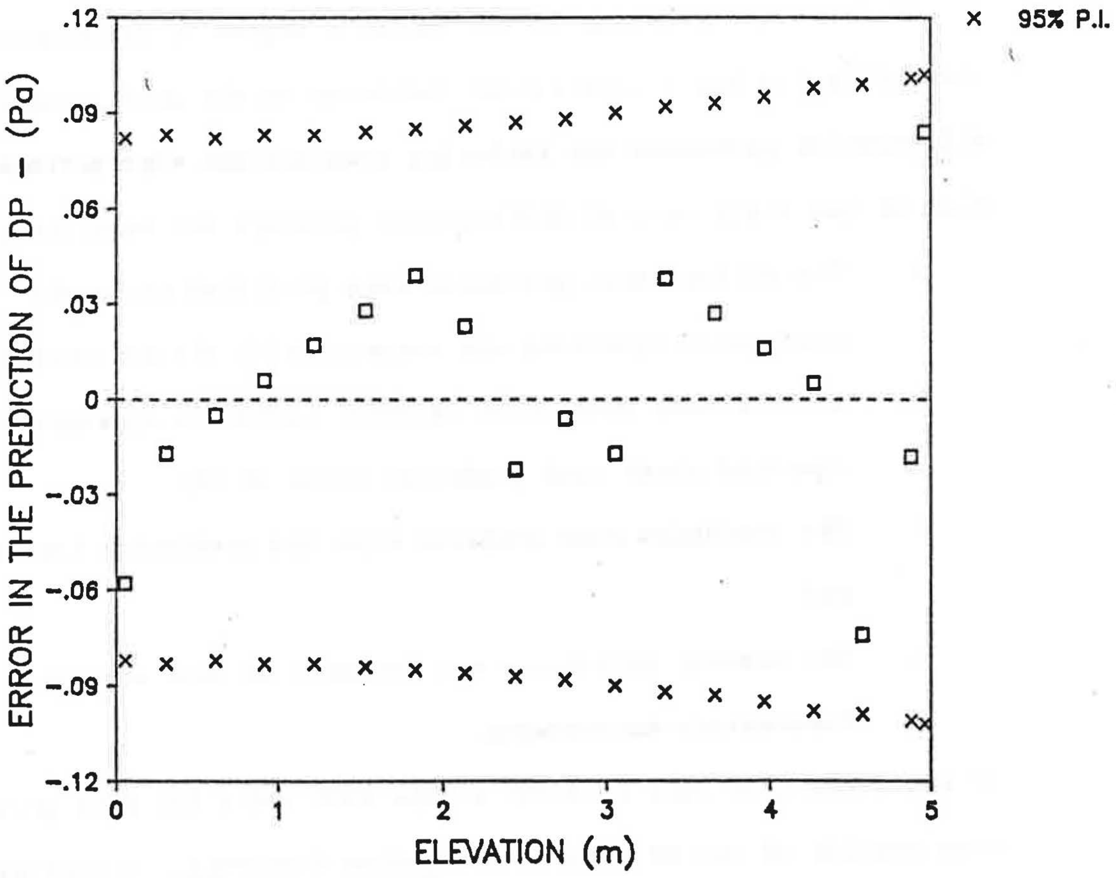

Figure 7.11 **Comparison of the observed and predicted differential pressures for a typical case (DP = pressure difference; P.I. = prediction interval; G1H1T1 Rep 3).**

profiles. As a result, it was concluded that the mean density difference between the two rooms, as opposed to the variation of $\Delta\rho$ with elevation, was the primary cause of the mass exchange between the two rooms.

The mean density difference may be determined from the data by the following three equations:

$$\overline{\Delta\rho}_{reg} = |\ b\ |/g \qquad (7.1a)$$

$$\overline{\Delta\rho} = (\overline{\rho}_c - \overline{\rho}_w) \qquad (7.1b)$$

$$\overline{\Delta\rho} = \overline{\rho}_c\ (\overline{\Delta T}/\overline{T}_w) \qquad (7.1c)$$

where; T_w = the warm room temperature (K).

The best estimate of the density difference available was $\Delta\rho_{reg}$, but in a practical situation either equation 7.1b or 7.1c would be used. Equation 7.1c is often used because of its simplicity of application. The mean density difference was computed using equations 7.1b and 7.1c for all sixty sets of data. The two methods of computing the mean density difference from the air properties have been compared with those obtained by equation 7.1a in Figure 7.12.

Comparison of the mean density difference computed by equation 7.1c with $\Delta\rho_{reg}$ indicates that equation 7.1c tends to underpredict the mean density difference. In fact, 62 percent of the differences were in the range of 0 to 0.004 kg/m^3 while 95 percent of the differences ranged from −0.004 to 0.008 kg/m^3.

Similarly, equation 7.1b tended to overpredict the mean density difference. It was determined that 72 percent of the differences were in the range of −0.004 to −0.012 kg/m^3 and only 65 percent of

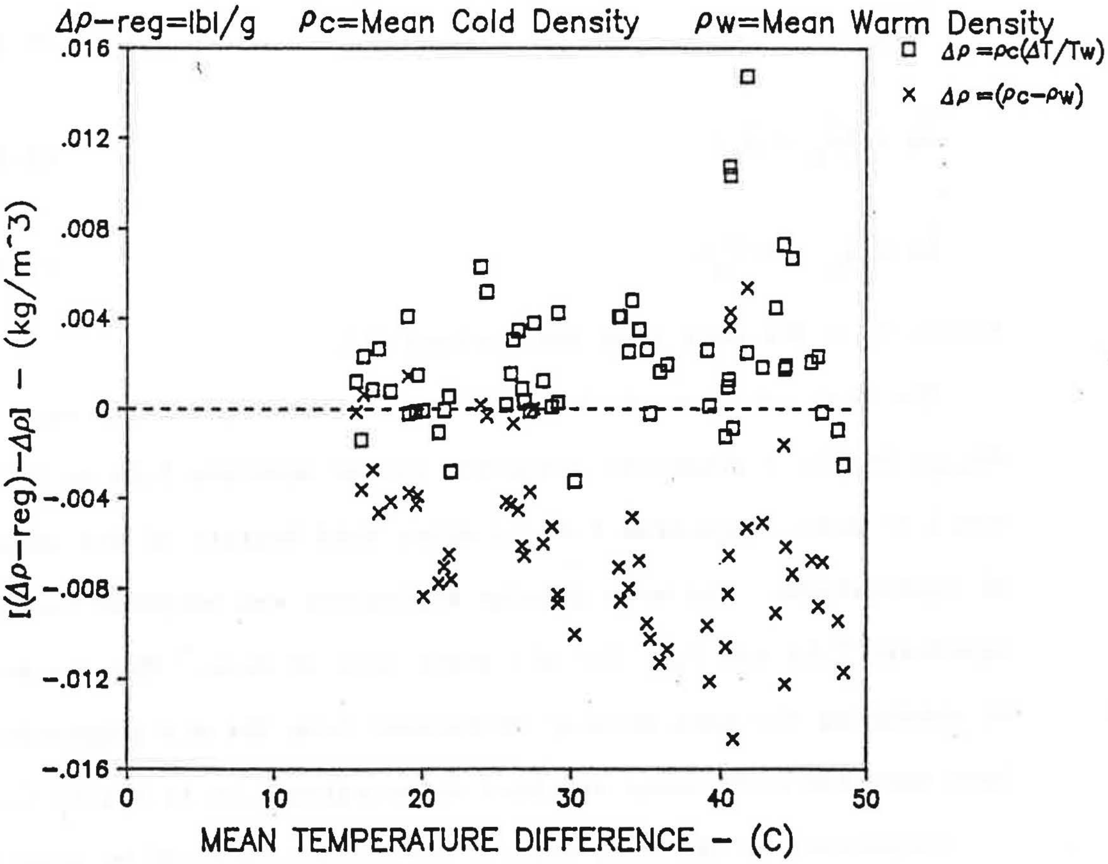

Figure 7.12 Comparison of the two methods of computing the mean density difference with the mean density difference obtained by regression.

the prediction agreed within +.004 to -0.008 kg/m^3. Therefore, the data of Figure 7.12 indicated that equation 7.1c is the preferred method of computing the mean density difference between the interior and the exterior of a structure. The predictions are skewed towards underprediction because the term ($\Delta T/T_w$) imposes the assumption that the humidity ratio (W = kg H_2O/kg dry air) was the same for the warm air as the cold air. The use of equation 7.1c had the advantage that the density of cold air was easier to estimate than the density of warm air.

Prediction of the Elevation of the NPA Neglecting the Background Leakage

The elevation of the neutral pressure axis was determined for each replication of the sixteen original treatments using the mass balancing technique. The mean density difference was determined from the slope of the differential pressure profile as described previously. The properties of the air (ρ and ν) flowing through a particular opening were determined from the measurements of the barometric pressure, the wet bulb temperature or dewpoint (depending upon direction of air flow) and the temperature measurement at the elevation of the opening (Appendix B). The only exceptions were for the low temperature difference cases (T3). In order to reach the relatively high cold room temperatures in a reasonable amount of time, heat was added to the cold room by means of 1500 Watts of electric heat placed down stream from the evaporator coils. As a result, the dewpoint measurement was lost. Therefore, the cold room air density was computed assuming the air was at 75 percent of saturation. This assumption was based upon a few dewpoint measurements that were obtained at the low temperature difference conditions (T3) during the initial trials. Also, a relatively large variation in the moisture content of cold air does not induce a large change in density.

A comparison between the observed and the predicted elevations of the NPA have been presented in Figure 7.13. The differences between the observed and the predicted elevations of the NPA ranged from -0.5 cm (0.2 in) to 55.9 cm (22.0 in).

The two opening groups with the largest total leakage areas (refer to Tables 6.1 and 6.2) were G2 and REC1. For the seven treatments (7 through 13) involving opening groups G2 and REC1, all of the predictions were within $\pm$7.0 cm (2.8 in). The greatest amount of error was for the treatment CYL (treatment number 15) which had the smallest total leakage area. For this case, the predicted NPA was on the average 54.3 cm (21.4 in) too low.

The data in Figure 7.13 suggested that a relationship existed between the size of the openings mounted in the test sections and the amount of disagreement between the observed and the predicted positions of the NPA. It was believed the presence of the background leakage was the source of the greater error in the prediction of the NPA for the smaller opening distributions (G1, REC2, CYL and CYLREC). Furthermore, it was likely that the degree which the background leakage influenced the position of the NPA depended upon the size of the individual openings in a distribution.

The influence of the background leakage was further inspected by computing the sum of the mass flow rates for each distribution using the observed position of the NPA and the observed pressure

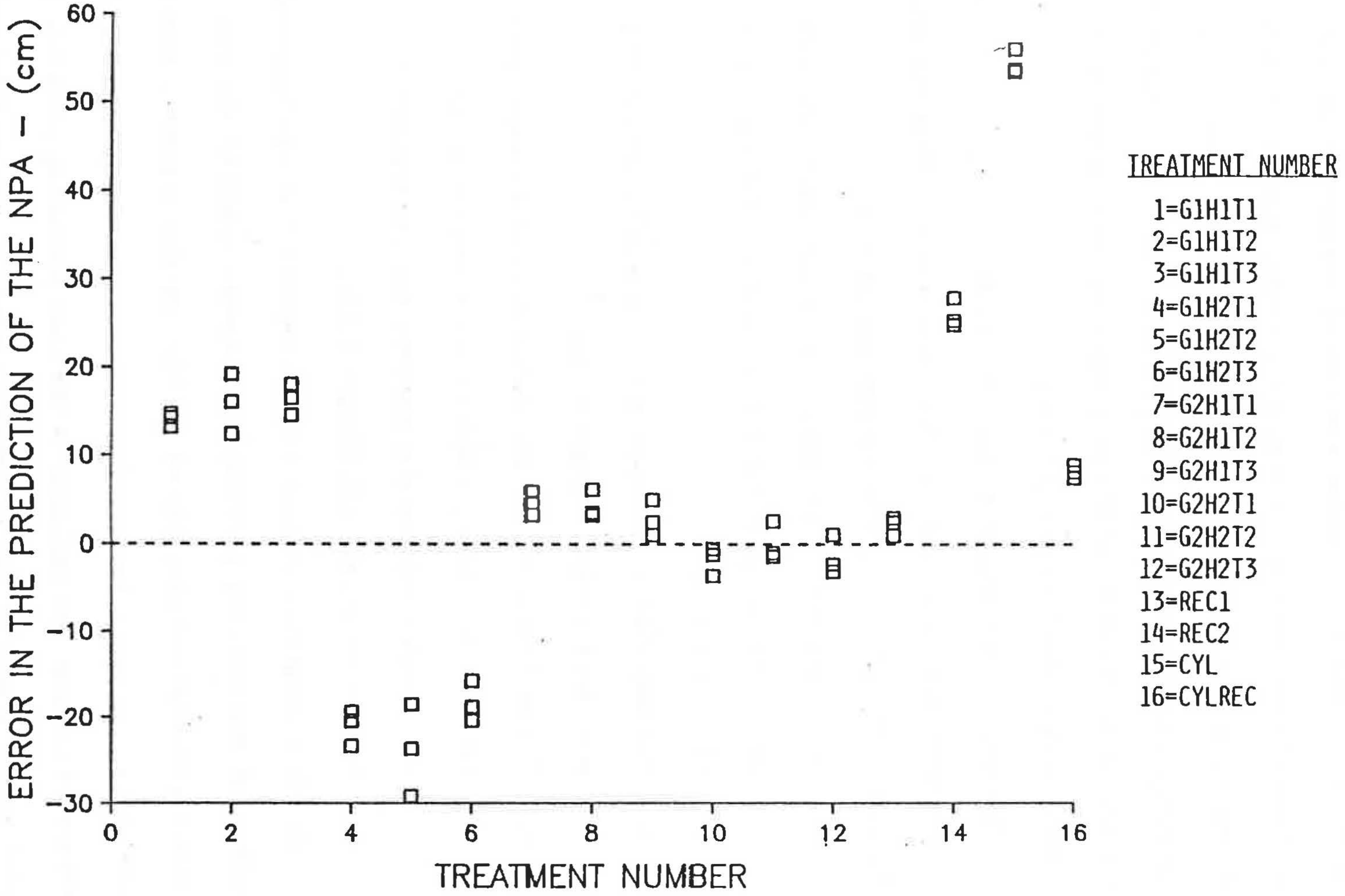

Figure 7.13 Comparison of the observed and predicted values of the NPA for the original sixteen treatments when the background leakage was not included.

differences. Theoretically, the sum of the mass flow rates should equal zero. Due to the various errors of measurement and the use of an assumed mean total minor loss coefficient, none of the mass flows of any distribution were expected to sum to zero. However, it was expected that the degree of imbalance would give some indication of the relative influence of the mass exchange between the two rooms resulting from the background leakage.

The sums of the mass flow through the defined openings for each of the treatments have been shown in Figure 7.14. From the data in the figure the following observations may be made:

a. The magnitude of the imbalance in the sum of the mass flow rates are the greatest for the smaller opening groups G1, REC2, and CYL;

b. The magnitudes of the imbalance generally decreases as the mean temperature decreases; and

c. The variation of the sum of the mass flows about zero followed the same pattern as the variation of the differences between the observed and the predicted elevations of the NPA (Figure 7.13).

The data presented in both figures implied that the background leakage of the two cell environmental chamber could be the factor which influenced the position of the NPA for the sixteen original treatments. In order to test this observation, the presence of the background leakage was included in the mass balancing procedure by modeling the effect of the background leakage as two hypothetical openings.

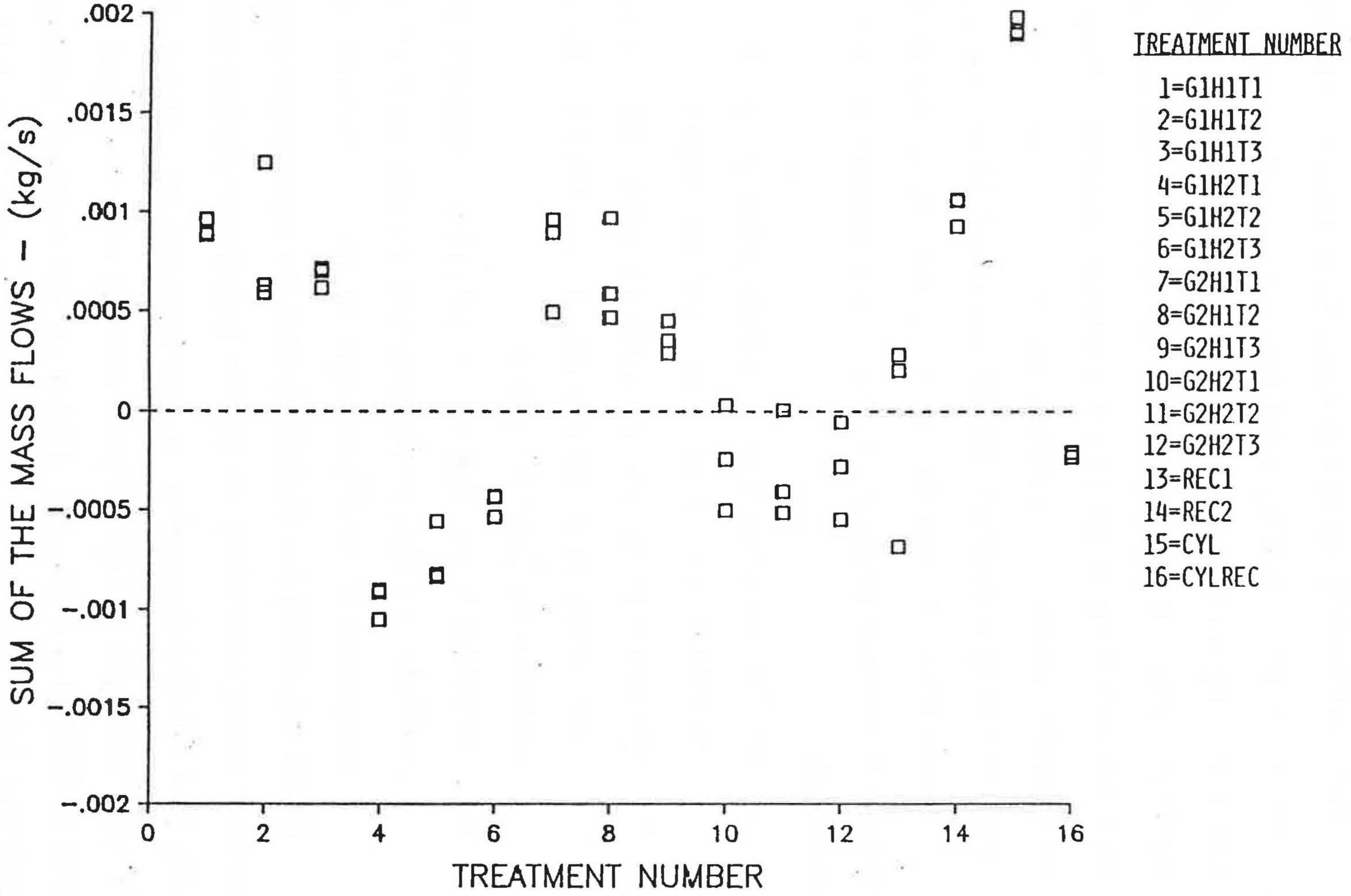

Figure 7.14 Sum of the mass flow rates through the defined openings of the sixteen original treatments excluding the influence of the background leakage.

Modeling the Background Leakage

The known primary sources of significant leakage were: the leaks around the mounting plates in the test sections; the leaks around the access door to the cold room; and the leaks in the ducts of the air handling system. The temperature of the warm room was maintained at about the same temperature as the laboratory in which the two cell environmental chamber was located. Therefore, the leakage between the warm room and the laboratory was not considered to be significant.

To facilitate the inclusion of the effects of the background leakage in the mass balancing technique the following assumptions were made:

1. The background leakage is uniformly and exclusively distributed across the ceiling and wall sections;
2. The mass flow through the lower portion of the test wall is equal to the mass flow out through the upper portion of the test wall and test ceiling; and
3. The background leakage may be modeled as two equivalent straight rectangular openings placed above and below the mean value of the NPA observed for the No Cracks treatments.

It was determined experimentally that the differential pressure varies linearly with elevation and the location of the NPA does not vary with the mean temperature of the two rooms. As a result, the elevations for the two hypothetical openings were determined from a general differential pressure profile for the No Cracks data as shown in Figure 7.15. The NPA was considered to be at 2.795 m (9.17 ft) which was the overall mean of the No Cracks treatments (refer to Table 7.2). In Figure 7.15 it can be seen that two right triangles

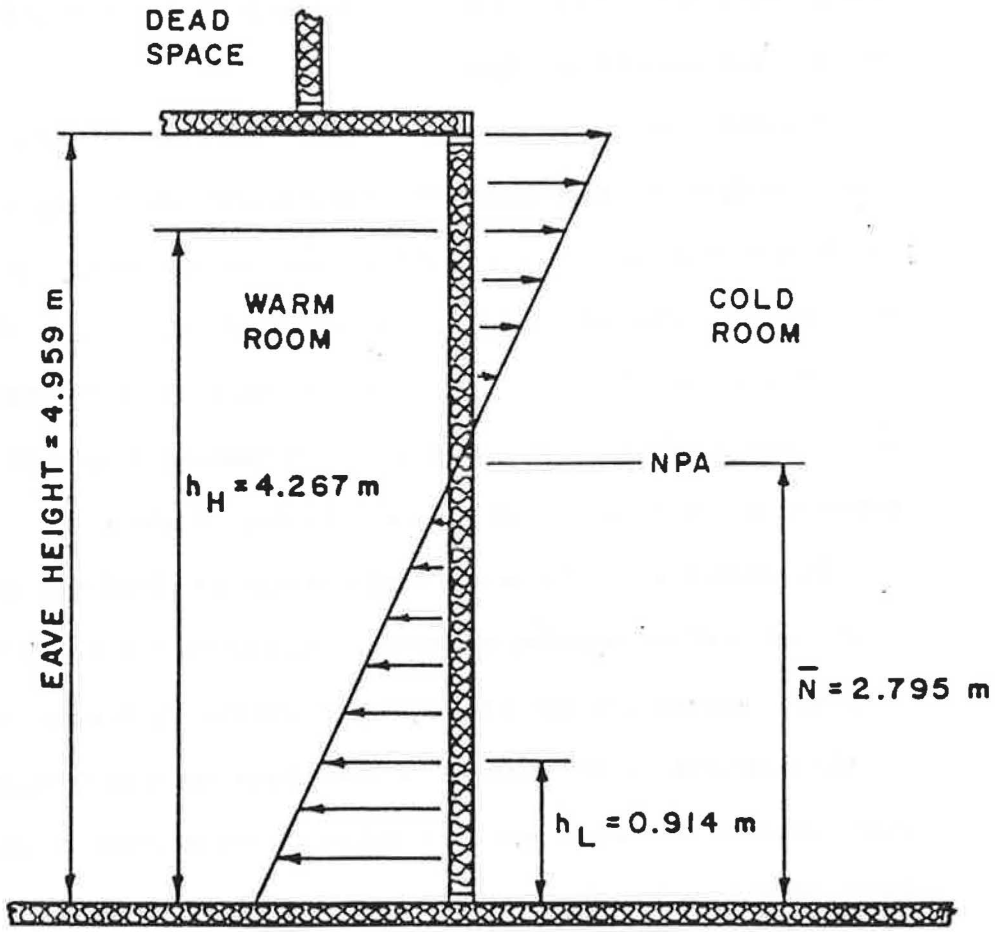

Figure 7.15 The general differential pressure profile for the No Cracks data.

are formed by the intersection of the differential pressure profile and the test wall. The two model openings were considered to be positioned at the elevations of the differential pressure measurements closest to the centroids of these two triangles. The equivalent opening placed at 4.267 m (14.0 ft) was identified as BGH (BackGround High) and the model opening positioned at 0.914 m (3.0 ft) was BGL (BackGround Low).

The first assumption suggests that the relative size of the two model openings is approximately proportional to the surface areas which they represent. The surface area (on the warm side) of the test wall and the test ceiling above the NPA was 12.153 m^2 and the surface area of the portion of the test wall below the NPA was 8.519 m^2. A ratio of these two surface areas indicated that BGH would be expected to be larger than BGL by a factor of about 1.4.

The modeling of the background leakage involved the determination of the equivalent opening parameters (A and γ) for both BGH and BGL such that assumption two is satisfied for the No Cracks treatments.

An equation to determine the equivalent opening parameters of a model opening was obtained by algebraic manipulation of the expression for the total pressure drop across a straight rectangular opening as given by equation 3.16:

$$\Delta P = \frac{1}{2}\rho\bar{V}^2 B\left(\frac{z}{D_h Re}\right) + \frac{1}{2}\rho\bar{V}^2 K$$

The mean velocity and the Reynolds number were defined in terms of the mass flow rate as follows:

$$\bar{V} = \frac{\dot{m}}{\rho A} \quad ; \text{ and} \tag{7.2a}$$

$$Re = \frac{\dot{m}\ D_h}{\rho A \nu} \tag{7.2b}$$

Substitution of these definitions into equation 3.16 gave an equation for the pressure drop across an opening of the following form:

$$\Delta P = \frac{\dot{m}\,\nu\, BzA}{2A^2 D_h^2} + \frac{\dot{m}^2 K}{2\rho A^2} \tag{7.3}$$

The definition of the hydraulic diameter was given in equation 3.9 as:

$$D_h = \frac{2d}{(1 + \alpha)}$$

Utilizing the equation for the hydraulic diameter gave the following expression for the term A/D_h^2 in equation 7.3:

$$\frac{A}{D_h^2} = \frac{(1 + \alpha)^2}{4\alpha} \tag{7.4}$$

Combining equations 7.3 and 7.4 and using the definition of gamma for a rectangular opening (equation 3.24) yielded the following modeling equation:

$$\Delta P = b\ X \tag{7.5}$$

where;

$$X = \left[\frac{\dot{m}\nu}{8\gamma} + \frac{\dot{m}^2 K}{2\rho}\right] \ (N * m^2),$$

$$b = (1/A^2)\ (m^{-4}); \text{ and}$$

$$\gamma = \frac{\alpha}{Bz(1 + \alpha)^2}$$

The air properties (ρ and ν) used in equation 7.5 were the properties of the air flowing through the modeling subject (i.e. cold air properties for BGL and warm air properties for BGH). A value of

1.5 was used for the total minor loss coefficient (K).

If the actual differential pressure and mass flow rates through the background leakage were known, then the area (A) and gamma (γ) of the model opening would be determined by the following procedure.

1. Successive approximations of γ would be made and the corresponding value of A would be determined by application of a least squares best fit to equation 7.5.
2. The mass flow rates would be predicted using the discharge coefficient method (equation 3.26 and 3.33) for each value of γ and its corresponding A.
3. The pair of opening parameters, A and γ, which best predicted the observed mass flow rates would be chosen to model the leakage of the modeling subject.

The equivalent opening parameters, A and γ, would describe the three dimensional geometry of the straight rectangular opening which would provide the same mass flow rates as the modeling subject under the same pressure differences.

Since the mass flow rates for the background leakage in this study were unknown, equation 7.5 could not be directly applied to determine the equivalent opening parameters of both BGH and BGL. Instead, it was required to set the dimensions of the lower opening (BGL) and compute the mass flow rates into the warm room using the pressure differences observed at an elevation of 0.914 m for the twelve replications of the No Cracks treatments. To maintain equilibrium, the same mass of air would be required to flow out through the upper opening (BGH) at the pressure differences observed at an elevation of 4.267 m. This process would generate a mass flow versus pressure curve for BGH, which could be used with the modeling equation to determine the equivalent opening parameters for BGH.

This procedure to estimate the geometry of the two openings to model the effects of the background leakage had an infinite number of pairs of openings which could satisfy the continuity requirements for the No Cracks data. Not all of the solutions would be adequate to describe the influence of the background leakage for the sixteen original treatments. For example, if an extremely small opening was chosen for BGL the modeling procedure would result in an equivalent opening for BGH which was also very small. This pair of openings would be adequate to model the effects of the background leakage on the NPA for the No Cracks treatments, but they would have mass flow rates so small that their influence would be insignificant when included with the defined openings of the other sixteen treatments. Therefore, the first step was to determine a set of dimensions for the lower opening (BGL) that would be useful in describing the effects of the background leakage on the NPA for all twenty treatments.

Several pairs of hypothetical openings (BGL and BGH) of various sizes were arbitrarily defined. Each pair of hypothetical openings were included with the defined opening groups G1, REC1 and REC2. Using the data of the treatments G1H1T1, G1H1T3, REC1, and REC2, the sum of the mass flows was computed using the measured differential pressures and air properties. The elevation of the NPA was then predicted using the mass balancing procedure. By trial and error different pairs of hypothetical openings were used until a pair was found that provided the greatest improvement in the prediction of the elevation of the NPA as well as the sum of the mass flows (refer to Figures 7.13 and 7.14). The dimensions of the ''best'' pair of hypothetical openings are presented in Table 7.5. The only dimension varied was the thickness, d.

Table 7.5
Dimensions of the Pair of Openings to Model the Background Leakage as Determined by Trial and Error

ID	d (cm)	w (cm)	A (cm)	z (cm)	γ (x 10^{-4} m^{-1})	Elevation (m)
BGH	0.20	50.0	10.0	5.08	8.173	4.267
BGL	0.17	50.0	8.5	5.08	6.9507	0.914

So that only the No Cracks data would be used in the modeling of the background leakage, the BGH opening given in Table 7.5 was not used to actually model the effects of the background leakage. Instead, another set of equivalent opening parameters were determined for BGH from the No Cracks data as outlined below.

1. The mass flow rates through BGL ($A = 8.5\ cm^2$ and $\gamma = 6.9507 \times 10^{-4}\ m^{-1}$) were computed from the observed pressure differences at an elevation of 0.914 m for each of the twelve replications of the No Cracks condition (using equations 3.26 and 3.33 with K = 1.5).
2. The twelve mass flow rates computed from BGL were paired with the appropriate differential pressures (at 4.267m) to give a pressure difference versus mass flow curve for BGH.
3. The value of gamma for BGH was assumed to be equal to that of BGL. That is, gamma was set at $6.9507 \times 10^{-4}\ m^{-1}$.

4. The air properties used were the average of the mean air properties of the warm room for all of the No Cracks treatments. The average density was 1.1456 kg/m^3 ($s = 0.0011$). The average kinematic viscosity was 1.5886×10^{-5} m^2/s ($s = 0.00207 \times 10^{-5}$).
5. The cross-sectional area for BGH was determined to be 11.0 cm^2 from a least squares best fit of equation 7.5. The coefficient of determination (r^2) was 0.795. The 95 percent confidence interval about the estimation of the area was $\pm$4.0 cm^2 ($\pm$36%, with 10 degrees of freedom).

The equivalent opening parameters of the two hypothetical openings used to model the effects of the background leakage on the position of the NPA are given in Table 7.6. It is interesting to note that the area of BGH is greater than the area of BGL by a factor of 1.3. Previously, it was estimated that BGH would be larger than BGL by a factor of 1.4 based upon a ratio of surface areas. This gave more credence to the assumption that the background leakage was uniformly distributed across the test sections.

Table 7.6
The Equivalent Opening Parameters of the Hypothetical Openings Used to Model the Effects of the Background Leakage

ID	A (cm^2)	γ (m^{-1})	$A\gamma$ (m)	Elevation (m)
BGH	11.0	6.9507×10^{-4}	7.6458×10^{-5}	4.267
BGL	8.5	6.9507×10^{-4}	5.9081×10^{-5}	0.914

The comparison of the mass flow rates computed using the equivalent opening parameters of BGH (given in Table 7.6) with the mass flows used to determine A and γ for BGH has been shown in Figure 7.16. Given the large scatter in the mass flow rates generated from the lower opening (BGL, in step 1), the equivalent opening parameters determined for BGH adequately predicted the mass flows from the warm room to the cold room.

The elevation of the NPA was predicted for the No Cracks treatments using the mass balancing procedure with the two hypothetical openings (Table 7.6). The differences between the observed and the predicted elevations of the NPA are shown in Figure 7.17. The mean of all of the predicted elevations was 284.7 cm with a standard deviation of 5.086 cm. The difference between the predicted overall mean NPA and the observed grand mean NPA (279.5 from Table 7.3) was 5.2 cm. Considering the variability of the No Cracks data, the equivalent openings (BGH and BGL) were believed to be adequate to describe the background leakage for the No Cracks treatments.

Prediction of the NPA Including the Effects of the Background Leakage

The elevation of the NPA as well as the sum of the mass flow rates were recomputed using the two hypothetical openings BGH and BGL to include the effect of the background leakage. A comparison of the errors in the prediction of the NPA before and after the effect of the background leakage was included has been presented in Figure 7.18. The corresponding errors in the sum of the mass flow rates have been given in Figure 7.19. Examination of these two figures indicated a great improvement in the prediction of the NPA and the degree of imbalance in the sum of the mass flow rates.

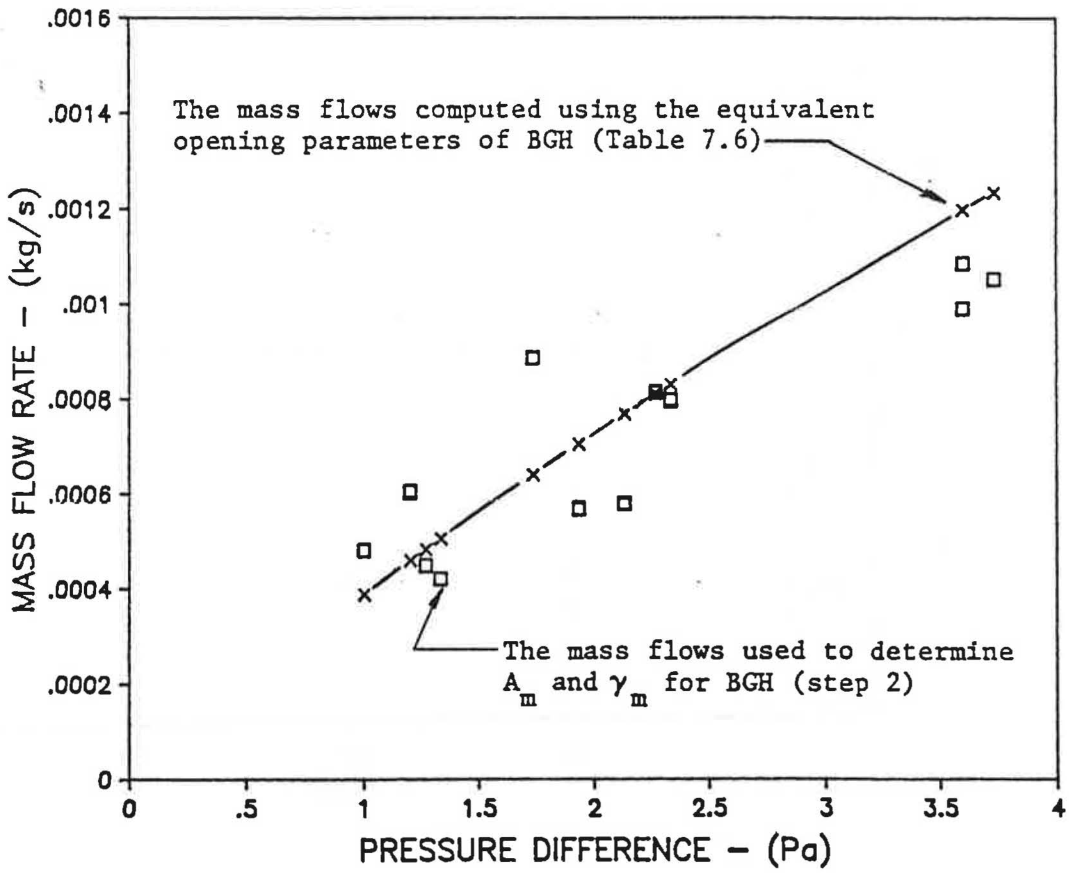

Figure 7.16 Comparison of the mass flows used with equation 7.5 to determine the equivalent opening parameters of BGH with the computed mass flows using BGH (pressure differences at 4.267 m).

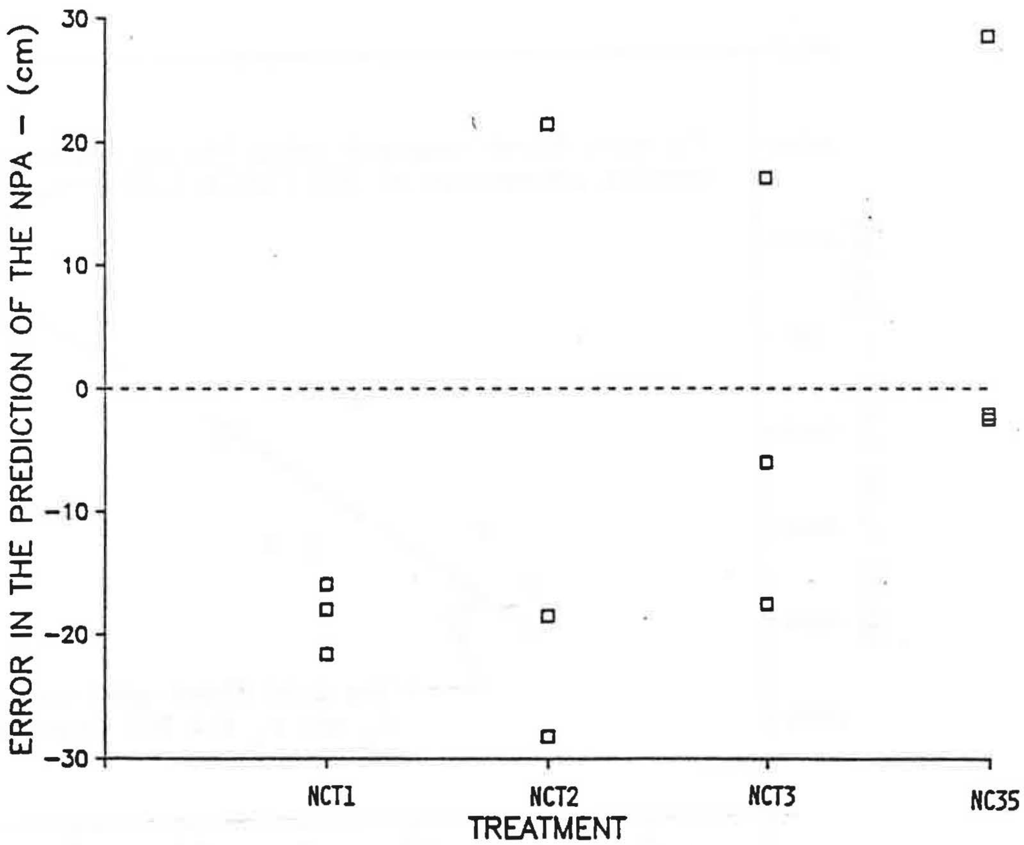

Figure 7.17 Comparison of the observed and predicted positions of the NPA for the No Cracks treatments.

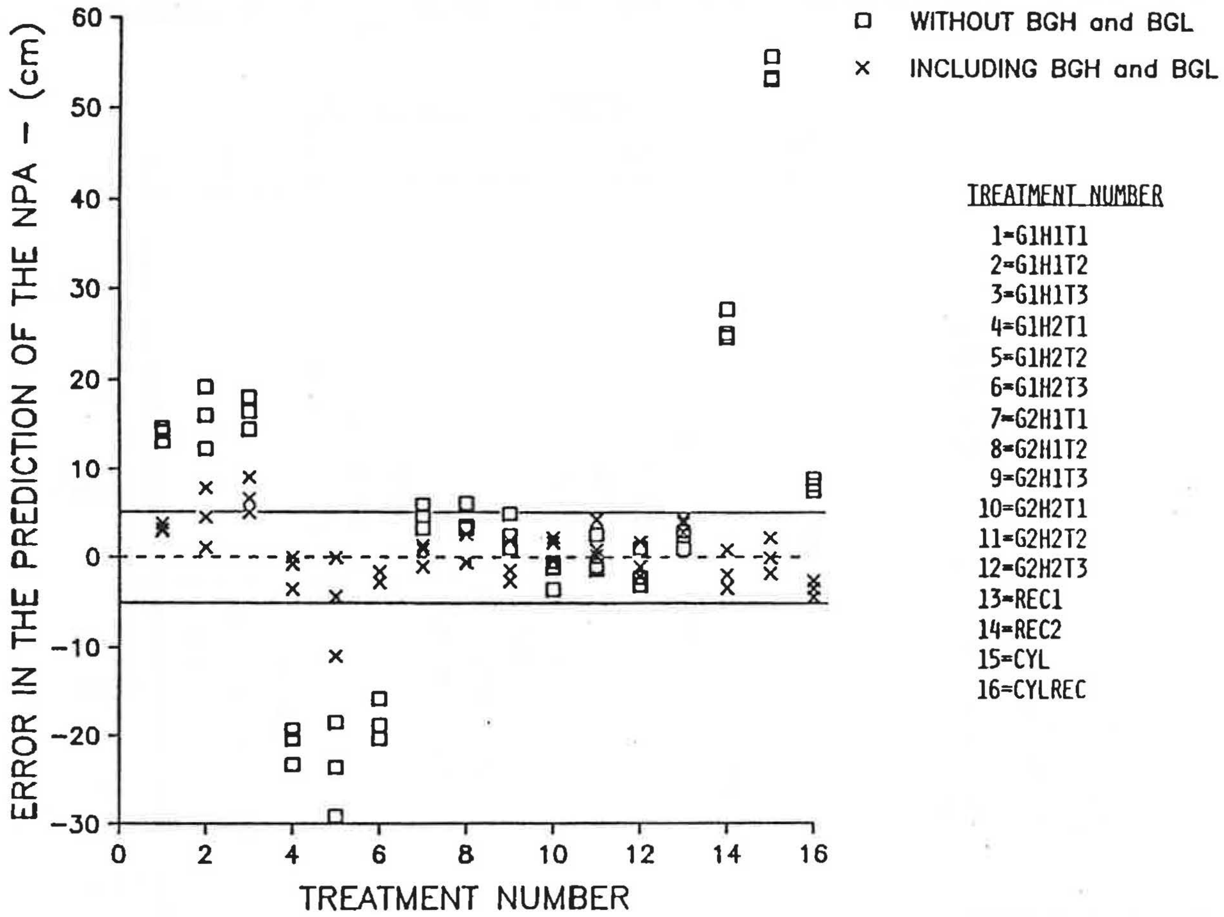

Figure 7.18 Comparison of the differences between the observed and predicted elevations of the NPA before and after the background leakage was included.

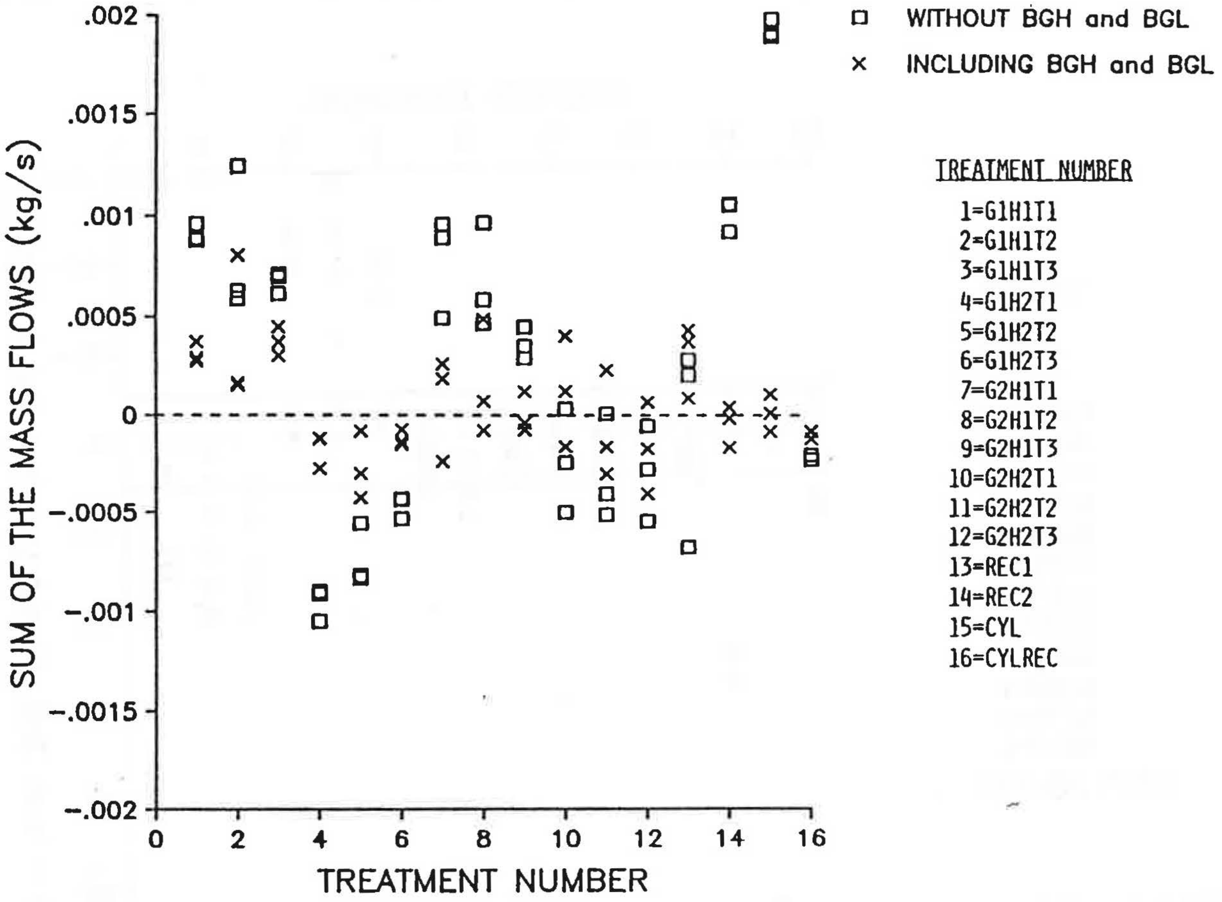

Figure 7.19 Comparison of the sum of the mass flow rates before and after the background leakage was included.

In particular, the results shown in Figure 7.18 indicated that when BGH and BGL were included with the defined openings the elevation of the NPA was predicted within ±5.0 cm (±1.97 in) for all but four of the 48 observed differential pressure profiles. The four cases with an error in prediction greater than ±5.0 cm were all treatments involving opening group G1. Three of these four cases were treatments for which the G1 openings were distributed according to placement H1. The greatest amount of error was -11.0 cm (4.33 in) for the third replication of G1H2T2 for which one of the openings was placed in the ceiling.

The additional scatter in the prediction of the NPA and the sum of the mass flows for the treatments involving opening group G1 was believed to be the result of the large variation of the background leakage. The variation of the NPA with respect to the day on which data were taken (refer to Figure 7.6) indicated that 67 percent of the No Cracks data were obtained on days 12 through 19. Examination of the laboratory records (refer to Appendix E) showed that 94 percent of all of the data for G1H1, G1H2, G2H1, and G2H2 (at any mean temperature difference) were taken before the twelfth day and 72 percent of the data were taken on days 2 through 9. The data for treatments REC1, REC2, CYL and CYLREC were obtained on days 14 through 18. The background leakage was modeled based upon the grand mean of all observed elevations of the NPA for the No Cracks case. Therefore, the two openings used to model the influence of the background leakage over the entire experiment best described the effects of the background leakage which existed between days 12 and 19.

This indicated a problem with the experimental design. The No Cracks data should have been taken at uniform time increments throughout the data taking period, but the importance of the variation of the background leakage was not realized until the analysis of the data was begun.

Additional evidence of this observation may be seen by comparing Figure 7.6 with Figure 7.17. It can be seen that the positions of the NPA for NCT1, taken on days 1, 4, and 9, were consistently overpredicted whereas the other differences were scattered about the mean.

An analysis of the propagation of the errors in measurement was performed on the summation of the mass flow rates and the mass balancing procedure for predicting the elevation of the NPA (NPA.PRED). A detailed summary of the computations as well as the tabulated results has been provided in Appendix F.

Theoretically, the sum of the mass flow rates should be zero. Due to the errors in measurement and the variation of the total minor loss coefficient (K) between openings the mass flow rates did not sum to zero for any opening distribution. The total minor loss coefficient was not measured. Therefore, the analysis only included measurement errors associated with opening dimensions, differential pressures, temperatures, and air properties. It also should be noted that the hypothetical openings, BGL and BGH, were not included in any estimation of uncertainty.

The uncertainty in the summation of the mass flow rates ($u_{\Sigma \dot{m}}$) was computed (see Appendix F) for each replication of the sixteen original treatments. The sum of the mass flow rates ($\Sigma \dot{m}_j$) has been compared with $u_{\Sigma\dot{m}}$ in Figure 7.20. The uncertainty in the summation of the mass flow rates was about the same for each replication. Hence, only the largest values of $u_{\dot{m}}$ have been shown (refer to Table F.2).

It was observed that the mass flow rates balanced within the uncertainty of the summation of the mass flow rates for all but 7 of the 48 differential pressure profiles. Five of the cases for which the mass flow rates did not balance within the uncertainty of the measurements were for treatments taken on days 3 through 12. Consequently, the additional variation in these treatments was believed to be the result of the variation of the background leakage. The other two points that fell outside the band of uncertainty were for two of the three replications of treatment CYL. Reference to Table 6.2b and Figure F.2 (Appendix F) indicates that this was the smallest opening group. Also, all of the openings in this group were cylindrical openings. Therefore, the error in selecting a total minor loss coefficient of 1.5 was probably the greatest for this treatment.

The uncertainty in the prediction of the NPA due to uncertainties in the measurements was expressed in terms of an uncertainty interval (U.I.) about NPA.PRED. The elevation of the NPA was computed by iteratively balancing the sum of the mass flow rates to within five decimal places (i.e. zero $\equiv \pm$ 0.000004 kg/s). The uncertainty in the prediction of the NPA was a function of the uncertainty of the summation of the mass flows for each replication of each distribution. The upper and lower limits of the uncertainty interval for the prediction of the NPA were determined by iteratively solving for

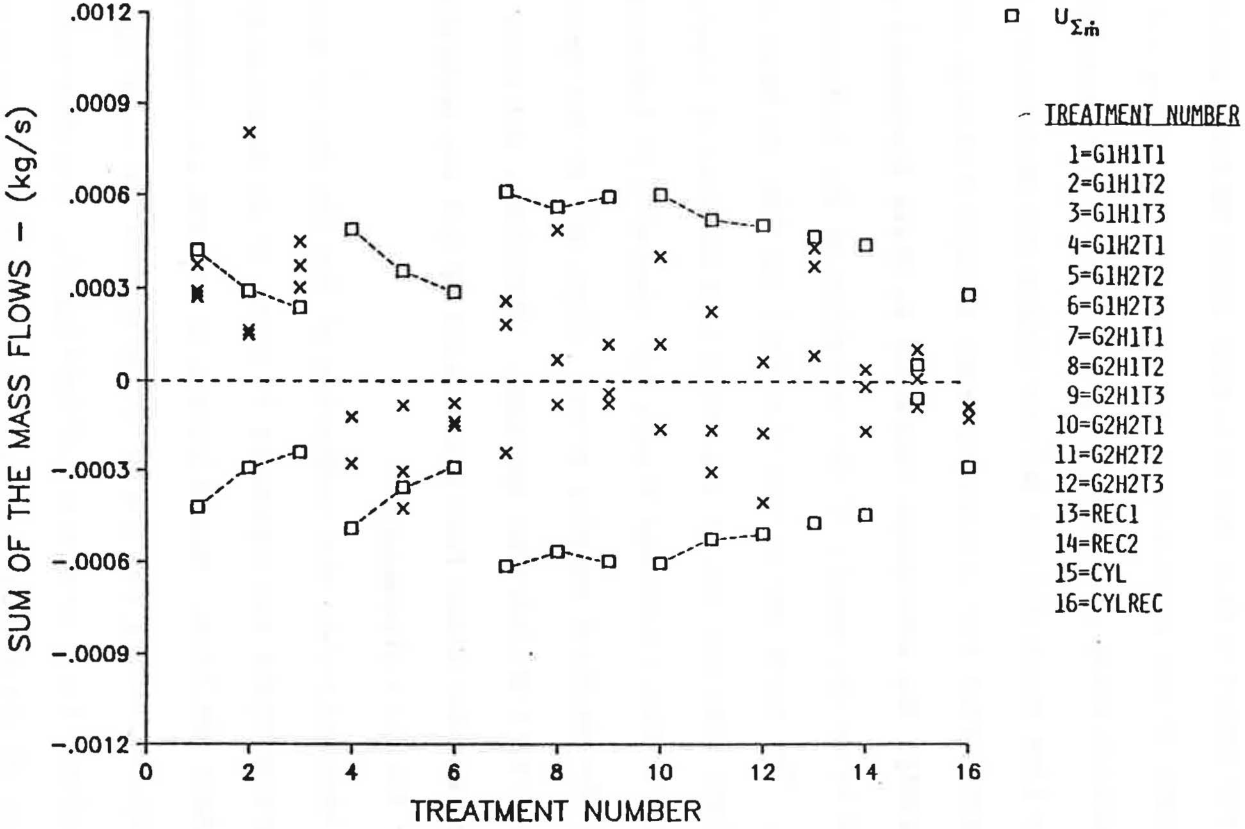

Figure 7.20 Comparison of the sum of the mass flow rates with the uncertainty in the summation of the mass flow rates.

the two elevations of the NPA which satisfied the following expression:

$$\sum_{j=1}^{n} \dot{m}_j = \pm\ u_{\Sigma \dot{m}} \qquad (7.6)$$

where; $u_{\Sigma \dot{m}}$ = the uncertainty in the summation of the mass flow rates for a particular case.

A 95 percent confidence interval (C.I.), based upon the variance about the regression line (Appendix D), was computed for each observed elevation of the NPA (NPA.DATA). The observed and predicted values of the NPA along with the corresponding confidence intervals and uncertainty intervals have been compared for the sixteen original treatments in Figure 7.21. The data shown indicates that the confidence intervals of the observed values and the uncertainty intervals of the predicted values overlap for all but two cases (Figure 7.21a). These two cases were the first replication of G1H1T2 and the third replication of G1H1T3. It is apparent from Figure 7.21a and Table 7.1 that the elevations of the NPA for these two replications were considerably higher than the other replications.

A general comparison of the scatter in the observed positions of the NPA indicated that there was generally less scatter associated with REC1, REC2, CYL and CYLREC than with the twelve treatments involving opening groups G1 and G2. The additional scatter in these observations (G1, G2) was believed to be the result of greater variation in the background leakage between the replications of these twelve treatments.

The differences between the observed and the predicted elevations

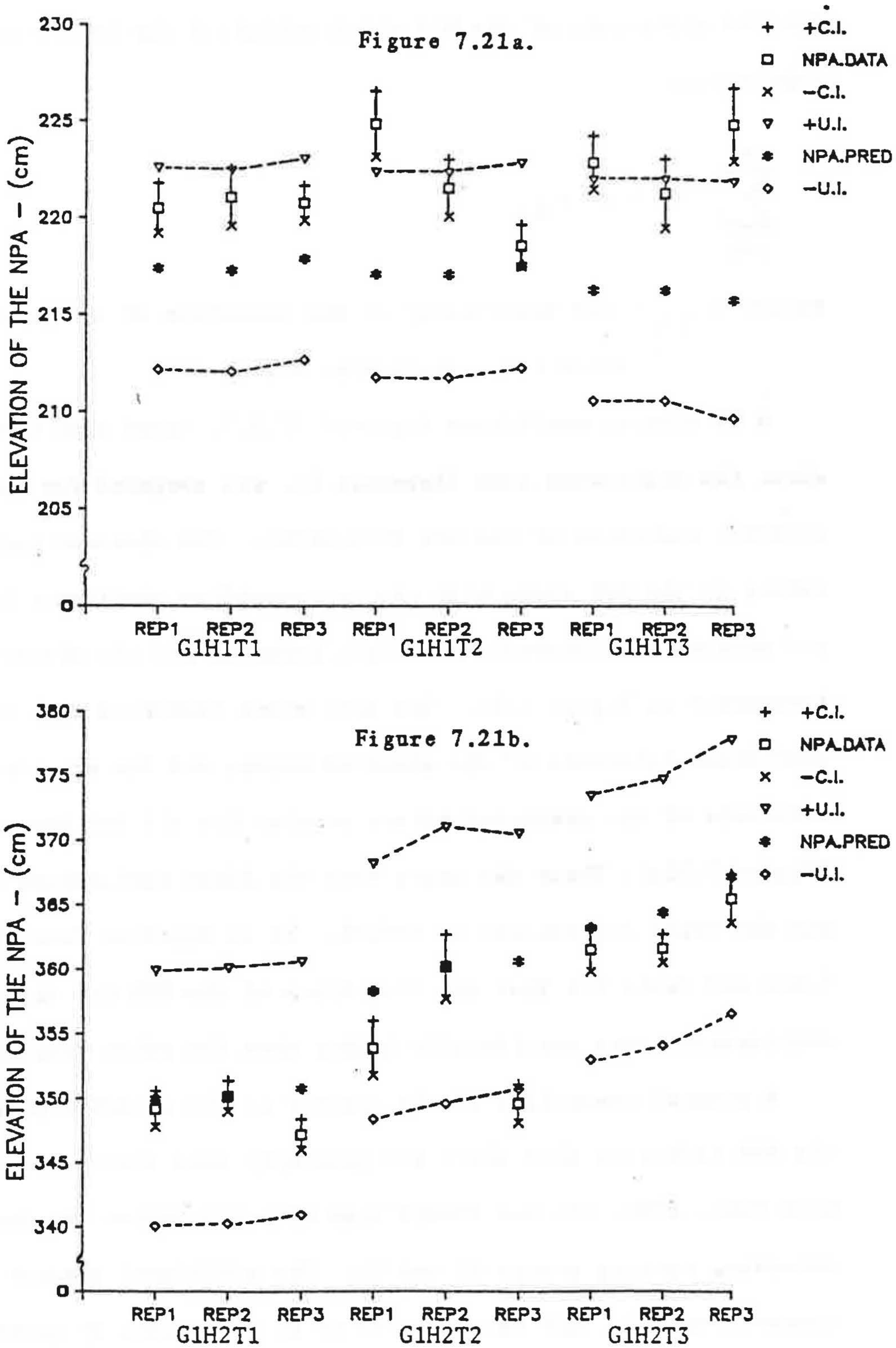

Figure 7.21 Comparison of the observed and predicted positions of the NPA along with their respective estimates of error (C.I. = 95% confidence interval; U.I. = uncertainty interval).

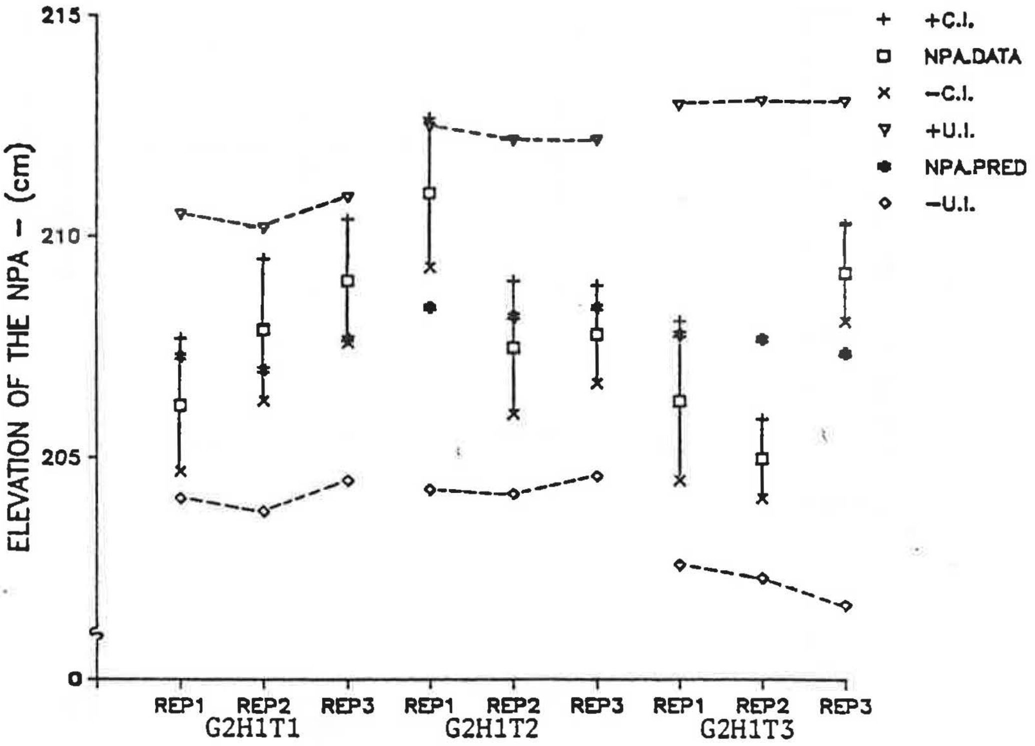

Figure 7.21c.

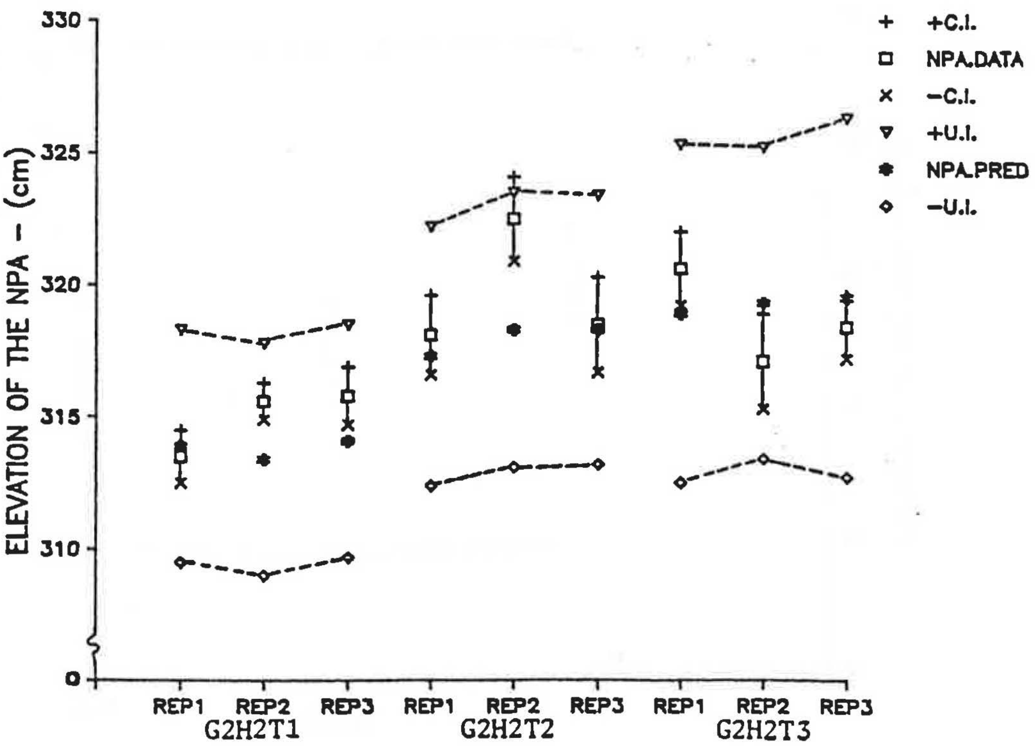

Figure 7.21d.

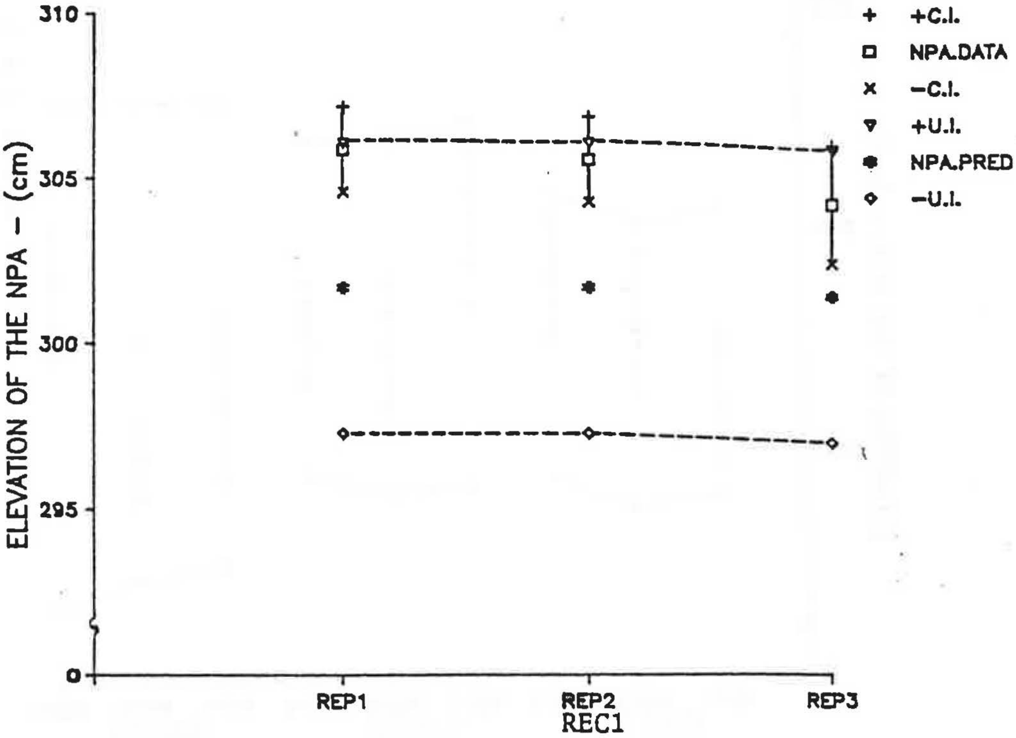

Figure 7.21e.

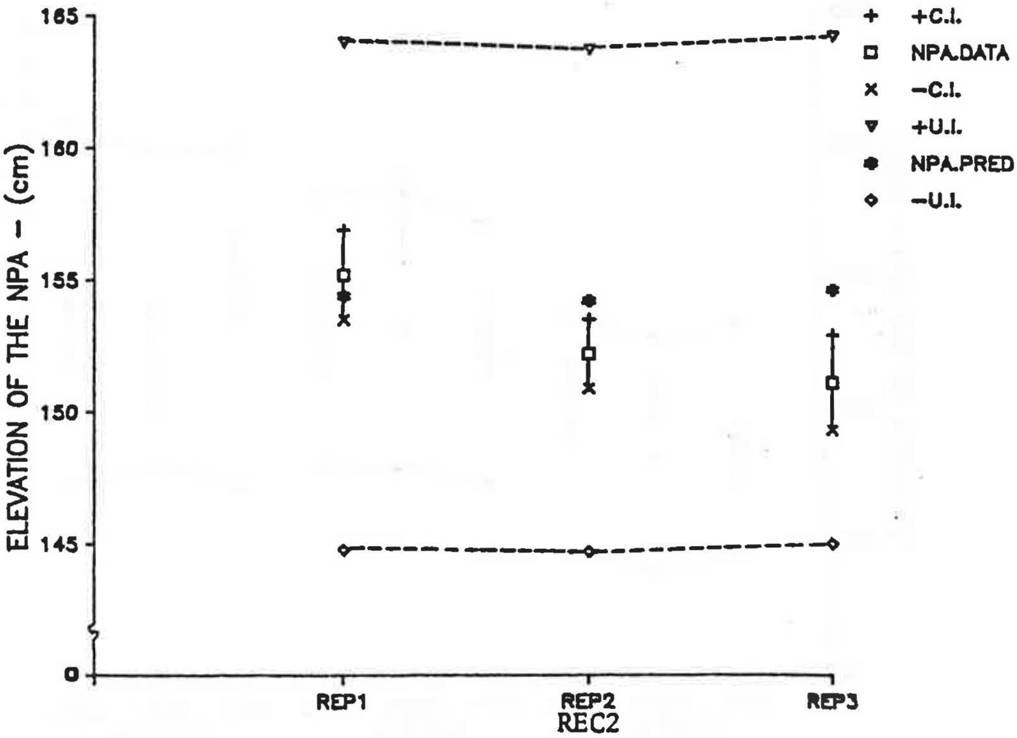

Figure 7.21f.

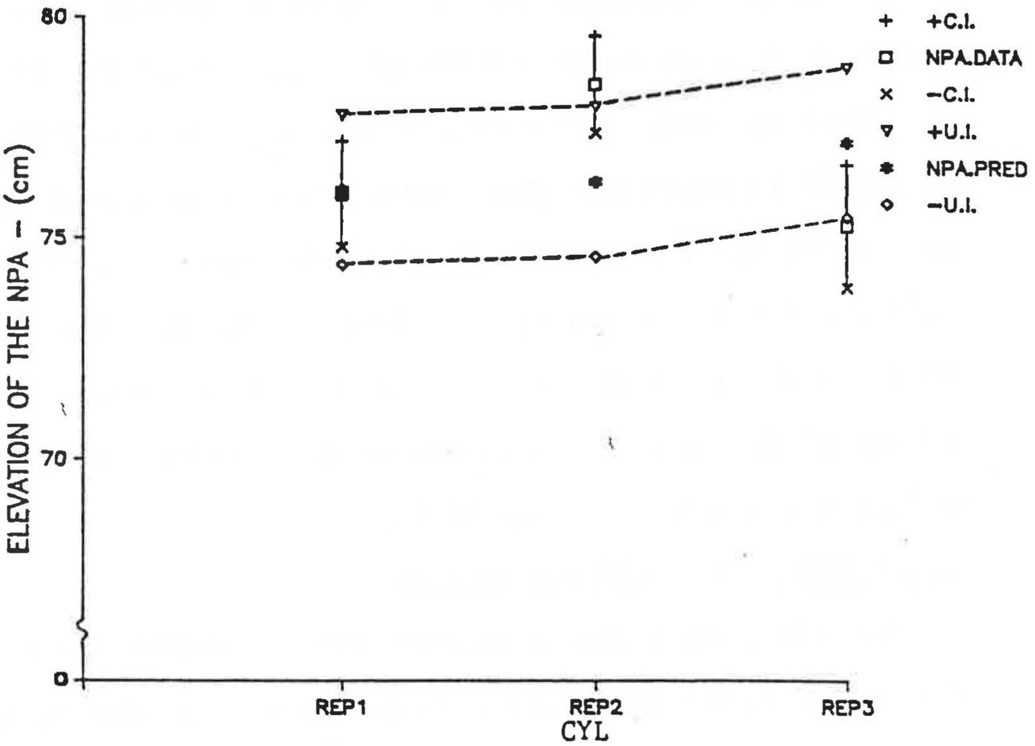

Figure 7.21g.

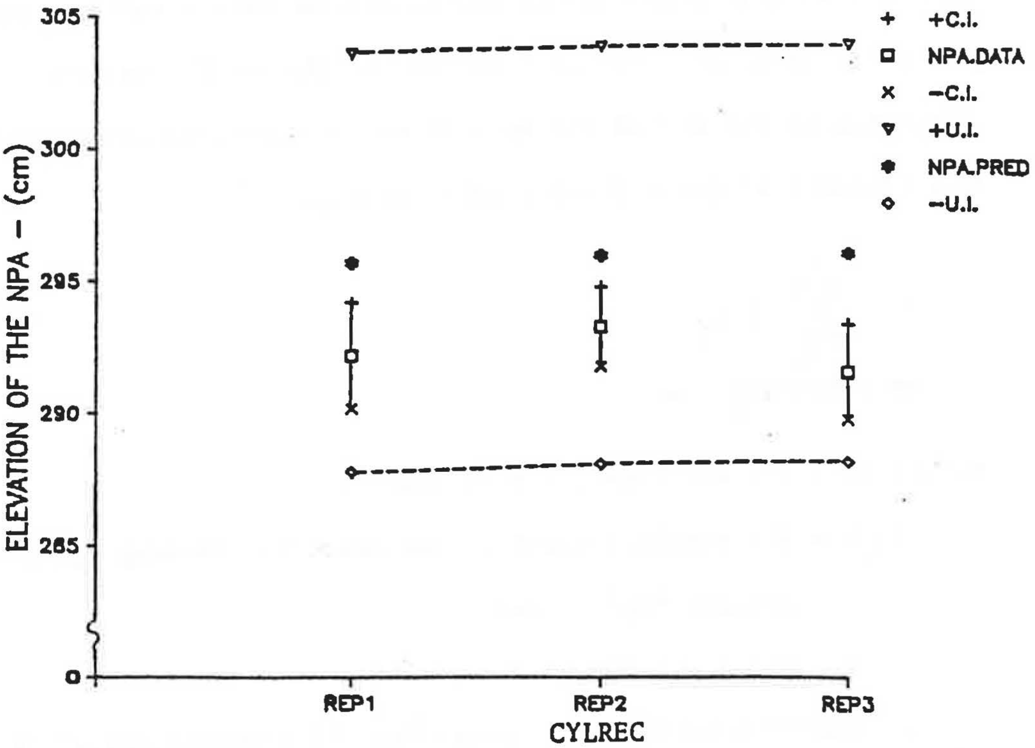

Figure 7.21h.

of the NPA were normalized with respect to the eave height of the test sections (eave height = 4.959 m). It was found that 91.7 percent of the predicted values were within ±1 percent of the eave height; 97.9 percent were predicted within ±2.0 percent of the eave height; and all of the elevations of the NPA were predicted within ±2.22 percent of the eave height. Furthermore, the elevation of the NPA was predicted to within ±1 percent of the eave height for 95.8 percent of the cases which included an opening placed in the test ceiling (G1H2, G2H2, REC1, and REC2).

Computation of the Infiltration Rate

The infiltration rate is defined, for the purpose of this discussion, as the total mass exchange between the interior and exterior of a structure resulting from the stack effect. By the continuity equation (equation 3.32), the infiltration rate may be computed as either the sum of the mass flow into a building or the sum of the mass flow out of a building. Due to the observed imbalance in the sum of the mass flows, the mean infiltration rate was computed by the following relationship:

$$IR = \frac{\sum_{j=1}^{n} | \dot{m}_j |}{2} \tag{7.7}$$

where; IR = the infiltration rate (kg/s),

$|\dot{m}_j|$ = the absolute value of the mass flow through the j^{th} opening (kg/s), and

n = the total number of openings.

The computed infiltration rates for all replications of the sixteen original treatments and the No Cracks treatments using the measured pressure differences have been displayed in Figures 7.22 and 7.23, respectively. Excluding the No Cracks situation, the minimum infiltration rate was 0.0017 kg/s for treatment G1H1T3 (replication 3) and the maximum infiltration rate was 0.0225 kg/s for G2H2T1 (replication 2). Therefore, the infiltration rate varied by a factor of 13.2 depending upon the relative size of the openings, the distribution of the openings, and the mean temperature difference. The infiltration rate computed for the No Cracks data was found to vary by a factor of 2.4 depending upon the mean temperature difference.

The contribution of each of the hypothetical openings, BGH and BGL, to the infiltration rate has been presented in Figure 7.24 for each replication of each treatment. In general, the contribution of the background leakage was a function of the size of the openings in a particular distribution. Comparison of Figure 7.24 with Figure 7.20 indicates that in general the cases for which the sum of the mass flows fell outside the band of uncertainty were also cases for which the contribution of the background leakage to the infiltration rate was the most important. The background leakage made the largest contribution to the infiltration rate of treatment CYL which had the smallest opening distribution.

The infiltration rates were normalized with respect to the warm room volume (V_{wr}) and the mean warm room density (ρ_w). The volume of the warm room was calculated to be 48.580 m^3 and ρ_w of all sixty data sets was 1.1520 kg/m^3 (s = 0.0017). The normalized infiltration rates were expressed in terms of air changes per hour

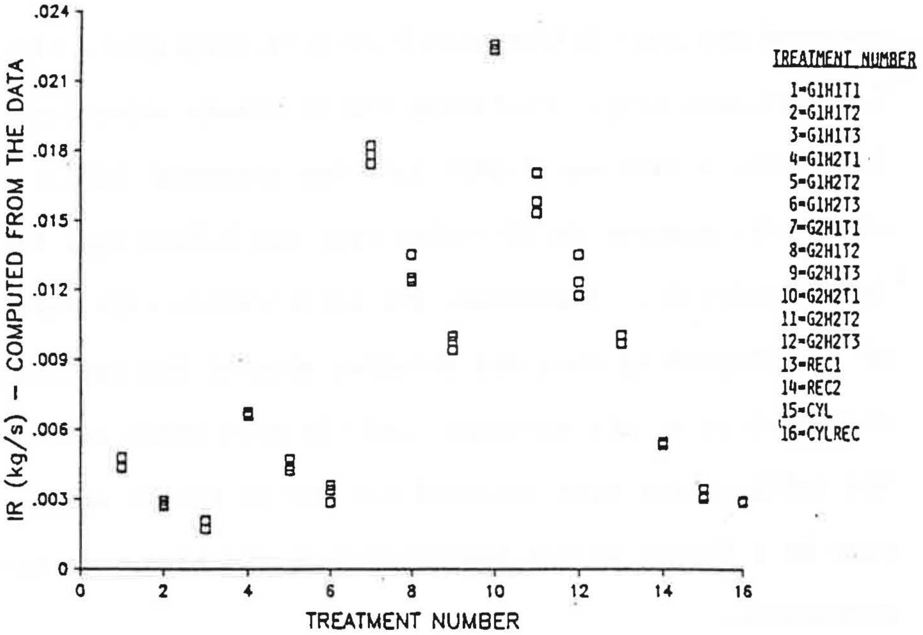

Figure 7.22 Infiltration rates for the original sixteen treatments computed from the measured differential pressures.

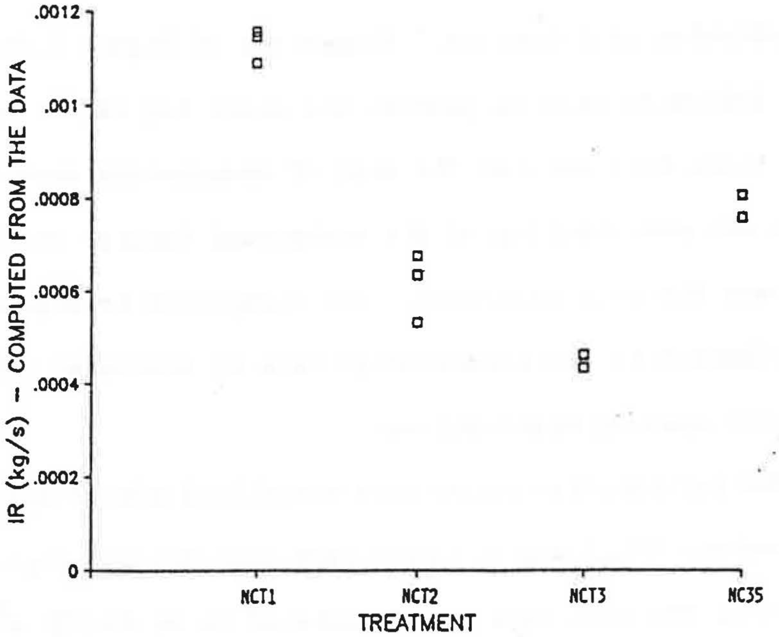

Figure 7.23 Computed infiltration rates for the No Cracks treatments.

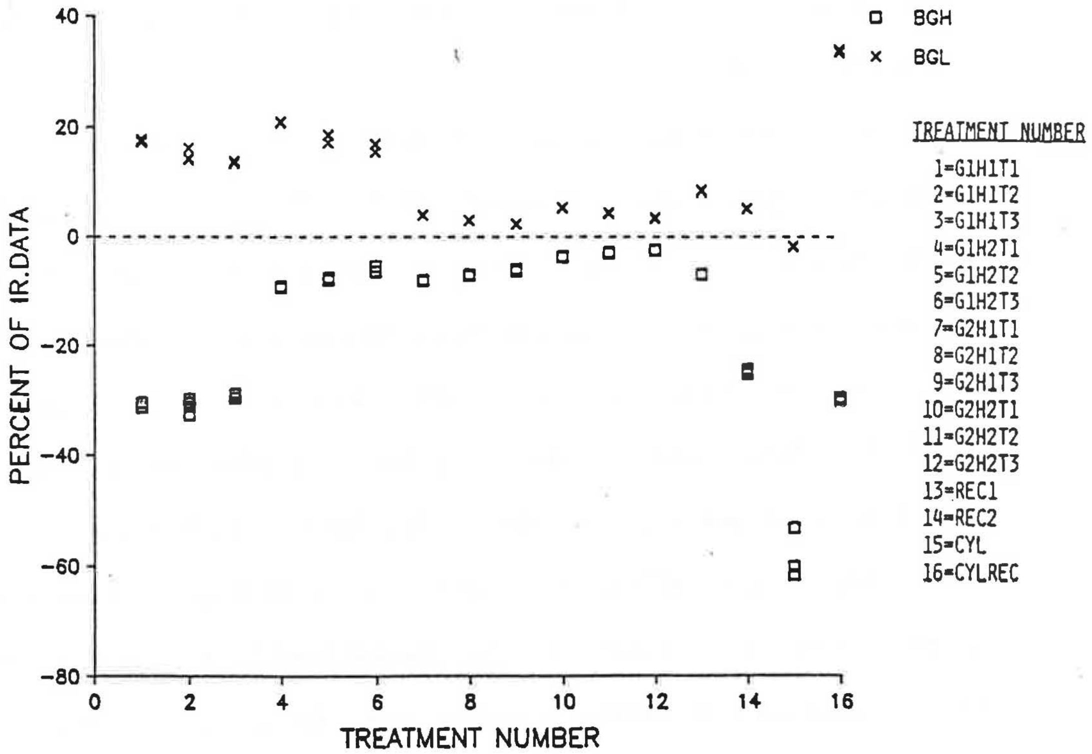

Figure 7.24 **Contribution of the two hypothetical openings to the infiltration rate (a positive value indicates flow into the warm room and a negative value indicates flow out).**

(ach) as follows:

$$IR_N = IR * \frac{3600}{\rho_w V_{wr}} = IR * 64.327 \tag{7.8}$$

Where: IR_N = the normalized infiltration rate (ach); and

IR = the infiltration rate (kg/s).

The infiltration rates ranged from 0.109 to 1.447 ach for the original sixteen treatments and from 0.028 to 0.075 ach for the No Cracks treatment.

Examination of all of the treatments for which the mean temperature difference was varied (G1H1, G1H2, G2H1, G2H2 and NC) suggested that the infiltration rate varied linearly with the mean temperature difference. The normalized infiltration rates correlated highly with the mean temperature difference as shown in Figure 7.25.

An important question which has not been addressed is: What influence does the error in the prediction of the NPA have on the prediction of the infiltration rate? In an attempt to answer this question the infiltration rate was calculated by equation 7.7 using the differential pressures computed based upon the predicted elevations of the NPA (NPA.PRED). The differences between the infiltration rates computed from the measured pressure differences (IR.DATA) and the infiltration rates computed based upon the predicted elevations of the NPA (IR.PRED) have been shown for all sixty cases in Figure 7.26 and 7.27. The uncertainty in the summation of the mass flow rates ($u_{\sum \dot{m}}$) is also the uncertainty in the calculation of the infiltration rate for the original sixteen treatments. The data of Figure 7.26 indicates that all but four

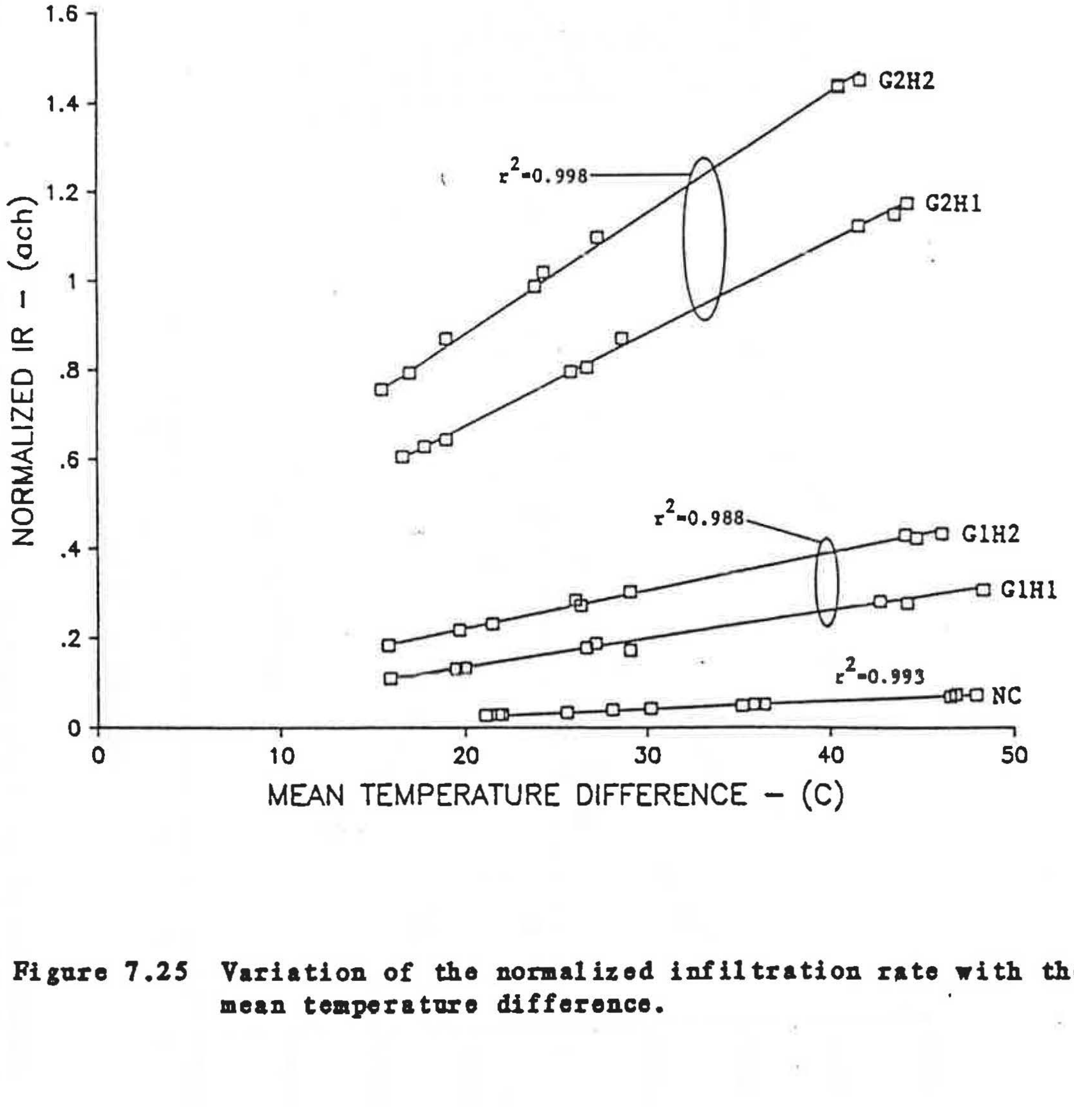

Figure 7.25 Variation of the normalized infiltration rate with the mean temperature difference.

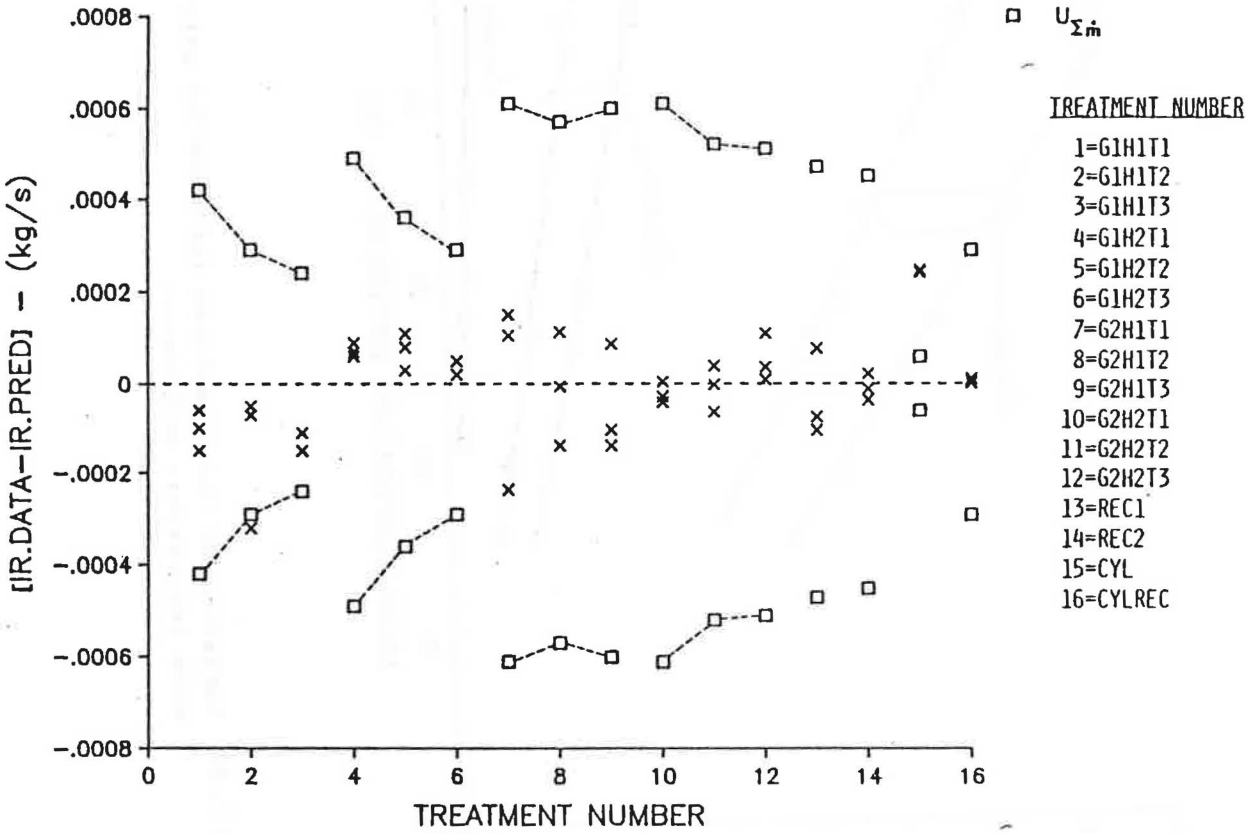

Figure 7.26 Comparison of the infiltration rates computed from the data (IR.DATA) and the infiltration rates computed based upon the predicted NPA (IR.PRED) for the original sixteen treatments.

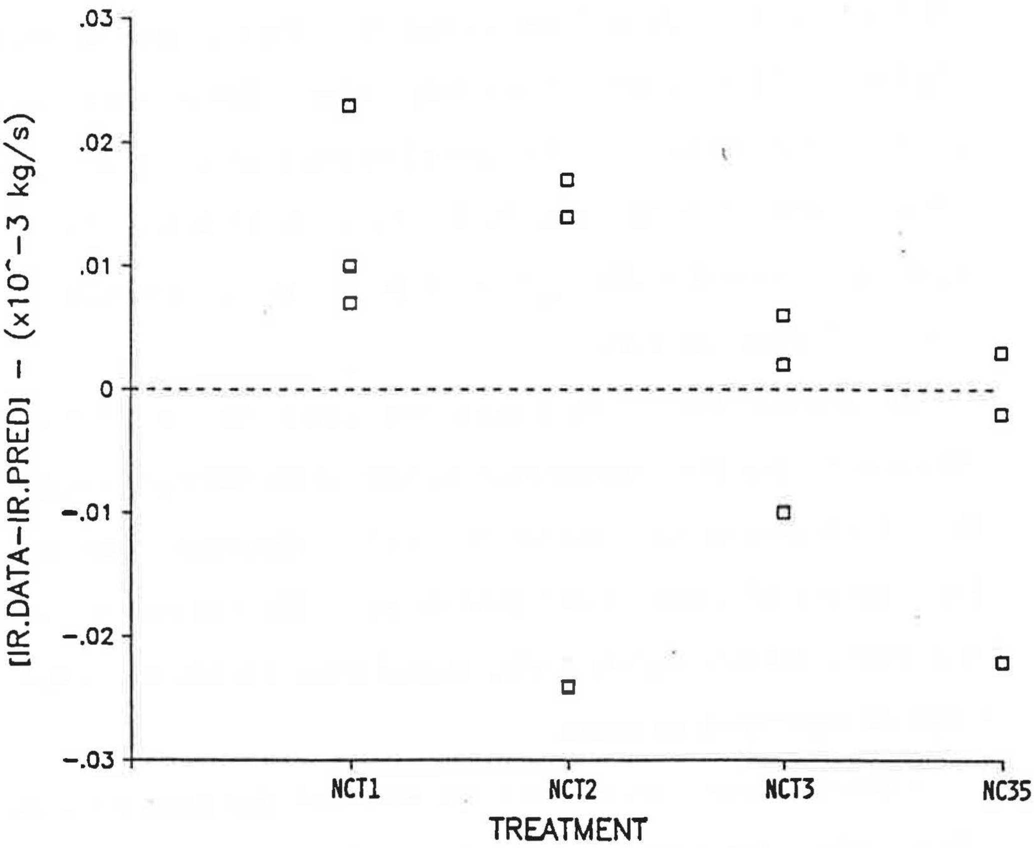

Figure 7.27 Comparison of the infiltration rates computed from the measured pressure differences (IR.DATA) and the infiltration rates computed based upon the predicted NPA (IR.PRED) for the No Cracks treatments.

infiltration rates agreed within the uncertainties due to the propagation of the errors in measurement (Appendix F).

The results for the original sixteen treatments, provided in Figure 7.26, indicated that 89.6 percent of the errors were within ±0.0002 kg/s (±0.013 ach). The greatest error was -0.00032 kg/s (-0.021 ach) for G1H1T2 (replication 1). This largest difference represented 11.9 percent of the total flow. The greatest consistent error was 8.0 percent for the distribution containing all cylindrical openings (CYL; 0.00024 kg/s, 0.016 ach). It is believed that the consistent error for CYL resulted from the use of a mean total minor loss coefficient of 1.5.

The results for the No Cracks treatments (Figure 7.27) showed that all of the differences were within ±0.000024 kg/s (±0.002 ach) or ±4.5 percent of the infiltration rate. Therefore, the seemingly large amount of error in the prediction of the NPA for the No Cracks treatments did not induce a very significant variation in the computed infiltration rates.

A direct comparison between the error in the prediction of the NPA and the error induced in the computed infiltration rate has been provided for the sixteen original treatments in Figure 7.28. From this figure it can be concluded that an error in the prediction of the NPA equal to ±1 percent of the eave height resulted in a variation in the computed infiltration rate of ±3.0 percent for 81.3 percent of the 48 cases. The errors in the computation of the infiltration rate were within ± 5.0 percent for all but five cases.

Initial Estimates of the Elevation of the NPA

The application of the mass balancing procedure required an

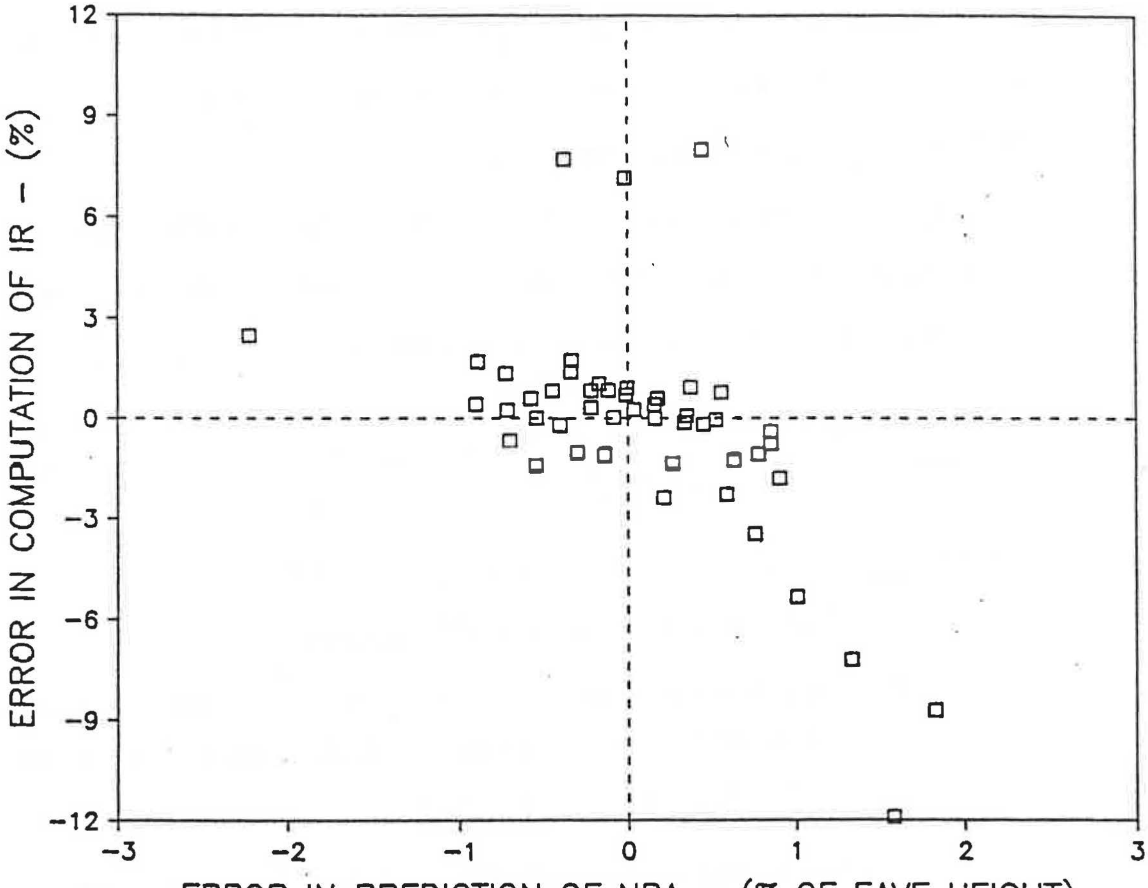

Figure 7.28 Error in the computed infiltration rate induced by the error in prediction of the position of the NPA.

initial estimate of the elevation of the NPA. Obviously, the number of iterations required to determine the predicted value of the NPA was a function of the quality of the initial estimate.

It was determined from the experimental investigation and from the literature cited (Emswiler, 1926; Lee et al., 1985) that the most important factors affecting the position of the NPA were the relative size of the openings in a distribution and their vertical placement. The factors which influenced the relative size of the openings were the cross-sectional area and the discharge coefficient. Based upon these observations the following empirical relationship was developed to provide an initial estimate of the NPA without iteration:

$$N_{est} = \sum_{j=1}^{n} h_j \, (C_{z_j} \, A_j)^k \Bigg/ \sum_{j=1}^{n} (C_{z_j} \, A_j)^k \tag{7.9}$$

where; N_{est} = the estimated elevation of the NPA,

h_j = the elevation of the j^{th} opening,

C_{z_j} = the discharge coefficient of the j^{th} opening computed at a ΔP of 4.0 Pa (using $\rho = 1.2236$ kg/m^3, $\nu = 1.4364 \times 10^{-5}$ m^2/s, T = 7.3°C (45°F)),

A_j = the cross-sectional area of the j^{th} opening, and

k = an empirical exponent of 1.24.

The exponent of 1.24 was determined as follows:

1. The overall average elevation of the observed NPA ($\bar{N}$) was computed for each opening group and placement combination (i.e., G1H1, G1H2, G2H1, G2H2, REC1, REC2, CYL, CYLREC, and NC);
2. The best value of k for each of these nine distributions was

iteratively determined by setting their respective values of $\bar{N}$ equal to equation 7.9; and

3. The average of these nine values of k was determined to be 1.24 (s = 0.645).

The values of N_{est} were computed by equation 7.9 (with k = 1.24) for each defined opening group and placement combination. These 9 estimates were compared with the 48 observed elevations of the NPA (NPA.DATA). The average error in the estimates was -0.12 percent of the eave height (0.6 cm; 0.24 in) and the maximum error was ±5.2 percent of the eave height (±25.8 cm; ±10.2 in). The overall average NPA of the No Cracks treatments was estimated within -4.6 percent of the eave height.

If the mass flow rates were balanced within ±0.000004 kg/s, then the initial estimation of the NPA obtained by equation 7.9 enabled the predicted elevation of the NPA to be determined by only 4 or 5 iterations. If the mass flow rates were balanced within ±0.00004 kg/s, then N_{est} enabled the predicted elevation of the NPA to be obtained in 2 or 3 iterations.

Chapter 8

THE EXPERIMENTAL VALIDATION OF THE DISCHARGE COEFFICIENT EQUATION AND THE APPLICATION OF THE THEORY TO THE MODELING OF ENVELOPE LEAKAGE

Introduction

The application of the mass balancing procedure to determine the elevation of the neutral pressure axis (NPA) of an actual structure would require a complete description of the vertical placement and the flow characteristics of the openings in the building envelope. Obviously, any attempt to locate and describe each individual opening would soon prove to be futile. A more feasible approach would be to model the flow through a building component, such as a window, as an equivalent opening. The equivalent opening would most likely be assigned to the elevation of the centroid of the modeled component. It may be necessary to model tall components as two equivalent openings placed at the elevations of the centers of the upper and lower halves of the actual component. If all of the components of the building envelope could be modeled in this manner then the elevation of the NPA and the resulting infiltration rate could be estimated from a blueprint.

The current practice (as described in chapter 3) consists of modeling structural components as an equivalent orifice with a constant discharge coefficient. The modeling parameter is termed the effective leakage area (equation 3.1) which is equivalent to the product of the cross-sectional area and a mean discharge coefficient. The results of the sensitivity analysis (chapter 6) indicated that for small openings, which are similar to envelope leakage, the discharge coefficient varied considerably with the relative size of the flow length. This suggests that the presence of the flow length should not be neglected.

Motivated by the conclusions of the sensitivity analysis and the measure of success experienced in modeling the influence of background leakage a supplementary experiment was performed to satisfy the following objectives:

a. To experimentally determine the importance of the flow length (i.e. friction loss) for small rectangular and cylindrical openings;

b. To experimentally validate the use of the discharge coefficient equation to compute the flow through small rectangular openings; and

c. To demonstrate the potential for the modeling of envelope leakage as an equivalent straight rectangular opening.

Description of the Experiment

An experiment was set up to validate the use of the discharge coefficient equation for the computation of laminar flow through short openings. Differential pressure measurements over a given range of volumetric flow rates were obtained for a group of rectangular and cylindrical openings. Flows to produce Reynolds numbers up to 3500 were used. All of the openings included in the experiment were short pipes with dimensionless flow lengths, z/D_h, from 2.0 to 15.9.

A description of the rectangular and cylindrical openings used in the experimental investigation has been presented in Tables 8.1 and

Table 8.1.
Geometric Description of the Rectangular Openings

ID.	d (mm)	z (mm)	w (mm)	A (cm^2)	α	B	γ $x10^{-4}$ (m^{-1})	($A\gamma$) $x10^{-5}$ (m)	D_h (mm)	z/D_h
A	0.8	25.4	500.1	4.00	0.0016	95.8	6.55	0.026	1.6	15.9
B	1.7	50.8	500.1	8.50	0.0034	95.6	6.95	0.059	3.4	14.9
C	2.0	12.7	500.1	10.00	0.0040	95.6	32.68	0.327	4.0	3.2
D	3.3	44.5	500.1	16.50	0.0066	95.3	15.36	0.253	6.6	6.7
E	6.3	88.9	499.3	31.45	0.0126	94.7	14.60	0.459	12.4	7.2
F	12.9	50.8	498.5	64.31	0.0259	93.2	51.98	3.334	25.1	2.0
G	13.4	152.4	500.1	67.01	0.0268	93.1	17.92	1.201	26.1	5.8

Table 8.2.
Geometric Description of the Cylindrical Openings

ID.	Number of Openings	D (mm)	z (mm)	A (cm^2)	γ $x10^{-4}$ (m^{-1})	($A\ \gamma$) $x10^{-5}$ (m)	z/D_h
X	2	6.4	50.8	0.32	979.05	0.313	7.9
Y	2	12.7	50.8	1.27	979.05	1.243	4.0

8.2, respectively. The seven rectangular openings have been divided into two classifications based upon the thickness of the opening (d) and the flow length (z). The openings labeled A through D are considered the most characteristic of structural leakage in a residence. The remaining openings are more representative of natural ventilation. In particular, slot F may be expected to behave in a manner similar to a window which has been slightly raised. Two different diameters of cylindrical openings were included and two openings of each size were fabricated to give a total of four openings. The construction of all of the openings used in this experiment was described previously in Chapter 4.

The dimensionless flow length, z/D_h, is shown for each of the rectangular and cylindrical openings. The size of the dimensionless flow length is an indicator of the relative importance of the contribution of the flow length to the total dimensionless pressure drop. An opening with a very small dimensionless flow length would be expected to contribute a negligible friction loss and behave as an orifice. Openings with relatively large values of z/D_h would contribute a significant friction loss characteristic of laminar flow through a pipe.

Four replications of air flow and differential pressure data were taken for each test specimen. For each replication the air properties were determined from a measurement of the local barometric pressure, and the wet-bulb and dry-bulb temperatures (Appendix C). The wet-bulb and dry-bulb temperatures were measured by means of a mechanical psychrometer and the barometric pressure reading was taken from a metallic coil barometer which was checked against a standard.

The experimental investigation was carried out in an airtight test box. The test box had a length of 1.54 m (60.5 in) and a cross-section of 0.93 m (36.63 in) by 0.63 m (24.63 in). In order to obtain an airtight test chamber with a smooth surface on the interior, the walls were constructed of plexiglass and all of the seams were sealed with silicone. The test chamber was tested for leakage and sealed where the leaks were found. An air diffuser, made of polyester filter material, was located 0.305 m (1 ft) downstream from the air supply inlet. A mounting plate for the test specimens was located 0.58 m (22.5 in) downstream from the air diffuser. The test openings were mounted within the test chamber by several bolts and gaps between the mounting plate and the openings were sealed with vacuum grease. Four 6.35 mm (0.25 in) copper tubing pressure taps were installed around the perimeter of the test chamber on each side of the mounting plate. Each set of four pressure taps were connected in parallel using copper tubing of like diameter. The mean static pressure drop across the openings was measured using a micromanometer that could be read within ±0.125 Pascals (0.0005 in of H_2O).

The air flow was supplied by a variable speed, positive displacement blower. The air flow was measured by variable area flow meters which were accurate to within ± 2.0 percent of full scale. For flow rates below 800.0 cm^3/s (1.7 cfm) the flow meter was calibrated against a positive displacement flow indicator.

Method of Data Analysis

All of the openings included in the experiment were classified as short pipes. A review of the literature indicated that the total minor loss coefficient (K) was an empirical value which can vary considerably between short pipes according to the degree of hydrodynamic development (K_{hd}) and the sharpness of the inlet (K_{inlet}). The value of K_{hd} for a particular short pipe will also vary with the Reynolds number and thus will vary with the flow rate. The magnitude of the variation of the minor loss coefficients in a particular opening is considerable for low flow rates.

The four replications of differential pressure and air properties data were averaged for each flow rate tested to give one flow versus pressure drop curve for each opening. A distribution of total minor loss coefficients was determined for each opening by applying the following relationship at each mean data point:

$$K = (K_{inlet} + K_{hd} + K_{ex}) = \frac{2\,\Delta P}{\rho\,\bar{V}^2} - B\left(\frac{z}{D_h Re}\right) \qquad (8.1)$$

The friction coefficient, B, was determined for the rectangular openings from equation 3.30. A friction coefficient of 64 was used for each of the cylindrical openings. The importance of the flow length for each of the openings was determined by a comparison of the magnitudes of the dimensionless friction losses and the total minor loss coefficients.

A mean total minor loss coefficient (K) was determined for each opening by averaging the minor loss coefficients obtained (using equation 8.1) over the entire range of pressure differences. In a practical situation it would be desirable to simplify the computation of a discharge coefficient by using a mean value of K over as a wide range of pressure differences as possible. Using the mean total minor loss coefficient (K) for each opening, the flow rates were computed using the discharge coefficient method (equation 3.26 with equation 3.21) and compared with the measured flow rates.

The purpose of this portion of the analysis was not to endorse the use of a particular value of K. Instead, the purpose was to determine if the discharge coefficient method is a reliable technique to compute the flow through a short opening provided the proper value of K is known.

The sensitivity analysis (Chapter 6) demonstrated that a 20 percent error in K would only induce a 0.3 to 8.7 percent error in the discharge coefficient depending upon the magnitude of ($A\gamma$) and the pressure difference. The error in the discharge coefficient would render the same percentage of error in the computation of the flow rate. Based upon the capabilities of the instrumentation, the uncertainty of the flow measurements ranged from $\pm$ 2.0 percent (at full scale) to $\pm$ 10.0 percent and the estimated error in the differential pressure measurements ranged from $\pm$ 0.2 to $\pm$ 8.9 percent. The uncertainty associated with the measurement of the cross-sectional dimensions of the openings was the source of the greatest consistent error. An analysis of the propagation of error in computing the area of the openings indicated that the greatest percentage of error was in the measurement of the slot thickness, d for the rectangular openings and the diameter (D) for the cylindrical openings (Appendix F). Also, the percentage of uncertainty in the calculation of the area for the rectangular openings was identical to the percentage of uncertainty in the measurement of the slot thickness. Recalling that the uncertainty of the measurement of the opening dimensions was $\pm$ 0.25 mm (0.01 in), the uncertainty of the area of each rectangular opening may be determined from Table 8.1. The uncertainty of the areas ranged from 1.9 to 31.7 percent. The uncertainty in the area for openings X and Y were ±8 and ±4 percent respectively. For most of the openings the flow prediction error associated with a 15 to 20 percent error in the estimation of K would be less than the errors associated with the air flow, differential pressure and opening dimension measurements.

The distribution of the total minor loss coefficients and the comparison of the measured and the computed volumetric flow rates are presented separately for the rectangular and cylindrical openings in the following sections. The data for each opening and the total minor loss coefficients for each opening are presented in Appendix G.

Results for the Rectangular Openings

For the rectangular openings A and B the Reynolds numbers ranged from 19 to 777. It was observed that for Reynolds numbers less than 400 the scatter of the values of K greatly increased as the Reynolds number continued to decrease.

The Reynolds number may be interpreted as the ratio of the inertia forces to the viscous forces and at large Reynolds numbers the viscous forces are considered negligible. The increase in scatter was believed to be related to the greater importance of the viscous forces at very low Reynolds numbers. As a result, only data points with Reynolds numbers greater than 400 were used with equation 8.1.

In order to determine the relative importance of the dimensionless flow length, the total minor loss coefficients for each rectangular opening were plotted against the term $B(z/D_hRe)$ (refer to Figure 8.1). As was expected, the dimensionless flow length,

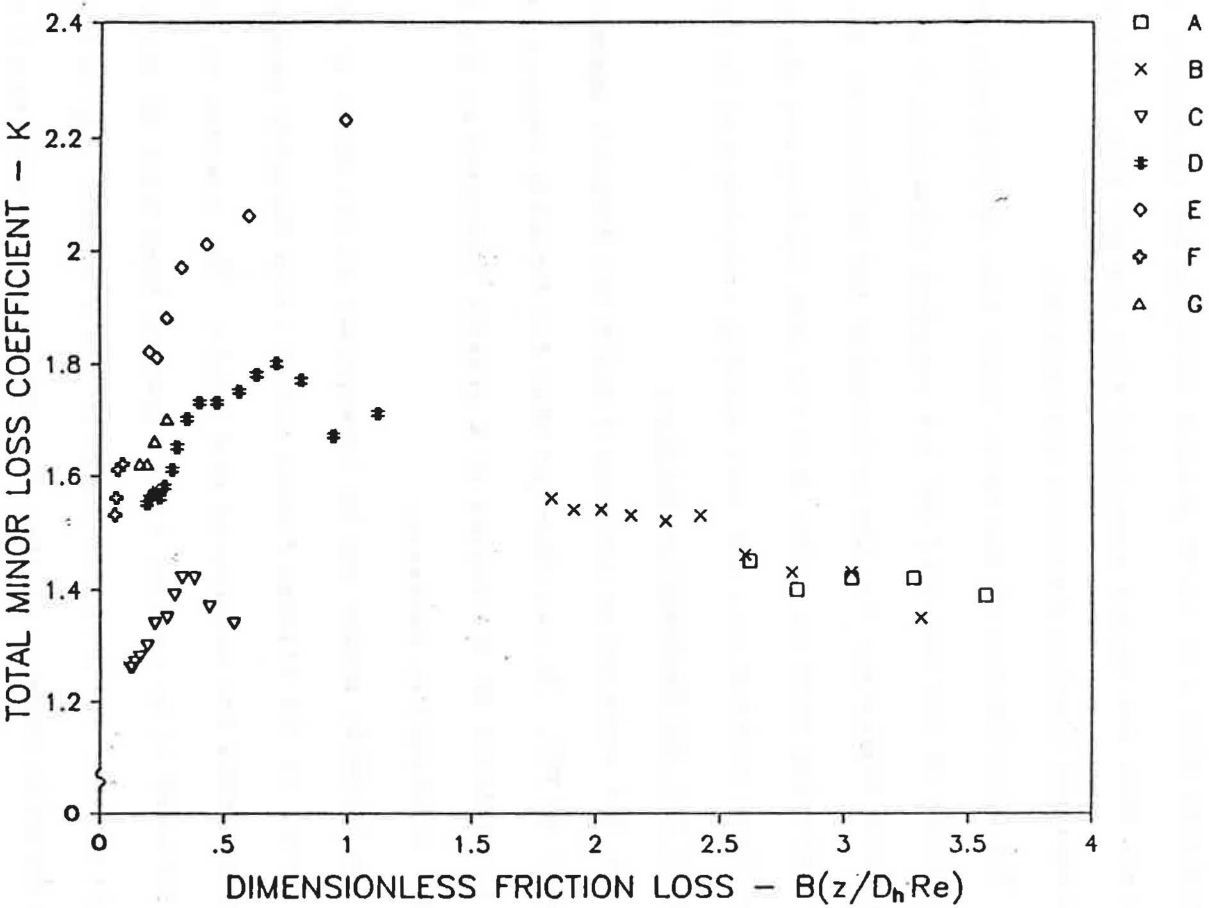

Figure 8.1 Comparison of the dimensionless friction loss and the total minor loss coefficients for the rectangular openings.

z/D_h, may be used to make a distinction among the different openings. The slots with the largest dimensionless flow lengths, namely A and B, provided a friction loss that was greater than the total minor loss coefficient at every point. This suggested that the flows in these two openings may have developed near the exit of the slots. The flow length is clearly not negligible. It was speculated that the decrease in K for these two openings was a result of the very low Reynolds numbers where the viscous forces became more important.

The remaining five slots had values of z/D_h ranging from 2.0 to 7.2. For all of these openings the minor loss coefficients were greater than the dimensionless friction loss at every point and the importance of the friction loss varied with the Reynolds number.

The relative importance of the flow length for this group of openings may be readily demonstrated by a closer examination of the data of slots D (z/D_h=6.7) and F (z/D_h=2.0). A comparison at the extreme values of Reynolds number (refer to Figure 8.1 and Table 8.3) indicated that the dimensionless friction loss of slot D contributed about 40 percent of the total pressure drop at a Reynolds number of 573 and 11 percent of the total pressure drop at Re equal to 3440. Even though the contribution of the dimensionless friction loss varied by a factor of 3.6, neglect of the flow length would incur significant error. For slot F the presence of the flow length accounted for 3.8 percent (at Re = 3356) to 5.3 percent (at Re = 2013) of the total dimensionless pressure drop. Therefore, slot F behaved the most like an orifice and over the range of data considered, the flow length could probably be neglected.

Table 8.3.
Mean Total Minor Loss Coefficients for the Rectangular Openings

ID.	z/D_h	$\bar{K}$	Std. Dev.	Maximum	Minimum	Range of Re
A	15.9	1.42	0.023	1.45	1.39	426 to 581
B	14.9	1.49	0.071	1.56	1.35	427 to 777
C	3.2	1.33	0.059	1.42	1.26	574 to 2524
D	6.7	1.67	0.088	1.80	1.55	573 to 3440
E	7.2	1.97	0.149	2.23	1.81	680 to 3400
F	2.0	1.58	0.042	1.62	1.53	2013 to 3356
G	5.8	1.65	0.038	1.70	1.62	2014 to 3347

In general, the pressure loss induced by the presence of the flow length should not be neglected for dimensionless flow lengths greater than 2.0. Furthermore, the slots which are the most characteristic of structural leakage (A through D) had dimensionless flow lengths ranging from 3.2 to 15.9. The data strongly implied that for the modeling of leakage characteristic of infiltration the effect of the flow length should be included.

The average total minor loss coefficients for each rectangular opening are presented along with the standard deviations and extremes in Table 8.3. Inspection of the magnitudes of the standard deviations reveals that they are all below 0.15 and the majority are below 0.10. Based on a review of literature pertaining to flow through rectangular channels, (Beavers et al. 1970; Etheridge, 1977; Fox and McDonald, 1973; Han, 1960) the observed variation of the total minor loss coefficients was not considered excessive. Furthermore, the subtractive process used to determine the individual values of K tended to accentuate the variation. Therefore, the flow rates were predicted over the entire range of observed pressure differences for each opening using its respective value of $\bar{K}$.

The flow rates predicted by the equations have been compared in Figure 8.2 with the observed flow rates. The flow measurement range was 77.7 cm^3/s (0.16 cfm) to 14160 cm^3/s (30.0 cfm) and the corresponding range of pressure drops was 1.4 Pa (.0056 in H_2O) to 83.4 Pa (0.3349 in H_2O). An equal range of flow and pressure differentials for each slot was not possible due to the limitations of the equipment or the occurrence of Reynolds numbers greater than 3500 at the higher pressure differentials.

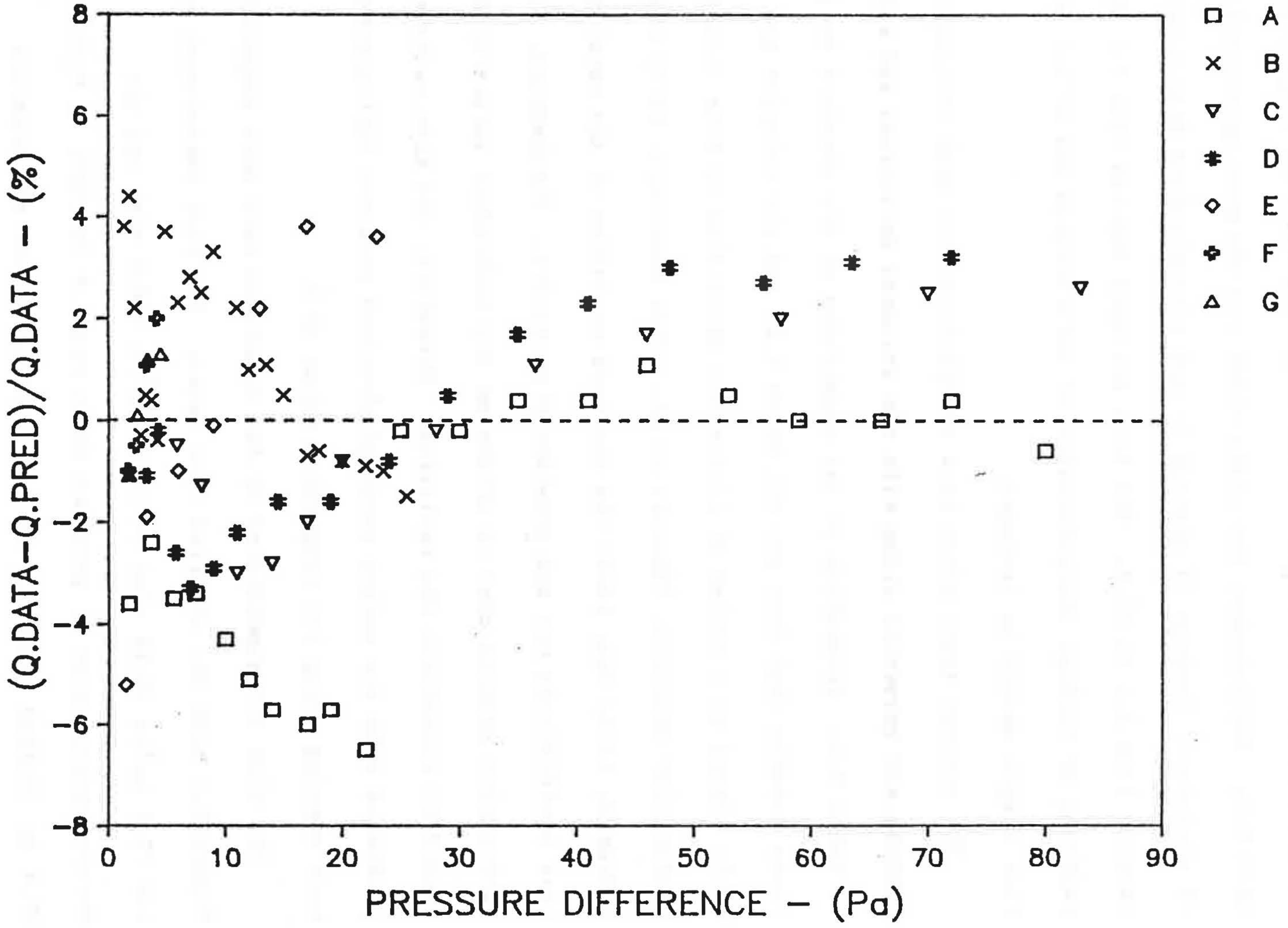

Figure 8.2 Comparison of the measured and calculated flow rates for the rectangular openings (using the average K values given in Table 8.3).

The majority of the flow predictions for the rectangular openings were within ± 4.0 percent of the measured values. A total of eight points were outside this band. Six of these points were from the data of slot A and they were measured using the same flow meter. The scatter of the data presented in Figure 8.2 implies that part of the error associated with these six points was due to an unknown systematic error. It is believed that the source of this error was in the flow measurement since the flows measured at differential pressures greater than 25 Pa used a different flow meter and the errors were less than 1 percent. In addition, the relatively low flow measurements for these points correspond to a range of Reynolds numbers from 95 to 197. It was stated previously that values of K were only determined from data at Reynolds numbers greater than 400.

The data point with the greatest percentage of error (−6.5 percent) was in the prediction of the flow rate for slot A at a pressure drop of 22.3 Pa. The flow measurement was 799.4 cm^3/s (1.69 cfm) and the error was 52.3 cm^3/s (0.11 cfm). The maximum absolute difference occurred for the prediction of flow through slot E at a ΔP of 22.9 Pa and a flow measurement of 14160 cm^3/s (30.0 cfm). The absolute difference was 516.4 cm^3/s (1.09 cfm) which corresponds to an error of 3.6 percent. The uncertainty of the flow measurements ranged from ± 2.0 percent (at full scale) to ± 10.0 percent. The estimated error in the differential pressure measurements based upon the capabilities of the instrument ranged from ±0.15 to ±8.9 percent. The uncertainty of the areas ranged from 31.2 percent for slot A to 1.9 percent for slot G.

Taking into consideration the errors discussed, it was concluded that the discharge coefficient method was able to predict the measured flow rates within the uncertainty of the measured quantities using a mean total minor loss coefficient. In particular, the results for slots A, C, and D indicated that a mean total minor loss coefficient may be applied over a differential pressure range as large as 1.5 to 80 Pascals for short rectangular channels with aspect ratios in the range of 0.0016 to 0.0066. In addition, the comparisons for slots A and B suggest that an average total minor loss coefficient which has been determined at Reynolds numbers greater than 400 may be applied relatively well for Reynolds numbers as low as 19. The results for slots F and C indicated that the discharge coefficient equation may be applied to rectangular openings with very small dimensionless flow lengths.

Results for the Cylindrical Openings

The sum of the minor loses and the losses induced by the flow length have been compared in Figure 8.3. As was true for the rectangular openings, each point shown represents four replications of data.

The distribution of the total minor loss coefficients for the cylindrical openings differ from the rectangular openings in two respects. The minor loss coefficients for the cylindrical openings increased with $B(z/D_hRe)$ at approximately three times the rate of the rectangular openings over a comparable range of $B(z/D_hRe)$ and z/D_h. Also, the distribution of the K values for all of the cylindrical openings appears to be monotonic. The contribution of the dimensionless friction loss to the total dimensionless pressure drop varied with the Reynolds number from 4.6 percent to a maximum of 19

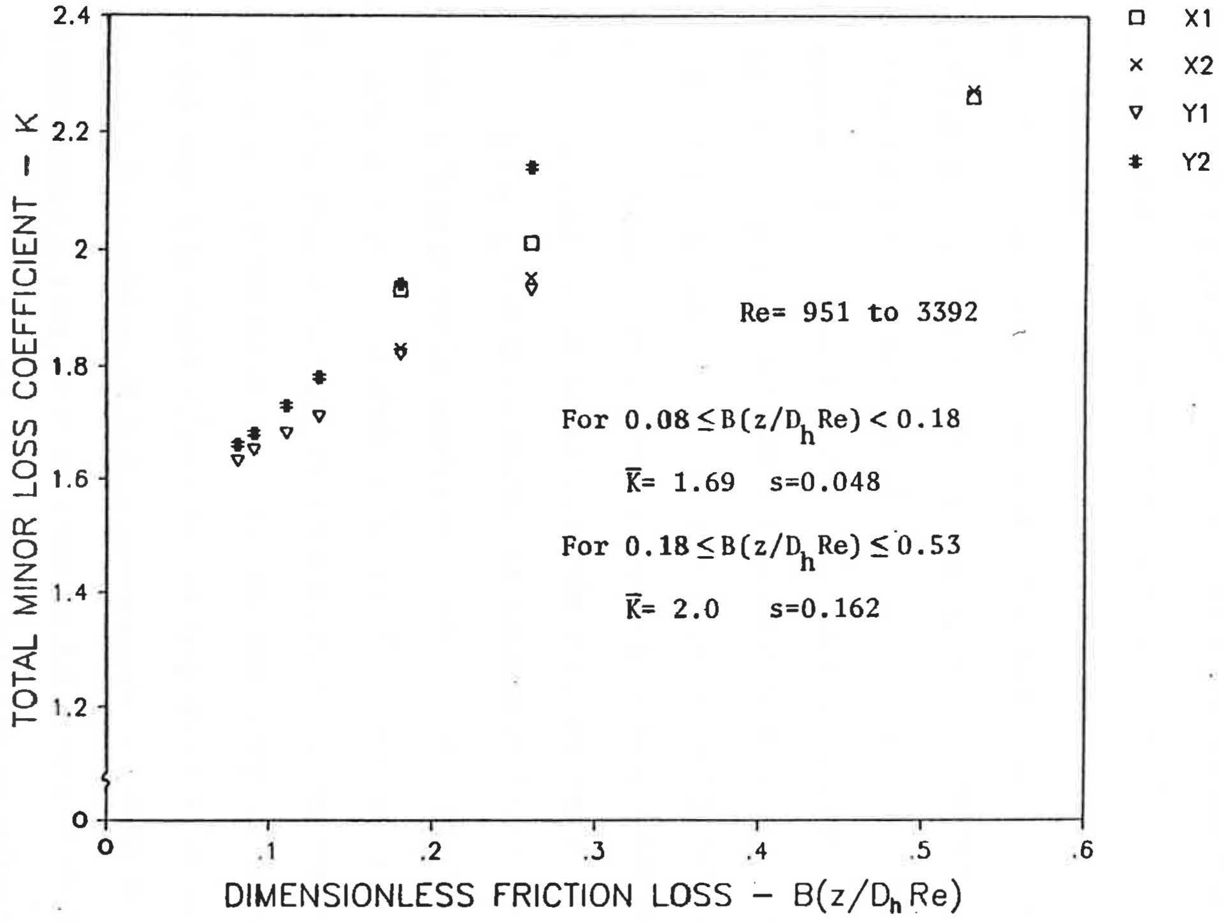

Figure 8.3 Comparison of the dimensionless friction loss and the total minor loss coefficients for the cylindrical openings.

percent. Therefore, the contribution of the dimensionless frictional loss should not be neglected.

Due to the great variability, the total minor loss coefficients of all four of the cylindrical openings were averaged over two ranges of the dimensionless friction loss. For values of $B(z/D_hRe)$ from 0.18 to 0.53 the flow rates were predicted by the discharge coefficient method using a $\bar{K}$ of 2.0 (std. dev. = 0.162). For values of $B(z/D_hRe)$ less than 0.18 a $\bar{K}$ of 1.69 (std. dev. = 0.048) was used. The minimum friction loss was 0.08. The criterion used for the selection of the ranges was the magnitude of the standard deviation of the mean total minor loss coefficients. It was desired to minimize the magnitudes of the standard deviations and thereby maximize the ranges of application. The comparison of the measured flows with those predicted have been presented in Figure 8.4. The residuals in percent were plotted against the dimensionless friction loss (Figure 8.4) to facilitate comparison with Figure 8.3.

For openings X1 and X2 the range of measured flow rates was 77.7 cm^3/s (0.16 cfm) to 307.2 cm^3/s (0.65 cfm). The corresponding pressure drops ranged from 9.3 Pa (0.0373 in H_2O) to 60.9 Pa (0.2446 in H_2O). The measured flow rates for Y1 and Y2 varied from 158.2 cm^3/s (0.34 cfm) to 549.0 cm^3/s (1.16 cfm) with differential pressure measurements of 2.0 Pa (0.0080 in H_2O) to 18.4 Pa (0.0739 in H_2O). All of the flow rates were measured with the same flow meter which had an error of $\pm$ 15.7 cm^3/s (0.03 cfm). The number of data points obtained was limited by the capabilities of the flow meter and the occurrence of Reynolds numbers greater than 3500 at pressure drops greater than the upper limits indicated.

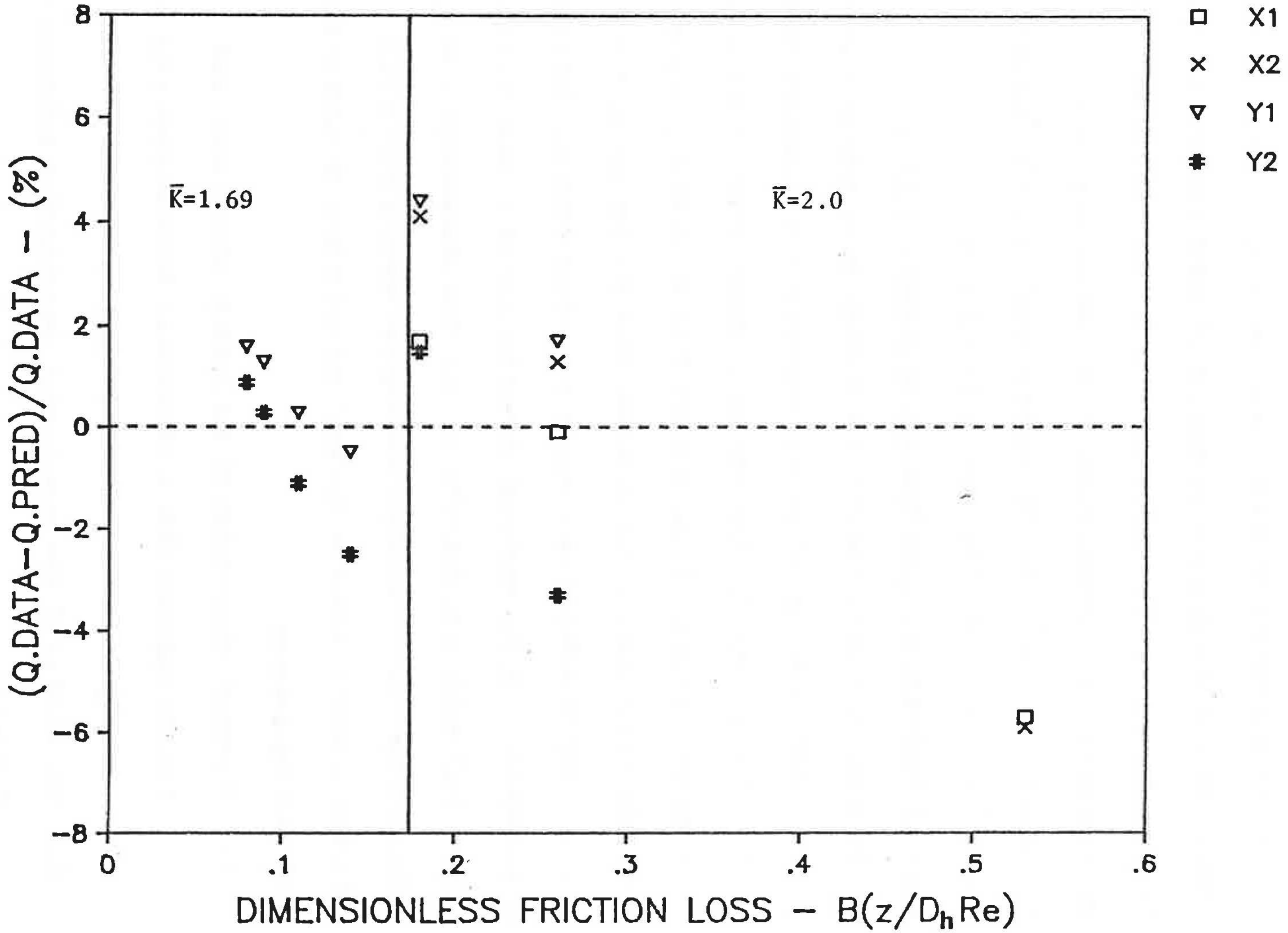

Figure 8.4 Comparison of the measured and calculated flow rates for the cylindrical openings (using values of $\bar{K}$ presented in Figure 8.3).

The majority of the flow rates measured were predicted within ± 4.0 percent and the points with errors greater than 4.0 percent were within the uncertainty of the measured quantities. The flow prediction with the greatest percentage of error was for X2. The flow measurement was 77.7 cm^3/s (at ΔP = 9.3 Pa) and the error in prediction was -5.9 percent which is equivalent to an absolute difference of 4.6 cm^3/sec. The maximum absolute difference was 10.3 cm^3/s (for Y1, Q = 232.6 cm^3/s; ΔP = 3.8 Pa).

Proposed Application to the Modeling of Structural Leakage

In order to compute the air flow through an opening at a given pressure difference and set of air properties the parameters that are required are A, γ and K. The same requirements apply to the modeling of structural leakage. It is proposed that if an appropriate average total minor loss coefficient is known, then the leakage of a building component may be modeled as a single equivalent opening. This would be accomplished by the empirical determination of an area (A_m) and a gamma (γ_m) which best describe the air flow characteristic of the building component. A straight rectangular opening with a small hydraulic diameter would be the most suitable type of opening for the following reasons.

1. A general observation of the leakage around doors and windows suggests that a rectangular cross-section with a small D_h would be the most appropriate.
2. The results of the experimental investigation indicated the following:
   a. The air flow through straight rectangular openings with dimensions most typical of infiltration (A through D)

may be predicted over a range of differential pressures as great as 1.5 to 72 Pascals using a single mean total minor loss coefficient; and

b. The flow through straight rectangular openings with hydraulic diameters in the range of 1.6 mm to 6.6 mm may be expected to remain laminar for differential pressures which greatly exceed those typical of infiltration.

The primary requirement to model a building component as an equivalent straight rectangular opening is to determine a mean total minor loss coefficient for modeling structural leakage, K_s. From Table 8.3, the value of K_s was determined to be 1.5 (std. dev. = 0.14) by averaging the mean total minor loss coefficients of openings A, B, C, and D. Referring to Table 8.1, it can be shown that the corresponding mean aspect ratio was 0.0039. Using an aspect ratio of 0.0039 sets the mean friction coefficient, B, at 95.6 (from Table 8.1 or equation 3.30). These values of K_s and B were in close agreement with the results presented by Etheridge (1977) for straight rectangular slots with dimensions typical of infiltration.

Rearranging the terms in equation 3.23 and setting K equal to K_s the dimensionless energy equation may be written in the following form:

$$\frac{2\Delta P}{\rho \overline{V}^2} = \frac{2\Delta P A^2}{\rho Q^2} = \frac{\nu}{4Q\gamma_m} + K_s \tag{8.2}$$

where:

$$\frac{\nu}{4Q\gamma_m} = B\left(\frac{z}{D_h Re}\right) = \text{the dimensionless friction loss}$$

The equation to be used for modeling a building component as an equivalent straight rectangular opening was obtained by solving equation 8.2 for the pressure drop, ΔP.

$$\Delta P = bX \tag{8.3}$$

where; $$X = \left[\frac{\mu Q}{8\gamma_m} + \frac{\rho K_s Q^2}{2} \right] \qquad [N * m^2]$$

$$b = \frac{1}{A_m^2} \qquad [m^{-4}]$$

The air flow through a building component would be modeled as a straight rectangular opening by determining the equivalent opening parameters (A_m and γ_m) according to the following procedure.

1. The pressure drop, ΔP, across the component and the corresponding flow rate, Q, would be measured over a wide range and the air properties would be determined.
2. Successive approximations of γ_m would be made and the corresponding A_m would be determined by application of a least squares best fit to equation 8.3.
3. The flow rates would be predicted using the discharge coefficient method for each γ_m and its corresponding A_m.
4. The A_m and γ_m which best predicts the observed volumetric flow rates would be chosen to model the leakage of the component.

In equation 8.2 it was shown that the total dimensionless pressure drop across any opening or building component is the sum of the dimensionless pressure drops given by the dimensionless friction loss, $\nu/4Q\gamma_m$, and the total minor loss coefficient, K_s. In essence, the modeling procedure involves the assignment of a value for the total minor loss coefficient, and then iterating on the three dimensional scale of the equivalent opening until a value of gamma, γ_m, is determined such that the sum of $\nu/4Q\gamma_m$ and K_s is equivalent equivalent to $2\Delta P/\rho\bar{V}^2$ over the range of data. If the total minor loss coefficient of the actual building component is greater than K_s then the additional pressure drop would be compensated by a smaller value of γ_m which would yield a greater dimensionless friction loss. From the definition of gamma for a rectangular opening (equation 3.24) it can be seen that a decrease in gamma would be the result of an increase in the flow length (z) or a decrease in the aspect ratio.

Up to this point the discussion has been devoted exclusively to the modeling of subjects which have straight flow paths. The actual flow paths of the leakage of a structure are often characterized by expansions, contractions and bends. The presence of these sources of minor loss can add from 0.2 to 1.3 to the total minor loss coefficient (ASHRAE, 1985; Fox and McDonald, 1978). Due to the extreme variability of these types of pressure losses, the more predictable situation of a near infinite straight rectangular opening is preferred. It is theorized that the increased pressure drop due to contractions, expansions, and bends would also be compensated by a decrease in the value of gamma of the equivalent straight rectangular opening.

For laminar flow the friction factor, B/Re, is not a function of the surface roughness of the opening (Fox and McDonald, 1978). For turbulent flows the surface roughness causes the friction factor to increase which in turn causes the dimensionless friction loss to increase. If the modeling procedure was applied to flows in the turbulent regime it is believed that the value of gamma of the equivalent rectangular opening would decrease to compensate for the increase in the dimensionless friction loss.

For the purpose of demonstration, the modeling procedure has been applied to the data of openings A, B, C, D, E, and Y1. Slots A through D were chosen because their cross-sectional dimensions were the most characteristic of infiltration. Slot E was selected because it was the rectangular opening with the largest value of $\bar{K}$ as well as the greatest variability (refer to Table 8.3). The opening Y1 was included to determine if a cylindrical opening could be modeled as an equivalent straight rectangular opening with a constant total minor loss coefficient.

It was determined that the easiest method to determine when the best pair of opening parameters (A_m and γ_m) had been obtained was by comparing the average error in the prediction of the flow rates. The pair of equivalent opening parameters that gave a mean error closest to zero was chosen. A plot depicting the use of this technique has been provided in Appendix H.

The results of the modeling procedure have been presented in Table 8.4 and the comparison of the flows using the equivalent opening parameters with the data have been shown in Figure 8.5. All but four of the predicted flow rates agreed with the measured flow rates within $\pm$ 3.0 percent and the error in each of the predictions was within the uncertainty of the measurements. Also, the average error in the prediction of flow was within $\pm$0.6 percent for all of the openings.

Table 8.4
Results of the Modeling Procedure

Opening ID	A_m (cm^2)	$(A-A_m)$ %	γ_m $x10^{-4}(m^{-1})$	$(\gamma-\gamma_m)$ %	$(A\gamma)_m$ $x10^{-5}(m^{-1})$	$(\bar{K}-K_s)$ %	r^2
A	4.29	-7.3	5.5	16.0	0.024	-5.3	0.9994
B	8.35	1.8	7.87	-13.2	0.066	-0.7	0.9997
C	11.07	-10.7	20.0	38.8	0.221	-11.3	0.9999
D	16.44	0.4	12.0	21.9	0.197	11.3	0.9997
E	29.61	5.9	10.0	31.5	0.296	31.3	0.9997
Y1	1.26	0.8	400.0	59.1	0.504	N/A	0.9999

Note: Values of $\bar{K}$ are from Table 8.3.

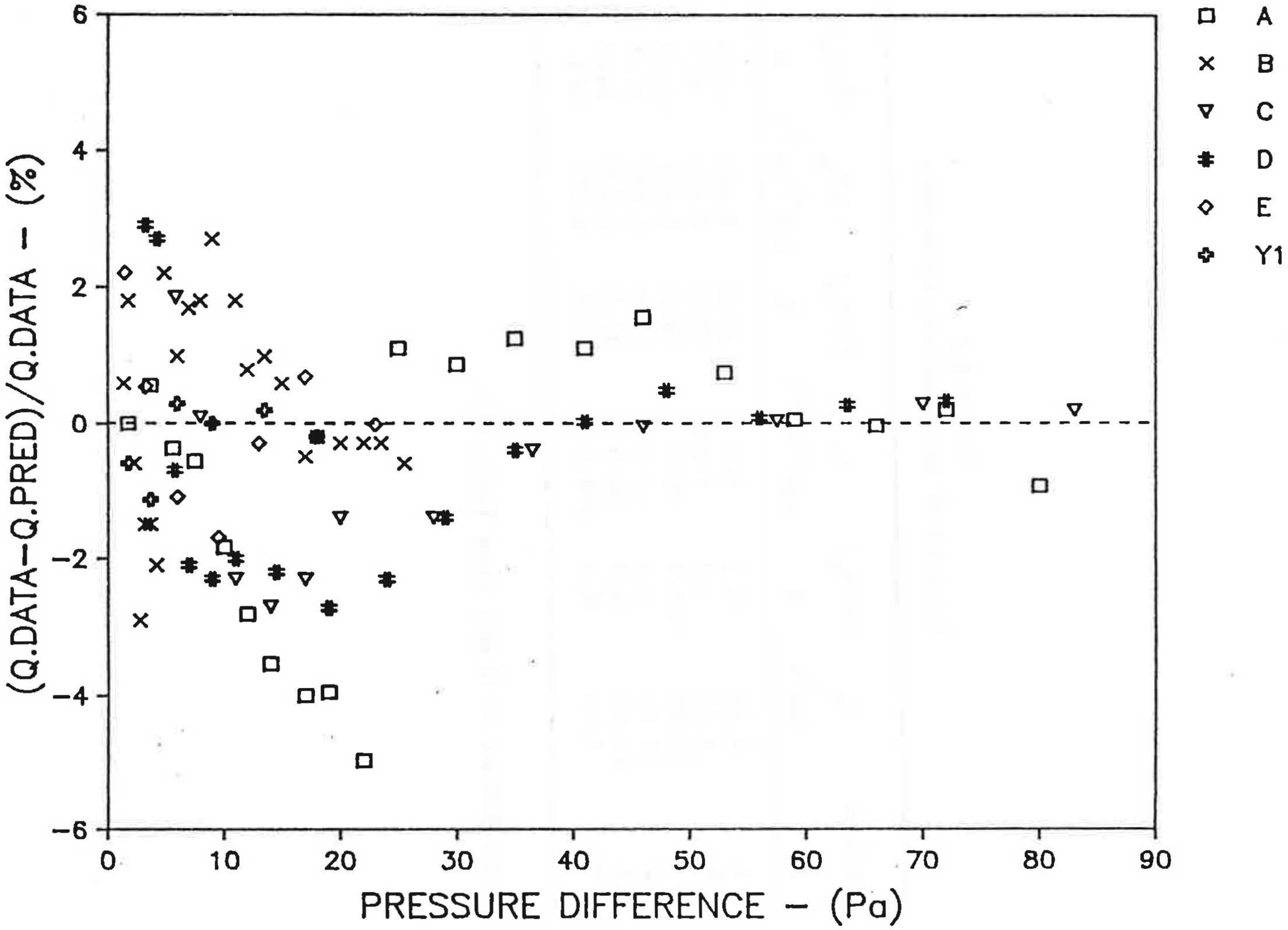

Figure 8.5 Comparison of the predicted flow rates with those observed using the equivalent opening parameters shown in Table 8.4 (K_s = 1.5).

Comparison of the equivalent opening parameters (Table 8.4) with the actual values (shown in Tables 8.1 and 8.2) indicated that the magnitude of the percent difference in area ranged from 0.4 to 10.7 percent while the magnitude of the difference in γ ranged from 13.2 to 59.1 percent. Therefore, the three dimensional scale of the model slot varied more than the cross-sectional area. Furthermore, the only cross-sectional area which was not predicted within the uncertainty of the measurements was for opening E. The uncertainty in the area for opening E was $\pm$ 4.0 percent. The additional error in the prediction of A for this opening was believed to be related to the larger magnitude of K for opening E. This also implied that the values of A_m had a relatively good degree of physical significance.

Comparison of the values of K in Table 8.3 with K_s indicated that the percent difference between γ and γ_m was the greatest when the percent difference between $\bar{K}$ and K_s was the greatest. Consequently, for the cases when K_s was less than the actual total minor loss coefficient the additional pressure drop required was provided by a smaller value of gamma. The smallest magnitude of percent difference between γ and γ_m was for opening B. Opening B had a mean total minor loss coefficient which was almost identical to K_s.

The dimensions of the model slots were determined by using an average aspect ratio of 0.0039 and a $\bar{B}$ of 95.6 and they are presented in Table 8.5. The flow length was determined by solving the defining equation of gamma for a rectangular opening (equation 3.24) for z. The thickness, d, was calculated by:

$$d = \sqrt{A_m \alpha} \tag{8.4}$$

Table 8.5
Dimensions of the Equivalent Straight
Rectangular Openings

$\bar{\alpha} = 0.0039$ $\bar{B} = 95.6$ $K_s = 1.5$

Opening ID.	d (mm)	w (mm)	z (mm)	D_h (mm)	z/D_h
A	1.3	330.0	74.1	2.6	28.6
B	1.8	463.9	51.3	3.6	14.3
C	2.1	527.1	20.5	4.2	4.9
D	2.5	657.6	33.4	5.0	6.7
E	3.4	870.9	40.6	6.8	6.0
Y1	0.7	180.0	1.0	1.4	0.7

The hydraulic diameter (D_h) and the dimensionless flow length, (z/D_h), were determined from the appropriate defining equations.

Noting that the resistance of a rectangular opening may be increased by either decreasing α or increasing z, comparison of the dimensions and parameters given in Table 8.5 with the physical measurements (Tables 8.1 and 8.2) allows the following general observations.

1. If the actual aspect ratio was greater than the α assumed then the values of D_h and $(A\gamma)$ of the model slot were less than the actual values.
2. A straight cylindrical opening has very little resistance due to the cross-section relative to a near infinite rectangular opening. As a result, the greatest reduction in D_h, $(A\gamma)$ and z occurred for opening Y1.

It must be emphasized that even though an average aspect ratio of 0.0039 was used for demonstration, this is not meant to imply that a value of 0.0039 should always be used. The actual modeling and computation of the flow characteristic of an opening depends entirely upon the magnitudes of the parameters A_m and γ_m. The assumption of an aspect ratio was only required to estimate the dimensions of the equivalent straight rectangular opening.

It is believed that the leakage of structural components may be modeled as an equivalent straight rectangular opening. Using a mean total minor loss coefficient for modeling structural leakage (K_s), the equivalent opening parameters A_m and γ_m would be determined by the outlined procedure. The advantages of using the modeling procedure described are:

1. The dimensions of the modeling equation (equation 8.3) are homogeneous.
2. The effect of the flow length as well as the dimensionless properties of the cross-section may be included.
3. The variation of the discharge coefficient with ($A\gamma$) as well as ΔP may be taken into account.

The modeling of structural leakage as an equivalent straight rectangular opening has been presented in concept only. In order to apply the modeling procedure to actual structural leakage the modeling procedure needs to be experimentally validated for actual building components. The effects of bends, contractions, and turbulent flows need to be experimentally determined also.

Chapter 9

SUMMARY AND CONCLUSIONS

A review of the literature indicated that the position of the neutral pressure axis (NPA) for envelope leakage under pure stack conditions is primarily dependent upon the relative size of the individual openings, their resistance to flow and their vertical distribution. The factor subject to the greatest ambiguity was the description of the flow resistance of relatively short openings common to infiltration.

A semi-empirical equation to directly compute the discharge coefficient was developed from the general energy equation for laminar flow through a straight channel of arbitrary cross-section. The discharge coefficient may be viewed as a dimensionless flow resistance described by the following functional statement:

$$C_Z = f[\ (A\gamma),\ \Delta P,\ K,\ \mu,\ \rho\ ]$$

The area-gamma product $(A\gamma)$, represents the total geometric contribution to the flow resistance of an opening. The geometric parameter, gamma, is a three dimensional scale factor which represents the resistance due to the geometry of the cross-section and the flow length. The total minor loss coefficient (K) represents the losses due to the inlet geometry, the degree of hydrodynamic development, and the exit. Hence, the total minor loss coefficient is the empirical portion of the equation.

The discharge coefficient equation was incorporated into a procedure to predict the elevation of the NPA for general distributions of rectangular or cylindrical openings. The procedure to predict the elevation of the NPA was an iterative technique based upon a direct application of the continuity equation written in terms of the mass flow rate.

A two cell environmental chamber was constructed to simulate the temperature gradients across the shell of a two story residence. An insulated wall and ceiling section divided the chamber into a cold room and a warm room. Idealized openings could be mounted in the test wall at nine different locations. The ceiling section had one location for mounting an opening and a circular mounting plate to facilitate the study of a chimney at a later date.

Several idealized straight rectangular and cylindrical openings were constructed of acrylic sheet. The dimensionless flow length (z/D_h) ranged from 1.0 to 15.9.

A collection of experiments were performed to investigate the factors which influence the location of the NPA and to test the validity of the mass balancing procedure of determining the elevation of the NPA. The parameters varied were: the total leakage area mounted in the test sections; the size of the individual openings; the geometry of the openings; the vertical placement and the mean temperature difference. The differential pressure across the test sections was measured as a function of elevation for six opening groups, five opening distributions and four ranges of temperature difference. The elevation of the NPA and the mean density difference were determined from each differential pressure profile using a regression technique. The observed elevations of the NPA ranged from 15.2 to 73.7 percent of the eave height of the test wall. The temperature was also measured with respect to elevation in each room to observe any stratification which may occur.

It was determined that a significant amount of unidentifiable and uncorrectable leakage existed in the two room environmental chamber. As a result, the chamber leakage (or background leakage) was treated as an additional opening group. Twelve replications of data were taken for the background leakage at several differential temperature conditions. The average elevation of the NPA was observed to be at 56.4 percent of the eave height. To facilitate inclusion of the effects of the background leakage in the mass balancing procedure, the leakage was modeled as two hypothetical openings based upon the differential pressure profiles observed for the environmental chamber.

The following results concerning the description of the pressure differences due to the stack effect were established from the linear regression on the observed differential pressure profiles.

1. The coefficients of determination (r^2) of the 60 differential pressure profiles observed were all greater than 0.9986.
2. These high levels of correlation yielded 95 percent confidence intervals for the elevations of the NPA from $\pm$0.7 cm ($\pm$0.26 in) to $\pm$3.1 cm ($\pm$1.22 in).
3. The mean density difference between the two rooms was also determined from the regression. The 95 percent confidence intervals were from $\pm$0.47 to $\pm$1.98 percent.
4. It was found that 99.3 percent of the observed differential pressures were within the 95 percent prediction interval

about each regression line. Therefore, the variation of the density difference with elevation induced by the observed degree of temperature stratification did not have a meaningful influence on the prediction of the differential pressures.

The following results were found concerning the factors which influence the position of the NPA.

1. A variation of the mean temperature difference from 16°C (28.8°F) to 48.4°C (87.1°F) had no significant effect on the position of the NPA.
2. The observed degree of temperature stratification had no distinguishable effect on the position of the NPA.
3. The elevation of the NPA was observed to vary by as much as 27 percent of the eave height depending upon the vertical placement of openings in a distribution (G1H1 and G1H2).
4. The elevation of the NPA was observed to vary by as much as 30.7 percent of the eave height due to a variation of the opening group used for a particular vertical placement (REC1 and REC2).
5. The elevation of the NPA was observed to vary by as much as 56.2 percent of the eave height depending upon the combined variation of the opening groups and the vertical placements.
6. For the cases with an opening placed in the test ceiling (H2) the NPA was observed to vary with the density of the cold air above the test ceiling. This variation was determined to induce a variation in the elevation of the NPA which was equivalent to 0.75 percent to 2.8 percent of the

eave height.

The prediction of the elevation of the NPA by means of the mass balancing procedure (including the effects of the background leakage) yielded the following results.

1. It was determined that the elevation of the NPA was predicted within the uncertainties of the measured quantities and the errors in regression for 95.8 percent of the cases which involved openings placed in the test sections.
2. For all of the treatments which involved openings placed in the test sections, the elevations of the NPA were predicted within ±1.0 percent of the eave height for 91.7 percent of the observations; within ±2.0 percent of the eave height for 97.9 of the observations; and within ±2.22 percent of the eave height for all observations.
3. The elevation of the NPA was predicted within ±1.0 percent of the eave height for 95.8 percent of the cases which included an opening placed in the ceiling.
4. The mean elevation of the NPA for the background leakage was predicted within ±1.05 percent of the eave height using the two model openings.
5. It was found that the infiltration rate varied linearly with respect to the mean temperature difference.
6. It was determined that an error in the prediction of the NPA equivalent to ±2.22 percent of the eave height, resulted in an error in the computed infiltration rate within ±5.0 percent (±0.013 ach) for all but five cases.

The following conclusions were developed based upon the results of the experiment.

1. The differential pressures due to the stack effect varied linearly with elevation.
2. The slope of the differential pressure distribution was a function of the mean density difference of the air in the two rooms.
3. The slope of the differential pressure profile was independent of the location of the NPA.
4. The elevation of the NPA was primarily a function of the relative size of the openings in a distribution, a variable resistance to flow (discharge coefficient) and the vertical placement.
5. The position of the NPA was not a function of the mean temperature difference.
6. The density of the air above an opening placed in the test ceiling induced a small variation in the position of the NPA.
7. The observed degree of temperature stratification had no effect on the position of the NPA.
8. The mass balancing procedure was able to predict the position of the NPA within ±2.22 percent of the eave height for each of the opening distributions.
9. The two largest sources of error in the prediction of the NPA were: the inability to describe the variation of the background leakage in the two cell environmental chamber and the use of a single total minor loss coefficient for all of

the openings.

Application of the mass balancing procedure to compute the elevation of the NPA for an actual structure would require a method to model the air flow through a building component (such as a window) as an equivalent opening. A supplementary experiment was performed to develop the concept of modeling components of envelope leakage as an equivalent straight rectangular opening.

Differential pressure measurements over a specified range of flow rates were obtained for a group of straight openings which ranged in cross-sectional geometry from a near infinite rectangular slot to a cylinder. The dimensionless flow length, z/D_h, of the openings was varied from 2.0 to 15.9. Furthermore, flows to produce Reynolds numbers up to 3500 were used.

A distribution of total minor loss coefficients, K, was determined for each opening by subtracting the dimensionless friction loss, $B(z/D_h Re)$, from the total dimensionless pressure drop, $2\Delta P/\rho\bar{V}^2$. A comparison of the magnitudes of $B(z/D_h Re)$ and K yielded the following observations.

1. The total minor loss coefficient varied from 1.26 to 2.23 for the rectangular openings depending upon the cross-sectional geometry and the degree of hydrodynamic development.
2. The rectangular openings with cross-sectional dimensions most characteristic of structural leakage had dimensionless flow lengths from 3.2 to 15.9 and aspect ratios from 0.0016 to 0.0066. Over a differential pressure range of about 1.5 to 80 Pascals the contribution of the dimensionless friction

loss to the total dimensionless pressure drop ranged from 8.7 to greater than 70 percent. Thus, the presence of the flow length should be included in the modeling of envelope leakage.

3. The total minor loss coefficient varied from 1.64 to 2.26 for the cylindrical openings depending upon the degree of hydrodynamic development.

4. It was determined that the contribution of the flow length to the total dimensionless pressure drop was not negligible for openings of any cross-section with dimensionless flow lengths greater than 2.0.

A mean total minor loss coefficient was determined for each rectangular opening and the flow rates were predicted using the discharge coefficient method (equations 3.26 and 3.21). It was found that a mean value of K was adequate for use with the discharge coefficient equation over the range of data obtained.

The total minor loss coefficient of the cylindrical openings varied with the degree of hydrodynamic development three times as much as rectangular openings with similar magnitudes of $B(z/D_hRe)$. As a result, it was concluded that a rectangular cross-section would be preferred for modeling structural leakage.

In order to model the air flow through a building component as an equivalent straight rectangular opening the parameters required are: an equivalent cross-sectional area (A_m); an equivalent gamma (γ_m); and a mean total minor loss coefficient for modeling structural leakage (K_s). The value of K_s was determined to be 1.5 by averaging the mean total minor loss coefficients of four rectangular openings which had cross-sectional dimensions most similar to those found about doors and windows of a residence. A modeling equation (equation 8.3) was developed from the dimensionless energy equation which, when applied according to the outlined procedure, could be used to determine the values of A_m and γ_m of the equivalent straight rectangular slot.

The modeling procedure was applied to the data of six openings to demonstrate its use. Openings with cross-sections ranging from a near infinite rectangular slot to a circular cross-section were used.

The modeling of the six defined openings as an equivalent near infinite straight rectangular slot provided the following results and conclusions.

1. The cross-sectional areas of the equivalent slots (A_m) agreed with the actual areas within the uncertainty of the measurements for all but one case. Therefore, the cross-sectional area of the equivalent rectangular slot had a good degree of physical significance.
2. The gammas of the equivalent slots (γ_m) differed from the actual gammas depending upon the agreement between the actual mean total minor loss coefficient of the particular opening and the value of K_s used in the modeling equation. Therefore, the three dimensional scale of the equivalent slot was not the same as the actual opening.
3. Using a single value of K_s and the equivalent opening parameters (A_m and γ_m), the measured flow rates were predicted within the uncertainties of the measurements for each of the defined openings.

Chapter 10

SUGGESTIONS FOR FURTHER RESEARCH

From the results of the experiments of the present study it was concluded that the mass balancing procedure can be used to determine the elevation of the neutral pressure axis (NPA) for any distribution of straight rectangular or cylindrical openings. Furthermore, the results of modeling the background leakage and a few of the fabricated openings as equivalent straight rectangular openings suggests that the leakage of individual building components may also be modeled as equivalent straight rectangular openings. Therefore, application of the mass balancing procedure to the envelope leakage of an actual building would require the further development of the modeling technique to describe the various sources of leakage in a residence. Several of the sources of leakage which would need to be included are doors, windows, penetrations for duct work and plumbing, electrical outlets and switches, and structural joints.

In addition, the appropriate elevation for an equivalent rectangular opening needs to be determined for each of the various types of leakage components. For most equivalent openings the elevation of the centroid of the actual component would probably be satisfactory. For sources of leakage that are much taller than they are wide it may be necessary to model the leakage as two equivalent openings. The openings would most likely be placed at the elevations of the centers of the upper and lower halves of the actual component.

The present study has only considered leakage in the envelope of a structure. One of the largest sources of infiltration that is not part of the shell of a structure is a chimney. The pressure drop across a chimney is a combination of the pressure difference due to the stack effect and a pressure difference resulting from the much higher temperatures at the base of a chimney. In order to include a chimney in the mass balancing procedure, a reliable method of computing the total pressure drop across a chimney must first be developed.

The other source of potential for infiltration which needs a large amount of study is the pressure distribution across the surface of a structure due to wind velocities. In general, wind pressures on the windward side of a structure are positive and pressures on the leeward side are negative. The pressures on the other surfaces of the structure can fluctuate from positive to negative depending upon the incident wind angle, fluctuations in the wind speed, and the shape of the building. If the three dimensional distribution of wind pressures could be determined for a design wind velocity, then the total three dimensional differential pressure profile across the shell of a structure would be obtained by simply adding the wind pressures to the differential pressures due to the stack effect. The total infiltration rate would be obtained by adding the magnitudes of the mass flows through all of the sources of infiltration and dividing by two. A practical method of computing the distribution of wind pressures across a structure is currently not available.

APPENDIX A

NOMENCLATURE

A_e	- equivalent leakage area
A	- cross-sectional area
A_m	- cross-sectional area of an equivalent rectangular opening
B	- friction coefficient
C	- flow coefficient ($m^3/s * Pa^n$)
C_d	- discharge coefficient for idealized laminar flow
C_z	- discharge coefficient for real laminar flow
D	- diameter of a cylindrical channel
D_h	- hydraulic diameter
d	- thickness of a rectangular channel
h	- elevation
IR	- infiltration rate
K	- total minor loss coefficient
K_{inlet}	- inlet loss coefficient
K_{hd}	- loss due to hydrodynamic development
K_{ex}	- exit loss coefficient
K_s	- mean total minor loss coefficient for modeling structural leakage
L_e	- the entrance length of a long pipe or duct
$\dot{m}$	- mass flow rate (kg/s)
NPA	- neutral pressure axis
N	- elevation of the NPA
ΔP	- pressure difference (Pa)
Q	- Volumetric flow rate (m^3/s)

Re	- Reynolds number
s	- standard deviation
$\bar{V}$	- average velocity (m/s)
W	- humidity ratio (kg_w/kg_a)
w	- width of a rectangular channel
z	- flow length
z/D_h	- dimensionless flow length
α	- aspect ratio
γ	- geometric parameter (m^{-1})
γ_m	- geometric parameter for an equivalent straight rectangular opening
$(A\gamma)$	- area-gamma product (m)
$(A\gamma)_m$	- area gamma product for an equivalent straight rectangular opening
ρ	- density (kg/m^3)
ν	- kinematic viscosity (m^2/s)
μ	- dynamic viscosity ($N * s/m^2$)

APPENDIX B

SOLUTION OF THE NAVIER-STOKES EQUATION FOR LAMINAR FLOW BETWEEN INFINITE PARALLEL FLAT PLATES

The case of fully developed laminar flow between two infinite parallel plates separated by a distance, d, is shown in Figure B.1.

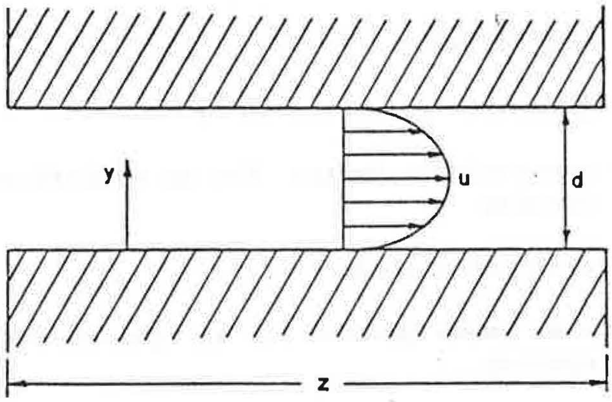

Figure B.1. Laminar flow between infinite parallel plates.

Using the coordinates as defined in the figure, the velocity vector is:

$$\vec{V} = (v,\ w,\ u) \tag{B.1}$$

$$\rho\left(\frac{\partial u}{\partial t} + v\,\frac{\partial u}{\partial x} + w\,\frac{\partial u}{\partial y} + u\,\frac{\partial u}{\partial z}\right) = -\,\frac{\partial P}{\partial z} - \rho g + \mu\left(\frac{\partial^2 u}{\partial x^2} + \frac{\partial^2 u}{\partial y^2} + \frac{\partial^2 u}{\partial z^2}\right) \tag{B.2}$$

where; P = pressure,

t = time,

ρ = density,

μ = dynamic viscosity, and

g = gravity.

The Navier-Stokes equation may be simplified by application of the following assumptions:

1. The fluid is viscid and incompressible;
2. The flow is laminar and fully developed;
3. The velocity is steady and in the z-direction only ($\partial u/\partial t = 0$; $v = w = 0$);
4. The velocity varies in the y-direction only ($u=f(y)$);
5. The pressure varies linearly and in the direction of flow ($P = f(z)$);
6. The gravity effects are negligible ($\rho g = 0$);
7. There are no entrance or exit losses; and
8. The full no-slip boundary condition exists ($u(0) = 0$; $u(d) = 0$).

Application of assumptions 3, 4 and 6 gives the following simplified Navier-Stokes equation.

$$0 = -\frac{dP}{dz} + \mu\left(\frac{d^2u}{dy^2}\right) \tag{B.3}$$

The fully developed laminar velocity profile may be obtained by integrating the simplified Navier-Stokes equation twice with respect to y. The generalized velocity profile is given by:

$$u(y) = \frac{1}{\mu}\left(\frac{dP}{dz}\right)\frac{y^2}{2} + Ay + B \tag{B.4}$$

The constants of integration, A and B, may be determined by application of the boundary condition at each interior surface of the flow channel.

$$u(0) = 0 \text{ requires that } B = 0$$

$$u(d) = 0 \text{ gives;} \qquad A = -\frac{1}{\mu}\left(\frac{dP}{dz}\right)\frac{d}{2} \tag{B.5}$$

Substitution of A and B into the general velocity profile gives the equation for the velocity distribution for fully developed laminar flow.

$$u(y) = \frac{1}{2\mu}\left(\frac{dP}{dz}\right) y(y-d) \tag{B.6}$$

The flow equation may be obtained by integrating equation B.6 across the cross-section of the channel.

$$Q = \int_0^w \int_0^d u(y)\, dy\, dx \tag{B.7}$$

The resulting equation for the flow per unit width is:

$$\frac{Q}{w} = \frac{-d^3}{12\mu}\left(\frac{dP}{dz}\right) \tag{B.8}$$

Based upon the assumption that the pressure gradient is linear in the direction of flow (assumption 5), the variables may be separated and integration of equation B.8 gives:

$$\frac{Q}{w} = \frac{-d^3\ \Delta P}{12\ \mu\ z} \tag{B.9}$$

Equation B.9 is identical to equation 3.4 except for the sign. The classical derivation of the full Navier-Stokes equation assumes that a negative pressure gradient yields a positive flow (Currie, 1974). The negative sign has been dropped in equation 3.4 because in many practical situations the sign convention used assumes that a positive pressure drop produces a positive flow. Furthermore, the air flow into a residence has been assumed to be positive and the result of a positive differential pressure (refer to equation 2.8).

APPENDIX C

RELATIONSHIPS USED TO COMPUTE AIR PROPERTIES

The dynamic or absolute viscosity of air is a function of the temperature only under normal atmospheric conditions. The dynamic viscosity of air was computed using the following empirical equation (Fox and McDonald, 1978):

$$\mu = \frac{b\sqrt{T}}{1 + S/T} \tag{C.1}$$

where: $b = 1.458 \times 10^{-6}$ (kg/m*s*$K^{1/2}$),

$S = 110.4$ (K),

T = the dry bulb temperature (K), and

μ = the dynamic viscosity, (N*s/m^2).

The density of the air, ρ, is equivalent to the inverse of the specific volume of a moist air mixture. The specific volume was computed from the following relationship (ASHRAE, 1981, Ch. 5):

$$v_{sp} = \frac{R_a\, T}{BP}(1 + 1.6078\ W) \tag{C.2}$$

where; R_a = the gas constant for dry air = 287.055 (J/kg*K),

BP = the barometric pressure (Pa),

W = the humidity ratio (kg_w/kg_a), and

v_{sp} = the specific volume (m^3/kg).

For the air in the warm room, the humidity ratio was determined from the equation given in ASHRAE (1981, Ch. 5) as:

$$W = \frac{(2501 - 2.381\ T_{wb})\ W_s^* - (T - T_{wb})}{(2501 + 1.805\ T - 4.186\ T_{wb})} \tag{C.3}$$

where; T_{wb} = the wet bulb temperature (°C),

T = the dry bulb temperature (°C),

W_s^* = the humidity ratio corresponding to saturation at T_{wb} (kg_w/kg_a).

The values of W_s^* were determined from the following regression equations:

For T_{wb} = 289 K to 300 K

$$\ln (W_s^*) = -109.41153 + 18.51963 \ln (T_{wb}) \qquad (C.4a)$$

For T = 283 K to 289 K

$$\ln(W_s^*) = -112.13592 + 19.00025 \ln (T_{wb}) \qquad (C.4b)$$

These two equations were determined from a linear regression on the psychrometric data given in the ASHRAE Fundamentals Handbook (1981, Table 1 pg 6.3).

For the air in the cold room, the humidity ratio (W) was set equal to the humidity ratio corresponding to the dew point temperature (T_{dp}). The values of W_s were determined from the following regression equations which were determined in the same manner as described previously.

For T_{dp} = 274 K to 283 K

$$\ln (W_s) = -115.10110 + 19.52567 \ln (T_{dp}) \qquad (C.5a)$$

For T_{dp} = 258 K to 273 K

$$\ln (W_s) = -135.75649 + 23.20829 \ln (T_{dp}) \qquad (C.5b)$$

For T_{dp} = 243 K to 258 K

$$\ln (W_s) = -143.86171 + 24.66858 \ln (T_{dp}) \qquad (C.5c)$$

The kinematic viscosity, ν, is defined by the following expression:

$$\nu = \mu/\rho \ (m^2/s). \tag{C.6}$$

APPENDIX D

SUMMARY OF THE REGRESSION COMPUTATIONS

The elevation of the neutral pressure axis and the mean density difference between the warm and the cold room were determined from each differential pressure profile by fitting the data to a linear equation of the following form:

$$y = a + bx \tag{D.1}$$

where; $y = \Delta P$ (Pa),

x = elevation (m),

$b = -g\,\overline{\Delta\rho}$ (Pa/m),

$a = g\overline{\Delta\rho}N$ (Pa),

$N = |a/b|$ = elevation of the NPA (m),

$\overline{\Delta\rho} = |b/g|$ = (kg/m^3).

The equations to compute the slope, y-intercept, coefficient of determination (r^2), and the 95 percent confidence intervals for the slope and the elevation of the NPA (N) are outlined in the following steps (Steel and Torrie, 1980; Younger, 1979).

1. Corrected Sums of Squares and Cross Products

$$S_{XX} = \Sigma x^2 - (\Sigma x)^2/n \tag{D.2a}$$

$$S_{YY} = \Sigma y^2 - (\Sigma y)^2/n \tag{D.2b}$$

$$S_{XY} = \Sigma xy - (\Sigma x)(\Sigma y)/n \tag{D.2c}$$

where; n = total number of ordered pairs = 18

2. Calculation of the slope and y-Intercept

$$b = S_{XY}/S_{XX} \tag{D.3}$$

$$a = \bar{y} - b\bar{x} \tag{D.4}$$

where; $\bar{x}$ = the mean of all elevations

$\bar{y}$ = the mean of all pressure differences

3. Calculation of the Coefficient of Determination

$$r^2 = (S_{XY})^2/S_{XX}(S_{YY}) \tag{D.5}$$

4. Estimation of the Variance About the Regression Line

$$s_{y.x}^{2} = S_{YY}^{2} - [(S_{XY})^2/S_{XX}] \tag{D.6}$$

5. The 95 Percent Confidence Interval for the Slope

$$95\%\ \text{C.I.} = b \pm t_{\alpha/2(n-2)} \sqrt{s^2_{y.x}/S_{XX}} \tag{D.7}$$

where; (n - 2) = the error degrees of freedom.

$t_{0.025(16)} = 2.12$

6. The 95 Percent Confidence Interval About the Elevation of the NPA.

The y-intercept of the regression equation was equal to the product of the slope and the elevation of the NPA. As a result, a straight forward method of computing a 95 percent confidence interval about the elevation of the NPA (N) was not available. Instead a confidence interval for the difference between a particular value of x (elevation) and $\bar{x}$ was computed from the following formula (P. L. Cornelius, personal communication, Feb. 1986; Snedecor and Cochran, 1980):

$$(x - \bar{x}) = \frac{1}{(1 - c^2)}\left[\hat{x} \pm \frac{t_{\alpha/2(n-2)}\ s_{y.x}}{b}\sqrt{\frac{(1-c^2)}{n} + \frac{\hat{x}^2}{\Sigma x^2}}\right] \tag{D.8}$$

where; $c^2 = \dfrac{1}{\Sigma x^2}\left(\dfrac{t_{\alpha/2(n-2)}\ s_{y.x}}{b}\right)^2$, and

$\hat{x} = (x - \bar{x})$.

For the case at hand, the value of x that is of interest is the elevation of the NPA, N. Therefore, a confidence interval was computed for the difference $(N - \bar{x})$. The resulting confidence interval for N was determined by simply adding $\bar{x}$ to the two final values.

7. <u>The 95 Percent Confidence Interval About An Individual Prediction of the Pressure Difference (y_i).</u>

$$y_i = t_{.025(n-2)} s_{y.x} \sqrt{1 + \frac{1}{n} + (x_i - \bar{x})} \qquad (D.9)$$

where; y_i = the predicted pressure difference, and

x_i = the corresponding elevation for Y_i.

This type of confidence interval is generally called a prediction interval (Younger, 1979).

APPENDIX E

DATA AND REGRESSION RESULTS

Table E.1
Chronological Order of the Data

DAY NUMBER	DATE (1986)
1	1/30
2	1/31
3	2/3
4	2/5
5	2/6
6	2/7
7	2/8
8	2/11
9	2/12
10	2/13
11	2/14
12	2/15
13	2/17
14	2/18
15	2/19
16	2/21
17	2/22
18	2/23
19	2/24

Table E.2
Day Number on Which Each Set of Data Were Taken

	DAY NUMBER		
TREATMENT	REP1	REP2	REP3
G1H1T1	2	4	8
G1H1T2	5	6	10
G1H1T3	3	7	12
G1H2T1	2	4	8
G1H2T2	3	6	10
G1H2T3	3	7	11
G2H1T1	2	4	8
G2H1T2	3	6	9
G2H1T3	3	7	12
G2H2T1	2	4	9
G2H2T2	2	6	10
G2H2T3	3	7	10
REC1	14	15	15
REC2	14	15	15
CYL	16	16	17
CYLREC	17	17	18
NCT1	1	4	9
NCT2	12	18	19
NCT3	4	12	19
NC35	13	13	16

Table E.3 Data and Regression Results

Definition of terms used in Table E.3

BP - Local barometric pressure, Pa

C - Temperature, Celsius

C.I. - 95% confidence interval (Appendix D)

den. - density

DP - Pressure difference

DT - Mean temperature difference

k.vis. - kinematic viscosity

Tc - cold room temperature

Tdp - dew point temperature

Tw - warm room temperature

Twb - wet bulb temperature

Dden-reg - the mean density difference determined from the regression equation (Appendix D)

Dden-temp - $g\rho_c(DT/Tw)$ (Tw in absolute scale)

NOTE: The cold room air properties for temperature condition three (T3) were computed assuming the air was 75% saturated.

Table E.3a

Test ID.= G1H1T1 Data at Time= 25 min.

Elev. (m)	Rep 1 DP (Pa)	Rep 1 Tw (C)	Rep 1 Tc (C)	Rep 2 DP (Pa)	Rep 2 Tw (C)	Rep 2 Tc (C)	Rep 3 DP (Pa)	Rep 3 Tw (C)	Rep 3 Tc (C)
0.052	4.80	18.8	-28.8	4.27	17.8	-26.0	4.27	15.1	-25.9
0.305	4.27			3.87			3.80		
0.610	3.60	20.9	-28.8	3.33	19.8	-25.7	3.20	17.3	-25.9
0.914	2.93			2.67			2.60		
1.219	2.20	20.5	-28.5	2.00	19.4	-25.7	2.00	17.0	-25.8
1.524	1.53			1.40			1.40		
1.829	0.85	21.4	-27.7	0.81	20.4	-24.7	0.80	18.1	-25.3
2.134	0.12			0.17			0.17		
2.438	-0.53	22.0	-27.5	-0.43	20.9	-24.4	-0.44	18.8	-25.1
2.743	-1.24			-1.07			-1.07		
3.048	-1.93	22.3	-27.2	-1.73	21.3	-24.2	-1.67	19.0	-25.1
3.353	-2.60			-2.33			-2.33		
3.658	-3.27	22.1	-27.1	-2.93	21.0	-23.8	-2.93	18.7	-24.8
3.962	-4.00			-3.53			-3.53		
4.267	-4.53	22.1	-26.4	-4.20	20.9	-23.6	-4.13	18.9	-24.7
4.572	-5.20			-4.80			-4.67		
4.877	-5.87	22.6	-25.1	-5.33	21.6	-22.2	-5.33	19.4	-23.6
4.959	-6.27		-23.1	-5.73		-19.9	-5.60		-21.5
MEANS ---->		21.4	-27.0		20.3	-24.0		18.0	-24.7
		DT= 48.4 C			DT= 44.3 C			DT= 42.8 C	

Mean Air Properties

		Warm Room			Cold Room		
Rep	BP (Pa)	Twb (C)	den. (kg/m^3)	k.vis. (m^2/s)	Tdp (C)	den. (kg/m^3)	k.vis. (m^2/s)
1	99017.8	12.2	1.1621	0.00001566	-31.2	1.4017	0.00001126
2	97324.6	14.4	1.1414	0.00001589	-29.4	1.3610	0.00001171
3	98238.9	9.4	1.1686	0.00001543	-31.5	1.3781	0.00001154

Regression Results Using the Model DP=a+(b*h)

Rep	NPA (m)	C.I.	Slope (Pa/m)	C.I.	r^2	Dden-reg (kg/m^3)	Dden-temp (kg/m^3)
1	2.205	0.013	-2.2360	0.0186	0.99975	0.2279	0.2304
2	2.211	0.015	-2.0341	0.0191	0.99969	0.2073	0.2056
3	2.208	0.009	-2.0051	0.0121	0.99987	0.2044	0.2026

Table E.3b

Test ID.= G1H1T2 Data at Time= 30 min.

Elev. (m)	Rep 1 DP (Pa)	Rep 1 Tw (C)	Rep 1 Tc (C)	Rep 2 DP (Pa)	Rep 2 Tw (C)	Rep 2 Tc (C)	Rep 3 DP (Pa)	Rep 3 Tw (C)	Rep 3 Tc (C)
0.052	2.67	20.8	-8.1	2.40	20.7	-5.4	2.53	17.7	-8.3
0.305	2.40			2.13			2.20		
0.610	2.00	21.8	-8.0	1.80	21.8	-5.6	1.87	19.5	-8.1
0.914	1.60			1.47			1.47		
1.219	1.27	21.2	-7.9	1.20	21.0	-5.5	1.15	19.2	-8.0
1.524	0.87			0.80			0.79		
1.829	0.53	22.0	-7.3	0.40	22.0	-4.8	0.43	20.0	-7.4
2.134	0.13			0.11			0.07		
2.438	-0.13	22.6	-7.0	-0.27	22.6	-4.7	-0.27	20.7	-7.4
2.743	-0.60			-0.60			-0.64		
3.048	-0.93	22.8	-7.0	-0.87	22.9	-4.5	-1.00	21.0	-7.2
3.353	-1.33			-1.27			-1.33		
3.658	-1.73	22.6	-7.0	-1.60	22.5	-4.4	-1.73	20.7	-7.1
3.962	-2.13			-2.00			-2.13		
4.267	-2.53	22.5	-6.7	-2.33	22.7	-4.3	-2.47	20.6	-6.8
4.572	-2.80			-2.67			-2.80		
4.877	-3.20	22.9	-6.0	-3.00	23.1	-3.8	-3.20	21.3	-6.2
4.959	-3.40		-5.0	-3.13		-2.7	-3.33		-5.2
MEANS ---->		22.1	-7.0		22.1	-4.5		20.1	-7.1
		DT= 29.1 C			DT= 26.7 C			DT= 27.2 C	

Mean Air Properties

		Warm Room			Cold Room		
Rep	BP (Pa)	Twb (C)	den. (kg/m^3)	k.vis. (m^2/s)	Tdp (C)	den. (kg/m^3)	k.vis. (m^2/s)
1	96985.9	13.9	1.1329	0.00001609	-9.6	1.2666	0.00001327
2	97663.2	13.3	1.1418	0.00001596	-6.6	1.2630	0.00001340
3	99525.7	10.0	1.1763	0.00001541	-9.5	1.3006	0.00001291

Regression Results Using the Model DP=a+(b*h)

Rep	NPA (m)	C.I.	Slope (Pa/m)	C.I.	r^2	Dden-reg (kg/m^3)	Dden-temp (kg/m^3)
1	2.249	0.017	-1.2270	0.0137	0.99956	0.1251	0.1248
2	2.216	0.015	-1.1285	0.0111	0.99965	0.1150	0.1142
3	2.186	0.011	-1.1837	0.0083	0.99982	0.1207	0.1208

Table E.3c

Test ID.= G1H1T3 Data at Time= 50 min.

Elev. (m)	Rep 1 DP (Pa)	Rep 1 Tw (C)	Rep 1 Tc (C)	Rep 2 DP (Pa)	Rep 2 Tw (C)	Rep 2 Tc (C)	Rep 3 DP (Pa)	Rep 3 Tw (C)	Rep 3 Tc (C)
0.052	1.73	20.8	1.5	1.73	21.4	2.7	1.47	22.3	6.6
0.305	1.60			1.47			1.28		
0.610	1.33	21.7	1.3	1.27	22.3	2.3	1.09	23.6	6.6
0.914	1.08			1.05			0.88		
1.219	0.84	21.1	1.4	0.80	21.7	2.4	0.67	23.0	6.7
1.524	0.59			0.55			0.48		
1.829	0.35	22.0	2.1	0.32	22.5	3.0	0.29	24.2	7.5
2.134	0.08			0.07			0.03		
2.438	-0.15	22.4	2.2	-0.16	23.0	3.1	-0.11	24.2	7.8
2.743	-0.39			-0.40			-0.32		
3.048	-0.67	22.7	2.2	-0.67	23.2	3.2	-0.53	24.4	8.1
3.353	-0.92			-0.91			-0.72		
3.658	-1.17	22.4	2.2	-1.15	22.9	3.0	-0.92	24.0	8.0
3.962	-1.47			-1.40			-1.12		
4.267	-1.67	22.5	2.2	-1.60	23.0	3.2	-1.31	24.1	8.3
4.572	-1.93			-1.87			-1.53		
4.877	-2.20	23.0	2.5	-2.13	23.4	3.7	-1.73	24.5	8.8
4.959	-2.27		2.6	-2.27		4.3	-1.87		10.2
MEANS ---->		22.0	2.0		22.6	3.1		23.8	7.8
		DT= 20.0 C			DT= 19.5 C			DT= 15.9 C	

Mean Air Properties

Rep	BP (Pa)	Warm Room Twb (C)	Warm Room den. (kg/m^3)	Warm Room k.vis. (m^2/s)	Cold Room Tdp (C)	Cold Room den. (kg/m^3)	Cold Room k.vis. (m^2/s)
1	98238.9	15.0	1.1456	0.00001591	75%	1.2379	0.00001394
2	98306.6	13.3	1.1479	0.00001590	Sat	1.2335	0.00001403
3	98713.0	13.9	1.1478	0.00001595	***	1.2148	0.00001444

Regression Results Using the Model DP=a+(b*h)

Rep	NPA (m)	C.I.	Slope (Pa/m)	C.I.	r^2	Dden-reg (kg/m^3)	Dden-temp (kg/m^3)
1	2.229	0.014	-0.8241	0.0075	0.99971	0.0840	0.0841
2	2.213	0.018	-0.7982	0.0089	0.99955	0.0814	0.0815
3	2.249	0.019	-0.6632	0.0081	0.99947	0.0676	0.0653

Table E.3d

Test ID.= G1H2T1 Data at Time= 20 min.

Elev. (m)	Rep 1 DP (Pa)	Rep 1 Tw (C)	Rep 1 Tc (C)	Rep 2 DP (Pa)	Rep 2 Tw (C)	Rep 2 Tc (C)	Rep 3 DP (Pa)	Rep 3 Tw (C)	Rep 3 Tc (C)
0.052	7.47	19.4	-26.6	7.20	17.9	-26.8	7.20	16.2	-27.0
0.305	6.93			6.80			6.67		
0.610	6.13	20.9	-26.8	6.13	19.8	-27.0	6.13	18.3	-27.1
0.914	5.47			5.47			5.47		
1.219	4.80	20.7	-26.6	4.80	19.5	-26.8	4.80	18.0	-27.1
1.524	4.27			4.13			4.13		
1.829	3.60	21.6	-25.9	3.53	20.2	-26.0	3.47	19.2	-26.4
2.134	2.93			2.93			2.80		
2.438	2.27	22.5	-25.6	2.27	21.0	-25.7	2.27	19.8	-26.3
2.743	1.60			1.60			1.53		
3.048	1.00	22.8	-25.3	0.95	21.3	-25.6	0.92	20.2	-26.2
3.353	0.32			0.33			0.29		
3.658	-0.31	22.4	-25.2	-0.29	20.8	-25.1	-0.35	19.7	-25.8
3.962	-1.00			-0.93			-1.01		
4.267	-1.67	22.5	-25.0	-1.60	20.8	-25.0	-1.67	19.8	-25.8
4.572	-2.33			-2.27			-2.33		
4.877	-2.93	23.3	-23.5	-2.87	21.5	-24.1	-3.00	20.5	-24.6
4.959	-3.27		-14.1	-3.20		-13.6	-3.27		-15.7
MEANS ---->		21.8	-24.4		20.3	-24.6		19.1	-25.2
		DT= 46.2 C			DT= 44.8 C			DT= 44.2 C	

Mean Air Properties

Rep	BP (Pa)	Warm Room Twb (C)	Warm Room den. (kg/m^3)	Warm Room k.vis. (m^2/s)	Cold Room Tdp (C)	Cold Room den. (kg/m^3)	Cold Room k.vis. (m^2/s)
1	99017.8	12.2	1.1609	0.00001569	-28.9	1.3871	0.00001147
2	97324.6	14.4	1.1415	0.00001589	-30.2	1.3641	0.00001166
3	98238.9	11.1	1.1624	0.00001556	-30.2	1.3804	0.00001150

Regression Results Using the Model DP=a+(b*h)

Rep	NPA (m)	C.I.	Slope (Pa/m)	C.I.	r^2	Dden-reg (kg/m^3)	Dden-temp (kg/m^3)
1	3.492	0.014	-2.1530	0.0179	0.99975	0.2195	0.2174
2	3.502	0.012	-2.1114	0.0151	0.99982	0.2152	0.2085
3	3.472	0.012	-2.1232	0.0155	0.99981	0.2164	0.2091

Table E.3e

Test ID.= G1H2T2 Data at Time= 40 min.

Elev. (m)	Rep 1 DP (Pa)	Rep 1 Tw (C)	Rep 1 Tc (C)	Rep 2 DP (Pa)	Rep 2 Tw (C)	Rep 2 Tc (C)	Rep 3 DP (Pa)	Rep 3 Tw (C)	Rep 3 Tc (C)
0.052	4.40	18.7	-10.5	4.00	20.5	-5.4	4.00	18.8	-6.8
0.305	4.13			3.73			3.67		
0.610	3.80	20.0	-9.9	3.40	21.6	-5.7	3.33	20.0	-7.0
0.914	3.47			3.13			2.93		
1.219	3.07	19.8	-9.8	2.67	21.1	-5.7	2.67	19.4	-6.9
1.524	2.67			2.40			2.27		
1.829	2.27	20.7	-9.0	2.07	21.9	-5.1	1.93	20.2	-6.3
2.134	1.80			1.67			1.67		
2.438	1.40	21.3	-9.0	1.33	22.6	-4.8	1.23	20.8	-6.2
2.743	1.05			1.00			0.87		
3.048	0.63	21.6	-8.9	0.73	22.9	-4.5	0.51	21.1	-6.2
3.353	0.24			0.27			0.19		
3.658	-0.13	21.2	-8.8	0.00	22.3	-4.6	-0.19	20.8	-5.9
3.962	-0.52			-0.33			-0.51		
4.267	-0.93	21.3	-8.7	-0.80	22.5	-4.5	-0.88	20.8	-5.9
4.572	-1.33			-1.20			-1.28		
4.877	-1.73	21.8	-7.9	-1.47	23.0	-3.9	-1.60	21.4	-5.3
4.959	-1.93		-1.4	-1.60		0.2	-1.73		-1.1
MEANS ---->		20.7	-8.4		22.0	-4.4		20.3	-5.8
		DT= 29.1 C			DT= 26.4 C			DT= 26.1 C	

Mean Air Properties

Rep	BP (Pa)	Warm Room Twb (C)	Warm Room den. (kg/m^3)	Warm Room k.vis. (m^2/s)	Cold Room Tdp (C)	Cold Room den. (kg/m^3)	Cold Room k.vis. (m^2/s)
1	98238.9	14.4	1.1509	0.00001578	-15.8	1.2913	0.00001296
2	97663.2	13.9	1.1410	0.00001597	-6.2	1.2620	0.00001342
3	99525.7	10.6	1.1745	0.00001545	-7.4	1.2932	0.00001304

Regression Results Using the Model DP=a+(b*h)

Rep	NPA (m)	C.I.	Slope (Pa/m)	C.I.	r^2	Dden-reg (kg/m^3)	Dden-temp (kg/m^3)
1	3.539	0.021	-1.2954	0.0166	0.99942	0.1320	0.1278
2	3.602	0.025	-1.1425	0.0175	0.99916	0.1165	0.1130
3	3.496	0.015	-1.1580	0.0107	0.99969	0.1180	0.1150

Table E.3f

Test ID.= G1H2T3 Data at Time= 50 min.

Elev. (m)	Rep 1 DP (Pa)	Rep 1 Tw (C)	Rep 1 Tc (C)	Rep 2 DP (Pa)	Rep 2 Tw (C)	Rep 2 Tc (C)	Rep 3 DP (Pa)	Rep 3 Tw (C)	Rep 3 Tc (C)
0.052	3.13	20.2	-0.8	2.93	20.1	1.2	2.27	20.5	5.3
0.305	2.93			2.73			2.13		
0.610	2.67	21.3	-0.6	2.47	21.2	1.0	1.93	21.5	4.9
0.914	2.40			2.27			1.73		
1.219	2.13	20.8	-0.4	2.00	20.7	1.0	1.60	20.9	5.1
1.524	1.87			1.73			1.33		
1.829	1.60	21.7	0.2	1.47	21.5	1.6	1.17	22.6	5.7
2.134	1.33			1.20			0.99		
2.438	1.07	22.3	0.2	0.96	22.2	1.8	0.77	22.1	5.8
2.743	0.80			0.72			0.59		
3.048	0.53	22.5	0.3	0.45	22.3	1.9	0.39	22.4	6.0
3.353	0.27			0.20			0.17		
3.658	-0.03	22.2	0.2	0.00	22.0	1.9	0.01	22.0	6.0
3.962	-0.27			-0.28			-0.20		
4.267	-0.57	22.3	0.5	-0.53	22.1	1.9	-0.37	22.0	6.3
4.572	-0.89			-0.79			-0.56		
4.877	-1.15	22.9	0.9	-1.04	22.6	2.5	-0.77	22.5	6.4
4.959	-1.25		2.7	-1.12		5.0	-0.88		8.5
MEANS ---->		21.8	0.3		21.6	2.0		21.8	6.0
		DT= 21.5 C			DT= 19.7 C			DT= 15.8 C	

Mean Air Properties

Rep	BP (Pa)	Warm Room Twb (C)	Warm Room den. (kg/m^3)	Warm Room k.vis. (m^2/s)	Cold Room Tdp (C)	Cold Room den. (kg/m^3)	Cold Room k.vis. (m^2/s)
1	98238.9	13.9	1.1486	0.00001586	75%	1.2464	0.00001377
2	98306.6	13.3	1.1510	0.00001582	Sat	1.2390	0.00001392
3	99525.7	12.8	1.1657	0.00001562	***	1.2342	0.00001414

Regression Results Using the Model DP=a+(b*h)

Rep	NPA (m)	C.I.	Slope (Pa/m)	C.I.	r^2	Dden-reg (kg/m^3)	Dden-temp (kg/m^3)
1	3.615	0.017	-0.8905	0.0089	0.99964	0.0908	0.0908
2	3.616	0.011	-0.8257	0.0056	0.99984	0.0842	0.0827
3	3.655	0.019	-0.6365	0.0073	0.99953	0.0649	0.0663

Table E.3g

Test ID.= G2H1T1 Data at Time= 15 min.

Elev. (m)	Rep 1 DP (Pa)	Rep 1 Tw (C)	Rep 1 Tc (C)	Rep 2 DP (Pa)	Rep 2 Tw (C)	Rep 2 Tc (C)	Rep 3 DP (Pa)	Rep 3 Tw (C)	Rep 3 Tc (C)
0.052	4.13	15.4	-27.4	4.13	14.8	-27.8	3.93	11.6	-27.6
0.305	3.73			3.73			3.53		
0.610	3.07	18.9	-27.7	3.07	18.0	-27.8	2.93	15.5	-27.0
0.914	2.47			2.40			2.40		
1.219	1.73	19.4	-27.4	1.73	18.8	-27.4	1.73	16.2	-27.1
1.524	1.11			1.12			1.15		
1.829	0.47	20.6	-26.3	0.48	19.8	-26.4	0.53	17.3	-26.4
2.134	-0.20			-0.16			-0.09		
2.438	-0.80	21.2	-25.5	-0.77	20.5	-25.5	-0.68	17.9	-26.1
2.743	-1.47			-1.47			-1.33		
3.048	-2.13	21.6	-24.1	-2.07	21.0	-24.2	-2.00	18.4	-25.3
3.353	-2.73			-2.67			-2.53		
3.658	-3.33	21.4	-23.2	-3.20	20.7	-23.2	-3.07	18.2	-24.6
3.962	-4.00			-3.87			-3.67		
4.267	-4.53	21.5	-22.1	-4.40	20.9	-22.4	-4.27	18.3	-23.5
4.572	-5.07			-5.07			-4.80		
4.877	-5.87	22.2	-20.9	-5.60	21.3	-21.2	-5.47	18.9	-22.1
4.959	-6.00		-17.4	-5.87		-16.5	-5.73		-18.9
MEANS ---->		20.2	-24.2		19.5	-24.2		16.9	-24.8
		DT= 44.4 C			DT= 43.7 C			DT= 41.7 C	

Mean Air Properties

Rep	BP (Pa)	Warm Room Twb (C)	Warm Room den. (kg/m^3)	Warm Room k.vis. (m^2/s)	Cold Room Tdp (C)	Cold Room den. (kg/m^3)	Cold Room k.vis. (m^2/s)
1	99085.5	11.1	1.1687	0.00001552	-29.6	1.3866	0.00001149
2	97324.6	13.9	1.1451	0.00001581	-29.4	1.3622	0.00001169
3	98238.9	9.4	1.1723	0.00001534	-31.5	1.3785	0.00001153

Regression Results Using the Model DP=a+(b*h)

Rep	NPA (m)	C.I.	Slope (Pa/m)	C.I.	r^2	Dden-reg (kg/m^3)	Dden-temp (kg/m^3)
1	2.062	0.015	-2.0783	0.0200	0.99967	0.2119	0.2100
2	2.079	0.016	-2.0410	0.0206	0.99964	0.2081	0.2036
3	2.090	0.014	-1.9707	0.0179	0.99971	0.2009	0.1984

Table E.3h

Test ID.= G2H1T2 Data at Time= 30 min.

Elev. (m)	Rep 1 DP (Pa)	Rep 1 Tw (C)	Rep 1 Tc (C)	Rep 2 DP (Pa)	Rep 2 Tw (C)	Rep 2 Tc (C)	Rep 3 DP (Pa)	Rep 3 Tw (C)	Rep 3 Tc (C)
0.052	2.33	19.1	-5.5	2.27	18.9	-7.1	2.53	17.4	-12.5
0.305	2.00			2.07			2.27		
0.610	1.67	21.4	-6.0	1.67	20.9	-7.1	1.87	19.0	-11.0
0.914	1.33			1.33			1.47		
1.219	0.99	21.3	-5.6	0.93	21.0	-6.8	1.08	18.8	-10.7
1.524	0.65			0.60			0.67		
1.829	0.29	22.3	-4.9	0.33	22.0	-6.0	0.28	19.7	-9.7
2.134	-0.03			-0.07			-0.08		
2.438	-0.37	22.9	-4.5	-0.40	22.5	-5.5	-0.47	20.4	-9.1
2.743	-0.72			-0.80			-0.85		
3.048	-1.08	23.3	-3.8	-1.13	23.0	-5.0	-1.23	20.8	-8.5
3.353	-1.40			-1.47			-1.60		
3.658	-1.73	22.8	-3.4	-1.80	22.5	-4.7	-2.00	20.3	-8.4
3.962	-2.13			-2.13			-2.40		
4.267	-2.40	22.9	-2.8	-2.53	22.5	-4.1	-2.73	20.5	-7.9
4.572	-2.67			-2.80			-3.07		
4.877	-3.00	23.6	-1.9	-3.13	23.3	-2.9	-3.47	21.1	-6.8
4.959	-3.13		0.4	-3.27		-1.1	-3.60		-4.9
MEANS ---->		22.2	-3.8		21.8	-5.0		19.8	-8.9
		DT= 25.9 C			DT= 26.8 C			DT= 28.7 C	

Mean Air Properties

Rep	BP (Pa)	Warm Room Twb (C)	Warm Room den. (kg/m^3)	Warm Room k.vis. (m^2/s)	Cold Room Tdp (C)	Cold Room den. (kg/m^3)	Cold Room k.vis. (m^2/s)
1	98238.9	12.2	1.1506	0.00001584	-9.4	1.2678	0.00001338
2	97663.2	12.8	1.1438	0.00001592	-8.8	1.2659	0.00001335
3	98916.2	11.1	1.1681	0.00001551	-8.2	1.3010	0.00001284

Regression Results Using the Model DP=a+(b*h)

Rep	NPA (m)	C.I.	Slope (Pa/m)	C.I.	r^2	Dden-reg (kg/m^3)	Dden-temp (kg/m^3)
1	2.110	0.017	-1.1080	0.0117	0.99960	0.1129	0.1114
2	2.075	0.015	-1.1341	0.0107	0.99968	0.1156	0.1153
3	2.078	0.011	-1.2515	0.0090	0.99982	0.1276	0.1275

Table E.3i

Test ID.= G2H1T3 Data at Time= 30 min.

Elev. (m)	Rep 1 DP (Pa)	Rep 1 Tw (C)	Rep 1 Tc (C)	Rep 2 DP (Pa)	Rep 2 Tw (C)	Rep 2 Tc (C)	Rep 3 DP (Pa)	Rep 3 Tw (C)	Rep 3 Tc (C)
0.052	1.53	19.8	1.5	1.47	20.7	3.2	1.40	21.7	5.6
0.305	1.33			1.28			1.23		
0.610	1.12	21.3	2.0	1.07	21.7	3.1	1.03	23.0	5.2
0.914	0.89			0.83			0.80		
1.219	0.67	21.2	2.1	0.60	21.1	3.2	0.57	22.5	5.5
1.524	0.47			0.39			0.37		
1.829	0.19	22.2	2.8	0.16	22.0	4.0	0.16	23.9	6.2
2.134	-0.01			-0.07			-0.03		
2.438	-0.27	22.5	2.8	-0.27	22.6	4.2	-0.25	24.0	6.7
2.743	-0.53			-0.49			-0.45		
3.048	-0.77	23.1	3.1	-0.75	22.9	4.5	-0.67	24.3	7.0
3.353	-1.01			-0.97			-0.85		
3.658	-1.20	22.6	3.2	-1.19	22.5	4.5	-1.07	23.8	7.3
3.962	-1.47			-1.40			-1.27		
4.267	-1.73	22.7	3.5	-1.60	22.6	4.8	-1.47	23.9	7.6
4.572	-2.00			-1.87			-1.67		
4.877	-2.20	23.2	4.0	-2.07	23.2	5.5	-1.87	24.5	8.4
4.959	-2.27		5.0	-2.13		6.7	-1.93		10.0
MEANS ---->		22.0	3.0		22.1	4.3		23.5	6.9
		DT= 19.0 C			DT= 17.8 C			DT= 16.6 C	

Mean Air Properties

Rep	BP (Pa)	Warm Room Twb (C)	Warm Room den. (kg/m^3)	Warm Room k.vis. (m^2/s)	Cold Room Tdp (C)	Cold Room den. (kg/m^3)	Cold Room k.vis. (m^2/s)
1	98238.9	12.8	1.1499	0.00001585	75%	1.2330	0.00001403
2	98306.6	13.9	1.1483	0.00001587	Sat	1.2272	0.00001415
3	98713.0	14.4	1.1476	0.00001594	***	1.2194	0.00001435

Regression Results Using the Model DP=a+(b*h)

Rep	NPA (m)	C.I.	Slope (Pa/m)	C.I.	r^2	Dden-reg (kg/m^3)	Dden-temp (kg/m^3)
1	2.063	0.018	-0.7790	0.0087	0.99955	0.0794	0.0796
2	2.050	0.009	-0.7333	0.0040	0.99990	0.0747	0.0740
3	2.092	0.011	-0.6771	0.0047	0.99983	0.0690	0.0682

Table E.3j

Test ID.= G2H2T1 Data at Time= 20 min.

Elev. (m)	Rep 1 DP (Pa)	Rep 1 Tw (C)	Rep 1 Tc (C)	Rep 2 DP (Pa)	Rep 2 Tw (C)	Rep 2 Tc (C)	Rep 3 DP (Pa)	Rep 3 Tw (C)	Rep 3 Tc (C)
0.052	6.00	12.9	-26.1	6.40	12.1	-27.4	6.13	11.7	-26.7
0.305	5.60			5.87			5.60		
0.610	5.07	17.0	-25.8	5.20	16.2	-27.6	5.07	16.0	-26.9
0.914	4.40			4.53			4.53		
1.219	3.80	18.1	-25.7	4.00	17.6	-27.1	3.87	17.1	-26.7
1.524	3.20			3.40			3.33		
1.829	2.60	19.4	-24.6	2.73	18.9	-26.5	2.67	18.2	-25.8
2.134	2.00			2.13			2.00		
2.438	1.40	20.1	-24.1	1.47	19.7	-25.9	1.47	19.0	-25.5
2.743	0.76			0.85			0.83		
3.048	0.17	20.8	-23.8	0.21	20.3	-25.4	0.23	19.6	-25.2
3.353	-0.43			-0.41			-0.41		
3.658	-1.07	20.3	-23.3	-1.07	19.9	-25.1	-1.00	19.2	-24.6
3.962	-1.67			-1.67			-1.60		
4.267	-2.27	20.5	-22.3	-2.27	20.0	-23.8	-2.27	19.2	-23.7
4.572	-2.87			-2.93			-2.80		
4.877	-3.40	21.3	-18.0	-3.53	20.7	-19.7	-3.40	20.0	-19.3
4.959	-3.60		-3.4	-3.67		-5.7	-3.60		-4.6
MEANS ---->		18.9	-21.7		18.4	-23.4		17.8	-22.9
		DT= 40.6 C			DT= 41.8 C			DT= 40.6 C	

Mean Air Properties

Rep	BP (Pa)	Warm Room Twb (C)	Warm Room den. (kg/m^3)	Warm Room k.vis. (m^2/s)	Cold Room Tdp (C)	Cold Room den. (kg/m^3)	Cold Room k.vis. (m^2/s)
1	99085.5	10.0	1.1749	0.00001538	-28.0	1.3728	0.00001170
2	97324.6	11.1	1.1538	0.00001564	-30.6	1.3578	0.00001176
3	98916.2	8.9	1.1785	0.00001529	-28.6	1.3770	0.00001162

Regression Results Using the Model DP=a+(b*h)

Rep	NPA (m)	C.I.	Slope (Pa/m)	C.I.	r^2	Dden-reg (kg/m^3)	Dden-temp (kg/m^3)
1	3.135	0.010	-1.9780	0.0119	0.99987	0.2016	0.1909
2	3.156	0.007	-2.0539	0.0097	0.99992	0.2094	0.1946
3	3.158	0.011	-1.9897	0.0135	0.99984	0.2028	0.1924

Table E.3k

Test ID.= G2H2T2 Data at Time= 40 min.

Elev. (m)	Rep 1 DP (Pa)	Rep 1 Tw (C)	Rep 1 Tc (C)	Rep 2 DP (Pa)	Rep 2 Tw (C)	Rep 2 Tc (C)	Rep 3 DP (Pa)	Rep 3 Tw (C)	Rep 3 Tc (C)
0.052	3.80	14.1	-13.4	3.33	17.7	-5.1	3.33	17.5	-5.9
0.305	3.53			3.07			3.13		
0.610	3.20	17.2	-11.7	2.80	19.8	-5.2	2.80	19.7	-5.9
0.914	2.87			2.53			2.53		
1.219	2.47	17.4	-11.6	2.13	20.0	-5.1	2.20	19.8	-5.8
1.524	2.07			1.87			1.87		
1.829	1.73	18.6	-10.6	1.47	20.9	-4.6	1.47	20.8	-5.1
2.134	1.31			1.19			1.17		
2.438	0.93	19.3	-10.4	0.87	21.5	-4.3	0.83	21.5	-4.6
2.743	0.55			0.49			0.48		
3.048	0.17	19.8	-10.1	0.19	22.0	-4.1	0.17	22.0	-4.5
3.353	-0.23			-0.13			-0.16		
3.658	-0.57	19.5	-9.9	-0.48	21.4	-3.9	-0.52	21.4	-4.4
3.962	-0.95			-0.77			-0.84		
4.267	-1.33	19.5	-9.3	-1.12	21.5	-3.4	-1.17	21.6	-4.0
4.572	-1.73			-1.47			-1.53		
4.877	-2.13	20.2	-6.8	-1.73	22.2	-1.7	-1.87	22.3	-1.8
4.959	-2.27		2.7	-1.87		5.5	-2.00		5.2
MEANS ---->		18.4	-9.1		20.8	-3.2		20.7	-3.6
		DT= 27.4 C			DT= 23.9 C			DT= 24.4 C	

Mean Air Properties

Rep	BP (Pa)	Warm Room Twb (C)	Warm Room den. (kg/m^3)	Warm Room k.vis. (m^2/s)	Cold Room Tdp (C)	Cold Room den. (kg/m^3)	Cold Room k.vis. (m^2/s)
1	99085.5	9.4	1.1775	0.00001533	-9.0	1.3042	0.00001281
2	97663.2	12.2	1.1482	0.00001582	-7.0	1.2567	0.00001352
3	99525.7	11.7	1.1713	0.00001551	-7.8	1.2832	0.00001323

Regression Results Using the Model DP=a+(b*h)

Rep	NPA (m)	C.I.	Slope (Pa/m)	C.I.	r^2	Dden-reg (kg/m^3)	Dden-temp (kg/m^3)
1	3.181	0.015	-1.2425	0.0117	0.99968	0.1267	0.1229
2	3.225	0.016	-1.0664	0.0106	0.99965	0.1087	0.1024
3	3.185	0.018	-1.0948	0.0122	0.99956	0.1116	0.1064

Table E.3l

Test ID.= G2H2T3 Data at Time= 40 min.

Elev. (m)	Rep 1 DP (Pa)	Rep 1 Tw (C)	Rep 1 Tc (C)	Rep 2 DP (Pa)	Rep 2 Tw (C)	Rep 2 Tc (C)	Rep 3 DP (Pa)	Rep 3 Tw (C)	Rep 3 Tc (C)
0.052	2.27	19.8	3.5	2.53	17.4	-0.3	2.00	19.5	5.3
0.305	2.07			2.40			1.87		
0.610	1.87	20.9	3.4	2.13	19.3	-0.2	1.67	20.8	4.7
0.914	1.60			1.87			1.47		
1.219	1.47	20.7	3.4	1.60	19.3	-0.2	1.28	20.6	4.8
1.524	1.20			1.33			1.09		
1.829	0.99	21.7	4.2	1.13	20.4	0.2	0.89	22.5	5.4
2.134	0.77			0.88			0.68		
2.438	0.57	22.3	4.2	0.63	21.1	0.4	0.47	22.0	5.5
2.743	0.35			0.37			0.29		
3.048	0.12	22.5	4.4	0.12	21.4	0.6	0.09	22.3	5.7
3.353	-0.09			-0.13			-0.12		
3.658	-0.32	22.2	4.4	-0.40	20.9	0.8	-0.29	21.9	5.8
3.962	-0.53			-0.64			-0.48		
4.267	-0.75	22.3	4.6	-0.88	21.0	1.0	-0.69	21.9	5.9
4.572	-0.99			-1.15			-0.92		
4.877	-1.23	22.8	5.5	-1.47	21.5	2.4	-1.09	22.4	6.8
4.959	-1.28		9.5	-1.53		7.9	-1.17		10.9
MEANS ---->		21.7	4.7		20.2	1.2		21.5	6.1
		DT= 17.0 C			DT= 19.0 C			DT= 15.5 C	

Mean Air Properties

Rep	BP (Pa)	Warm Room Twb (C)	Warm Room den. (kg/m^3)	Warm Room k.vis. (m^2/s)	Cold Room Tdp (C)	Cold Room den. (kg/m^3)	Cold Room k.vis. (m^2/s)
1	98238.9	15.0	1.1467	0.00001588	75%	1.2246	0.00001420
2	98306.6	11.1	1.1594	0.00001564	Sat	1.2425	0.00001385
3	99525.7	12.2	1.1676	0.00001559	***	1.2338	0.00001415

Regression Results Using the Model DP=a+(b*h)

Rep	NPA (m)	C.I.	Slope (Pa/m)	C.I.	r^2	Dden-reg (kg/m^3)	Dden-temp (kg/m^3)
1	3.206	0.014	-0.7182	0.0065	0.99971	0.0732	0.0706
2	3.171	0.018	-0.8293	0.0094	0.99955	0.0845	0.0804
3	3.184	0.012	-0.6476	0.0049	0.99979	0.0660	0.0648

Table E.3m

Test ID.= REC1　　Data at Time= 20 min.

Elev. (m)	Rep 1 DP (Pa)	Rep 1 Tw (C)	Rep 1 Tc (C)	Rep 2 DP (Pa)	Rep 2 Tw (C)	Rep 2 Tc (C)	Rep 3 DP (Pa)	Rep 3 Tw (C)	Rep 3 Tc (C)
0.052	4.40	17.7	-14.5	4.40	17.7	-14.9	4.53	18.0	-15.6
0.305	4.00			4.07			4.27		
0.610	3.67	19.7	-14.8	3.67	19.9	-15.3	3.73	19.8	-15.8
0.914	3.20			3.20			3.20		
1.219	2.80	19.7	-14.6	2.80	20.0	-15.1	2.80	19.8	-15.8
1.524	2.27			2.27			2.40		
1.829	1.87	20.9	-13.9	1.87	21.0	-14.3	1.87	21.1	-15.1
2.134	1.33			1.33			1.33		
2.438	0.92	21.6	-13.8	0.92	21.5	-14.0	0.93	21.6	-14.6
2.743	0.45			0.45			0.40		
3.048	0.03	21.9	-13.2	-0.01	21.8	-13.5	0.00	21.9	-14.2
3.353	-0.45			-0.47			-0.53		
3.658	-0.89	21.4	-12.9	-0.88	21.5	-13.2	-1.00	21.6	-13.8
3.962	-1.33			-1.33			-1.47		
4.267	-1.80	21.7	-12.1	-1.87	21.5	-12.5	-1.87	21.7	-13.2
4.572	-2.27			-2.27			-2.27		
4.877	-2.67	22.2	-9.4	-2.67	22.3	-9.9	-2.73	22.2	-10.5
4.959	-2.80		-6.2	-2.80		-7.7	-2.93		-8.4
MEANS ---->		20.7	-12.5		20.8	-13.0		20.8	-13.7
		DT= 33.2 C			DT= 33.8 C			DT= 34.5 C	

Mean Air Properties

Rep	BP (Pa)	Warm Room Twb (C)	Warm Room den. (kg/m^3)	Warm Room k.vis. (m^2/s)	Cold Room Tdp (C)	Cold Room den. (kg/m^3)	Cold Room k.vis. (m^2/s)
1	97019.8	14.4	1.1366	0.00001598	-17.6	1.2958	0.00001275
2	96748.9	13.3	1.1354	0.00001600	-18.2	1.2947	0.00001275
3	96748.9	13.3	1.1352	0.00001600	-16.7	1.2978	0.00001268

Regression Results Using the Model DP=a+(b*h)

Rep	NPA (m)	C.I.	Slope (Pa/m)	C.I.	r^2	Dden-reg (kg/m^3)	Dden-temp (kg/m^3)
1	3.059	0.013	-1.4787	0.0120	0.99977	0.1507	0.1467
2	3.056	0.013	-1.4851	0.0121	0.99976	0.1514	0.1489
3	3.042	0.018	-1.5287	0.0170	0.99956	0.1558	0.1523

Table E.3n

Test ID.= REC2　　Data at Time= 30 min.

Elev. (m)	Rep 1 DP (Pa)	Rep 1 Tw (C)	Rep 1 Tc (C)	Rep 2 DP (Pa)	Rep 2 Tw (C)	Rep 2 Tc (C)	Rep 3 DP (Pa)	Rep 3 Tw (C)	Rep 3 Tc (C)
0.052	2.13	17.7	-13.4	2.27	17.4	-15.3	2.13	16.7	-15.2
0.305	1.93			1.87			1.87		
0.610	1.33	20.8	-13.6	1.33	20.7	-15.2	1.33	19.9	-15.3
0.914	0.95			0.93			0.93		
1.219	0.49	20.4	-13.4	0.47	20.6	-15.1	0.45	19.5	-15.2
1.524	0.05			0.03			0.00		
1.829	-0.40	21.4	-12.7	-0.47	21.7	-14.4	-0.47	20.7	-14.4
2.134	-0.84			-0.93			-0.92		
2.438	-1.29	22.2	-12.5	-1.33	22.4	-14.0	-1.33	21.1	-14.2
2.743	-1.80			-1.87			-1.87		
3.048	-2.20	22.4	-12.2	-2.40	22.6	-13.9	-2.40	21.3	-14.2
3.353	-2.67			-2.80			-2.80		
3.658	-3.07	22.0	-12.0	-3.27	22.2	-13.7	-3.20	21.0	-13.7
3.962	-3.53			-3.73			-3.73		
4.267	-4.00	22.3	-11.7	-4.27	22.2	-13.5	-4.27	21.0	-13.5
4.572	-4.40			-4.67			-4.67		
4.877	-4.80	22.6	-10.4	-5.20	22.8	-12.5	-5.07	21.7	-12.3
4.959	-5.07		-6.5	-5.33		-9.0	-5.33		-9.1
MEANS ---->		21.3	-11.8		21.4	-13.6		20.3	-13.7
		DT= 33.1 C			DT= 35.0 C			DT= 34.0 C	

Mean Air Properties

Rep	BP (Pa)	Warm Room Twb (C)	Warm Room den. (kg/m^3)	Warm Room k.vis. (m^2/s)	Cold Room Tdp (C)	Cold Room den. (kg/m^3)	Cold Room k.vis. (m^2/s)
1	97019.8	13.9	1.1359	0.00001601	-17.8	1.2924	0.00001281
2	96748.9	14.4	1.1314	0.00001608	-18.2	1.2979	0.00001269
3	96748.9	12.8	1.1379	0.00001594	-16.7	1.2980	0.00001269

Regression Results Using the Model DP=a+(b*h)

Rep	NPA (m)	C.I.	Slope (Pa/m)	C.I.	r^2	Dden-reg (kg/m^3)	Dden-temp (kg/m^3)
1	1.552	0.017	-1.4663	0.0148	0.99964	0.1495	0.1454
2	1.522	0.013	-1.5403	0.0118	0.99979	0.1570	0.1544
3	1.511	0.018	-1.5230	0.0165	0.99958	0.1553	0.1504

Table E.3o

Test ID.= CYL Data at Time= 30 min.

Elev. (m)	Rep 1 DP (Pa)	Rep 1 Tw (C)	Rep 1 Tc (C)	Rep 2 DP (Pa)	Rep 2 Tw (C)	Rep 2 Tc (C)	Rep 3 DP (Pa)	Rep 3 Tw (C)	Rep 3 Tc (C)
0.052	1.20	18.5	-19.4	1.31	18.8	-19.1	1.24	17.4	-21.6
0.305	0.80			0.80			0.79		
0.610	0.27	20.5	-19.5	0.33	20.5	-19.4	0.24	19.6	-21.6
0.914	-0.23			-0.20			-0.24		
1.219	-0.80	19.9	-19.5	-0.73	19.9	-19.4	-0.84	19.0	-21.6
1.524	-1.40			-1.33			-1.40		
1.829	-1.87	20.9	-19.0	-1.87	20.8	-18.8	-2.00	20.1	-20.9
2.134	-2.40			-2.40			-2.53		
2.438	-2.93	21.6	-18.8	-2.93	21.5	-18.5	-3.07	20.8	-20.9
2.743	-3.47			-3.47			-3.67		
3.048	-4.00	21.8	-18.5	-4.00	21.6	-18.4	-4.27	21.1	-20.4
3.353	-4.53			-4.53			-4.80		
3.658	-5.07	21.3	-18.4	-5.07	21.4	-18.4	-5.33	20.5	-20.4
3.962	-5.60			-5.60			-5.87		
4.267	-6.13	21.2	-18.2	-6.13	21.5	-17.8	-6.53	20.7	-20.3
4.572	-6.67			-6.67			-7.07		
4.877	-7.20	22.0	-17.5	-7.20	21.9	-17.2	-7.60	21.2	-19.7
4.959	-7.47		-15.3	-7.47		-15.0	-7.87		-17.8
MEANS ---->		20.8	-18.4		20.9	-18.2		20.0	-20.5
		DT= 39.2 C			DT= 39.1 C			DT= 40.5 C	

Mean Air Properties

Rep	BP (Pa)	Warm Room Twb (C)	Warm Room den. (kg/m^3)	Warm Room k.vis. (m^2/s)	Cold Room Tdp (C)	Cold Room den. (kg/m^3)	Cold Room k.vis. (m^2/s)
1	97832.5	13.9	1.1468	0.00001584	-24.0	1.3377	0.00001213
2	97832.5	13.9	1.1467	0.00001584	-24.0	1.3365	0.00001215
3	98137.3	11.1	1.1581	0.00001565	-24.5	1.3530	0.00001191

Regression Results Using the Model DP=a+(b*h)

Rep	NPA (m)	C.I.	Slope (Pa/m)	C.I.	r^2	Dden-reg (kg/m^3)	Dden-temp (kg/m^3)
1	0.760	0.012	-1.7538	0.0114	0.99985	0.1788	0.1786
2	0.785	0.011	-1.7677	0.0105	0.99987	0.1802	0.1776
3	0.753	0.014	-1.8482	0.0138	0.99980	0.1884	0.1871

Table E.3p

Test ID.= CYLREC Data at Time= 30 min.

Elev. (m)	Rep 1 DP (Pa)	Rep 1 Tw (C)	Rep 1 Tc (C)	Rep 2 DP (Pa)	Rep 2 Tw (C)	Rep 2 Tc (C)	Rep 3 DP (Pa)	Rep 3 Tw (C)	Rep 3 Tc (C)
0.052	5.07	19.2	-21.6	5.20	19.4	-20.8	5.07	19.4	-20.8
0.305	4.80			4.80			4.67		
0.610	4.27	19.9	-21.7	4.27	20.4	-21.0	4.13	20.3	-20.9
0.914	3.73			3.67			3.60		
1.219	3.20	19.3	-21.8	3.13	19.8	-21.1	3.07	19.5	-21.0
1.524	2.67			2.60			2.53		
1.829	2.00	20.2	-21.2	2.07	20.7	-20.5	2.00	20.5	-20.4
2.134	1.47			1.47			1.47		
2.438	0.93	20.8	-20.9	0.93	21.3	-20.1	0.92	20.9	-20.3
2.743	0.35			0.37			0.37		
3.048	-0.23	21.1	-20.7	-0.16	21.6	-19.9	-0.19	21.3	-20.0
3.353	-0.79			-0.75			-0.76		
3.658	-1.33	20.7	-20.7	-1.33	21.1	-19.9	-1.33	21.0	-19.9
3.962	-1.87			-1.87			-1.87		
4.267	-2.47	20.7	-20.5	-2.40	21.3	-19.7	-2.40	21.0	-19.6
4.572	-3.07			-2.93			-2.93		
4.877	-3.60	21.3	-19.5	-3.60	21.7	-18.5	-3.60	21.6	-18.9
4.959	-3.87		-16.3	-3.87		-15.5	-3.87		-15.5
MEANS ---->		20.3	-20.5		20.8	-19.7		20.6	-19.7
		DT= 40.8 C			DT= 40.4 C			DT= 40.3 C	

Mean Air Properties

Rep	BP (Pa)	Warm Room Twb (C)	Warm Room den. (kg/m^3)	Warm Room k.vis. (m^2/s)	Cold Room Tdp (C)	Cold Room den. (kg/m^3)	Cold Room k.vis. (m^2/s)
1	98137.3	14.4	1.1509	0.00001576	-24.8	1.3530	0.00001192
2	98137.3	12.2	1.1537	0.00001574	-24.4	1.3486	0.00001198
3	98103.4	12.2	1.1539	0.00001573	-24.3	1.3483	0.00001199

Regression Results Using the Model DP=a+(b*h)

Rep	NPA (m)	C.I.	Slope (Pa/m)	C.I.	r^2	Dden-reg (kg/m^3)	Dden-temp (kg/m^3)
1	2.922	0.020	-1.8386	0.0229	0.99945	0.1874	0.1883
2	2.933	0.015	-1.8310	0.0174	0.99968	0.1866	0.1857
3	2.916	0.018	-1.8034	0.0212	0.99951	0.1838	0.1850

Table E.3q

Test ID.= NCT1 Data at Time= 30 min.

Elev. (m)	Rep 1 DP (Pa)	Rep 1 Tw (C)	Rep 1 Tc (C)	Rep 2 DP (Pa)	Rep 2 Tw (C)	Rep 2 Tc (C)	Rep 3 DP (Pa)	Rep 3 Tw (C)	Rep 3 Tc (C)
0.052	5.60	17.3	-29.8	5.33	20.6	-26.5	5.47	21.4	-27.0
0.305	5.07			4.80			4.93		
0.610	4.53	18.0	-29.9	4.13	21.0	-26.5	4.40	22.1	-26.5
0.914	3.87			3.60			3.80		
1.219	3.13	17.4	-29.8	2.93	20.4	-26.4	3.20	21.3	-26.8
1.524	2.47			2.27			2.33		
1.829	1.80	18.1	-28.9	1.60	21.0	-25.8	1.80	22.1	-26.3
2.134	1.07			0.93			0.99		
2.438	0.43	19.1	-28.7	0.33	21.7	-25.7	0.41	22.6	-26.1
2.743	-0.24			-0.40			-0.27		
3.048	-0.93	19.3	-28.6	-1.00	22.0	-25.3	-0.93	22.9	-25.9
3.353	-1.60			-1.73			-1.60		
3.658	-2.33	19.0	-28.4	-2.33	21.6	-25.4	-2.40	22.5	-25.9
3.962	-2.93			-3.07			-3.07		
4.267	-3.60	18.9	-28.2	-3.60	21.9	-25.0	-3.73	22.6	-25.8
4.572	-4.40			-4.27			-4.40		
4.877	-5.07	19.5	-27.2	-4.93	22.3	-24.6	-5.07	23.2	-24.8
4.959	-5.33		-24.9	-5.33		-21.8	-5.33		-22.8
MEANS ---->		18.5	-28.4		21.4	-25.3		22.3	-25.8
		DT= 46.9 C			DT= 46.6 C			DT= 48.0 C	

Mean Air Properties

Rep	BP (Pa)	Warm Room Twb (C)	Warm Room den. (kg/m^3)	Warm Room k.vis. (m^2/s)	Cold Room Tdp (C)	Cold Room den. (kg/m^3)	Cold Room k.vis. (m^2/s)
1	99153.2	9.4	1.1779	0.00001533	-33.0	1.4119	0.00001113
2	97324.6	13.3	1.1402	0.00001595	-31.0	1.3681	0.00001160
3	98916.2	12.2	1.1581	0.00001575	-30.8	1.3932	0.00001138

Regression Results Using the Model DP=a+(b*h)

Rep	NPA (m)	C.I.	Slope (Pa/m)	C.I.	r^2	Dden-reg (kg/m^3)	Dden-temp (kg/m^3)
1	2.619	0.014	-2.2286	0.0202	0.99971	0.2272	0.2273
2	2.562	0.016	-2.1495	0.0214	0.99965	0.2191	0.2168
3	2.595	0.020	-2.2144	0.0282	0.99942	0.2257	0.2267

Table E.3r

Test ID.= NCT2 Data at Time= 80 min.

Elev. (m)	Rep 1 DP (Pa)	Rep 1 Tw (C)	Rep 1 Tc (C)	Rep 2 DP (Pa)	Rep 2 Tw (C)	Rep 2 Tc (C)	Rep 3 DP (Pa)	Rep 3 Tw (C)	Rep 3 Tc (C)
0.052	3.20	23.0	-3.3	3.20	20.0	-10.8	3.07	21.0	-7.2
0.305	3.00			2.93			2.93		
0.610	2.73	23.3	-3.1	2.53	20.8	-10.2	2.53	21.6	-7.1
0.914	2.33			2.13			2.13		
1.219	2.00	22.6	-3.0	1.73	19.9	-10.1	1.80	20.7	-7.1
1.524	1.73			1.33			1.40		
1.829	1.40	23.6	-2.4	0.93	20.6	-9.4	1.00	21.7	-6.6
2.134	1.03			0.53			0.67		
2.438	0.69	23.7	-2.1	0.13	21.2	-9.4	0.27	22.1	-6.3
2.743	0.40			-0.27			-0.07		
3.048	0.09	24.1	-2.2	-0.53	21.5	-9.3	-0.40	22.3	-6.5
3.353	-0.27			-0.93			-0.80		
3.658	-0.53	23.8	-2.0	-1.33	21.0	-9.3	-1.20	22.0	-6.4
3.962	-0.93			-1.73			-1.47		
4.267	-1.20	23.8	-1.8	-2.13	21.2	-9.2	-1.93	22.2	-6.2
4.572	-1.60			-2.53			-2.20		
4.877	-1.93	24.1	-1.4	-2.93	21.7	-8.8	-2.60	22.4	-5.7
4.959	-2.07		0.2	-3.07		-7.3	-2.80		-4.5
MEANS ---->		23.5	-2.1		20.9	-9.4		21.8	-6.3
		DT= 25.6 C			DT= 30.2 C			DT= 28.1 C	

Mean Air Properties

Rep	BP (Pa)	Warm Room Twb (C)	Warm Room den. (kg/m^3)	Warm Room k.vis. (m^2/s)	Cold Room Tdp (C)	Cold Room den. (kg/m^3)	Cold Room k.vis. (m^2/s)
1	98713.0	12.2	1.1517	0.00001589	-7.8	1.2654	0.00001347
2	98103.4	12.2	1.1531	0.00001576	-9.4	1.2928	0.00001291
3	97595.5	12.8	1.1432	0.00001593	-9.9	1.2716	0.00001324

Regression Results Using the Model DP=a+(b*h)

Rep	NPA (m)	C.I.	Slope (Pa/m)	C.I.	r^2	Dden-reg (kg/m^3)	Dden-temp (kg/m^3)
1	3.102	0.020	-1.0744	0.0133	0.99946	0.1095	0.1093
2	2.581	0.014	-1.2730	0.0115	0.99971	0.1298	0.1330
3	2.689	0.020	-1.2007	0.0155	0.99941	0.1224	0.1212

Table E.3s

Test ID.= NCT3 Data at Time= 80 min.

Elev. (m)	Rep 1 DP (Pa)	Rep 1 Tw (C)	Rep 1 Tc (C)	Rep 2 DP (Pa)	Rep 2 Tw (C)	Rep 2 Tc (C)	Rep 3 DP (Pa)	Rep 3 Tw (C)	Rep 3 Tc (C)
0.052	2.47	22.0	0.4	2.53	23.1	1.7	2.27	21.2	-0.4
0.305	2.27			2.40			2.13		
0.610	2.00	22.6	0.4	2.13	23.6	1.9	1.87	21.8	-0.8
0.914	1.73			1.87			1.60		
1.219	1.47	21.9	0.4	1.60	22.8	2.0	1.33	21.0	-0.6
1.524	1.17			1.33			1.07		
1.829	0.88	22.5	0.9	1.07	24.0	2.4	0.80	21.8	-0.1
2.134	0.65			0.80			0.53		
2.438	0.41	23.0	1.1	0.53	24.0	2.7	0.27	22.1	0.1
2.743	0.13			0.27			0.00		
3.048	-0.13	23.4	1.1	0.00	24.3	2.9	-0.27	22.6	0.2
3.353	-0.49			-0.20			-0.53		
3.658	-0.73	22.9	1.2	-0.47	23.8	2.9	-0.73	22.1	0.2
3.962	-0.99			-0.73			-1.07		
4.267	-1.27	23.1	1.2	-1.00	23.9	2.7	-1.33	22.2	0.2
4.572	-1.53			-1.27			-1.60		
4.877	-1.87	23.4	1.2	-1.53	24.4	3.1	-1.87	22.7	0.4
4.959	-1.93		1.5	-1.67		4.4	-2.13		0.6
MEANS ---->		22.7	0.9		23.7	2.6		21.9	-0.0
		DT= 21.8 C			DT= 21.1 C			DT= 22.0 C	

Mean Air Properties

Rep	BP (Pa)	Warm Room Twb (C)	Warm Room den. (kg/m^3)	Warm Room k.vis. (m^2/s)	Cold Room Tdp (C)	Cold Room den. (kg/m^3)	Cold Room k.vis. (m^2/s)
1	97324.6	14.4	1.1339	0.00001610	75%	1.2317	0.00001396
2	98713.0	15.0	1.1458	0.00001598	Sat	1.2408	0.00001393
3	97595.5	12.8	1.1427	0.00001594	***	1.2398	0.00001383

Regression Results Using the Model DP=a+(b*h)

Rep	NPA (m)	C.I.	Slope (Pa/m)	C.I.	r^2	Dden-reg (kg/m^3)	Dden-temp (kg/m^3)
1	2.844	0.017	-0.8964	0.0097	0.99958	0.0914	0.0908
2	3.079	0.017	-0.8557	0.0091	0.99959	0.0872	0.0883
3	2.729	0.031	-0.8787	0.0174	0.99861	0.0896	0.0924

Table E.3t

Test ID.= NC35 Data at Time= 40 min.

Elev. (m)	Rep 1 DP (Pa)	Rep 1 Tw (C)	Rep 1 Tc (C)	Rep 2 DP (Pa)	Rep 2 Tw (C)	Rep 2 Tc (C)	Rep 3 DP (Pa)	Rep 3 Tw (C)	Rep 3 Tc (C)
0.052	4.53	20.8	-14.9	4.40	21.8	-15.5	4.27	21.3	-15.0
0.305	4.27			4.00			4.00		
0.610	3.87	21.4	-14.8	3.53	22.1	-15.2	3.60	21.9	-15.0
0.914	3.40			3.00			3.07		
1.219	3.00	20.3	-15.0	2.53	21.4	-15.1	2.60	20.9	-14.9
1.524	2.53			2.07			2.00		
1.829	2.07	21.3	-14.2	1.60	22.0	-14.5	1.47	21.8	-14.2
2.134	1.47			1.07			1.00		
2.438	1.07	21.7	-14.1	0.60	22.6	-14.3	0.53	22.3	-14.0
2.743	0.60			0.07			0.00		
3.048	0.07	22.0	-13.9	-0.33	22.9	-14.2	-0.40	22.7	-13.8
3.353	-0.33			-0.87			-0.93		
3.658	-0.80	21.6	-13.8	-1.33	22.5	-14.1	-1.33	22.3	-13.9
3.962	-1.27			-1.87			-1.73		
4.267	-1.73	21.6	-13.5	-2.33	22.6	-13.9	-2.27	22.4	-13.8
4.572	-2.27			-2.80			-2.80		
4.877	-2.67	22.2	-13.6	-3.33	23.0	-13.2	-3.27	23.0	-13.1
4.959	-2.93		-10.8	-3.47		-11.1	-3.40		-11.0
MEANS ---->		21.4	-13.8		22.3	-14.1		22.1	-13.8
		DT= 35.2 C			DT= 36.4 C			DT= 35.9 C	

Mean Air Properties

Rep	BP (Pa)	Warm Room Twb (C)	Warm Room den. (kg/m^3)	Warm Room k.vis. (m^2/s)	Cold Room Tdp (C)	Cold Room den. (kg/m^3)	Cold Room k.vis. (m^2/s)
1	97324.6	13.3	1.1402	0.00001596	-17.6	1.3065	0.00001260
2	97324.6	15.0	1.1341	0.00001608	-18.4	1.3079	0.00001258
3	97832.5	15.0	1.1408	0.00001598	-18.4	1.3135	0.00001253

Regression Results Using the Model DP=a+(b*h)

Rep	NPA (m)	C.I.	Slope (Pa/m)	C.I.	r^2	Dden-reg (kg/m^3)	Dden-temp (kg/m^3)
1	3.120	0.023	-1.5322	0.0223	0.99925	0.1562	0.1564
2	2.808	0.008	-1.6001	0.0078	0.99991	0.1631	0.1612
3	2.806	0.022	-1.5834	0.0226	0.99928	0.1614	0.1598

APPENDIX F

ERROR ANALYSIS

An analysis of the propagation of the errors in measurement was performed for the calculation of the mass flow rate through each of the defined openings ($\dot{m}_j$), the summation of the mass flow rates ($\Sigma \dot{m}_j$), the calculation of the infiltration rate (IR), and the prediction of the elevation of the NPA (NPA.PRED). The uncertainty analysis was based upon the methods presented by Holman (1978).

<u>Uncertainty of the Cross-Sectional Area and the Area-Gamma Product.</u>

The cross-sectional area (A) of the rectangular openings was simply the product of the thickness, d, and the width, w. Therefore, the uncertainty in computing the area from the measured dimensions was founded by:

$$u_A = \sqrt{\left(u_d \frac{\partial A}{\partial d}\right)^2 + \left(u_w \frac{\partial A}{\partial w}\right)^2} \tag{F.1}$$

The uncertainty in the measurement of each of the cross-sectional dimensions (u_d and u_w) was ± 0.254 mm (± 0.01 in). The resulting equation for the uncertainty in the area was given by:

$$u_A = \sqrt{(u_d w)^2 + (u_w d)^2} \tag{F.2}$$

If was found that u_A was ± 1.27 cm^2 for all of the rectangular openings. The greatest source of error was the uncertainty associated with the slot thickness. Also, it was determined that the uncertainty of A in percent was almost identical to the uncertainty of d in percent. That is,

$$u_A = (u_d/d) * 100 \qquad (F.3)$$

The uncertainty in the area of the cylindrical openings was only a function of the uncertainty in the measurement of the diameter D. The uncertainty of D was also ± 0.254 mm. As a result, u_A for the cylindrical openings was computed as follows:

$$u_A = u_D \, |\partial A/\partial D| = u_D \, (\pi D/2) \qquad (F.4)$$

The equation for the uncertainty of the area-gamma product for both the rectangular and the cylindrical openings was:

$$u_{(A\gamma)} = \sqrt{(u_A\gamma)^2 + (u_\gamma A)^2} \qquad (F.5)$$

The geometric parameter, gamma, for a rectangular opening was defined in equation 3.24 as;

$$\gamma = \frac{\alpha}{Bz(1 + \alpha)^2}$$

where; $\alpha = d/w$ (equation 3.10), and

$B = 96 - 106.67\alpha$ (equation 3.3).

The uncertainties of gamma for the rectangular openings were determine by the following equation:

$$u_\gamma = \sqrt{\left(u_\alpha \frac{\partial\gamma}{\partial\alpha}\right)^2 + \left(u_z \frac{\partial\gamma}{\partial z}\right)^2 + \left(u_B \frac{\partial\gamma}{\partial B}\right)^2} \qquad (F.6)$$

where; $u_\alpha = \sqrt{[u_d \; (1/w)]^2 + [u_W(-d/w^2)]^2} = \pm 5.08 \times 10^{-4}$

$u_z = \pm 2.54 \times 10^{-4}$ m, and

$u_B = u_\alpha * 106.67 = \pm 0.054$.

The uncertainties in gamma for the rectangular openings ranged from ± 5 percent for opening H (the largest opening) to ± 31.6 percent for opening A (the smallest opening). The greatest source of error was u_α.

The defining equation of gamma for the cylindrical openings was given in equation 3.29 as:

$$\gamma = \frac{1}{B\,\pi\,z} \quad .$$

Where, the value of B was equal to 64 and z was equal to 5.08 x 10^{-2} m for each of the cylindrical openings. Consequently, the uncertainty in γ was a constant for all of the cylindrical openings given by:

$$u_z = u\ |\partial\gamma/\partial z| = \pm 4.89 \times 10^{-4}\ m^{-1} \qquad (F.7)$$

where; $u_z = \pm 2.54 \times 10^{-4}$ m.

Since, all of the cylindrical openings had a value of γ equal to 979.05 x 10^{-4} m^{-1} the uncertainty in γ was $\pm$0.5 percent.

The uncertainties in the cross-sectional area (A) and the area-gamma product ($A\gamma$), for all of the defined openings have been presented in Table F.1.

Table F.1
Uncertainties in A and ($A\gamma$) for Each of the Defined Openings

Opening ID.	A (cm^2)	u_A (%)	($A\gamma$) x 10^{-5} (m)	$u_{(A\gamma)}$ (%)
A	4.00	31.7	0.026	44.8
B	8.50	14.9	0.059	21.1
C	10.00	12.7	0.327	18.0
D	16.50	7.7	0.253	10.9
E	31.45	4.0	0.459	5.6
F	64.31	2.0	3.343	2.8
H	80.02	1.6	2.097	2.2
X	0.32	8.0	0.313	8.0
Y	1.27	4.0	1.243	4.0
Z	20.27	1.0	19.845	1.1

Uncertainty in the Calculation of the Air Properties

The equations used to compute the dynamic viscosity (μ), the density (ρ) and the kinematic viscosity (ν) have been provided in Appendix C.

Equation C.1 indicates that the dynamic viscosity is a function of the dry-bulb temperature of the air (T_{db}). It was assumed that the thermocouples used to measure the dry bulb temperature had an error of $\pm 0.6°C$. It was determined from equation C.1 that a 0.6°C error in T_{db} would result in an uncertainty of μ equal to $\pm 3.0 \times 10^{-8}$ ($N*s/m^2$).

The density was computed by inverting the specific volume (v_{sp}) of the air as computed by equation C.2. The uncertainty in the specific volume in percent was equal to the uncertainty in the density in percent. The uncertainty in the specific volume was computed from the following relationship:

$$u_{v_{sp}} = \left[\left(u_{T_{db}} \frac{\partial v_{sp}}{\partial T_{db}}\right)^2 + \left(u_W \frac{\partial v_{sp}}{\partial W}\right)^2 + \left(u_{BP} \frac{\partial v_{sp}}{\partial BP}\right)^2\right]^{1/2} \quad \text{(F.8)}$$

where; u_{BP} = uncertainty in the local barometric pressure, and

u_W = uncertainty in the humidity ratio.

Since the mean barometric pressure was used for each day on which data were taken the uncertainty in the barometric pressure was assumed to be ± 1.0 percent based upon the means and standard deviations of the individual readings. The humidity ratio (W) of the air in the warm room was computed using equation C.3 and the uncertainty in W for the air in the warm room was determined by:

$$u_W = \sqrt{\left(u_{T_{db}} \frac{\partial W}{\partial T_{db}}\right)^2 + \left(u_{T_{wb}} \frac{\partial W}{\partial T_{wb}}\right)^2 + \left(u_{W_s^*} \frac{\partial W}{\partial W_s^*}\right)^2} \quad \text{(F.9)}$$

where; $u_{T_{wb}}$ = the uncertainty of the wet-bulb temperature,

u_{W^*} = the uncertainty of the humidity ratio corresponding to saturation at T_{wb}.

The uncertainty in the wet-bulb temperature measurement was assumed to be ± 1.0°C. The uncertainty in W_s^* corresponding to a 1.0°C error in T_{wb} was determined to be ± 7.0 percent from the regression equations given by equation C.4.

The humidity ratio of the air in the cold room was equal to the humidity ratio corresponding to the dewpoint temperature (T_{dp}). The error in T_{dp} was assumed to be ± 1.0°C. The uncertainty in the humidity ratio (W_s) corresponding to a 1.0°C error in T_{dp} was determined from the regression equations given by equation C.5 to be ± 10.0 percent.

The resulting uncertainty in the density (ρ) of both the warm and the cold air was ± 1.03 percent. The greatest source of error was due to the uncertainty of the barometric pressure measurements.

The kinematic viscosity, ν, was defined in equation C.6. The uncertainty in was found to be ± 1.04 percent.

Uncertainty in the Calculation of the Discharge Coefficient

The discharge coefficient equation was given as (equation 3.26):

$$\frac{1}{C_z^2} = \frac{2K}{\left[1 + (A\ \gamma)^2\ \frac{128\ K\ \Delta\ P}{\rho\ \nu^2}\right]^{0.5} - 1} + K$$

where; K = 1.5.

The uncertainty in the squared inverse of the discharge coefficient ($1/C_z^2$) was computed by the following expression:

$$u_{1/C_z^2} = \left[\left(u_{(A\gamma)} \frac{\partial\ 1/C_z^2}{\partial (A\gamma)}\right)^2 + \left(u_{\Delta P} \frac{\partial\ 1/C_z^2}{\partial\ \Delta P}\right)^2 + \left(u_\rho \quad \frac{\partial\ 1/C_z^2}{\partial \rho}\right)^2 + \left(u_\nu \quad \frac{\partial\ 1/C_z^2}{\partial \nu}\right)^2\right]^{1/2}$$

where; $u_{\Delta P}$ = the uncertainty in the differential pressure measurement.

The three scales used on the pressure transducer (MKS Baratron) had resolutions of 0.0001 mm Hg (full scale = 0.003 mm Hg), 0.0002 mm Hg (full scale = 0.010 mm Hg) and 0.001 mm Hg (full scale = 0.03 mm Hg). Due to fluctuations in these very low differential pressure measurements, the smallest scale could only be read to the nearest $\pm$0.0002 mm Hg ($\pm$0.027 Pa). As a result, two uncertainties were used for the differential pressure measurements as defined below:

for $\Delta P < 1.33$ Pa $\quad u_{\Delta P} = \pm 0.027$ Pa ($\pm$0.0002 mm Hg)

for $\Delta P \geq 1.33$ Pa $\quad u_{\Delta P} = \pm 0.133$ Pa ($\pm$0.001 mm Hg)

It was desired to know the uncertainty in the discharge coefficient, C_z, not $1/C_z^2$. Therefore, the discharge coefficient, C_z, was expressed as follows:

$$C_z = \sqrt{1/\lambda} \tag{F.11}$$

where; $\lambda = 1/C_z^2$

The uncertainty in the discharge coefficient resulting from the propagation of uncertainties in measurements was determined by:

$$u_{C_z} = |u_{1/C_z^2} \quad (-\frac{1}{2}\lambda^{3/2})| \tag{F.12}$$

It was determined that the greatest source of error in the calculation of C_z (or $1/C_z^2$) was due to the uncertainties associated with $(A\gamma)$. The next most important error was $u_{\Delta P}$.

The variation of the uncertainty of the discharge coefficient with respect to the pressure difference has been presented for each of the defined openings in Figure F.1.

Uncertainty of the Calculation of the Mass Flow Rate

The equation to compute the mass flow rate through an individual opening was given in equation 3.33 as:

$$\dot{m}_j = (C_z\ A)_j \sqrt{2\ \Delta P_j\ \rho_j}$$

where; $\dot{m}_j$ = the mass flow rate through the j^{th} opening.

Typical mass flow rates through each of the defined openings have been provided in Figure F.2.

The uncertainty in the mass flow rate was determined as follows;

$$u_{\dot{m}} = \sqrt{\left(u_A \frac{\partial \dot{m}}{\partial A}\right)^2 + \left(u_{C_z} \frac{\partial \dot{m}}{\partial C_z}\right)^2 + \left(u_{\Delta P} \frac{\partial \dot{m}}{\partial \Delta P}\right)^2 + \left(u_\rho \frac{\partial \dot{m}}{\partial \rho}\right)^2} \qquad (F.13)$$

The variation of the uncertainty in the mass flow rate with respect to the pressure difference for each of the defined openings has been presented in Figure F.3. It was found that the greatest source of error in the computation of the mass flow rate was due to the uncertainty in the cross-sectional area. The next largest source of error was the uncertainty of C_z.

Uncertainty of the Sum of the Mass Flow Rates

Theoretically, the NPA assumes an elevation such that the mass flow into a structure is equal to the mass flow out. Due to the errors of measurement the sum of the mass flow rates was not zero for any opening distribution. Therefore, it was desired to estimate the magnitude of the uncertainty in the summation of the mass flows due to the propagation of the uncertainties in measurement. The

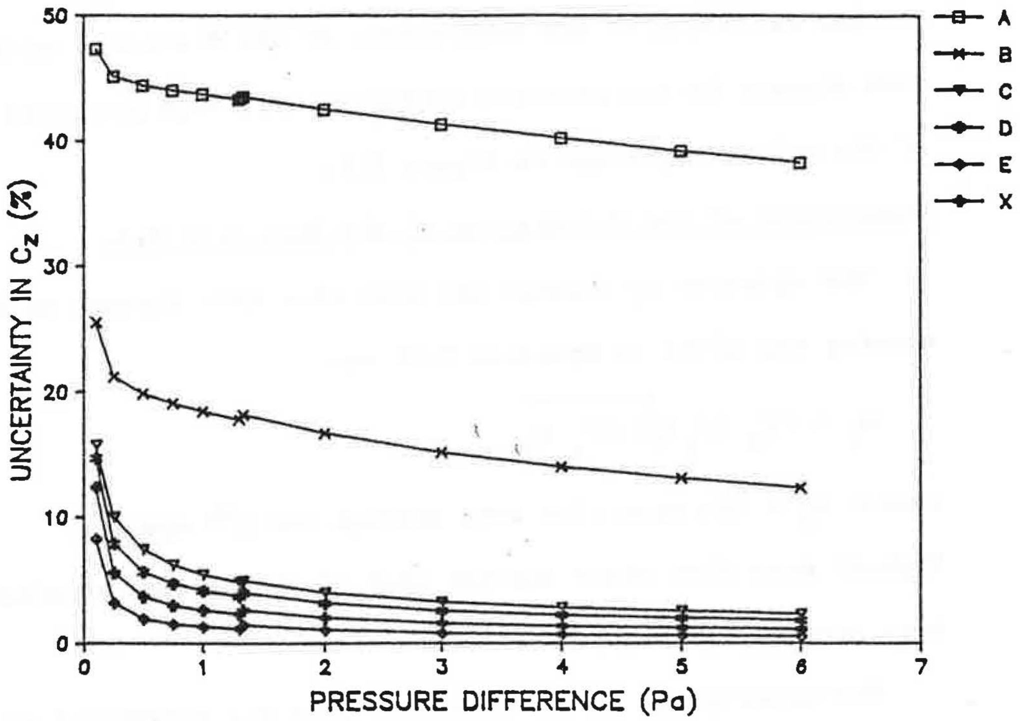

Figure F.1a.

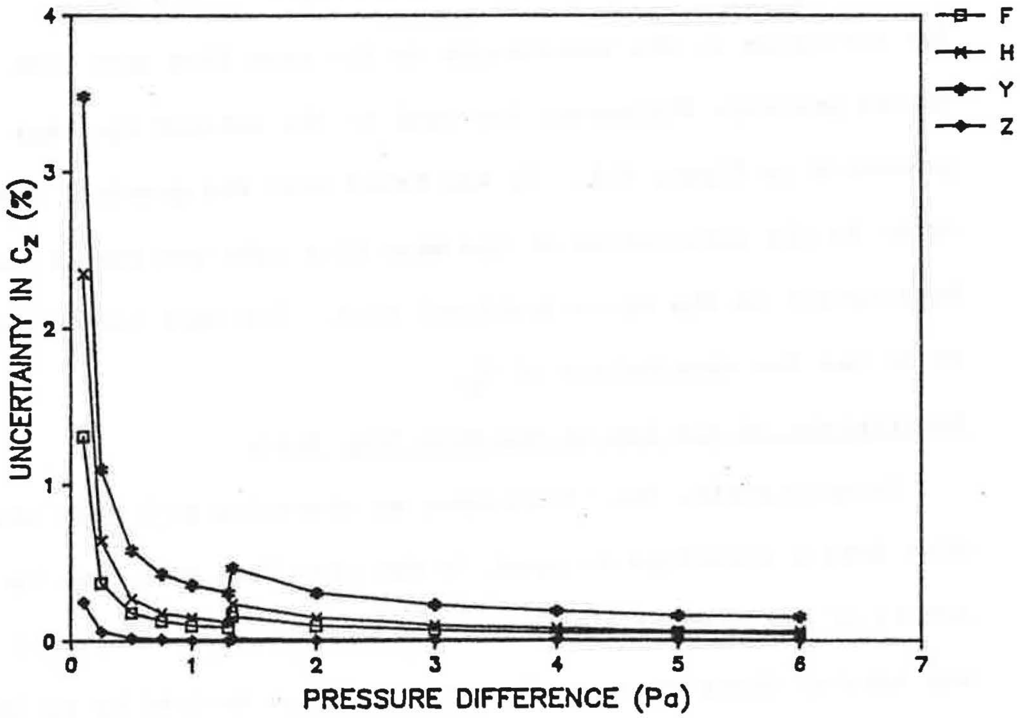

Figure F.1b.

Figure F.1 Uncertainty in the discharge coefficient for each of the defined openings.

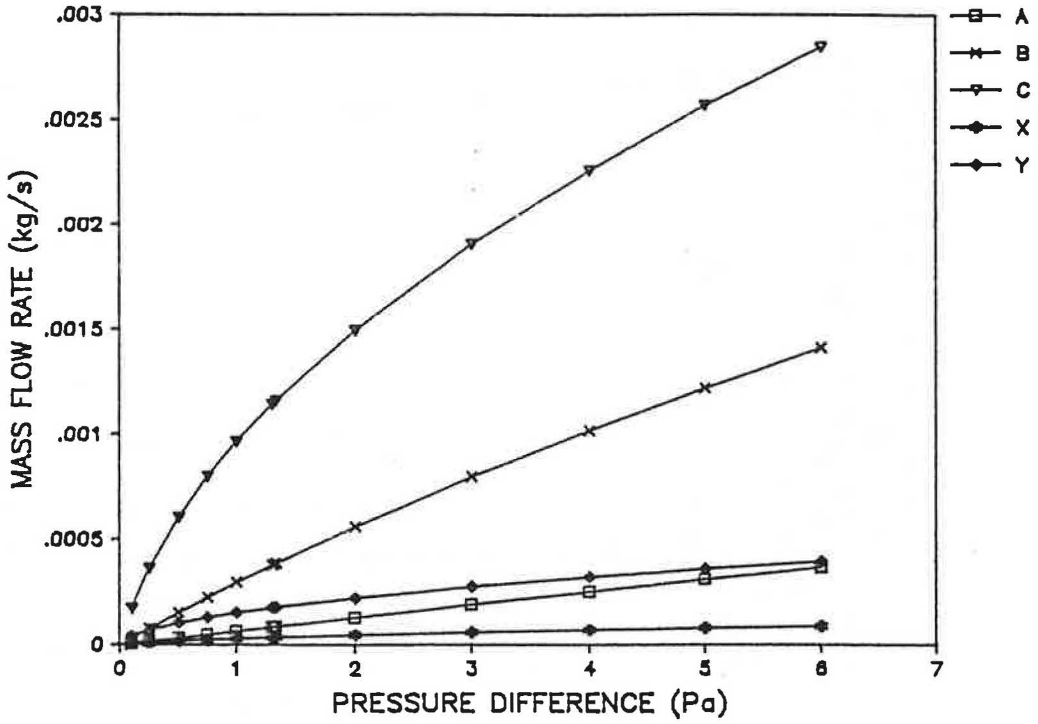

Figure F.2a.

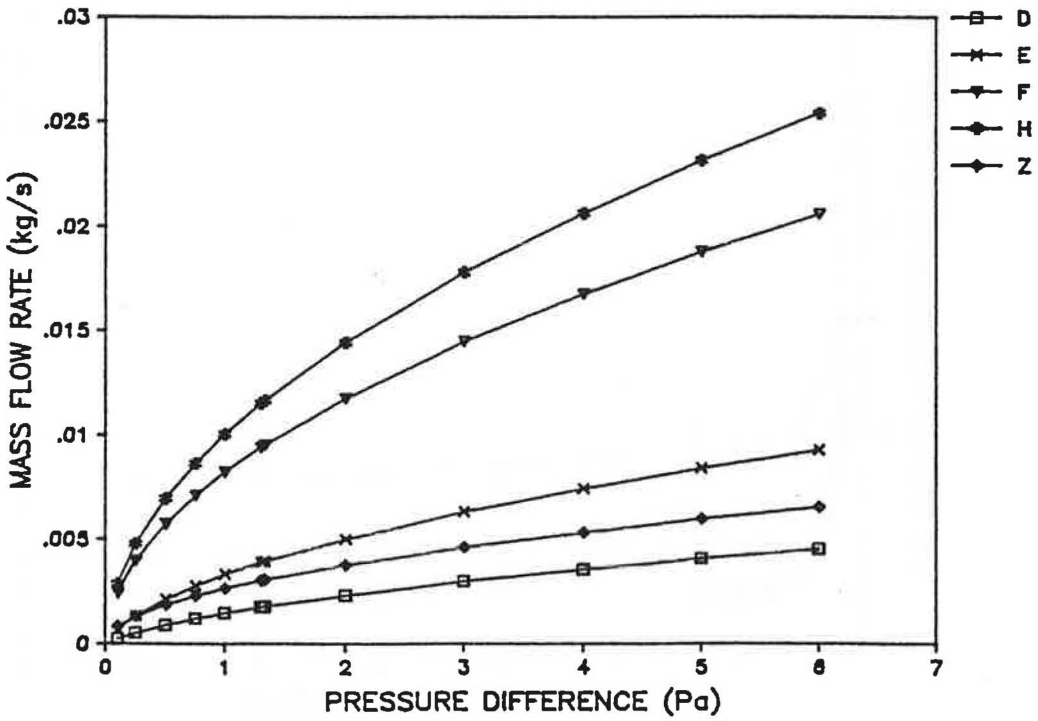

Figure F.2b.

Figure F.2 Typical mass flow rates through the defined openings.

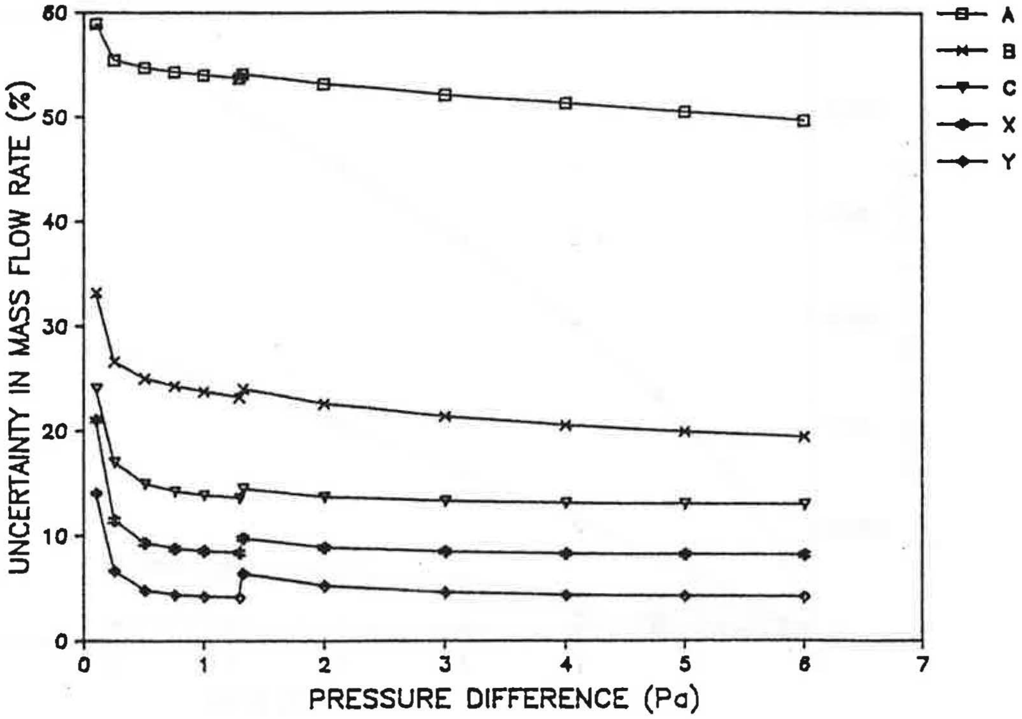

Figure F.3a.

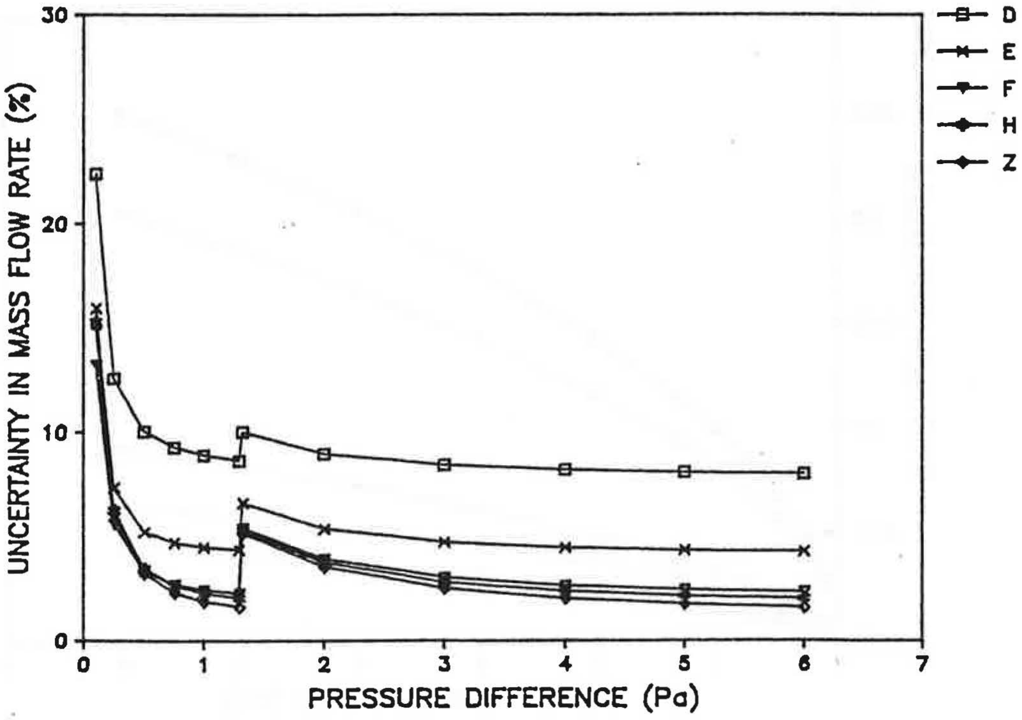

Figure F.3b.

Figure F.3 Uncertainty of the mass flow rate for each of the defined openings.

uncertainty of the sum of the mass flow rates about zero for an opening distribution was estimated as follows:

$$u_{\Sigma \dot{m}} = \left[\sum_{j=1}^{n} (u_{\dot{m}_j})^2 \right]^{1/2} \quad \text{(F.14)}$$

where; $u_{\Sigma \dot{m}}$ = the uncertainty in the sum of the mass flow rates for n openings,

$u_{\dot{m}_j}$ = the uncertainty of the mass flow rate through an individual opening in the distribution (eq. F.13).

The infiltration rate was computed for each opening distribution as follows (equation 7.7):

$$IR = \frac{\sum_{j=1}^{n} | \dot{m}_j |}{2}$$

Therefore, the uncertainty in the sum of the mass flow rates was also the estimate of the uncertainty in the calculation of the infiltration rate.

The sum of the mass flow rates, the uncertainty in the sum of the mass flow rates, and the infiltration rate using the measured differential pressures (IR.DATA) for each replication of each treatment have been presented in Table F.2 (also refer to Figures 7.20 and 7.26). It was determined that the sum of the mass flow rates ($\Sigma \dot{m}_j$) was greater than $u_{\Sigma \dot{m}}$ in only 7 of the 48 observations.

It should be noted that the mass flow rates of the hypothetical openings BGH and BGL are included in the values of $\Sigma \dot{m}_j$ and IR.DATA. The uncertainty in the summation of the mass flow rates ($u_{\Sigma \dot{m}}$) was computed exclusively from the defined openings in each

Table F.2
Results of the Error Analysis on the Mass Balancing Procedure

TREATMENT	REP	$\Sigma\dot{m}$ (kg/s)	$u_{\Sigma\dot{m}}$ (kg/s)	IR.DATA (kg/s)	NPA.DATA (cm)	C.I.	NPA.PRED (cm)	U.I.
G1H1T1	1	.00029	.00042	.00479	220.5	1.3	217.4	5.2
	2	.00038	.00039	.00432	221.1	1.5	217.3	5.2
	3	.00027	.00040	.00438	220.8	.9	217.9	5.2
G1H1T2	1	.00081 +	.00029	.00269	224.9 *	1.7	217.1	5.3
	2	.00017	.00028	.00278	221.6	1.5	217.1	5.3
	3	.00015	.00029	.00293	218.6	1.1	217.6	5.3
G1H1T3	1	.00037 +	.00024	.00208	222.9	1.4	216.3	5.7
	2	.00030 +	.00024	.00206	221.3	1.8	216.3	5.7
	3	.00045 +	.00022	.00172	224.9 *	1.9	215.8	6.1
G1H2T1	1	-.00012	.00049	.00674	349.2	1.4	350.0	9.9
	2	-.00012	.00048	.00658	350.2	1.2	350.2	9.9
	3	-.00028	.00048	.00669	347.2	1.2	350.8	9.8
G1H2T2	1	-.00030	.00036	.00472	353.9	2.1	358.3	9.9
	2	-.00008	.00036	.00424	360.2	2.5	360.3	10.7
	3	-.00043 +	.00034	.00443	349.6	1.5	360.6	9.9
G1H2T3	1	-.00015	.00029	.00360	361.5	1.7	363.2	10.2
	2	-.00007	.00028	.00339	361.6	1.1	364.4	10.3
	3	-.00014	.00025	.00287	365.5	1.9	367.2	10.6
G2H1T1	1	-.00024	.00061	.01822	206.2	1.5	207.3	3.2
	2	.00019	.00060	.01783	207.9	1.6	207.0	3.2
	3	.00026	.00060	.01743	209.0	1.4	207.7	3.2
G2H1T2	1	.00049	.00056	.01237	211.0	1.7	208.4	4.1
	2	.00007	.00056	.01252	207.5	1.5	208.2	4.0
	3	-.00008	.00057	.01353	207.8	1.1	208.4	3.8
G2H1T3	1	-.00004	.00059	.01001	206.3	1.8	207.8	5.2
	2	-.00008	.00059	.00977	205.0	.9	207.7	5.4
	3	.00012	.00060	.00941	209.2	1.1	207.4	5.7
G2H2T1	1	-.00016	.00060	.02227	313.5	1.0	313.9	4.4
	2	.00041	.00061	.02251	315.6	.7	313.4	4.4
	3	.00012	.00060	.02234	315.8	1.1	314.1	4.4
G2H2T2	1	-.00017	.00052	.01705	318.1	1.5	317.3	4.9
	2	.00023	.00050	.01533	322.5	1.6	318.3	5.2
	3	-.00030	.00051	.01583	318.5	1.8	318.3	5.1
G2H2T3	1	.00007	.00050	.01233	320.6	1.4	318.9	6.4
	2	-.00041	.00050	.01353	317.1	1.8	319.3	5.9
	3	-.00017	.00051	.01176	318.4	1.2	319.5	6.8
REC1	1	.00038	.00046	.00969	305.9	1.3	301.7	4.4
	2	.00044	.00046	.00968	305.6	1.3	301.7	4.4
	3	.00009	.00047	.01004	304.2	1.8	301.4	4.4
REC2	1	.00004	.00044	.00534	155.2	1.7	154.4	9.6
	2	-.00002	.00045	.00547	152.2	1.3	154.2	9.5
	3	-.00017	.00045	.00542	151.1	1.8	154.6	9.6
CYL	1	.00001	.00006	.00345	76.0	1.2	76.1	1.7
	2	.00011 +	.00006	.00305	78.5	1.1	76.3	1.7
	3	-.00009 +	.00006	.00315	75.3	1.4	77.2	1.7
CYLREC	1	-.00008	.00029	.00293	292.2	2.0	295.7	7.9
	2	-.00009	.00029	.00291	293.3	1.5	296.0	7.9
	3	-.00012	.00029	.00288	291.6	1.8	296.1	7.9

+ - Cases for which $\Sigma\dot{m}$ was greater than $u_{\Sigma\dot{m}}$.

* - Cases for which the 95% confidence interval (C.I.) and the uncertainty interval (U.I.) did not overlap.

opening distribution.

Uncertainty of the Mass Balancing Procedure to Predict the Elevation of the NPA.

The uncertainty of the sum of the mass flow rates was also the means by which the uncertainty in the prediction of the NPA (NPA.PRED) due to the propagation of the errors of measurement could be estimated. The elevation of the NPA was determined by iteratively balancing the sum of the mass flow rates to five decimal places (i.e. zero $\equiv \pm 0.000004$ kg/s). An uncertainty interval (U.I.) about NPA.PRED was determined by iteratively balancing the sum of the mass flow rates until the sum of the mass flow rates was equal to the uncertainty in the sum of the mass flow rates. That is, until the following relationship was satisfied (equation 7.6):

$$\sum_{j=1}^{n} \dot{m}_j = \pm u_{\Sigma \dot{m}}$$

The upper limit of the uncertainty interval on NPA.PRED was the elevation of the NPA which corresponded to $\Sigma \dot{m}_j = -u_{\Sigma \dot{m}}$ and the lower limit was the elevation of the NPA which corresponded to $\Sigma \dot{m}_j = +u_{\Sigma \dot{m}}$.

As was shown in Appendix D, a 95 percent confidence interval (C.I.), based upon the variance about the regression line, was computed about each observed NPA (NPA.DATA). The values of NPA.DATA and NPA.PRED along with the corresponding confidence intervals (C.I.) and uncertainty intervals (U.I.) for the original sixteen treatments have also been presented in Table F.2 (also refer to Figures 7.21a through 7.21h). The only two cases for which the 95 percent confidence interval (C.I.) of NPA.DATA and the uncertainty interval of NPA.PRED did not overlap were for G1H1T2 (Rep 1) and G1H1T3 (Rep 3). In each of these cases the observed elevation of the NPA was considerably higher than the other replications. The additional error for the two cases was believed to be due to the results of the variation of the background leakage.

APPENDIX G

DATA FOR THE VALIDATION OF THE DISCHARGE COEFFICIENT EQUATION

Definition of the symbols used in the tables

BP - Local barometrio pressure, Pa

C - Temperature, degree Celsius

DYN.VISC - Dynamic viscosity, $N*s/m^2$

KIN.VISC - Kinematic viscosity, m^2/s

Tdb - Dry bulb temperature

Q - Volumetric flow rate, m^3/s

Re - Reynolds number

STD - Standard deviation

C.V. - Coefficient of variation, %

W - Humidity ratio, kg.w/kg

$(1/C_z\wedge 2)$ - Total dimensionless pressure drop

$B(z/D_hRe)$ - Dimensionless friction loss

K - Total minor loss coefficient

Table G.1 Differential Pressure, Volumetric Flow, and Air Properties Data

Table G.1a

DATA FOR OPENING A AREA=4.00 (cm^2)
GAMMA=6.55x10^-4 (m^-1)

	REP	BP (Pa)	Tdb (C)	Twb (C)
	1	97951.03	24.4	12.2
	2	97849.44	25.3	13.3
	3	97883.31	25.6	13.3
	4	97883.31	25.8	13.3
MEAN		97891.78	25.3	13.1
STD		52.26	.6	.56
C.V-%		.05	2.37	4.26

	REP	W kg.w/kg	DENSITY kg/m^3	DYN.VISC N*s/m^2	KIN.VISC m^2/s
	1	.0039189	1.1394	.0000183	.0000161
	2	.0046946	1.1337	.0000184	.0000162
	3	.0045822	1.1332	.0000184	.0000162
	4	.0044698	1.1324	.0000184	.0000163
MEAN		.0044164	1.1347	.0000184	.0000162
STD		.0003441	.0032	2.917e-8	7.068e-8
C.V.-%		7.79	.28	.16	.44

		PRESSURE DIFFERENCE (Pa)				
Q (m^3/s)	Re	REP1	REP2	REP3	REP4	MEAN
.0000777	19	1.74	1.92	1.57	1.97	1.80
.0001582	39	3.54	3.87	3.52	3.82	3.68
.0002326	57	5.46	5.76	5.31	5.76	5.57
.0003072	76	7.40	7.65	7.15	7.70	7.47
.0003835	95	9.50	9.81	9.29	9.72	9.58
.0004703	116	11.96	12.38	11.81	12.13	12.07
.0005490	135	14.23	14.72	14.15	14.58	14.42
.0006306	155	16.74	17.17	16.57	17.12	16.90
.0007134	176	19.31	19.86	18.98	19.46	19.40
.0007994	197	22.12	22.77	22.07	22.32	22.32
.0009439	233	25.43	25.33	25.01	25.18	25.24
.0011012	271	30.42	30.62	29.99	30.31	30.33
.0012585	310	35.55	35.82	34.87	35.35	35.40
.0014159	349	41.00	41.40	40.30	40.93	40.91
.0015732	388	46.38	46.78	45.66	46.41	46.31
.0017305	426	53.03	53.16	51.76	52.78	52.68
.0018878	465	59.86	59.76	58.34	59.48	59.36
.0020451	504	66.36	66.46	64.89	65.86	65.89
.0022024	543	72.53	73.10	72.11	71.61	72.34
.0023597	582	80.00	81.65	79.06	80.95	80.42

Table G.1b

DATA FOR OPENING B — AREA=8.50 (cm^2), GAMMA=6.95x10^-4 (m^-1)

	REP	BP (Pa)	Tdb (C)	Twb (C)
	1	98120.36	25.0	13.9
	2	98221.94	25.6	13.3
	3	98425.13	24.4	13.3
	4	98289.68	25.6	14.4
MEAN		98264.28	25.14	13.75
STD		122.55	.53	.53
C.V.-%		.13	2.12	3.87

	REP	W kg.w/kg	DENSITY kg/m^3	DYN.VISC N*s/m^2	KIN.VISC m^2/S
	1	.0053820	1.1366	.0000184	.0000162
	2	.0045822	1.1371	.0000184	.0000162
	3	.0050322	1.1429	.0000183	.0000161
	4	.0057442	1.1358	.0000184	.0000162
MEAN		.0051852	1.1381	.0000184	.0000161
STD		.0004961	.0032	2.433e-8	6.608e-8
C.V.-%		9.57	.28	.13	.41

Q (m^3/s)	Re	PRESSURE DIFFERENCE (Pa) REP1	REP2	REP3	REP4	MEAN
.0003072	76	1.18	1.42	1.40	1.57	1.39
.0003835	95	1.54	1.77	1.77	1.94	1.75
.0004703	116	2.09	2.24	2.27	2.39	2.25
.0005490	135	2.49	2.79	2.82	2.89	2.75
.0006306	156	2.97	3.22	3.29	3.27	3.18
.0007134	176	3.42	3.67	3.74	3.87	3.67
.0007994	197	3.89	4.28	4.33	4.43	4.23
.0009439	233	4.61	4.98	4.93	5.11	4.91
.0011012	272	5.78	6.08	6.01	6.18	6.01
.0012585	311	6.95	7.12	7.05	7.05	7.04
.0014159	349	8.10	8.17	8.20	8.27	8.18
.0015732	388	9.15	9.32	9.32	9.27	9.26
.0017305	427	10.49	10.71	10.71	10.66	10.64
.0018878	466	11.98	12.23	12.11	12.18	12.12
.0020451	505	13.48	13.63	13.30	13.50	13.48
.0022024	544	14.90	15.27	14.77	15.10	15.01
.0023597	582	16.62	17.07	16.77	16.72	16.79
.0025171	621	18.18	18.43	18.41	18.36	18.34
.0026744	660	19.85	20.28	19.95	20.05	20.03
.0028317	699	21.40	22.15	21.80	21.65	21.75
.0029890	738	23.34	23.89	23.36	23.51	23.52
.0031463	777	25.46	25.90	25.41	25.26	25.51

Table G.1c

DATA FOR OPENING C AREA=10.00 (cm^2)
GAMMA=32.68x10^-4 (m^-1)

REP	BP (Pa)	Tdb (C)	Twb (C)
1	97951.03	24.4	20.6
2	98594.46	26.1	21.7
3	98560.59	26.1	22.2
4	98594.46	25.0	21.1
MEAN	98425.12	25.4	21.4
STD	317.86	.83	.72
C.V.-%	.32	3.28	3.35

REP	W kg.w/kg	DENSITY kg/m^3	DYN.VISC N*s/m^2	KIN.VISC m^2/s
1	.0136627	1.1220	.0000183	.0000164
2	.0145503	1.1215	.0000184	.0000164
3	.0153712	1.1197	.0000184	.0000165
4	.0142131	1.1263	.0000184	.0000163
MEAN	.0144493	1.1223	.0000184	.0000164
STD	.0007153	.0028	3.989e-8	6.664e-8
C.V.-%	4.95	.25	.22	.41

		PRESSURE DIFFERENCE (Pa)				
Q(m^3/s)	Re	REP1	REP2	REP3	REP4	MEAN
.0023597	574	5.81	5.91	5.88	5.86	5.86
.0028317	688	8.02	8.25	8.15	8.20	8.15
.0033036	803	10.91	11.19	10.86	11.19	11.04
.0037756	918	13.50	14.23	14.05	14.15	13.98
.0042475	1033	16.42	17.36	17.06	17.31	17.04
.0047195	1147	19.43	21.28	19.81	20.35	20.21
.0056634	1377	27.68	28.27	27.85	28.35	28.03
.0066073	1606	35.32	37.29	35.92	37.41	36.48
.0075512	1836	44.16	47.35	46.28	47.40	46.30
.0084951	2065	54.92	58.96	57.24	58.98	57.52
.0094390	2295	66.88	71.53	69.07	71.23	69.68
.0103829	2524	78.11	88.92	82.44	84.29	83.44

Table G.1d

DATA FOR OPENING D AREA=16.50 (cm^2)
GAMMA=15.36x10^-4 (m^-1)

	REP	BP (Pa)	Tdb (C)	Twb (C)
	1	98086.49	24.4	21.7
	2	98492.86	25.6	22.2
	3	98594.46	24.4	22.2
	4	98628.31	25.0	21.1
MEAN		98450.53	24.9	21.8
STD		247.87	.5	.53
C.V.-%		.25	2.14	2.44

	REP	W kg.w/kg	DENSITY kg/m^3	DYN.VISC N*s/m^2	KIN.VISC m^2/s
	1	.0152472	1.1207	.0000183	.0000164
	2	.0156038	1.1206	.0000184	.0000164
	3	.0160697	1.1251	.0000183	.0000163
	4	.0142131	1.1267	.0000184	.0000163
MEAN		.0152835	1.1233	.0000184	.0000164
STD		.0007890	.0031	2.433e-8	5.441e-8
C.V.-%		5.16	.28	.13	.33

Q (m^3/s)	Re	PRESSURE DIFFERENCE (Pa) REP1	REP2	REP3	REP4	MEAN
.0023597	573	3.27	3.02	3.49	3.29	3.27
.0028317	688	4.19	4.06	4.58	4.46	4.32
.0033036	803	5.53	5.61	6.08	6.03	5.81
.0037756	917	7.05	7.15	7.72	7.57	7.37
.0042475	1032	8.52	8.82	9.29	9.22	8.96
.0047195	1147	10.29	10.44	11.01	10.84	10.64
.0056634	1376	13.93	14.37	15.02	14.85	14.54
.0066073	1606	18.96	18.76	19.36	19.61	19.17
.0075512	1835	24.29	23.54	24.16	24.36	24.09
.0084951	2064	28.32	29.19	29.27	30.09	29.22
.0094390	2294	33.11	34.30	35.07	36.31	34.70
.0103829	2523	39.20	40.13	41.65	42.79	40.94
.0113268	2752	44.96	47.45	48.80	49.14	47.58
.0122707	2982	53.10	55.22	55.89	58.01	55.56
.0132146	3211	61.15	61.92	64.41	66.43	63.47
.0141585	3441	69.07	71.16	73.46	74.65	72.08

Table G.1e

DATA FOR OPENING E AREA=31.45 (cm^2)
GAMMA=14.60x10^-4 (m^-1)

	REP	BP (Pa)	Tdb (C)	Twb (C)
	1	98391.28	26.1	22.8
	2	98594.46	26.1	22.2
	3	98526.72	26.1	22.2
	4	98594.46	26.1	22.8
MEAN		98526.72	26.1	22.5
STD		104.51	.00	.32
C.V-%		.11	.00	1.43

	REP	W kg.w/kg	DENSITY kg/m^3	DYN.VISC N*s/m^2	KIN.VISC m^2/s
	1	.0162129	1.1163	.0000184	.0000165
	2	.0153712	1.1200	.0000184	.0000165
	3	.0153712	1.1193	.0000184	.0000165
	4	.0162129	1.1186	.0000184	.0000165
MEAN		.0157921	1.1185	.0000184	.0000165
STD		.0004860	.0016	0	2.508e-8
C.V.-%		3.08	.15	.00	.15

Q (M^3/S)	Re	PRESSURE DIFFERENCE (Pa) REP1	REP2	REP3	REP4	MEAN
.0028317	680	1.35	1.64	1.44	1.42	1.46
.0047195	1133	3.24	3.47	3.39	3.29	3.35
.0066073	1587	5.73	6.33	5.88	6.16	6.02
.0084951	2040	8.95	9.68	9.64	9.37	9.41
.0103829	2493	12.78	12.98	13.10	13.58	13.11
.0122707	2947	17.02	17.34	17.17	18.06	17.39
.0141585	3400	22.62	22.54	22.69	23.76	22.90

Table G.1f

DATA FOR OPENING F   AREA=64.31 (cm^2)
GAMMA=51.98x10^-4 (m^-1)

	REP	BP (Pa)	Tdb(C)	Twb (C)
	1	98594.46	26.7	22.8
	2	98628.31	26.1	22.2
	3	98594.46	26.1	22.2
	4	98594.46	27.8	21.7
MEAN		98602.92	26.7	22.2
STD		16.91	.8	.5
C.V.-%		.02	2.9	2.0

	REP	W kg.w/kg	DENSITY kg/m^3	DYN.VISC N*s/m^2	KIN.VISC m^2/s
	1	.0159799	1.1169	.0000185	.0000165
	2	.0153712	1.1204	.0000184	.0000164
	3	.0153712	1.1200	.0000184	.0000165
	4	.0138552	1.1165	.0000185	.0000166
MEAN		.0151443	1.1185	.0000185	.0000165
STD		.0009061	.0021	3.7e-8	6.114e-8
C.V.-%		5.98	.19	.20	.37

Q (m^3/s)	Re	PRESSURE DIFFERENCE (Pa) REP1	REP2	REP3	REP4	MEAN
.0084951	2014	1.74	1.57	1.72	1.57	1.65
.0103829	2461	2.59	2.37	2.44	2.27	2.42
.0122707	2909	3.32	3.19	3.32	3.19	3.25
.0141585	3356	4.33	4.16	4.33	4.09	4.23

Table G.1g

DATA FOR OPENING G   AREA=67.01 (cm^2)
GAMMA=17.91x10^-4 (m^-1)

	REP	BP (Pa)	Tdb (C)	Twb (C)
	1	97781.72	26.7	21.1
	2	98594.46	25.0	21.1
	3	98662.18	25.6	22.2
	4	98662.18	26.1	21.7
MEAN		98425.13	25.8	21.5
STD		429.33	.7	.53
C.V.-%		.44	2.78	2.47

	REP	W kg.w/kg	DENSITY kg/m^3	DYN.VISC N*s/m^2	KIN.VISC m^2/s
	1	.013518	1.1120	.0000185	.0000166
	2	.0142131	1.1263	.0000184	.0000163
	3	.0156038	1.1225	.0000184	.0000164
	4	.0145503	1.1223	.0000184	.0000164
MEAN		.0144714	1.1207	.0000184	.0000164
STD		.0008686	.0062	3.441e-8	.0000001
C.V.-%		6.00	.55	.19	.72

Q (m^3/s)	Re	PRESSURE DIFFERENCE (Pa) REP1	REP2	REP3	REP4	MEAN
.0084951	2014	1.74	1.64	1.82	1.89	1.77
.0103829	2462	2.42	2.57	2.57	2.57	2.53
.0122707	2910	3.34	3.27	3.47	3.52	3.40
.0141585	3357	4.38	4.28	4.63	4.51	4.45

Table G.1h

DATA FOR OPENING X1 AREA=0.32 (cm^2)
GAMMA=979.05x10^-4 (m^-1)

REP	BP (Pa)	Tdb (C)	Twb (C)
1	97849.44	24.4	13.6
2	97883.31	25.8	13.9
3	97951.03	26.1	16.1
4	97951.03	26.4	13.3
MEAN	97908.71	25.7	14.2
STD	52.26	.86	1.27
C.V.-%	.05	3.36	8.92

REP	W kg.w/kg	DENSITY kg/m^3	DYN.VISC N*s/m^2	KIN.VISC m^2/s
1	.0053183	1.1357	.0000183	.0000162
2	.0050440	1.1313	.0000184	.0000163
3	.0073625	1.1269	.0000184	.0000164
4	.0042451	1.1315	.0000184	.0000163
MEAN	.0054925	1.1313	.0000184	.0000163
STD	.0013272	.0036	3.989e-8	8.297e-8
C.V.-%	24.16	.32	.22	.51

Q (m^3/s)	Re	PRESSURE DIFFERENCE (Pa) REP1	REP2	REP3	REP4	MEAN
.0000777	958	9.15	9.20	9.37	9.24	9.24
.0001582	1950	30.69	31.49	31.11	30.76	31.01
.0002326	2867	62.92	62.80	62.12	61.32	62.29

Table G.1i

DATA FOR OPENING X2 AREA=0.32 (cm^2)
GAMMA=979.05x10^-4 (m^-1)

REP	BP (Pa)	Tdb (C)	Twb (C)
1	97917.18	24.4	14.4
2	97815.59	24.4	13.9
3	97883.31	25.6	14.2
4	97883.31	25.8	16.7
MEAN	97874.84	25.1	14.8
STD	36.95	.73	1.27
C.V.-%	.04	2.91	8.59

REP	W kg.w/kg	DENSITY kg/m^3	DYN.VISC N*s/m^2	KIN.VISC m^2/s
1	.0061961	1.1349	.0000183	.0000162
2	.0056075	1.1348	.0000183	.0000162
3	.0054488	1.1317	.0000184	.0000163
4	.0081199	1.1258	.0000184	.0000164
MEAN	.0063431	1.1318	.0000184	.0000162
STD	.0012274	.0043	3.387e-8	8.982e-8
C.V.-%	19.35	.38	.18	.55

Q (m^3/s)	Re	PRESSURE DIFFERENCE (Pa) REP1	REP2	REP3	REP4	MEAN
.0000777	960	10.71	8.80	8.75	8.84	9.27
.0001582	1953	31.98	29.32	29.37	30.19	30.21
.0002326	2872	62.47	58.39	58.23	58.56	59.41

Table G.1j

DATA FOR OPENING Y1

AREA=1.27 (cm^2)
GAMMA=979.05x10^-4 (m^-1)

	REP	BP (Pa)	Tdb (C)	Twb (C)
	1	97849.44	25.3	12.5
	2	97917.18	25.6	12.8
	3	97951.03	26.1	12.2
	4	97951.03	27.2	13.1
MEAN		97917.18	26.0	12.6
STD		36.95	.86	.36
C.V.-%		.04	3.30	2.84

	REP	W kg.w/kg	DENSITY kg/m^3	DYN.VISC N*s/m^2	KIN.VISC m^2/s
	1	.0038559	1.1352	.0000184	.0000162
	2	.0040203	1.1346	.0000184	.0000162
	3	.0032467	1.1343	.0000184	.0000162
	4	.0036265	1.1294	.0000185	.0000164
MEAN		.0036873	1.1334	.0000184	.0000163
STD		.0003352	.0026	3.989e-8	7.376e-8
C.V.-%		9.09	.23	.22	.45

Q (m^3/s)	Re	PRESSURE DIFFERENCE (Pa) REP1	REP2	REP3	REP4	MEAN
.0001582	976	1.82	1.99	1.92	2.02	1.93
.0002326	1435	3.74	3.99	3.89	3.64	3.82
.0003072	1895	6.03	6.21	6.23	6.08	6.14
.0003835	2366	9.17	9.52	9.22	9.24	9.28
.0004703	2901	13.45	13.78	13.48	13.50	13.55
.0005490	3386	18.01	18.48	18.31	18.01	18.20

Table G.1k

DATA FOR OPENING Y2

AREA=1.27 (cm^2)
GAMMA=979.05x10^-4 (m^-1)

	REP	BP (Pa)	Tdb (C)	Twb (C)
	1	97883.31	25.6	12.2
	2	97815.59	25.6	13.9
	3	97849.44	24.4	12.2
	4	97883.31	25.6	12.5
MEAN		97857.91	25.3	12.7
STD		32.43	.56	.80
C.V.-%		.03	2.20	6.28

	REP	W kg.w/kg	DENSITY kg/m^3	DYN.VISC N*s/m^2	KIN.VISC m^2/s
	1	.0034705	1.1352	.0000184	.0000162
	2	.0051566	1.1314	.0000184	.0000163
	3	.0039189	1.1383	.0000183	.0000161
	4	.0037438	1.1347	.0000184	.0000162
MEAN		.0040724	1.1349	.0000184	.0000162
STD		.0007460	.0028	2.508e-8	6.022e-8
C.V.-%		18.32	.25	.14	.37

Q (m^3/s)	Re	PRESSURE DIFFERENCE (Pa) REP1	REP2	REP3	REP4	MEAN
.0001582	979	2.19	2.56	1.79	1.97	2.13
.0002326	1439	4.09	4.71	3.59	3.82	4.05
.0003072	1901	6.43	7.25	5.73	6.16	6.39
.0003835	2374	9.54	10.69	8.77	9.24	9.56
.0004703	2910	13.78	15.07	12.98	13.45	13.82
.0005490	3397	18.41	19.85	17.76	17.99	18.50

Table G.2 Total Minor Loss Coefficients.

Table G.2a

OPENING A

Re	$(1/C_z\hat{}2)$	$(z/D_h Re)$	$B(z/D_h Re)$	K
426	4.9632	.03729	3.57350	1.39
465	4.6990	.03418	3.27547	1.42
504	4.4444	.03155	3.02344	1.42
543	4.2074	.02930	2.80782	1.40
582	4.0744	.02734	2.61999	1.45

Table G.2b

OPENING B

Re	$(1/C_z\hat{}2)$	$(z/D_h Re)$	$B(z/D_h Re)$	K
427	4.6583	.03455	3.30402	1.35
466	4.4597	.03167	3.02860	1.43
505	4.2235	.02923	2.79526	1.43
544	4.0556	.02715	2.59635	1.46
582	3.9527	.02534	2.42326	1.53
621	3.7953	.02375	2.27121	1.52
660	3.6715	.02236	2.13829	1.53
699	3.5550	.02111	2.01875	1.54
738	3.4515	.02000	1.91260	1.54
777	3.3778	.01900	1.81697	1.56

Table G.2c

OPENING C

Re	$(1/C_z\hat{}2)$	$(z/D_h Re)$	$B(z/D_h Re)$	K
574	1.8759	.00556	.53137	1.34
688	1.8121	.00463	.44249	1.37
803	1.8022	.00397	.37941	1.42
918	1.7482	.00347	.33163	1.42
1033	1.6834	.00309	.29531	1.39
1147	1.6177	.00278	.26568	1.35
1377	1.5581	.00232	.22172	1.34
1606	1.4897	.00198	.18923	1.30
1836	1.4474	.00174	.16629	1.28
2065	1.4209	.00154	.14718	1.27
2295	1.3941	.00139	.13284	1.26
2524	1.3798	.00126	.12042	1.26

Table G.2d

OPENING D

Re	$(1/C_z\hat{}2)$	$(z/D_h Re)$	$B(z/D_h Re)$	K
573	2.8413	.01184	1.12823	1.71
688	2.6132	.00986	.93956	1.67
803	2.5811	.00845	.80520	1.78
917	2.5078	.00740	.70515	1.80
1032	2.4083	.00658	.62701	1.78
1147	2.3168	.00592	.56412	1.75
1376	2.1982	.00493	.46978	1.73
1606	2.1289	.00423	.40308	1.73
1835	2.0483	.00370	.35257	1.70
2064	1.9632	.00329	.31350	1.65
2294	1.8884	.00296	.28206	1.61
2523	1.8415	.00269	.25633	1.59
2752	1.7985	.00247	.23537	1.56
2982	1.7892	.00228	.21726	1.57
3211	1.7626	.00211	.20106	1.56
3441	1.7436	.00197	.18772	1.56

Table G.2e

OPENING E

Re	$(1/C_z\hat{}2)$	$(z/D_h Re)$	$B(z/D_h Re)$	K
680	3.2284	.01051	.99477	2.23
1133	2.6559	.00630	.59630	2.06
1587	2.4401	.00450	.42593	2.01
2040	2.3065	.00350	.33128	1.98
2493	2.1511	.00287	.27165	1.88
2947	2.0435	.00242	.22905	1.81
3400	2.0213	.00210	.19877	1.82

Table G.2f

OPENING F

Re	$(1/C_z\hat{}2)$	$(z/D_h Re)$	$B(z/D_h Re)$	K
2014	1.7171	.00100	.09321	1.62
2461	1.6830	.00081	.07550	1.61
2909	1.6211	.00069	.06431	1.56
3356	1.5839	.00060	.05593	1.53

Table G.2g

OPENING G

Re	$(1/C_z\hat{}2)$	$(z/D_h Re)$	$B(z/D_h Re)$	K
2014	1.9708	.00290	.27008	1.70
2462	1.8791	.00237	.22072	1.66
2910	1.8062	.00201	.18719	1.62
3357	1.7799	.00174	.16205	1.62

Table G.2h

OPENING X1

Re	$(1/C_z\hat{}2)$	$(z/D_h Re)$	$B(z/D_h Re)$	K
958	2.7983	.00835	.53440	2.26
1950	2.2674	.00410	.26240	2.01
2867	2.1064	.00279	.17856	1.93

Table G.2i

OPENING X2

Re	$(1/C_z\hat{}2)$	$(z/D_h Re)$	$B(z/D_h Re)$	K
960	2.8078	.00834	.53376	2.27
1953	2.2082	.00410	.26240	1.95
2872	2.0082	.00279	.17856	1.83

Table G.2j

OPENING Y1

Re	$(1/C_z\hat{}2)$	$(z/D_h Re)$	$B(z/D_h Re)$	K
976	2.1886	.00410	.26240	1.93
1435	1.9968	.00279	.17856	1.82
1895	1.8417	.00211	.13504	1.71
2366	1.7871	.00169	.10816	1.68
2901	1.7348	.00138	.08832	1.65
3386	1.7103	.00118	.07552	1.63

Table G.2k

OPENING Y2

Re	$(1/C_z\hat{}2)$	$(z/D_h Re)$	$B(z/D_h Re)$	K
979	2.4037	.00409	.26176	2.14
1439	2.1168	.00278	.17792	1.94
1901	1.9156	.00210	.13440	1.78
2374	1.8379	.00169	.10816	1.73
2910	1.7669	.00137	.08768	1.68
3397	1.7362	.00118	.07552	1.66

APPENDIX H

THE TECHNIQUE USED TO DETERMINE THE BEST SET OF OPENING PARAMETERS

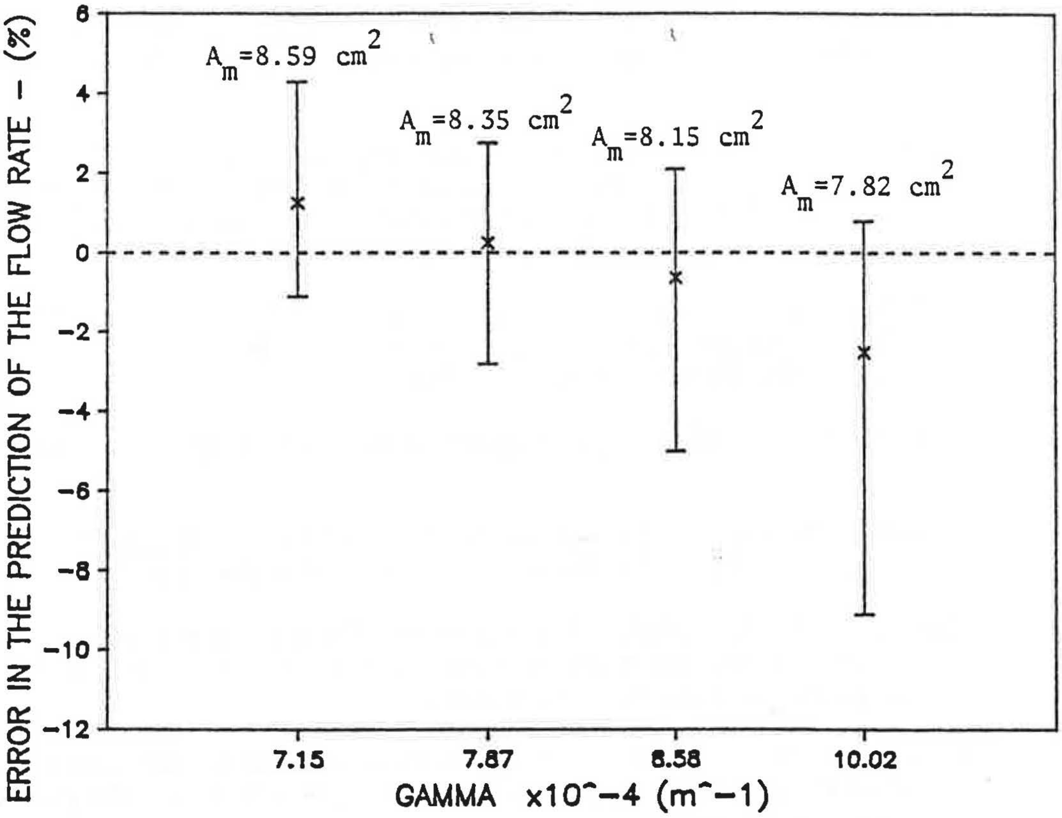

Figure H.1 The error in the prediction of the flow rates for opening B using several choices of gamma and the areas determined by a least squares best fit of equation 8.3.

REFERENCES

ASHRAE, 1981. ASHRAE Handbook of Fundamentals. American Society of Heating, Refrigerating and Air-Conditioning Engineers, Inc., Atlanta.

ASHRAE, 1985. ASHRAE Handbook of Fundamentals. American Society of Heating, Refrigerating and Air-Conditioning Engineers, Inc., Atlanta.

ASTM, 1985. ASTM E779-81: Standard Practice for Measuring Air Leakage By the Fan Pressurization Method. ASTM, Philadelphia, PA.

Beavers, G. S., Sparrow, E. M. and Magnuson, R. A. 1970. ''Experiments on Hydrodynamically Developing Flow in Rectangular Ducts of Arbitrary Aspect Ratio.'' International Journal of Heat and Mass Transfer, vol. 13, pp. 689-702.

Colliver, D. G., Walton, L. R. and Parker, B. F. 1982. ''Wind Speed Effect on Residential Energy Usage.'' ASAE Paper No. 82-4521, ASAE, St. Joseph, Michigan 49085.

Currie, I. G. 1974. Fundamental Mechanics of Fluids. McGraw-Hill, Inc.

Diamond, R. C., and Grimsrud, D. T., 1984. Manual On Indoor Air Quality. Electric Power Research Institute, pp. 2-1 to 2-9.

Emswiler, J. E. 1926. ''The Neutral Zone in Ventilation.'' Transactions American Society of Heating and Ventilating Engineers, vol. 32, pp. 59-74.

Etheridge, D. W., 1977. ''Crack Flow Equations and Scale Effect.'' Building and Environment, vol. 12, pp. 181-189. Pergamon Press, Great Britain.

Fox, R. W. and McDonald, A. T., 1973. Introduction to Fluid Mechanics. Second edition, John Wiley and Sons, Inc.

Han, L. S., 1960. ''Hydrodynamic Entrance Lengths for Incompressible Laminar Flow in Rectangular Ducts.'' Journal of Applied Mechanics, Transactions of ASME, pp. 403-405, Sept.

Holman, J. P., 1978. Experimental Methods for Engineers. pp. 44-50, McGraw-Hill, Inc.

Hopkins, L. P. and Hansford, B., 1974. ''Air Flow Through Cracks.'' Building Service Engineer, vol. 42, pp. 123-131, Sept.

Indoor Air Quality Research Strategy, 1984. U.S. Interagency Committee on Indoor Air Quality, U.S. Environmental Protection Agency, Office of Research and Development, Washington, DC.

Kays, W. M. and Crawford, M. E., 1980. Convective Heat and Mass Transfer. McGraw-Hill, Inc.

Keil, D. E., Wilson, D. J. and Sherman, M. H., 1985. ''Air Leakage Flow Correlations for Varying House Construction Types.'' ASHRAE Transactions, vol. 91 (2A), pp. 560-575.

Langhaar, H. L., 1942. ''Steady Flow in the Transition Length of a Straight Tube.'' Transactions of the ASME, pp. A-55 to A-58, June.

Lee, K. H., Lee, T. and Tanaka, H., 1985. ''Thermal Effect on Pressure Distribution in Simulated High Rise Buildings: Experiment and Analysis.'' ASHRAE Transactions, vol. 91(2).

Liddament, M. and Allen, C. 1983. The Validation and Comparison of Mathematical Models of Air Infiltration. International Energy Agency, Air Infiltration Center, Sept., Great Britain.

McNall, P. E., 1986. ''Indoor Air Quality.'' ASHRAE Journal, pp. 39-48, June.

Nazaroff, W. W., Boegel, M. L., Hollowell, C. D. and Roseme, G. D., 1981. ''The Use of Mechanical Ventilation with Heat Recovery for Controlling Radon and Radon-Daughter Concentrations in Houses.'' Atmospheric Environment, vol. 15, pp. 263-270. Pergamon Press, Great Britain.

Nero, A. V., 1986. ''The Indoor Radon Story.'' Technology Review, vol. 89, pp. 28-40, January.

Office of Technology Assessment. 1979. Residential energy conservation. OTA-E-92. U.S. Government Printing Office, Washington, D.C.

Shaw, C. Y. and Tamura, G. T., 1977. ''The Calculation of Air Infiltration Rates Caused by Wind and Stack Action for Tall Buildings.'' ASHRAE Transactions, vol. 82(2), pp. 145-157.

Shaw, C. Y., 1980. ''Wind and Temperature Induced Pressure Differentials and An Equivalent Pressure Difference Model for Predicting Air Infiltration in Schools.'' ASHRAE Transactions, vol. 86(1), pp. 268-278.

Shaw, C. V. and Brown, W. C., 1982. ''Effect of a Gas Furnace Chimney on the Air Leakage Characteristic of a Two-Story Detached House.'' Proceedigns of the 3rd IEA Conference of the Air Infiltration Centre, London.

Sherman, M. H., 1980. ''Air Infiltration in Buildings.'' University of California, Berkeley. Ph.D. Thesis, University Microfilms International.

Snedecor, G. W. and Cochran, W. G., 1980. Statistical Methods. seventh edition, The Iowa State University Press, Ames, Iowa.

Steel, R. G. D. and Torrie, J. H., 1980. Principles and Procedures of Statistics, A Biometrical Approach. second edition, McGraw-Hill, Inc.

Tamura, G. T. and Shaw, C. Y., 1976. ''Studies on Exterior Wall Air Tightness and Air Infiltration of Tall Buildings.'' ASHRAE Transactions, vol. 82(1), pp. 122-134.

Tamura, G. T. and Wilson, A. G., 1966. ''Pressure Differences for a Nine-Story Building as a Result of Chimney Effect and Ventilation System Operation.'' ASHRAE Transactions, vol. 82(1), pp. 122-134.

Tamura, G. T. and Wilson, A. G., 1967. ''Building Pressures Caused by Chimney Action and Mechanical Ventilation.'' ASHRAE Transactions, vol. 73(2).

Younger, M. S., 1979. A Handbook for Linear Regression. Duxburg Press, Massachusetts.

VITA

John Perkins Chastain

Born: October 2, 1960, Atlanta, Georgia

Education:

B.S. Agricultural Engineering, University of Georgia, 1982

M.S. Agricultural Engineering, University of Kentucky, 1987

Professional Positions:

Research Specialist, Agricultural Engineering Department, University of Kentucky, October 1986 to present

Research Assistant, Agricultural Engineering Department, University of Kentucky, January 1984 to October 1986

Instructor and Agricultural Consultant, Chamuhawi Christian Training and Rural Development Center, Tanzania, East Africa, September 1982 to September 1983

Student Research Technician, Agricultural Engineering Department, University of Georgia, June 1981 to August 1982

Scholastic and Professional Honors:

Phi Eta Sigma
E. G. Dawson Scholarship, 1980
Hugar F. Wilkes Scholarship, 1981
Engineer in Training, 1982
Alpha Epsilon
Tau Beta Pi
Gamma Sigma Delta

Date